

GAS ABSORPTION IN MOBILE BEDS OF SPHERICAL PACKINGS

A thesis submitted in accordance with the requirements  
for the Degree of Doctor of Philosophy

by

ALI HEKMAT-NAZEMI  
BSc, MSc

Under the direction of

Dr. D. Handley

Department of Chemical Engineering  
Houldsworth School of Applied Science  
University of Leeds  
Leeds, England

March 1992

# CONTENTS

	<u>Page</u>
ACKNOWLEDGEMENTS	
ABSTRACT	
CHAPTER 1	
1 Introduction	1
1.1 Hydrodynamic Performance of Turbulent Contact Absorber (TCA)	1
1.2 Mass Transfer Performance of (TCA)	3
1.3 Present Work	4
1.3.1 Hydrodynamic Studies	5
1.3.2 Mass Transfer Studies	5
CHAPTER 2	
2 Literature Review	6
2.1 Hydrodynamics of Turbulent Contact Absorber	6
2.2 Mass Transfer Characteristics of (TCA)	21
CHAPTER 3	
3 Mass Transfer Theories	29
3.1 The Diffusion Process	29
3.2 Physical Absorption	30
3.2.1 Models of Absorption	32
3.2.1.1 The Film Model (Whitman's Model)	32
3.2.1.2 Penetration Theory (Higbie's Model)	33
3.2.1.3 Surface - Renewal Theory (Danckwerts' Model)	35
3.3 Absorption in Presence of Chemical Reactions	37
3.3.1 Slow Reaction	38
3.3.2 Fast Reaction	39
3.3.3 Instantaneous Reaction	41
3.3.4 Equations of Rate of Absorption with (m,n-th) Order Irreversible Chemical Reaction	43

3.3.4.1	Film Theory	43
3.3.4.2	Penetration Theory	45
3.3.5	Determination of Interfacial Area	52
3.3.6	Determination of Liquid Film Transfer Coefficient	53
CHAPTER 4		
4	Equipment and Experimental Methods	55
4.1	Test Rig Design and Specifications	55
4.2	Experimental Procedures	57
4.2.1	Hydrodynamics Experimental Procedures	57
4.2.1.1	Pressure Drop	57
4.2.1.2	Expanded Bed Height	60
4.2.1.3	Liquid Hold Up	60
4.2.1.4	Minimum Expanding Velocity	60
4.2.2	Mass Transfer Experimental Procedures	60
CHAPTER 5		
5	Results and Discussion	62
5.1	Hydrodynamic Results and Discussion	62
5.1.1	Pressure Drop	62
5.1.2	Minimum Expanding Velocity	67
5.1.3	Wall Effect	72
5.1.4	Bed Expansion Characteristics	91
5.1.5	Liquid Hold Up	106
5.1.6	Summary of Comparative Hydrodynamic Studies	106
5.2	Mass Transfer Results and Discussion	122
5.2.1	Theoretical Model and Treatment of Data	122
5.2.2	Absorption of CO <sub>2</sub> in NaOH Solutions	123
5.2.3	Estimation of Interfacial Area (a) and Liquid Film Transfer Coefficient (k <sub>L</sub> )	124
5.2.4	Comparative Mass Transfer Performance for Different Systems	151

CHAPTER 6		
6	Graphical Presentation of Interphase Mass Transfer	156
CHAPTER 7		
7	Conclusions	162
	7.1 Hydrodynamics	162
	7.2 Mass Transfer	165
CHAPTER 8		
8	Recommendations for Further Work	168
APPENDICES		
A	Determination of The Physico-Chemical Parameters	169
B	Tables of Mass Transfer Results	173
C	Alternative Method of Estimation of $(a)$ and $(k_L)$	179
NOMENCLATURE		183
REFERENCES		187

## LIST OF FIGURES

		<u>Page</u>
Fig. 3.1	Concentration-profile of diffusing solute.	36
Fig. 3.2	Effect of chemical reaction on concentration profile in diffusion film.	36
Fig. 3.3	Interface behaviour for the liquid phase reaction.	40
Fig. 3.4	Concentration profiles for instantaneous reaction with varying concentrations of reactant.	42
Fig. 3.5	Enhancement factors for second order reaction; for quiescent liquid or agitated liquid.	50
Fig. 4.1	Rig arrangement.	56
Fig. 4.2	Type of Packings.	59
Fig. 5.1.1	Plot of pressure drop characteristics of plain packing, packing dia. = 38 mm, bed static height = 10.5 cm for various superficial liquid velocities.	63
Fig. 5.1.2	Plot of pressure drop characteristics of plain packing, packing dia. = 38 mm, bed static height = 16.5 cm, for various superficial liquid velocities.	64
Fig. 5.1.3	Plot of pressure drop characteristics of plain packing, packing dia. = 38 mm, H = 10.5 cm and H = 16.5 cm, for dry bed.	65
Fig. 5.1.4	Plot of pressure drop characteristics of plain packing, packing dia. = 38 mm, H = 10.5 cm and H = 16.5 cm, for superficial liquid velocity = $6.58 \times 10^{-3}$ m/s.	66
Fig. 5.1.5	Plot of minimum expanding velocity with liquid rate for plain packing, packing dia. = 38 mm, bed static height = 10.5 cm.	68
Fig. 5.1.6	Plot of variation of minimum expanding velocity with liquid rate for oblate spheroid packing, packing dia. = 50 x 38 mm, bed static height = 10.5 cm.	69
Fig. 5.1.7	Plot of variation of minimum expanding velocity with liquid rate for plain packing, packing dia. 25 mm, bed static height = 10.5 cm.	70

Fig. 5.1.8	Plot of variation of minimum expanding velocity with liquid rate for slotted packing, packing dia. = 25 mm, bed static height = 10.5 cm.	71
Fig. 5.1.9	Plot of pressure drop characteristics of oblate spheroid packing, packing dia. = 50 x 38 mm, bed static height = 10.5 cm, for various superficial liquid velocities.	73
Fig. 5.1.10	Plot of pressure drop characteristics of plain packing, packing dia. = 25 mm, bed static height = 10.5 cm, for various superficial liquid velocities.	74
Fig. 5.1.11	Plot of pressure drop characteristics of slotted packing, packing dia. = 25 mm, open area = 11%, bed static height = 10.5 cm, for various superficial liquid velocities.	75
Fig. 5.1.12	Plot of pressure drop characteristics of oblate spheroid packing, packing dia. = 50 x 38 mm, bed static height = 16.5 cm, for various superficial liquid velocities.	76
Fig. 5.1.13	Plot of pressure drop characteristics of plain sphere packing, packing dia. = 25 mm, bed static height = 16.5 cm, for various superficial liquid velocities.	77
Fig. 5.1.14	Plot of pressure drop characteristics of slotted packing, packing dia. = 25 mm, open area = 11%, bed static height = 16.5 cm, for various superficial liquid velocities.	78
Fig. 5.1.15	Plot of pressure drop characteristics of oblate spheroid packing, packing dia. = 25 mm, H = 10.5 cm and H = 16.5 cm, superficial liquid velocity = $8.77E-3$ m/s.	79
Fig. 5.1.16	Plot of pressure drop characteristics of plain sphere packing, packing dia. = 25 mm, H = 10.5 cm and H = 16.5 cm, superficial liquid velocity = $8.77E-3$ m/s.	80
Fig. 5.1.17	Plot of pressure drop characteristics of slotted packing, packing dia. = 25 mm, H = 10.5 cm and H = 16.5 cm, superficial liquid velocity = $8.77E-3$ m/s.	81
Fig. 5.1.18	Influence of wall effect on pressure drop for oblate spheroid packing, packing dia. = 50 x 38 mm, bed static height = 10.5 cm, superficial liquid velocity = $2.32E-3$ m/s.	83
Fig. 5.1.19	Influence of wall effect on pressure drop for plain sphere packing, packing dia. = 38 mm,	

bed static height = 10.5 cm, superficial liquid velocity = $2.32E=3$ m/s.	84
Fig. 5.1.20 Influence of wall effect on pressure drop for plain sphere packing, packing dia. = 25 mm, bed static height = 10.5 cm, superficial liquid velocity = $2.32E=3$ m/s.	85
Fig. 5.1.21 Influence of wall effect on pressure drop for slotted packing, packing dia. = 25 mm, open area = 11%, bed static height = 10.5 cm, superficial liquid velocity = $1.32E-3$ m/s.	86
Fig. 5.1.22 Influence of pressure drop for oblate spheroid packing, packing dia. = 50 x 38 mm, bed static height = 10.5 cm, superficial liquid velocity = $6.58E-3$ m/s.	87
Fig. 5.1.23 Influence of wall effect on pressure drop for plain sphere packing, packing dia. = 38 mm, bed static height = 10.5 cm, superficial liquid velocity = $6.58E-3$ m/s.	88
Fig. 5.1.24 Influence of wall effect on pressure drop for plain sphere packing, packing dia. = 25 mm, bed static height = 10.5 cm, superficial liquid velocity = $6.58E-3$ m/s.	89
Fig. 5.1.25 Influence of wall effect on pressure drop for slotted packing, packing dia. = 25 mm, open area = 11%, bed static height = 10.5 cm, superficial liquid velocity = $6.58E-3$ m/s.	90
Fig. 5.1.26 Plot of variation of bed height with superficial air velocity for plain sphere packing, packing dia. = 38 mm, bed static height = 10.5 cm, for various superficial liquid velocities.	92
Fig. 5.1.27 Plot of variation of bed height with superficial air velocity for plain sphere packing, packing dia. = 25 mm, bed static height = 10.5 cm, for various superficial liquid velocities.	93
Fig. 5.1.28 Plot of variation of bed height with superficial air velocity for oblate spheroid packing, packing dia. = 50 x 38 mm, bed static height = 10.5 cm, for various superficial liquid velocities.	94
Fig. 5.1.29 Plot of variation of bed height with superficial air velocity for slotted packing, packing dia. = 25 mm, bed static height = 10.5 cm, for various superficial liquid velocities.	95

- Fig. 5.1.30 Plot of variation of bed height with superficial air velocity for plain sphere packing, packing dia. = 38 mm, bed static height = 16.5 cm, for various superficial liquid velocities. 96
- Fig. 5.1.31 Plot of variation of bed height with superficial air velocity for plain sphere packing, packing dia. = 25 mm, bed static height = 16.5 cm, for various superficial liquid velocities. 97
- Fig. 5.1.32 Plot of variation of bed height with superficial air velocity for oblate spheroid packing, packing dia. = 50 x 38 mm, bed static height = 16.5 cm, for various superficial liquid velocity. 98
- Fig. 5.1.33 Plot of variation of bed height with superficial air velocity for slotted packing, packing dia. = 25 mm, bed static height = 16.5 cm, for various superficial liquid velocities. 99
- Fig. 5.1.34 Plot of variation of fluctuation of bed height with air velocity for oblate spheroid packing, packing dia. = 50 x 38 mm,  $H = 10.5$  cm and  $H = 16.5$  cm, superficial liquid velocity =  $2.32E-3$  m/s. 101
- Fig. 5.1.35 Plot of variation of fluctuation of bed height with air velocity for plain packing, packing dia. = 38 mm,  $H = 10.5$  cm and  $H = 16.5$  cm, superficial liquid velocity =  $2.32E-3$  m/s. 102
- Fig. 5.1.36 Plot of variation of fluctuation of bed height with air velocity for plain packing, packing dia. = 25 mm,  $H = 10.5$  cm and  $H = 16.5$  cm, superficial liquid velocity =  $2.32E-3$  m/s. 103
- Fig. 5.1.37 Plot of variation of fluctuation of bed height with air velocity for slotted packing, packing dia. = 25 mm,  $H = 10.5$  cm and  $H = 16.5$  cm, superficial liquid velocity =  $2.32E-3$  m/s. 104
- Fig. 5.1.38 Sequence of formation of slugs in slugging bed. 105
- Fig. 5.1.39 Plot of variation of liquid hold up with air velocity for plain sphere packing, packing dia. = 38 mm, bed static height = 10.5 cm, for various superficial liquid velocity. 107
- Fig. 5.1.40 Plot of variation of liquid hold up with air velocity for plain sphere packing, packing

dia. = 25 mm, bed static height = 10.5 cm, for various superficial liquid velocity.	108
Fig. 5.1.41 Plot of variation of liquid hold up with air velocity for oblate spheroid packing, packing dia. = 50 x 38 mm, bed static height = 10.5 cm, for various superficial liquid velocity.	109
Fig. 5.1.42 Plot of variation of liquid hold up with air velocity for slotted sphere packing, packing dia. = 25 mm, bed static height = 10.5 cm, for various superficial liquid velocity.	110
Fig. 5.1.43 Plot of variation of minimum expanding velocity with liquid rate for mobile bed packings, bed static height = 10.5 cm.	111
Fig. 5.1.44 Plot of pressure drop characteristics of mobile packings superficial liquid velocity = 2.32E-3 m/s, bed static height = 10.5 cm, for different packings.	113
Fig. 5.1.45 Plot of pressure drop characteristics of mobile packings superficial air velocity = 3 m/s, bed static height = 10.5 cm, for different packings.	114
Fig. 5.1.46 Plot of variation of liquid hold up with air velocity for mobile packings, superficial liquid velocity = 2.32E-3 m/s, bed static height = 10.5 cm.	115
Fig. 5.1.47 Plot of variation of liquid hold up with liquid rate for mobile packings, superficial air velocity = 3 m/s, bed static height = 10.5 cm.	116
Fig. 5.1.48 Plot of variation of bed static height with liquid hold up for mobile packings, bed static height = 10.5 cm, superficial liquid velocity = 2.32E-3 m/s.	118
Fig. 5.1.49 Plot of variation of bed height with air velocity for mobile packings, bed static height = 10.5 cm, superficial liquid velocity = 2.32E-3 m/s.	119
Fig. 5.1.50 Plot of variation of fluctuation of bed height with air velocity for mobile bed packings, bed static height = 10.5 cm.	120
Fig. 5.1.51 Plot of variation of bed height with air velocity for mobile bed packings, bed static height = 10.5 cm, liquid superficial velocity = 8.77E-3 m/s.	121

Fig. 5.2.1	Plot of overall mass transfer coefficient vs caustic concentration for oblate air velocity = 2.1 m/s, packing dia. = 50 x 38 mm, bed static height = 10.5 cm, for various superficial velocity.	125
Fig. 5.2.2	Plot of overall mass transfer coefficient vs caustic concentration for slotted packing, air velocity = 2.1 m/s, packing dia. = 25 mm, open area = 11%, bed static height = 10.5 cm for various superficial liquid velocities.	126
Fig. 5.2.3	Plot of overall mass transfer coefficient vs caustic concentration for plain sphere packing, air velocity = 2.1 m/s, packing dia. = 25 mm, bed static height = 10.5 cm for various superficial liquid velocities.	127
Fig. 5.2.4	Plot of overall mass transfer coefficient vs liquid rate at superficial air velocity = 2.1 m/s, bed static height = 10.5 cm, for mobile packings, caustic concentration = 1.5 k.mol/m <sup>3</sup> .	128
Fig. 5.2.5	Plot of mass transfer characteristics of oblate packing at superficial liquid velocity = 6.58E-3 m/s, packing dia. = 50 x 38 mm, bed static height = 10.5 cm for various superficial air velocity.	129
Fig. 5.2.6	Plot of mass transfer characteristics of oblate packing at superficial air velocity = 2.1 m/s, packing dia. = 50 x 38 mm, bed static height = 10.5 cm, for various superficial liquid velocities.	130
Fig. 5.2.7	Plot of mass transfer characteristics of slotted packing at superficial liquid velocity = 6.58E-3 m/s, packing dia. = 25 mm, open area = 11%, bed static height = 10.5 cm for various superficial air velocities.	131
Fig. 5.2.8	Plot of mass transfer characteristics of slotted packing at superficial air velocity = 2.1 m/s, packing dia. = 25 mm, open area = 11%, bed static height = 10.5 cm for various superficial liquid velocities.	132
Fig. 5.2.9	Plot of interfacial area per unit volume of static bed vs superficial air velocity, static bed height = 10.5 cm, superficial liquid velocity = 6.58E-3 m/s for mobile packings.	134
Fig. 5.2.10	Plot of interfacial area per unit volume of static bed vs superficial liquid velocity, static bed height = 10.5 cm, superficial air velocity = 2.1 m/s, for mobile packings.	135

Fig. 5.2.11	Plot of interfacial area per unit volume of liquid hold up vs superficial liquid velocity, bed static height = 10.5 cm, superficial air velocity = 2.1 m/s, for mobile packings.	138
Fig. 5.2.12	Plot of interfacial area per unit volume of liquid hold up vs superficial air velocity, bed static height = 10.5 cm, superficial liquid velocity = 6.58E-3 m/s, for mobile packings.	139
Fig. 5.2.13	Plot of interfacial area per unit volume of expanded bed vs superficial air velocity, bed static height = 10.5 cm, superficial liquid velocity = 6.58E-3 m/s, for mobile packings.	142
Fig. 5.2.14	Plot of interfacial area per unit volume of expanded bed vs superficial liquid velocity, bed static height = 10.5 cm, superficial air velocity 2.1 m/s, for mobile packings.	143
Fig. 5.2.15	Plot of liquid film transfer coefficient vs superficial liquid velocity, bed static height = 10.5 cm, superficial air velocity = 2.1 m/s, for mobile packings.	145
Fig. 5.2.16	Plot of liquid film transfer coefficient vs superficial air velocity, bed static height = 10.5 cm, superficial liquid velocity = 6.58E-3 m/s, for mobile packings.	146
Fig. 5.2.17	Plot of volumetric liquid mass transfer coefficient vs superficial liquid velocity, bed static height = 10.5 cm, superficial air velocity = 2.1 m/s, for mobile packings.	149
Fig. 5.2.18	Plot of volumetric liquid mass transfer coefficient vs superficial air velocity, bed static height = 10.5 cm, superficial liquid velocity = 6.58E-3 m/s, for mobile packings.	150
Fig. 5.2.19	Plot of operational mass transfer efficiency vs superficial liquid velocity, bed static height = 10.5 cm, superficial air velocity = 2.1 m/s, for mobile packings.	152
Fig. 5.2.20	Plot of operational mass transfer efficiency vs superficial air velocity = 6.58E-3 m/s, for mobile packings.	153
Fig. 6.1	Dimensionless plot of relative absorption efficiency $\eta_{rel}$ vs the transfer coefficient ratio $\gamma$ .	159

## LIST OF TABLES

	<u>Page</u>
Table 2.1 Correlation Equations for Pressure Drop in a Single-Stage TCA.	14
Table 2.2 Correlation equations for liquid and gas hold up in TCA.	19
Table 4.1 Specifications of packings used in present work.	58
Table 5.2.1 Comparison of $a_s$ and $a_L$ at different gas velocities.	136
Table 5.2.2 Comparison of $a_s$ and $a_L$ at different liquid velocities.	136
Table 5.2.3 Variation of $\epsilon(H_L)$ and $\epsilon(A)$ with liquid velocity for different packings.	140
Table 5.2.4 Variation of $\epsilon(H_L)$ and $\epsilon(A)$ with gas velocity for different packings.	141
Table 5.2.5 Comparison of $\epsilon(A)$ and $\epsilon(H_{dy})$ with liquid velocity for slotted packing with respect to oblate and plain packings.	147
Table 5.2.6 Comparison of (a) for different packings at constant gas velocity of 2.1 m/s.	147
Table 5.2.7 Comparison of (a) for different packings at constant liquid velocity of $6.58 \times 10^{-3}$ m/s.	147
Table B1 Variation of $K_L$ with liquid velocity at $V_g = 2.1$ m/s in present work estimated from Danckwerts' plot.	173
Table B2 Variation of $K_L$ with gas velocity at $V_L = 6.58 \times 10^{-3}$ m/s in present work estimated from Danckwerts' plot.	172
Table B3 Variation of $\eta_{op}$ with liquid velocity at $V_g = 2.1$ m/s	174
Table B4 Variation of $\eta_{op}$ with air velocity at $V_L = 6.58 \times 10^{-3}$ m/s in present work.	174
Table B5 Typical values of interfacial area in TCA.	175-176
Table B6 Typical values of $k_L$ in TCA.	177
Table B7 Typical values of liquid film mass transfer coefficient and interfacial area for sieve plates.	178

Table C1	Variation of $(a_s)$ and $k_L$ with liquid velocity at $V_g = 2.1$ m/s using short and full Danckwerts' models.	181
Table C2	Variation of $(a)$ and $(k_L)$ with gas velocity at $V_l = 6.58 \times 10^{-3}$ m/s using short and full Danckwerts' models.	182

This work is dedicated to my parents,  
my wife and children to whom  
I am indebted for  
their love and support.

## ACKNOWLEDGEMENTS

I would like to express my gratitude to all who helped bring this work to completion:

My supervisor, Dr. D. Handley, for his continued encouragement, constructive criticism, technical advice and invaluable guidance throughout my study.

To Professor G.G. Haselden for his help and advice.

To all the technical staff, Ernest, Ian, John, Peter, Michael, Bill and especially Martin.

To my wife who has borne a disproportionate share of the family duties, and my children who occasionally missed my uninterrupted attention over this period.

To Mrs. Sheilagh Ogden for her patience in typing this work.

## ABSTRACT

Experiments have been conducted to investigate the hydrodynamics and mass transfer performance of some alternative mobile bed packings. The polypropylene packings used in this work were 50 x 38 mm oblate spheroids, 38 mm diameter plain spheres, 25 mm diameter plain spheres and 25 mm diameter slotted spheres.

The perspex column was 22 cm internal diameter and 144 cm high and was fitted with a supporting grid having 72% open area.

In the hydrodynamics studies, air and water were passed counter currently through the column. Bed pressure drop, mean expanded bed height, minimum expanding gas velocity and volume of liquid hold up for all of the packings were measured at different air and water rates and with two bed static heights of 10.5 and 16.5 cm.

The general hydrodynamic behaviour of the fluidized packings has been observed and factors influencing pressure drop, liquid hold up, expanded bed height and minimum expanding velocity have been identified. Evidence for gas and liquid flow through the interiors of the slotted packings and giving rise to higher liquid hold up and a smoother quality of fluidization as compared with the other packings has been found.

Plain spheres and oblate spheroid packings appeared to have almost identical hydrodynamic behaviour, although the oblate spheroid was found to show more slugging fluctuation in the bed height at high gas velocities.

In mass transfer studies, dilute  $\text{CO}_2$  (2% vol/vol) was absorbed into sodium hydroxide solutions and the interfacial area and liquid film transfer coefficient were thereby established employing the pseudo first

order reaction model for the rate of absorption (known generally as the Danckwerts' model) (41).

The experimental results on the Danckwerts' plot lay on a straight line and therefore confirmed the applicability of the Danckwerts' model from which ( $k_L$ ) and ( $a$ ) could be estimated.

The interfacial area per unit volume of expanded bed ( $a$ ) and per unit volume static bed ( $a_s$ ) was found to be higher for the slotted packings than for the plain sphere packings and the oblate spheroid packings.

The interfacial area per unit volume of liquid hold up ( $a_L$ ) was higher for the plain sphere packing than for the oblate spheroid and the slotted sphere packings, however, the ( $a$ ) and ( $a_s$ ) for the plain sphere packings were higher than for the oblate spheroid packings.

The liquid film transfer coefficient for the slotted sphere packings was higher than for the other packings and was found to be almost the same for the plain sphere and the oblate spheroid packings.

The operational mass transfer efficiency (defined as the ratio of the volumetric liquid film mass transfer coefficient to the fluid energy consumption in the bed) for the oblate spheroid packings was found to be higher than for the plain and slotted sphere packings. This efficiency ratio was also found to be higher for the slotted packings than for the plain sphere packings. Finally, the slotted packings appear to offer high volumetric mass transfer coefficients with a smoother quality of fluidization and homogeneous contacting of gas and liquid.

## CHAPTER 1

### INTRODUCTION

#### 1.1. Hydrodynamic Performance of Turbulent Contact Absorber (TCA)

Turbulent Contact Absorbers with mobile packings have been used in industry for producing intimate contact between gas and liquid. In essence, it is a packed tower using low density spheres as packings.

Typically, the spherical packings are made of low density polystyrene foam and thus are easily set in motion by an upward-flowing gas. The simultaneous down-flow of the liquid phase increases the motion of the entire bed towards greater homogeneity. Thus a state of vigorous contacting between liquid and gas may be obtained over a wide range of flow rates as a result of the motion of the packing.

A gas-liquid contactor with movable packing possesses some significant advantages over a conventional gas-liquid contactor with fixed bed packing. The motion of the packing prevents plugging and bypassing which may occur, when gases or liquids containing suspended solid particles are used.

Fundamental studies of the hydrodynamics of mobile beds such as pressure drop, operating regime, liquid hold-up, minimum fluidization velocity, and bed expansion have been conducted by a number of investigators. The bed pressure drop is believed to be the sum of contributions due to the weight of the dry packing and the liquid hold up. Three successive hydrodynamic states are observed as the gas flow rate is increased at a constant liquid irrigation rate.

At low gas rates the bed is static and the pressure drop in this region increases sharply with an increase in gas velocity. This

condition continues until the gas velocity reaches the minimum fluidization velocity. After this point with further increase in the gas velocity, the packing spheres begin to move vigorously and are lifted by the upward drag and inertia forces of the gas flow causing the bed to expand. The pressure drop across the bed stays constant or increases only gradually with increasing gas velocity since fluidisation of the packing offers less resistance to the gas flow, however, eventually at very high gas rates the bed becomes flooded.

It is generally known that the bed pressure drop increases when either the static bed height, liquid flow rate, or the packing density are increased and when the packing diameter is decreased (20, 21, 23, 51).

The liquid hold up is reported to increase with an increase in liquid rate and decrease in packing diameter (2, 8, 21), however Chen and Douglas (21), Uchida et al (3) and Kito et al (2) reported that the liquid hold up is not significantly affected by gas velocity, whereas, Rao et al (24), Gelperin et al (8) and Groeneveld (55) found that the liquid hold up increases with increasing gas velocity.

The minimum fluidization velocity has been found to decrease with increase in liquid flow rate and with decrease in packing diameter (10,, 22, 53). It has been reported that the bed static height does not affect the minimum fluidization velocity (22, 50).

The expanded bed height increases with increasing air and liquid flow rates after the minimum fluidization velocity has been reached. The bed static height affects the mode of fluidization. The beds with a bed static height shorter than the column diameter, fluidize more

uniformly, while slugging is commonly observed in deeper beds (18, 23, 51, 54).

Tichy et al (18), Tichy and Douglas (53) reported that some wall effect was present during their experiments and this effect was more pronounced with increasing liquid rate and static bed height. Rao et al (24) also reported similar observations.

## 1.2. Mass Transfer Performance of (TCA)

The turbulent contact absorber (TCA), has been increasingly finding application as an alternative to the conventional packed bed in absorption, desorption, distillation and in pollution control (11, 20, 60, 61). It possesses significant advantages over the packed bed as it permits higher throughputs without flooding and processing of dusty gases, slurries and crystallizing liquids without clogging. Recently the TCA has been used for  $\text{SO}_2$  absorption and for particulate removal from stack gases (20).

Douglas et al (60) found that the combined high gas and liquid flow rates, far in excess of those possible in conventional packed towers, greatly increased the absorption capacity for a given tower size. Overall mass transfer rates as much as two orders of magnitude higher than in packed columns were also reported.

Kossev et al (35) also reported that on average, the mass transfer performance of a TCA is about 1.5 to 2 times greater than in a conventional plate column.

Some research has been carried out on the gas-liquid interfacial area, which is an important contributory factor in the design and operational performance of turbulent contact absorbers. Kossev et al

(35) investigated the gas-liquid contact area in a TCA at the high gas velocities of 2.85 to 4.15 m/s and found that the interfacial area per unit volume of expanded bed increased with increasing gas and liquid velocities up to 3 m/s and 0.022 m/s respectively, following which it decreased. Gelperin et al (26) correlated the static bed height,  $H_s$ , with the interfacial area. Wozniak and Ostergaard (30) studied the effect of the velocity of the liquid at a constant gas velocity of 0.7 m/s.

Subsequently, Wozniak (28) proposed a correlation for the interfacial area with the gas hold up, the pressure drop and expanded bed height. Kito et al (27) measured the interfacial area present in batch liquid fluidised absorption systems over a wide range of gas velocities, distributor types and column and packing diameters.

Strumillo and Kudra (37) studied the effects of packing size, gas and liquid velocities and the height of the static bed on the interfacial area and reported an empirical correlation.

### 1.3 Present Work

Turbulent contact absorbers have generally employed plain hollow plastic spheres and have been shown to offer high mass transfer rates and be capable of cleaning dusty gases. The possibility of achieving even better performance characteristic is offered by changing the shape of the packing and by providing slots for improving the gas and liquid contact.

The purpose of this study therefore was to investigate the hydrodynamic and mass transfer characteristics of novel packings available in the form of slotted spheres and oblate spheroids over a

wide range of experimental conditions and to compare their hydrodynamic and mass transfer performance with those of conventional plain sphere packings.

### 1.3.1. Hydrodynamic Studies

These were carried out in order to establish pressure drop, liquid hold up, expanded bed height, minimum expanding velocity and bed height fluctuation at two bed static heights of 10.5 and 16.5 cm over a wide range of water and air velocities.

### 1.3.2. Mass Transfer Studies

- (i) These were intended to estimate interfacial area per unit volume of static bed height ( $a_s$ ), per unit volume of expanded bed height ( $a$ ) and per unit volume of liquid hold up ( $a_L$ ) under different gas and liquid velocities.
- (ii) They were also intended to establish the liquid film transfer coefficient under the same conditions and to investigate the operational mass transfer efficiency,  $\eta_{op}$ , (defined as the ratio of volumetric liquid film transfer coefficient ( $k_L a$ ) to the fluid energy consumed in the bed) under corresponding gas and liquid rates.

## CHAPTER 2

### LITERATURE REVIEW

#### 2.1 Hydrodynamics of Turbulent Contact Absorber (TCA)

The hydrodynamics of turbulent contact absorbers have been studied by a number of investigators (2, 3, 8, 18-21). All of them have reported that at a given liquid rate, as the air velocity is increased three successive hydrodynamic states are observed, the static bed, the fluidized and the flooding bed states.

Douglas et al (1) reported that flooding occurs when the packing spheres start to congregate below the upper grids. There are two possible explanations for the occurrence of this condition. One is that the expanded bed height reaches the distance between the supporting grids so that a portion of spheres adhere to the upper grid. Another case is that the gas velocity has attained the terminal velocity of the wetted packing spheres, so that most of the packing is pushed up by the upward flow of gas and congregates below the upper grid. Therefore to avoid the problem of flooding either the bed static height should be short or the distance between the two grids should be large.

According to Kito et al (2) the expanded bed height,  $H$ , in a turbulent contact absorber can be estimated by

$$\frac{H}{H_s} = \frac{1 + \epsilon_L - \epsilon}{1 - \epsilon_g}$$

where

$$\epsilon_L = \frac{H_L}{H_s} \quad \epsilon_G = 0.41 V_g^{0.44}$$

Above the flooding point, the TCA acts like a fixed bed because of the congregation of the packings under the upper grid, the pressure drop is higher than that of TCA operated below the flooding point. They used the data obtained by Epstein et al (3) which is well above the flooding point and proposed the following correlation:

$$\Delta P_{hf} = 1.275 \times 10^{10} (\mu_L)^{2.3} (f)^{-0.42} (dp/D)^{-0.84} (dp)^{-0.84} (\rho_p)^{0.18} \times (H_s)^{3.52} (U_g)^{2.54} (U_L)^{6.16} \quad (2.1)$$

Equation (2.1) shows that the liquid hold up is a strong function of gas and liquid velocity when the TCA is operated above the flooding point.

Levesh et al (4) conducted empirical studies of a fluidized bed using rings of a material with a small specific weight as the packing. The bed height dependent on gas velocity ( $w$ ), the density of irrigation ( $V_L$ ) and the initial height of the bed.

The experimental data showed that the gas velocity has a power flux effect on the bed height which increases proportionally to the square of gas velocity, while changes in the wetting rate have relatively little effect on this parameter. They stated that the height of the fluidized bed could be given by,

$$H = 0.13 H_0 V_L^n w^2 \quad (2.2)$$

where  $n = 0.43$  for  $V_L < 28 \text{ m}^3/\text{m}^2 \text{ hr}$      $w < 2.5 \text{ m/s}$

$n = 0.35$  for  $V_L > 28 \text{ m}^3/\text{m}^2 \text{ hr}$      $w < 2.5 \text{ m/s}$

Fluidization of the packing produced in the apparatus used by Levesh et al (4) is a combination of fluidization of packing in the gas

streams and bubbling of the gas through the layer of liquid held up on the packing and supporting screen. The pressure drop of this bed was represented as

$$\Delta P = \Delta P_1 + \Delta P_2 + \Delta P_g \quad (2.3)$$

where  $\Delta P_1$  and  $\Delta P_2$  are the pressure drops of fluidization of the packing with gas and the bubbling of gas through the layer of liquid held in the column.

$\Delta P_g$  is the resistance due to the dry support screen.

$\Delta P_1$  is determined from the relationship

$$\Delta P_1 = \frac{G_p}{F}$$

$G_p$  is the packing weight,  $F$  is the cross sectional area of the column.

They suggest the following empirical equation for pressure drop of bubbling gas through the liquid in the bed,

$$\Delta P_2 = 0.155 V_L^{0.55} w \left[ \frac{H_o}{70} \right]^m \quad (2.4)$$

where  $m = 1$  for  $V_L = 28.8 - 61.5 \text{ m}^3/\text{m}^2 \text{ hr}$

$m = 0.75 - 0.8$  for  $V_L < 28.8 \text{ m}^3/\text{m}^2 \text{ hr}$

$m$ , increases with increasing irrigation rate and this is explained by the increase in the liquid hold up as a result of which the effect of  $H_o$  on  $\Delta P_2$  becomes greater.

The mean error in equation (2.4) is reported to be 8 - 12%.

Blyakher et al (5) assumed that the hydraulic resistance ( $\Delta P$ ) of an apparatus for a two phase system can be expressed as

$$\Delta P = \Delta P_d + \Delta P_L \quad (2.5)$$

where  $\Delta P_d$  and  $\Delta P_L$  are the hydraulic resistance corresponding to the dry apparatus and to the flow of the liquid phase respectively.

For a mobile packing, the hydraulic resistance of the dry column is composed of the packing ( $\Delta P_p$ ), and of the resistance of the grid ( $\Delta P_g$ ), while that corresponding to the flow of the liquid phase is made of the hydraulic resistance of the liquid froth layer and the grid ( $\Delta P_f$ ) and of the liquid inside the bed, ( $\Delta P_b$ ).

It can be written (6, 7)

$$\Delta P_g = \xi_g \frac{W^2 \gamma_g}{2 g} \quad (2.6)$$

where  $\xi_g$  is the hydraulic resistance coefficient for the grid and  $W$  is the gas velocity.  $\gamma_g$  is the density of gas and  $g$  is acceleration due to gravity.

They introduced the following relationship for pressure drop across the column:

$$\begin{aligned} \Delta P &= \Delta P_g + \Delta P_p + \Delta P_f + \Delta P_b \\ &= \xi_g \frac{W^2 \gamma_g}{2 g} + 6.13 (\gamma_p - \gamma_g) H_p + \xi_f W^{1.75} Q^{0.5} + \xi_b Q_L H_p \quad (2.7) \end{aligned}$$

where  $\gamma_p$  is density of packing,  $H_p$  is the static bed height,  $\xi_f$  is a coefficient which depends on the geometric characteristics of the grid

and  $Q_L$  is the liquid loading and  $\xi_b$  is a factor which depends on the characteristics of the grid and of the packing.

Blyakher et al (5) carried out some experiments to determine the effect of gas velocity and liquid flow rate on the height of bed (H), on a column of 350 mm diameter and a distributing grid which had an open flow area of ( $F_o = 41\%$ ), they found the following empirical relationship.

$$\frac{H}{H_p} = 1.17 + A (W - W_{cr})^{1.25} \quad (2.8)$$

where  $W$  is the air velocity.  $A$  is a coefficient which depends on the liquid loading. Values of  $W_{cr}$  depend on the properties of the packing and also upon the liquid loading.

They found for the packing density of  $180 \text{ kg/m}^3$

$$W_{cr} = W_{cr}^0 + \frac{W_{cr}^0 Q_L^{0.9}}{37.5 + Q_L^{0.9}} \quad (2.9)$$

where  $W_{cr}^0$  is the minimum fluidization velocity for dry packing.

Gelperin et al (8) found the point of transition to complete fluidization, the gas velocity in the system of water-air depends on the ratio of the liquid load to the gas load,  $V_l/V_g$ , the packing diameter ( $d_{sph}$ ) and the open cross section of the gratings ( $F_{op}$ ), but it is practically independent of slit width and relative density of the packing.

Analysis of their experimental data expressed the relation between these parameters and is given by an equation similar to that of Bain and Hogen for packed columns (9).

$$\frac{W_{cr}^2}{g d_{sph}} = 46 \times 10^3 \times F_{op}^{1.54} \exp\left[-12.6 \left(\frac{V_1}{V_g}\right)^{0.25}\right] \quad (2.10)$$

They expressed the pressure loss of the gas flow in the bed during complete fluidization as the combination of the resistances of the dry grid, ( $\Delta P_{fr}$ ) of the bed of the packing, ( $\Delta P_{sph}$ ) and finally of the pressure of liquid column supported by the bed  $\Delta P_1$ .

$$\Delta P_b = \Delta P_{fr} + \Delta P_{sph} + \Delta P_1 \quad (2.11)$$

$$\text{and } \Delta P_{fr} = \xi_{gr} \frac{\gamma_g}{2g} \left[ \frac{W_{go}}{1-\tau} \right]^2 \quad (2.12)$$

where  $\xi_{gr}$  is the coefficient of hydraulic resistance of the grid,

$W_{go}$  is the gas velocity referred to open cross section of dry grid

and  $\tau$  is the proportion of open cross section of grid occupied by liquid.

$$\Delta P_{sph} = \gamma_{sph} (1 - \epsilon_o) H_{st} \quad (2.13)$$

The mean static pressure of the liquid column supported by the bed is,

$$\Delta P_1 = \frac{h_L}{F} \gamma_1 \quad (2.14)$$

where

$h_L$  is the volume of liquid retained in the column.

$F$  is the cross sectional area of column.

$\gamma_1$  is the density of liquid.

According to Kuroda and Tabei (10) up to the moment when the packed particles begin to fluidize, their surface is covered with a

liquid film, rather like a trickling irrigated packed column. As the gas velocity is raised the thickness of the liquid film and the liquid hold-up both increase.

Two types of fluidization in TCA have been reported by O'Neill et al (11). Type I (TCA) and Type II (TCA). For type I (TCA) the packing is of very low density and the onset of fluidization occurs at a gas velocity below the flooding velocity for the equivalent counter current packed bed. For type II (TCA) the onset of fluidization for packing with a density higher than about  $300 \text{ kg m}^{-3}$  (for air-water systems) always occurs at the flooding point of the equivalent counter current packed bed. The true flooding point is reached when the packing is pushed up to the upper retaining grid, where they form a packed bed.

An estimation of the onset of the true flooding point for type I (TCA) from the flooding chart for the packed bed was shown to be possible by Uchida et al (12). The chart developed by Lobo and Sherwood (13) et al was used. Uchida et al (12) considered the TCA as a kind of fixed bed with an enlarged voidage.

The effect of the open area and geometry of the grid on the flooding condition was highlighted by Gelperin et al (8) who proposed an empirical correlation equation to estimate the flooding condition of the TCA with grid openings of 25 to 70%. The height of the unexpanded bed considerably affects the mode of fluidization. The beds with static bed height shorter than the column diameter fluidize uniformly, while slugging is commonly observed in deep beds (14). A flow regime map for a TCA using 13 to 19 mm packing was presented by Barile et al (15) who showed that the stable operation regime narrows with increasing static bed heights.

Wozniak (16) gave a steady-state macroscopic force balance for the TCA.

$$\Delta P_c = (\rho_s \epsilon_s + \rho_L \epsilon_l + \rho_g \epsilon_g) gH + F_g \quad (2.15)$$

The effect of supporting grid geometry on pressure drop across the grid ( $\Delta P_g$ ) observed by Blyakher (5), Gelperin (8), Levesh (4) and Mayak and Martrozov (17). Tichy et al (18) found that  $\Delta P_g$  was negligible for a grid opening of 83%.

Several authors have reported experimental data on the pressure drop and macroscopic models to correlate the pressure drop in TCA.

Table (2.1) summarizes the correlations for pressure drop in the TCA which are either purely empirical or developed on the basis of equation (2.15). It can be seen that the liquid hold up needs to be correlated in order to be able to estimate the pressure drop.

Vunjak-Novakovic et al (19) reported two operating regimes in TCA, the fluidization before flooding (type I) and fluidization at the flooding point of a fixed bed (type II). The change over from fixed bed to fluidized bed operation was explained and the corresponding hydrodynamic characteristics of the two modes of contacting were related. The first attempt in this direction was made by O'Neill et al (11) and the flooding sets an upper limit to counter current operation in a bed of fixed packing. In a bed of low density packing the bed pressure drop reaches the weight of both the packing and the liquid hold up.

$$(\Delta P)_{\text{fixed bed}} = \rho_p g H_o (1 - \epsilon_o) + \rho_L H_o \epsilon_L g \quad (2.16)$$

Table 2.1 Correlation Equations for Pressure Drop in a Single-Stage TCA.

Investigators	$f$	$\rho_s$ [kg/m <sup>3</sup> ]	$D_c/dp$	Correlation Equations*
Blvaker et al. (1967)	0.41	90, 180	9.2	$\Delta P_c = \xi_R \frac{U^2 \rho_R}{2} + (1 - \epsilon_0)(\rho_s - \rho_R) g H_0 + \xi_f U^2 U_l^{0.75} + \xi_b U_l H_0$ $\xi_R, \xi_f$ and $\xi_b$ are constants
Gel'perin et al. (1968b)	0.345 ~ 0.70	160 ~ 900	1.7 ~ 61.7	$\Delta P_c = \xi_R \frac{U^2 \rho_R}{2(1 - \tau')} + (1 - \epsilon_0) \rho_s g H_0 + 0.138 U_l^{0.75} H_0^{0.75} d_p^{-0.6} \rho_l g + F_a$
Levsh et al.** (1968a)				$\Delta P_c = \frac{W_g}{S} + 14.0 U_l^{0.55} U_R (14.29 H_0)^m + F_a + F_R$
Tichy et al. (1972)	0.78	155	11.4 ~ 7.5	$\log \left( \frac{2 \rho_R \Delta P_c D_c}{G_R^2 H_0} \frac{1}{1 + CG_d} \right) = 4.003 - 2.240 C_R + 0.840 C_R^2 - 0.127 C_R^3$ $C$ is a constant which depends on $H_0/D_c$
Uchida et al. (1977)				$\Delta P_c = (1 - \epsilon_0) \rho_s g H_0 + 9.38 \times 10^8 \mu_l^{-0.42} \left( \frac{D}{D} \right)^{-0.84} d_p^{-0.84} \rho_s^{0.18} H_0 U_l + 788 U_R^{0.91} U_l^{2.7}$
Wosniak (1977)	0.6	266	10.2	$\frac{(\Delta P_c - W_g/S)}{\rho_R U_R^2} = 4.672 \times 10^5 \left( \frac{H_0}{D_c} \right)^{0.4515} \left( \frac{d_p U_l \rho_l}{\mu_R} \right)^{-1.798} \left( \frac{d_p U_l \rho_l}{\mu_l} \right)^{0.8261}$
Barile and Meyer (1971)	0.82	109, 160	7.5, 15	
Kito et al. (1976c)	0.71 ~ 0.84	170 ~ 1,250	3.6 ~ 10.3	$\frac{\Delta P_c}{g} = (1 - \epsilon_0) \rho_s H_0 + a_{Lst} \rho_l H_0$ Correlation equations for $a_{Lst}$ are given in Table 7.
Vunjak-Novakovic et al. (1980)	0.36, 0.52 and 0.78	200, 400 and 700	3.6 ~ 29	

\* Use SI units for variables involved in the equations.

\*\* Special type of packing (plastic ring) was used.

According to Vunjak-Novakovic et al (19) before the flooding point for ( $\rho_p = 156 \text{ kg/m}^3$ ) with further increase in the gas flow rate, the bed expands but the value of bed pressure drop and liquid hold up remains constant and equal to those in a fixed bed at minimum fluidization velocity. A packed bed with heavier packing ( $\rho_p = 380$  and  $680 \text{ kg/m}^3$ ) cannot fluidize before the flooding point is reached. The pressure drop is insufficient to support the packing and the liquid hold up. The sufficient increase in liquid hold up which causes the flooding of a fixed bed reaches an advanced stage. An increase in  $\rho_p$  requires the corresponding advance in flooding, i.e. the increase in the liquid hold up.

Vunjak-Novakovic et al (20) reported that for a given packing diameter and given liquid flow rate, there is a limiting packing density. The boundary between two modes of contacting is located at the flooding point. They gave the following equation:

$$\left[ \frac{\Delta P}{H_o} \right]_{\text{at flooding}} = \rho_p g (1 - \epsilon_o) + \rho_l g \epsilon_{1,op} \quad (2.17)$$

where  $\epsilon_{1,op}$  is the operating liquid hold up.

They also suggested that the pressure drop can be calculated by the following equations:

$$\Delta P = \rho_p g H_o (1 - \epsilon_o) + \epsilon_1 H_o \rho_l g \quad (2.18)$$

$$\frac{H}{H_o} = (1 + \epsilon_1 + \epsilon_o) / 1 - \epsilon_g \quad (2.19)$$

where  $\epsilon_g = 0.628 U_g^{0.237}$  and  $\epsilon_1$  is defined by equations (2.30) and (2.31), for type I and type II fluidization respectively.

For type (I) fluidization minimum fluidization velocity is given by

$$\frac{U_{mf}}{(\epsilon_g)_{mf}} = 1.59 (U_m)_{fd}^{0.763} \quad (2.20)$$

for type II

$$(U_m)_{fd} = 0.545 \left[ \frac{U_{mf}}{\epsilon_o - h_L} \right]^{1.31} \quad (2.21)$$

Chen and Douglas (21) reported that minimum fluidization velocity decreases with increasing liquid rate, but increases as the packing diameter is increased. On the basis of the experimental results they proposed the following empirical equation, for the minimum fluidization velocity

$$G_{mf} = 229 (d_p)^{1.15} (10)^\gamma (V_L)^{\gamma} \quad (2.22)$$

with  $\gamma = -5.17 \times 10^{-5}$ .

Kito et al (22) found that the minimum fluidization velocity decreases as the packing size and density decreases and the liquid rate increases but static bed height seems to have little effect. From analysis of the experimental results they gave the following correlation equation:

$$\frac{U_{mf}}{(U_{mf})_{V_L=0}} = 3.14 \left[ f \frac{d}{D} \right]^{0.46} V_L^{-0.58} \quad (2.23)$$

for  $\left[ f \frac{d}{D} \right] \leq 0.05$

$$\text{and } \frac{U_{mf}}{(U_{mf})_{V_L=0}} = 0.78 V_L^{-0.36} \quad (2.24)$$

$$\text{for } \left[ f \frac{d}{D} \right] > 0.05$$

where  $(U_{mf})_{V_L=0}$  is the minimum fluidization velocity at zero liquid rate.

Douglas et al (18), Gelperin et al (23) and Rao et al (24) reported that in some of the experiments with the ratio of packing to column diameter less than 10, there was occasional wall effect present and the notion of packing near the wall was constrained. In cases where the wall effect was significant the packing congregated at the wall and a quasi-static layer of packing was built at the wall. This caused the effective bed height to be lowered and the pressure drop was also lowered.

Douglas et al (18) observed that the wall effect is increased by increasing the liquid rate. Chen and Douglas (21), Uchida et al (3) and Kito et al (2) found that the liquid hold up increases as the liquid rate increases and packing diameter decreases, but it is not significantly affected by the air velocity. Kito et al (2) proposed the following correlation equation for liquid hold up.

$$H_L = 12.8 (H_{st})^{0.6} (D_p)^{-0.84} (\rho_p)^{0.18} \left[ f \frac{d}{D} \right]^{-0.58} (V_L)^{0.64} (\mu_L)^{0.16} (\sigma)^{0.34} \quad (2.25)$$

Kito et al (2) expressed the expanded bed height as,

$$\frac{H}{H_s} = \frac{1 + \epsilon_{SL} - \epsilon_{sp}}{1 - \epsilon_g} \quad (2.26)$$

$$\epsilon_L = H_L/H_s)/(H_s/H) = \epsilon_{sL}/(H/H_s) \quad (2.26a)$$

From equations (2.26) and (2.26a),  $\epsilon_L$  can be represented as

$$\epsilon_L = \frac{\epsilon_{sL} (1 - \epsilon_g)}{1 + \epsilon_{sL} - \epsilon_{sp}} \quad (2.27)$$

Empirical correlations of hold up in fixed beds were presented by a number of investigators. Leva's correlation (25) for the air-water system is in the form

$$h_o \propto \left[ \frac{V_L}{d_p} \right]^{0.6}$$

Chen and Douglas (21) produced a general correlation for the range of variables investigated as follows,

$$h_t = 2.83 \times 10^{-4} (V_L)^{0.6} (d_p)^{-0.5} + 0.02 \quad (2.28)$$

They reported that bed height increases with increasing gas velocity and also increases with increasing liquid velocity. The reduced bed height  $H/H_o$  is independent of both the bed static height and the packing density for low density packing.

The reduced bed height can be calculated from a simultaneous volume balance in the liquid and solid phases,

$$\frac{H}{H_o} = \frac{1 - \epsilon_o + \epsilon_{l.st}}{1 - \epsilon_g}$$

Table (2.2) summarises correlation equations for bed expansion in a TCA.

A small fractional open area in the supporting grid strongly affects the bed expansion since a liquid layer builds up immediately

Table 2.2 Correlation Equations for Liquid and Gas Holdups in a TCA.

Investigators	$f$	$\rho_s$ [kg/m <sup>3</sup> ]	$D_c/d_p$	Correlation Equations*
Chen and Douglas (1968)	0.80	156 ~ 170	8 ~ 24	$\epsilon_l = 0.02 + 2.371 \times 10^{-3} G_i^0 d_p^{-0.5}$
Gel'perin et al. (1968b)		See Table 5		$\epsilon_{l,st} = 0.138 U_i^{0.5} H_0^{-0.25} d_p^{-0.6}$ $\epsilon_g = 0.93 \left( \frac{d_p U_g \rho_g}{\mu_g} \right)^{0.4} \left[ \frac{d_p^3 (\rho_s - \rho_g) \rho_g g}{\mu_g^2} \right]^{-0.2}$
Barile and Meyer (1971)		See Table 5		$\epsilon_{l,st} = 1,160 \left( \frac{G_i^2}{d_p g \rho_l^2} \right)^{0.78} \left( \frac{d_p C_i}{\mu_l} \right)^{-0.51} \left( \frac{H_0}{d_p} \right)^{-0.36}$
Kito et al. (1976a,b)**	0.0127 ~ 0.315	300 ~ 1,100	1.89 ~ 9.09	$\frac{\epsilon_g}{ \epsilon_g(1 - \epsilon_g)^2 ^{0.44}} = 0.5 \left( \frac{D_c U_g^2 \rho_l}{\sigma} \right)^{0.11} \left( \frac{U_g}{\sqrt{g d_p}} \right)^{0.22}$
Kito et al. (1976c)		See Table 5		$\epsilon_{l,st} = 0.06 + 3.018 \times 10^{-3} \left( \frac{d}{D} \right)^{-0.84} d_p^{-0.84} \rho_s^{0.18} H_0^{0.4} U_l$ $\epsilon_g = 0.417 U_g^{0.44}$
Kito et al. (1978)		Same as those of Kito et al. (1976c)		$\epsilon_{l,st} = 12.8 \left( \frac{H_0}{d_p} \right)^{-0.4} \left( \frac{d}{D} \right)^{-0.58} \left( \frac{g d_p^3 \rho_l^2}{\mu_l^2} \right)^{0.09} \left( \frac{U_l}{\sqrt{g d_p}} \right)^{1.66} \left( \frac{d_p U_l \rho_l}{\mu_l} \right)^{-0.31} \left( \frac{d_p U_l^2 \rho_l}{\sigma} \right)^{-0.31}$ $\epsilon_g = 0.19 \left( \frac{d_p U_g^2 \rho_l}{\sigma} \right)^{0.11} \left( \frac{U_g}{\sqrt{g d_p}} \right)^{0.22}$
Uysal (1978)		See Table 6		$\epsilon_{l,st} = 1.15 \times 10^{-4} G_i^{0.825} d_p^{-1.289}$
Vunjak-Novakovic et al. (1980)		See Table 5		$\epsilon_{l,st} = 6.4848 Re_l^{-0.1387} Fr_l^{0.4287} \left( \frac{H_0}{D_c} \right)^{-0.5672} + 0.02$ (Type I TCA) $\epsilon_{l,st} = 7.326 Re_l^{-0.0591} Fr_l^{0.4354} \left( \frac{H_0}{D_c} \right)^{0.4328} \left( \frac{\rho_s}{\rho_l} \right)^{0.0684} + 0.02$ (Type II TCA) $\epsilon_g = 0.628 U_g^{0.237}$

\* Use SI units for variables involved in the equations.

\*\* Stagnant liquid system.

above the grid. This behaviour of such beds may resemble that of a bubble column or a sieve tray. A number of correlations for the liquid hold up have been given in Table (2.3).

Gelperin et al (8) defined two liquid hold ups, the liquid hold up in the region near the grid and in the fluidized bed. They presented an empirical correlation for the latter, showing that the liquid hold up is affected by the static bed height.

Barile and Meyer (14) carried out dimensional analysis, considering the variables  $h_t$ ,  $V_L$ ,  $\Delta p$ ,  $H_o$ ,  $\rho_L$ ,  $\mu_L$  and  $g$ . Liquid hold up ( $h_t$ ) was related to the  $Re$ ,  $Fr$  and  $H_o/D_p$ . They performed a least squares regression analysis with data measured in their work at minimum fluidization velocity which yielded the correlation,

$$h_{to} = 1160 Fr^{0.78} Re^{-0.51} \left[ \frac{H_o}{D_p} \right]^{-0.36} \quad (2.29)$$

In terms of dimensioned variables the hold up is,

$$h_t \propto V_L^{1.06} D_p^{-0.93} H_o^{0.36}$$

Novakovic and Vukovic (20) expressed the total liquid hold up as a liquid volume fraction of the static bed volume and reported that up to the loading point, the total liquid hold up in a packed bed of spherical packing is independent of gas flow rate and for type I fluidization it is given by,

$$h_L = 6.49 Re_L^{-0.139} Fr_L^{0.429} \left[ \frac{H_o}{D_c} \right]^{-0.567} + 0.02 \quad (2.30)$$

Liquid hold up for type II operation is given by,

$$h_L = 7.33 \text{ Re}_L^{-0.059} \text{ Fr}_L^{0.435} \left[ \frac{H_o}{D_c} \right]^{-0.433} \left[ \frac{\rho_p}{\rho_L} \right]^{0.09} + 0.02 \quad (2.31)$$

According to Novakovic and Vukovic (20) when the particle density exceeds about 300 kg/m<sup>3</sup>, type I operation is impossible and for particle densities above about 1300 kg/m<sup>3</sup>, only packed bed operation is possible.

## 2.2 Mass Transfer Characteristics of TCA

Gelperin et al (26) absorbed CO<sub>2</sub> into NaOH and investigated interfacial area in a turbulent contact absorber by neglecting the gas phase resistance which contributes up to a maximum of 10 percent of the total resistance. A column of 14.5 cm inner diameter with polyethylene spheres of 1.55 cm diameter with a density of 470 kg/m<sup>3</sup> was used. The liquid rate was varied from 20 to 60 m<sup>3</sup>/m<sup>2</sup> hr and the air velocity from 1.5 to 4 m/s, the bed static height was also changed between 4.5 to 18 cm. They introduced a term phase contact area, A<sub>f</sub>, which consists of the contact surface in the bed (A<sub>bed</sub>) plus the contact surface in the separation space (A<sub>s</sub>). The unit phase contact surface in the separation space was determined on the basis of the total phase contact surface, A<sub>f</sub>, with different heights of the bed.

$$a_s = \frac{A_{f1} - A_{f2}}{H_1 - H_2} = \frac{\Delta A_f}{\Delta H} \quad (2.2.1)$$

H<sub>1</sub> and H<sub>2</sub> are the heights of column sections, A<sub>f1</sub> and A<sub>f2</sub> are the corresponding total phase contact surfaces in the section.

Equation (2.2.1) was used to evaluate a<sub>s</sub> and A<sub>s</sub> was related to a<sub>s</sub> by the following relationship.

$$A_s = a_s (H - H_{dyn})$$

where  $H_{\text{dyn}}$  is the dynamic bed height.

From the analysis of experimental results, Gelperin et al (26) proposed

$$a_s = 7.4 V_L^{0.35} W^{0.31} \quad (2.2.2)$$

They also considered the effect of gas and liquid velocities and grid open areas on  $A_{\text{bed}}$ . The correlation of experimental data yielded the relation:

$$A_{\text{bed}} = A_b \left[ \frac{1.685 \times 10^5 F_{\text{op}}^{1.1}}{A_b^{1.55} W^{0.29}} \right]^{H_{\text{st}}} \quad (2.2.3)$$

where  $A_b = 1.6 V_L^{0.44} W_o^{0.92}$  and is the contact area in the bubbling bed in the absence of packing and  $W_o = W/F_{\text{op}}$  is the gas velocity calculated on the basis of the open area of the grid ( $F_{\text{op}}$ ).

The experimental data indicated that the static bed height ( $H_{\text{st}}$ ) has a substantial effect on the value of the phase contact surface  $A_{\text{bed}}$ . Kito et al (27) investigated the effect of gas flow rate, the distributing plate open ratio, the static bed height, the column diameter, the packing diameter and density on the interfacial area by absorbing  $\text{CO}_2$  into an aqueous solution of sodium hydroxide. They measured the interfacial area based on the unit liquid volume ( $a_L$ ) and the interfacial area per unit column volume was calculated from

$$a = a_L \epsilon_L$$

where  $\epsilon_L$  is the fractional liquid hold-up per unit volume of bed. It was found that both  $a$  and  $a_L$  increases with gas velocity but ( $a$ ) starts to decrease when the gas velocity exceeds 2 m/s.

The interfacial area ( $a$  and  $a_L$ ) was shown to be independent of the column diameter and ( $a$ ) was not affected by particle size in the range of 1.1 - 2.85 cm or particle density in the range of 0.59 - 1 gr/cm<sup>3</sup>.

Wozniak (28) measured the interfacial area of a mobile packing of polypropylene spheres with 1.96 cm diameter and density 266 kg/m<sup>3</sup>. The column diameter was 20 cm having a supporting grid of 60% open area and the static bed height was varied from 20 - 40 cm. By absorbing CO<sub>2</sub> into NaOH he found that the interfacial area per unit area of bed static height increases with both gas and liquid rates.

The gas velocity was varied between 1.7 - 3.0 m/s and liquid velocity between 0.009 - 0.028 m/s. Within the range of experimental condition the interfacial area per unit volume of bed static height ranged between 100 to 1000 m<sup>2</sup>/m<sup>3</sup>. Wozniak (28) modified the correlation developed by Colar (29) on a sieve plate and introduced the dimensionless effective interfacial area and suggested the following empirical equation:

$$A = 6.189 \times 10^{-7} \left[ \frac{\epsilon_g}{1-\epsilon_g} \right]^{0.8022} \left[ \frac{h\Delta P}{U_g \mu_g} \right]^{0.9337} \quad (2.2.4)$$

The experimental data obtained in the following dimensionless number ranges

$$10 \leq \frac{h_{st}}{d_p} \leq 21, \quad 2200 \leq Re_g \leq 4100, \quad 100 \leq Re_L \leq 520$$

were,

$$A = \frac{a_{st}}{a_b}$$

$a_{st}$  = Interfacial area per unit volume of bed static height.

$a_b$  = Geometric surface area of packing per unit volume of bed static height.

$h_{st}$  = Bed static height.

$h$  = Dynamic bed height.

$d_p$  = Packing diameter.

Wozniak and Ostergaard (30) determined the interfacial area of polypropylene sphere packing of density  $388 \text{ kg/m}^3$  and of  $0.97 \text{ cm}$  diameter in a column of  $10 \text{ cm}$  diameter.

The effect of liquid velocity on the interfacial area was studied and it was varied from  $0.02$  to  $0.07 \text{ m/s}$  at a constant gas velocity of  $0.7 \text{ m/s}$ .

Dilute  $\text{CO}_2$  was absorbed into sodium hydroxide solutions of  $0.15$  -  $1.5 \text{ gmol/lit}$ . This system was considered to be liquid film controlled as the maximum gas film resistance amounted to  $10\%$  of the total resistance.

They found that the overall volumetric mass transfer coefficient,  $K_G a$  increases with both liquid rate and sodium hydroxide concentration. This is in agreement with other workers' findings (31, 32).

Wozniak and Ostergaard (30) showed that interfacial area per unit volume of bed static height ( $a_{st}$ ) increases with liquid velocity. These values amounting to  $15$  to  $16 \text{ cm}^2/\text{cm}^3$ . If they are calculated per unit volume of the dynamic bed height they would drop to  $1.2$  to  $3 \text{ cm}^2/\text{cm}^3$ .

Palaty (33) investigated the interfacial area in TCA in a column of 5.8 cm diameter and supporting grid with open area of 65.5% free area, the packing was polystyrene balls of 0.6 cm diameter and 1000 kg/m<sup>3</sup> density. The reaction system was CO<sub>2</sub> - NaOH with CO<sub>2</sub> and NaOH concentration of 3% by volume and 3.0 N respectively. Gas film resistance was considered to be negligible, the effects of the superficial gas and liquid velocities and bed static height on the interfacial area per unit volume of expanded bed was investigated. The gas velocity was varied from 1.0 to 3.0 m/s, and three different liquid velocities of 5.36 x 10<sup>-3</sup>, 8.93 x 10<sup>-3</sup> and 12.5 x 10<sup>-3</sup> m/s was used.

The bed static heights were 2.1, 3.2 and 4.7 cm. Palaty reported that the interfacial area per unit volume of expanded bed height increases with both gas and liquid velocities and that it also increases as the bed static height increases. The interfacial area was reported to vary from 0.82 to 1.45 cm<sup>-1</sup>. On the basis of experimental data the following empirical equation was suggested:

$$a = 2.34 \times 10^2 U_g^{0.35} U_l^{0.11} h_{st}^{0.12} \quad (2.2.5)$$

Tabei et al (34) studied the effect of gas and liquid rates on the interfacial area in a mobile bed absorber which consisted of a column of 10 cm diameter and supporting grid of 0.817 fraction open area.

The packing diameter was 1.95 cm and density 170 kg/m<sup>3</sup>. The liquid rate varied between 0.01 to 0.025 m/s at a constant air velocity of 2.0 m/s whilst the air rate was changed from 1.4 to 2.6 m/s at constant liquid velocity of 0.02 m/s. Carbon dioxide was absorbed into sodium hydroxide solution with concentrations ranging from 2% - 5% by volume and 0.01 to 0.3 kmol/m<sup>3</sup> respectively. They found that the interfacial area per unit volume of expanded bed increases with gas

velocity and passes through a maximum at a gas velocity of 2 to 2.5 m/s and consequently decreased beyond a bed expansion ratio  $H_{dy}/H_{st}$  of about 3.0.

From analysis of the experimental data, Tabei et al (34) proposed the following relationship for interfacial area:

$$a = 2100 \epsilon_g^{1.25} \epsilon_L^{0.75} \quad (\text{m}^{-1}) \quad (2.2.6)$$

Kossev et al (35) determined the interfacial area in a turbulent contact absorber with a column diameter of 19 cm and with a plastic packing of 1.8 cm diameter and 167 kg/m<sup>3</sup> density by absorbing CO<sub>2</sub> into NaOH solution. It was found that the interfacial area depends greatly on the hydrodynamic conditions and varies between 156 to 256 m<sup>2</sup>/m<sup>3</sup>. These values are higher than the areas obtained in froth on the bubble cap plates and is lower that of dispersions on sieve tray columns. It was also found that increasing the gas and the liquid velocities up to certain limits (gas velocity of 3 m/s and liquid velocity of 0.022 m/s) causes the interfacial area per unit volume of bed to increase. However beyond these velocities the interfacial area tends to decrease. In the second part of their investigation regarding the mass transfer performance of mobile beds, Kossev and Elenkov (36) investigated the effect of the supporting grid open area, packing density and the liquid and gas rates on the liquid side mass transfer coefficient by desorbing oxygen from water. In this study the gas velocity was varied between 1.2 to 6.4 m/s and liquid rate from  $5.6 \times 10^{-3}$  to  $2.4 \times 10^{-2}$  m<sup>3</sup>/m<sup>2</sup>s.

Three types of grids having 41.7, 60 and 79 percent free areas were used. The packings used were of hollow polystyrene spheres, 18 mm diameter and density 167 kg/m<sup>3</sup>, and of solid polystyrene spheres with 17 mm diameter and density of 930 kg/m<sup>3</sup>.

They reported that in the case of hollow spheres, having a bed static height of 20 cm with a grid open area of 42 percent, the liquid film transfer coefficient increases with the liquid rate up to about 80 m<sup>3</sup>/m<sup>2</sup>h, after this point, however, it decreases. At a given liquid rate, the liquid film transfer coefficient increases with gas velocity and decreasing grid open area. Similar behaviour was observed when a grid of 49 percent open area was used. Kossev and Elenkov (36) carried out some experiments using solid spheres with a static height of 17 cm and a grid of 79 percent open area and found that the variation of liquid film transfer coefficient with gas, liquid velocities and grid open area is similar to the case of hollow spheres.

On the basis of experimental data they proposed the following empirical equation:

$$k_L A = 0.024 \frac{D_1}{h_p} R_{eL}^{0.1} R_{eg}^{1.5} SC_L^{0.5} \quad (2.2.7)$$

$$\text{where } h_p = \frac{\Delta P - \Delta P_{\text{grid}}}{\rho_1}$$

$\Delta P$  = pressure drop of mobile bed.

$\Delta P_{\text{grid}}$  = pressure drop of grid.

It was reported that on average the liquid film transfer coefficient is about 1.5 to 2 times greater than the corresponding values in the conventional plate columns.

Strumillo and Kudra (37) measured the interfacial area in a TCA with a column diameter of 8.5 cm and a supporting grid of 65 percent open area by using CO<sub>2</sub> - NaOH reaction and applied the Danckwerts' plot

as in the work of W. Pasiuk-Bronikowska (38), who measured interfacial area and liquid film transfer coefficient in a sieve plate.

The CO<sub>2</sub> and NaOH concentrations in Strumillo and Kudra's (37) work was 3% by volume and 2 to 3 N respectively. Gas film resistance was found to be negligible since its contribution to total resistance was only 3%. The packing density was 1050 kg/m<sup>3</sup> with different diameters of 5, 7.5 and 10 mm. Bed static heights of 20 to 160 mm whilst liquid and air rates ranges of 33 to 110 m<sup>3</sup>/m<sup>2</sup> h and 0.5 to 3.5 m/s were used respectively.

They found that the total interfacial area ranges from 0.17 x 10<sup>4</sup> to 0.51 x 10<sup>4</sup> cm<sup>2</sup> and the surface renewal rate was about 1 x 10<sup>3</sup> s<sup>-1</sup> (k<sub>L</sub> = 0.12 m/s).

It was reported that an increase in gas velocity and bed static height up to certain values (about 3 m/s and 120 mm respectively) leads to an increase in the total interfacial area. At higher values of these parameters the total interfacial area decreases. It has been stated that in this range of gas velocity and bed static height, the homogeneity of the bed was increasingly disturbed.

Strumillo and Kudra (38) correlated their experimental results for conditions where  $U_g \leq 3$  m/s and  $H_{st} \leq 120$  mm by the following equation:

$$A = 2.15 U_g^{0.92} V_L^{0.34} H_{st}^{0.93} d_w^{-0.94} \quad \text{m}^2/\text{m}^2. \quad (2.2.8)$$

## CHAPTER 3

### MASS TRANSFER THEORIES

#### 3.1 The Diffusion Process

The transfer of heat by conduction is due to random molecular motions and is described by the mathematical equation of heat conduction derived by Fourier (40). By analogy with diffusional heat transfer, Fick (39) found the rate of transfer of diffusing substance through unit area of cross section is proportional to the concentration gradient measured normal to the section, i.e.

$$F_A = - D_A \frac{\partial C_A}{\partial x} \quad (3.1)$$

where  $\partial C_A / \partial x$  is the concentration gradient at  $x$  at the given moment and  $D_A$  is the diffusion coefficient of the solute whose concentration is  $C_A$ .

In general, the concentration varies with time as well as with position. The partial differential equation relating concentration, time, and position is established as follows. Considering an element of differential thickness,  $dx$ , and of unit cross-sectional area, disposed perpendicular to the  $x$  axis (Fig. 3.1). The concentration gradient at  $x$  (AB) is  $\partial C_A / \partial x$ . The concentration gradient at  $(x + dx)$  (CD) is:

$$\left[ \frac{\partial C_A}{\partial x} + dx \frac{\partial^2 C_A}{\partial x^2} \right].$$

Thus, diffusant is diffusing into the element at the rate

$$- D_A \frac{\partial C_A}{\partial x}, \text{ and out at the rate } - D_A \left[ \frac{\partial C_A}{\partial x} + dx \frac{\partial^2 C_A}{\partial x^2} \right],$$

the rate of accumulation is the rate of increase of concentration in the element, multiplied by its volume, i.e.

$$dx \frac{\partial C_A}{t} . \text{ Thus}$$

$$\text{diffusion in} - \text{diffusion out} = \text{accumulation}$$

or

$$- D_A \frac{\partial C_A}{x} + D_A \left[ \frac{\partial C_A}{\partial x} + dx \frac{\partial^2 C_A}{\partial x^2} \right] = dx \frac{\partial C_A}{\partial t} \quad (3.2)$$

whence

$$D_A \frac{\partial^2 C_A}{\partial x^2} = \frac{\partial C_A}{\partial t} \quad (3.3)$$

This is the basic equation which is used to describe the diffusion process, in the absence of chemical reactions.

### 3.2 Physical Absorption

The theory of gas absorption processes has been reviewed by Danckwerts (41) and Astarita (42). The physical absorption of a gas into a liquid phase takes place in three steps.

1. Diffusion of the gas towards the liquid surface.
2. Dissolution of the diffusing gas in the liquid phase.
3. Transport of dissolved gas from the surface of the liquid phase to the bulk of the liquid.

The surface of the liquid first comes into contact with the gas at time  $t = 0$  and it is assumed that from then on the concentration in the plane of the surface is uniformly equal to  $C_{Ai}$ .

This concentration corresponds to the solubility of the gas at the partial pressure prevailing above the surface of the liquid and is then assumed to be constant. It is also assumed that the diffusion of dissolved gas into the liquid does not appreciably affect the temperature or other physical properties of the liquid. Under these circumstances, the variation in time and space of the concentration ( $c$ ) of dissolved gas in the liquid in the absence of reaction, (i.e. physical absorption) is given by the diffusion equation

$$D_A \frac{\partial^2 C_A}{\partial x^2} = \frac{\partial C_A}{\partial t}$$

and the rate of transfer of dissolved gas across unit area of any plane parallel to the surface is

$$R_x = - D_A \frac{\partial C_A}{\partial x} \tag{3.4}$$

Here,  $x$  is the distance measured from the surface, where  $x = 0$  and  $D_A$  is the diffusivity of the dissolved gas. Thus the rate of absorption of gas at any time is,

$$R = - D_A \left[ \frac{\partial C_A}{\partial x} \right]_{x=0} \tag{3.5}$$

### 3.2.1 Models of absorption

#### 3.2.1.1 The film model (Whitman's model) (43)

This model owes a good deal to Nernst's (44) (1904) idea of a 'diffusion layer', and to the simplified models of heat transfer from a solid surface to a moving fluid. It pictures a stagnant film of thickness,  $x$ , at the surface of liquid next to the gas. The diffusion of solute molecules in a liquid is brought about by the random thermal motion of the molecules so that there is a net transport from regions of higher concentration to regions of lower concentration. The concentration in the film falls from  $C_{Ai}$  at its surface to  $C_{Ao}$  at its inner edge, there is no convection in the film, while the rest of the liquid is kept uniform in composition by agitation.

By integrating the differential equation for steady state diffusion, i.e. equation (3.4) and applying the pertinent boundary conditions, the average absorption rate per unit surface area ( $R$ ) is given by

$$R = (C_{Ai} - C_{Ao}) \frac{D_A}{x_L} \quad (3.6)$$

where  $K_L = \frac{D_A}{x_L}$ .

The hydrodynamic properties of the system are accounted for by the parameter  $x_L$  (the film thickness), which depends on the geometry, liquid agitation, physical properties.

Predictions based on the film model are usually similar to those based on more sophisticated models, and indeed sometimes identical.

### 3.2.1.2 Penetration theory (Higbie's model) (45)

This model takes as its basis the replacement at intervals of elements of liquid at the surface by liquid from the interior which has the local mean bulk composition. While the element of liquid is at the surface and is exposed to the gas, it absorbs gas as though it were quiescent and infinitely deep, the rate of absorption is a function of time of exposure of the element. In general, the rate of absorption is rapid or infinite initially, and decreases with time.

The replacement of liquid at the surface by fresh liquid of the bulk composition might be brought about by turbulent motion of the body of the liquid. It is assumed that every element of surface is exposed to the gas for the same length of time,  $\theta$ , before being replaced by liquid of bulk composition. Finally it is assumed that the exposure time is too short and the depth of penetration after this time is much less than the depth of the element itself, so that the steady state diffusion cannot be established. During the exposure time the element of liquid absorbs the same amount of gas per unit area as though it were stagnant and infinitely deep.

The average rate of absorption is therefore  $Q/\theta$ , and this is also the rate of absorption ( $\bar{R}$ ) per unit area averaged over the interface in a representative region of a steady state absorption system in which the bulk composition is statistically uniform.

The exposure time,  $\theta$ , is determined by the hydrodynamic properties of the system and is the only parameter required to account for their effect on the transfer coefficient,  $k_L$ , and

$$Q = \int_0^t R \, dt .$$

The differential equation for the transient-diffusion process within each element and the boundary conditions is:

$$\frac{\partial C_A}{\partial t} = D_A \frac{\partial^2 C_A}{\partial x^2} \quad (3.7)$$

Boundary conditions are

$$t = 0 \quad C_A = C_{A0} \quad (3.8)$$

$$x = 0 \quad C_A = C_{Ai} \quad (3.9)$$

$$x \longrightarrow \infty \quad C_A \longrightarrow C_{A0}$$

The average absorption rate during the exposure time  $\theta$  of an element is given by

$$\bar{R} = \frac{1}{\theta} \int_0^\theta R \, dt \quad (3.10)$$

where  $R$  is the instantaneous absorption rate into an element, which is obtained by integrating the differential equation (3.7) and applying the above boundary conditions to give the following result.

$$\begin{aligned} R &= - D_A \left. \frac{\partial C_A}{\partial x} \right|_{x=0} \\ &= (C_{Ai} - C_{A0}) \sqrt{\frac{D_A}{\pi t}} \end{aligned} \quad (3.11)$$

and integration of equation (3.10) gives the average rate of absorption

$$\bar{R} = (C_{Ai} - C_{Ao}) \left[ 2 \sqrt{\frac{D_A}{\pi\theta}} \right] \quad (3.12)$$

comparing this with equation (3.6), which is obtained by film theory, it can be seen that

$$k_L = 2 \sqrt{\frac{D_A}{\pi\theta}}$$

### 3.2.1.3 Surface-renewal theory (Danckwerts' model) (46)

Danckwerts' model is a version of the penetration theory in which volumes or elements of interfacial region are constantly exchanged with new elements of liquid from the bulk region. This idea of replacement or "surface renewal" makes the penetration theory a part of the overall process.

The penetration theory assumes the same time of exposure for all elements of surface. The Danckwerts' model supposes, instead, that the chance of an element of surface being replaced with fresh liquid is independent of the length of time for which it has been exposed to the gas. Stated another way, it is assumed that the interfacial region is uniformly accessible, so that any surface element is equally likely to be withdrawn. This leads to a stationary distribution of exposure times in which the fraction of surface which at any given instant has been exposed to the surface for times between  $\theta$  and  $(\theta + d\theta)$  is  $s e^{-s\theta} d\theta$ . Here  $s$  is the fraction of the area of surface which is replaced with fresh liquid in unit time. Thus, if  $R$  is the instantaneous rate of absorption per unit area of surface which has been exposed for time,  $\theta$ , then, for physical absorption

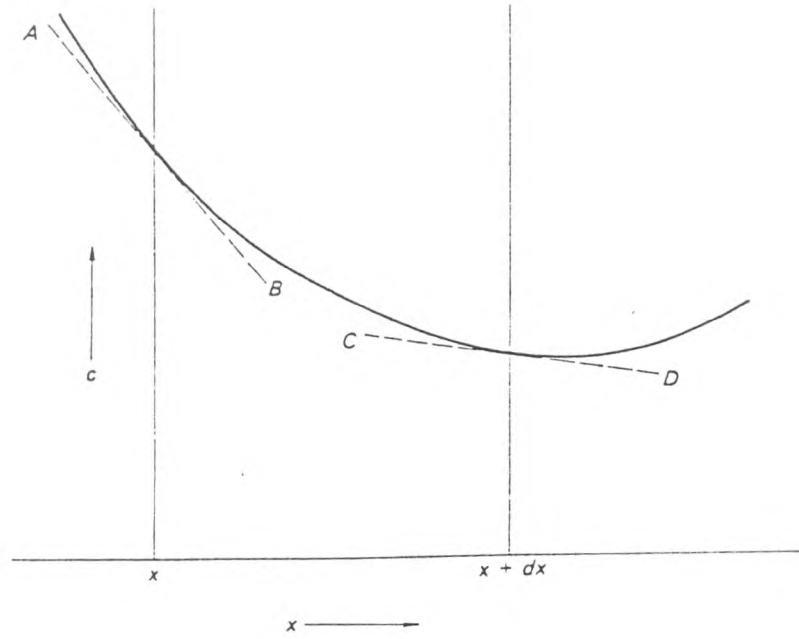


Fig. 3.1 Concentration-profile of diffusing solute.

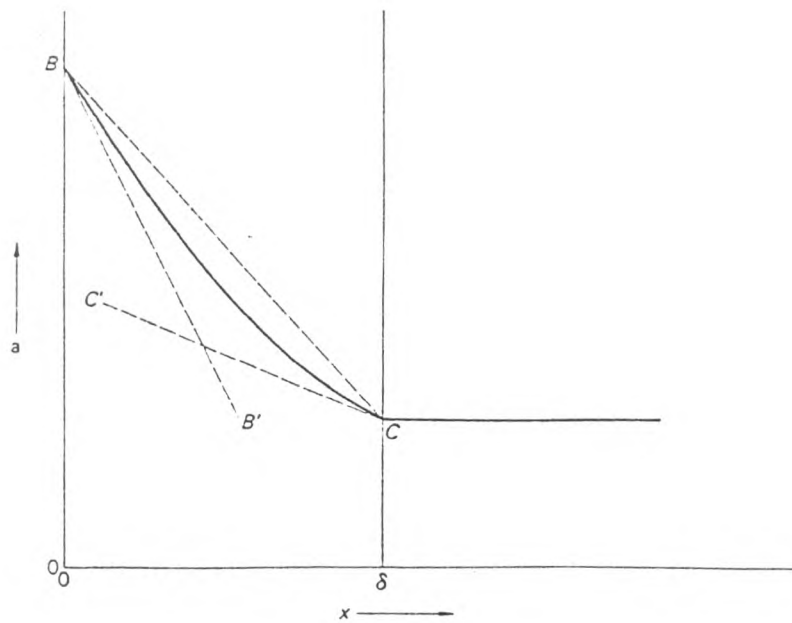


Fig. 3.2 Effect of chemical reaction on concentration profile in diffusion film.

$$R = (C_{Ai} - C_{Ao}) \sqrt{\frac{D_A}{\pi\theta}}$$

and the average rate of absorption into the surface is the  $R$  averaged over all elements of the surface, having exposure times between 0 and  $\infty$ .

$$\bar{R} = S \int_0^{\infty} R e^{-s\theta} d\theta$$

$$= (C_{Ai} - C_{Ao}) s \sqrt{\frac{D_A}{\pi}} \int_0^{\infty} \frac{e^{-s\theta}}{\sqrt{\theta}} d\theta$$

$$\bar{R} = (C_{Ai} - C_{Ao}) \sqrt{D_A S} \quad (3.13)$$

$$\text{Hence } k_L = \sqrt{D_A S}$$

The film theory predicts that  $k_L$  is proportional to the diffusivity of gas,  $D_A$ , but both Higbie and Danckwerts' models predict a square root - dependency on  $D_A$ .

### 3.3 Absorption in Presence of Chemical Reactions

Absorption is accompanied by chemical reaction according to the following steps.

1. Diffusion of dissolved gas from the interface where physical equilibrium is assumed to be established.
2. Diffusion of dissolved gas from the interface into the bulk of liquid.
3. Chemical reaction within the liquid phase.

4. Diffusion of reactant and/or products from the bulk of liquid phase towards the interface.

When the diffusant is being destroyed by some chemical reaction, the difference between the rates of diffusion into and out of the element is equal to the sum of the accumulation and the rate of reaction. If the rate of reaction of diffusant per unit volume of liquid at some distance  $x$  is  $r$ , the equation for diffusion with reaction becomes,

$$D_A \frac{\partial^2 C_A}{\partial x^2} = \frac{\partial C_A}{\partial t} + r \quad (3.14)$$

The chemical reaction increases the rate of interfacial mass transfer.

The effect of a chemical reaction is usually expressed in terms of the enhancement factor,  $E$ , which is the ratio of the amount of gas absorbed in a given time into a reacting liquid, to the amount which would be absorbed if there were no reaction.

The reaction reduces local concentration of reagent or better the equilibrium partial pressure of the gas is reduced, thus increasing the concentration gradient between the bulk of gas phase and interface and its flux.

### 3.3.1 Slow Reaction

When the reaction is slow, and a negligible proportion of the gas absorbed reacts in the diffusion film, according to the penetration theory, this means the time during which the surface liquid elements are exposed to the gas is much less than the time required for the reaction to take place appreciably within the elements. Hence the process is essentially one of physical absorption followed by reaction in the bulk.

In that case the concentration of the reactant is virtually constant through the liquid phase during the exposure time and the whole liquid becomes and remains saturated with the unreacted gas (at a concentration corresponding to its partial pressure above the liquid). The concentration profile in the diffusion film is shown in Fig. 3.2 according to the film model. The rate at which unreacted gas diffuses out of the film into the bulk liquid is the same as the rate at which it diffuses into the film from the surface. Thus the concentration profile of gas in the film is a straight line and the rate of absorption is that of physical absorption, i.e.

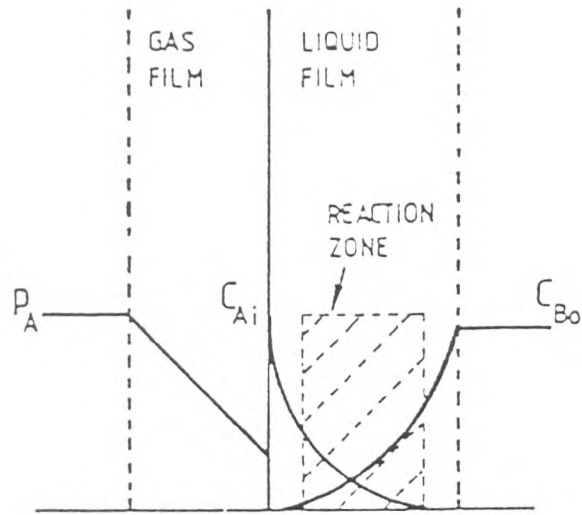
$$R_a = k_L a (C_{A_i} - C_{A_o}).$$

### 3.3.2 Fast Reaction

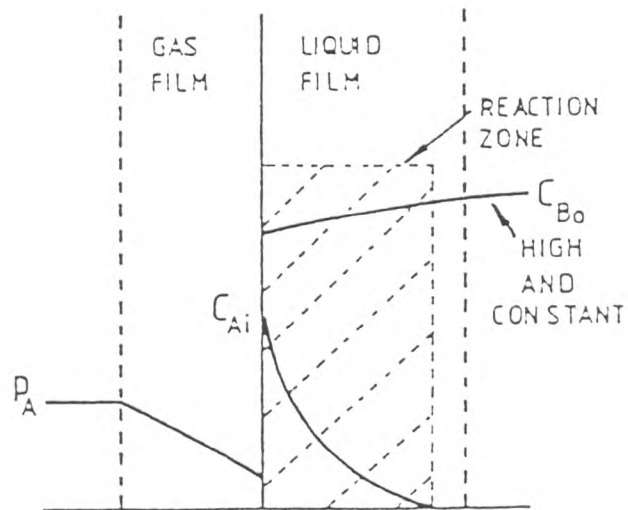
According to the film theory, when the reaction is fast enough for a substantial amount of the absorbed gas to react in the film, rather than to be transferred unreacted to the bulk the concentration profile is curved so that the concentration gradient at the surface, BB', is greater than that at the inner boundary of the film that is CC' Fig. 3.2.

The ratio of the rate of absorption to the rate of transfer of unreacted gas into the bulk is the ratio of the slopes of BB' and CC'. The enhancement factor is the ratio of the slopes of BB' and CC'. For the case of second-order reaction the concentration profile is shown in Fig. 3.3a.

The reaction plane spreads into a zone of reaction in which both gas and liquid are present but no reactant reaches the liquid surface



(a)



(b)

Fig. 3.3 Interface behaviour for the liquid phase reaction.

and no gas enters the bulk of the liquid to react there and the reaction zone remains totally within the liquid film.

For the special case where the concentration of reactant (liquid) is high and therefore does not drop appreciably within the film, it can be taken to be constant throughout, and the reaction in the liquid film becomes pseudo first order. Physically, this means that the reactant diffuses towards the surface fast enough to prevent the reaction causing any significant depletion Fig. 3.3b.

### 3.3.3 Instantaneous Reaction

In this case the dissolved gas reacts instantaneously with a dissolved reactant. According to the film model there is a plane beneath the interface, where the concentration of both is zero, and the rate of reaction is equal to the rate at which both gas and reactant diffuse towards the reaction plane. The actual kinetics of the reaction are immaterial and a change in partial pressure of gas ( $P_A$ ) or bulk concentration of the liquid will move the reaction plane one way or the other Fig. 3.4a).

Concentration profiles for instantaneous reaction with varying liquid concentration is shown in Fig. 3.4.

When the gas concentration at the interface,  $P_{A_i}$ , and the liquid concentration at the interface,  $C_{A_i}$ , are both zero, the dissolved liquid reaches the surface by diffusion through the liquid as fast as the gas reaches it by diffusion through the gas (Fig. 3.4b).

As the liquid concentration is further increased so that it is sufficiently high, the interfacial concentration of the liquid is greater than zero. This means that the transport of the liquid towards

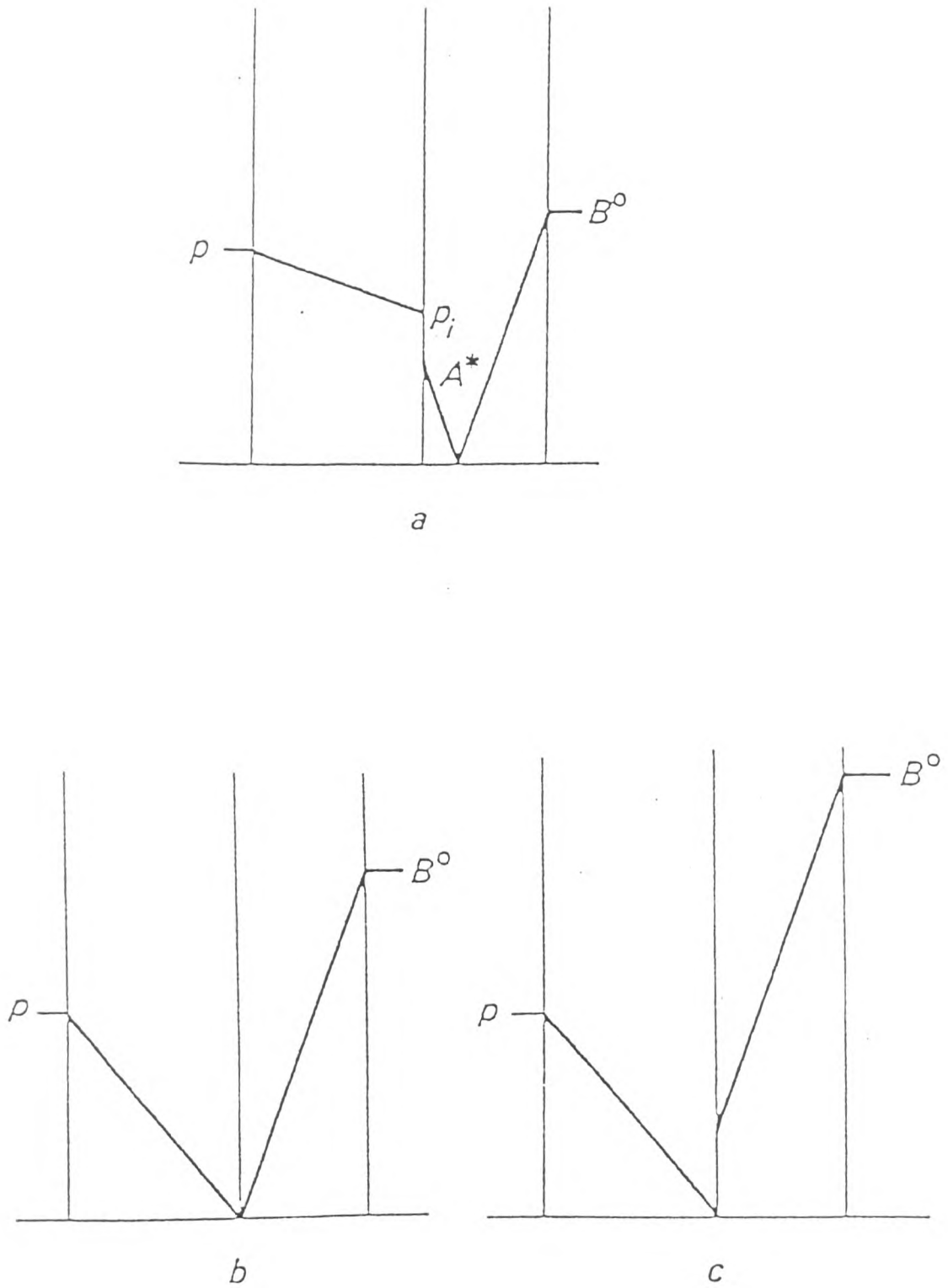


Fig. 3.4 Concentration profiles for instantaneous reaction with varying concentration of reactant.

the surface is faster than the gas. For this special case the reaction plane moves to the gas-liquid interface, hence the absorption process becomes entirely gas film controlled (i.e. by the transport of gas across the gas film).

Raising the liquid concentration further has no effect on the overall rate (Fig. 3.4c).

### 3.3.4 Equations of Rate of Absorption with (m, n-th) order Irreversible Chemical Reaction

Hikita and Asai (47) derived the equations of the rate of absorption and enhancement factor for m, n-th order irreversible reaction based on the film theory and penetration theory assuming the gas phase resistance is negligible.

They considered the absorption of a gas, A, in a liquid containing reactant, B. The reaction takes place by an (m, n-th) order irreversible reaction according to



The reaction rate can be represented by

$$r = - \frac{dC_A}{dt} = - \frac{a}{b} \frac{dC_B}{dt} = K_{m,n} C_A^m C_B^n \quad (3.16)$$

#### 3.3.4.1 Film Theory

Equation (3.16) is for the case where gas absorption is accompanied by an (m,n)-th order irreversible reaction. The fundamental diffusion equations for components A and B within the film are given as follows:

$$D_A \left[ \frac{d^2 C_A}{dx^2} \right] = K_{m,n} C_A^m C_B^n \quad (3.17)$$

$$D_A \left[ \frac{d^2 C_B}{dx^2} \right] = \left[ \frac{b}{a} \right] K_{m,n} C_A^m C_B^n \quad (3.18)$$

The boundary conditions are

$$x = 0 \quad C_A = C_{Ai} \quad \frac{dC_B}{dx} = 0 \quad (3.19)$$

$$x = x_f \quad C_A = 0 \quad C_B = C_{Bo} \quad (3.20)$$

The boundary condition  $dC_B/dx = 0$  in equation (3.19) is based on the assumption that the reactant B is non-volatile and does not diffuse into the gas phase through the phase boundary.

Equations (3.17) and (3.18) cannot be solved analytically except for the cases where the combination of  $m$  and  $n$  are given as follows:

$$m = 0 \quad n = 0$$

$$m = 0 \quad n = 1$$

$$m = 1 \quad n = 0$$

Thus, as an approximate equation for the enhancement factor,  $E$ , which may be applicable to a combination of any  $m$  and  $n$  values, can be given by

$$E = \frac{M \eta}{\tanh M \eta} \quad (3.20)$$

where

$$M = \frac{\sqrt{\frac{2 D_A K_{m,n} C_{Ai}^{m-1} C_{Bo}^n}{(m+1)}}}{K_L} \quad (3.21)$$

$$\eta = \left[ \frac{E_i - E}{E_i - 1} \right]^{\frac{n}{2}} \quad (3.22)$$

$$E_i = \left[ 1 + \frac{a D_B C_{Bo}}{b D_A C_{Ai}} \right] \quad (3.23)$$

$E_i$  is the enhancement for instantaneous reaction.

### 3.3.4.2 Penetration theory

The fundamental differential equations based on the penetration theory for the diffusion accompanied by an (m, n)-th order chemical reaction are

$$D_A \left( \frac{\partial^2 C_A}{\partial x^2} \right) - \frac{\partial C_A}{\partial t} = K_{m,n} C_A^m C_B^n \quad (3.24)$$

$$D_B \left( \frac{\partial^2 C_B}{\partial x^2} \right) - \frac{\partial C_B}{\partial t} = K_{m,n} C_A^m C_B^n \quad (3.25)$$

The boundary conditions are

$$t > 0, x = 0 \quad C_A = C_{Ai}, \quad \frac{\partial C_B}{\partial x} = 0 \quad (3.26)$$

$$t \geq 0, x = \infty \quad C_A = 0, \quad C_B = C_{Bo} \quad (3.27)$$

$$t = 0, x \geq 0 \quad C_A = 0, \quad C_B = C_{Bo} \quad (3.28)$$

Equations (3.24) and (3.25) cannot be solved analytically, but it is possible to solve it by approximation method.

Similar to the film theory, it may be assumed that the concentration of liquid ( $C_B$ ) in the liquid film, at least up to the penetration depth of  $C_A$ , is constant and independent of  $x$ . Furthermore, it is assumed that the constant  $C_B$  concentration is equal to  $C_{Bi}$ , the interphase concentration, and that  $C_{Bi}$  is independent of time. Then the equation (3.24) may be reduced to

$$D_A \left[ \frac{\partial^2 C_A}{\partial x^2} \right] - \frac{\partial C_A}{\partial t} = (K_{m,n} C_{Bi}^n) C_A^m \quad (3.29)$$

Thus the following approximate equation is obtained for  $E$ .

$$E = [M\eta + (\pi/8M\eta)] \operatorname{erf} (2 M\eta / \sqrt{\pi}) + \frac{1}{2} \exp(-4 M^2 \eta^2 / \pi) \quad (3.30)$$

where  $M$  and  $\eta$  are dimensionless groups defined by

$$M = \sqrt{[\pi/2 (m+1)] K_{m,n} C_{Ai}^{m-1} C_{Bo}^n t} \quad (3.31)$$

The equivalent form of this equation in terms of film model is,

$$M = \sqrt{[2/(m+1)] K_{m,n} D_A C_{Ai}^{m-1} C_{Bo}^n / k_L} \quad (3.32)$$

$$\text{and } \eta = \left[ \frac{C_{Bi}}{C_{Bo}} \right]^{\frac{n}{2}} \quad (3.33)$$

Similar to equation (3.22) of the film theory, the relationship between  $C_{Bi}$  and  $C_B$  is

$$\eta = \left[ \frac{C_{Bi}}{C_{Bo}} \right]^{\frac{n}{2}} = \left[ \frac{E_i - E}{E_i - 1} \right]^{\frac{n}{2}} \quad (3.34)$$

Three limiting cases can be considered here:

### Case 1

When  $M$  approaches infinity,  $\eta$  is equal to zero and  $E$  becomes  $E_i$  where reaction can be considered as an instantaneous reaction.

In the case of absorption accompanied by second order reaction, the condition for the reaction to be considered instantaneous is (48)

$$\sqrt{\frac{D_A K_2 C_{Bo}}{k_L}} \gg 10 \left[ 1 + \left( \frac{a}{b} \right) \left( \frac{D_B}{D_A} \right) \left( \frac{C_{Bo}}{C_{Ai}} \right) \right]$$

and  $E = E_i$ .

The average rate of absorption is given by

$$\bar{R} = k_L C_{Ai} \left[ 1 + \left( \frac{a}{b} \right) \left( \frac{D_B}{D_A} \right) \left( \frac{C_{Bo}}{C_{Ai}} \right) \right] \quad (3.35)$$

For Film Theory

and

$$\bar{R} = k_L C_{Ai} \left[ 1 + \left( \frac{a}{b} \right) \left( \sqrt{\frac{D_B}{D_A}} \right) \left( \frac{C_{Bo}}{C_{Ai}} \right) \right] \quad (3.36)$$

For Penetration Theory

For the special case when the concentration of liquid reactant,  $C_{B_0}$ , is considerably greater than  $C_{A_i}$ , then the rate of diffusion of liquid reactant towards the reaction plane is much higher than the rate of diffusion of gas.

The rate of absorption is therefore determined by the rate of diffusion of liquid reactant towards the interface, and is independent of the partial pressure of the gas. Hence equations (3.35) and (3.36) reduce to

$$\bar{R} = k_L \left[ \frac{a}{b} \right] \left[ \frac{D_B}{D_A} \right] C_{B_0} \quad (3.35a)$$

$$\bar{R} = k_L \left[ \frac{a}{b} \right] \left[ \sqrt{\frac{D_B}{D_A}} \right] C_{B_0} \quad (3.36a)$$

### Case 2

When the value of  $M$  approaches zero,  $\eta$  and  $E$  are equal to unity, which means the reaction is slow enough for the absorption process to be considered as a physical one.

For an irreversible second order reaction the condition for physical absorption is

$$M = \sqrt{\frac{D_A K_2 C_{B_0}}{k_L^2}} \ll 1$$

Physically this represents the condition where no appreciable proportion of the gas absorbed is to react in the film (i.e. no reaction in the film).

Case 3

When  $E_i$  approaches infinity,  $\eta$  is equal to unity then equations (3.20) and (3.21) reduce to

$$E = \frac{M}{\tanh M} \quad (3.37)$$

For Film Theory

and

$$\begin{aligned} \text{and } E = & \left[ M + \left[ \frac{\pi}{8M} \right] \right] \operatorname{erf} (2 M / \sqrt{\pi}) \\ & + \left[ \frac{1}{2} \right] \exp \left[ - \frac{4M^2}{\pi} \right] \end{aligned} \quad (3.38)$$

For Penetration Theory respectively.

For the special case when the reactant diffuses towards the surface fast enough to prevent the reaction causing any significant depletion there, the concentration of liquid reactant is everywhere equal to its bulk concentration, i.e.  $C_{Bo}$ . The reaction then becomes pseudo-mth order in gas. The condition for this situation is:

$$M = \frac{\sqrt{\frac{D_A K_{m,n} C_{Ai}^{m-1} C_{Bo}^n}{(m+1)}}}{k_L} < \frac{1}{2} \left[ 1 + \frac{a}{b} \left( \frac{D_B C_{Bo}}{D_A C_{Ai}} \right) \right]$$

The average rate of absorption is given by

$$\bar{R} = K_L C_{Ai} \sqrt{1 + M^2} \quad (3.39)$$

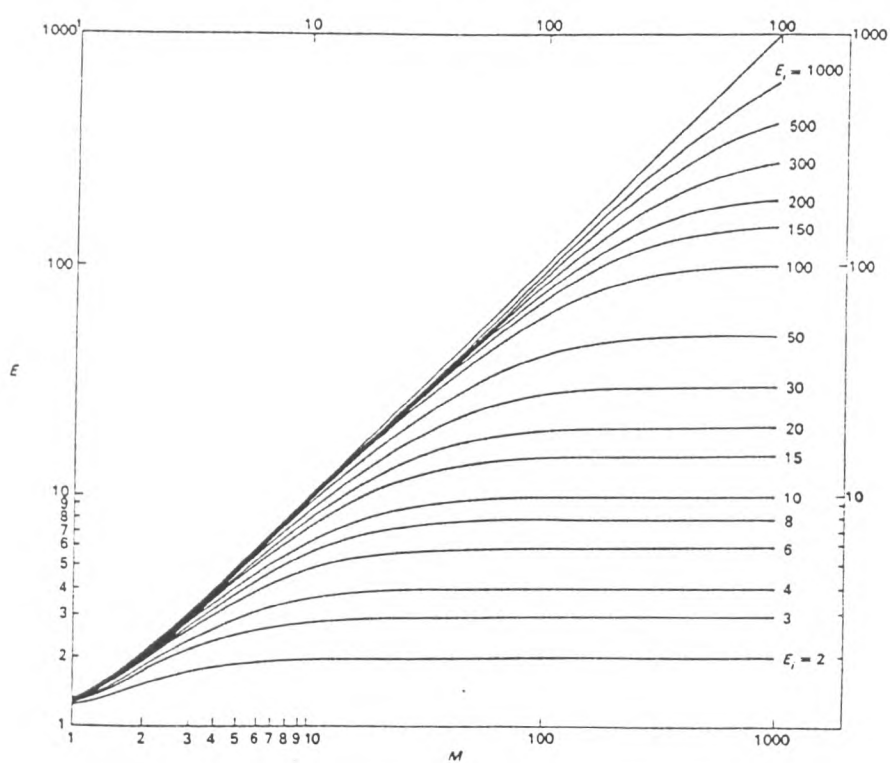


Fig. 3.5 Enhancement factors for second order reaction; for quiescent liquid or agitated liquid (film or Higbie models).

when  $M^2$  is sufficiently large ( $M^2 \gg 1$ ), both film and penetration theories predict that  $E$  is equal to  $M$  and the absorption process is said to be a fast pseudo- $m$ th order reaction.

The average rate of absorption is then given by:

$$\bar{R} = C_{Ai} \sqrt{\left[ \frac{2}{(m+1)} \right] K_{m,n} D_A C_{Bo}} \quad (3.39a)$$

Thus the rate of absorption is independent of the liquid hydrodynamic conditions, i.e. liquid film thickness and gas-liquid contacting time for the film and penetration models respectively. This corresponds to a sufficiently long contact-time or fast reaction.

Figure (3.5) shows the effect of second-order reaction on absorption rate.

Several limiting types of behaviour can be identified in Fig. 3.6 when  $M \ll 1$ ,  $E \approx 1$ , in these circumstances the time of contact between gas and liquid is very short, or the reaction is very slow, so that physical absorption predominates and the reaction has negligible effect.

When  $M < \frac{1}{2} E_i$ , the point representing  $E$  lies on the A-B-C forming the envelope of the family of curves on the figure, the reaction is then pseudo-first order. This means that the reactant diffuses towards the surface fast enough to prevent the reaction causing any significant depletion there. When  $1 \ll M \ll E_i$  the point representing  $E$  lies on the straight part (B-C) of the envelope. This corresponds to a sufficiently long contact-time or fast reaction. Then  $E = M$  and the rate of absorption is independent of the contact-time or hydrodynamic condition.

Finally, when  $M \gg E_i$ , then  $E = E_i$ , this occurs when the reaction is very fast, the contact-time, long, or the concentration of reactant, small.

The reactant is depleted in the neighbourhood of the surface to the extent that the rate of reaction is determined by diffusion alone.

Sharma and Danckwerts (49) introduced the standard methods of measuring interfacial area and the liquid and gas phase transfer coefficients in systems consisting of a gas and a liquid or of two liquids. One of the fluids (e.g. gas) dissolves in the other and there undergoes a reaction with the dissolved reactant.

By suitably choosing the solubility, the concentration of the reactant and the rate of reaction, either the interfacial area or the mass transfer coefficients, can be deduced from the overall rate of absorption.

### 3.3.5 Determination of Interfacial Area

Considering equation (3.39) the average rate of absorption per unit volume of bed for a first-order reaction is,

$$\bar{R}_a = a C_{A_i} \sqrt{D_A K_2 C_{B_0}} \quad (3.40)$$

Thus, provided  $\bar{R}$  can be measured experimentally and  $C_{A_i}$ ,  $D_A$ ,  $K_2$ ,  $C_{B_0}$  are known, then the interfacial area is determined directly from the rate of absorption.

If the solute gas is diluted by a carrier gas it is necessary to confirm that the gas side resistance is negligible, this will be the general case if

$$K_g \gg M \frac{k_L}{He} \quad (3.41)$$

where  $He$  is the Henry law constant relating the interfacial partial pressure,  $P_{Ai}$ , to  $C_{Ai}$ :

$$P_{Ai} = He C_{Ai} \quad (3.42)$$

If it is not possible to keep the gas side resistance negligible by satisfying condition (3.41) it is still possible to determine the interfacial area by using the following equation:

$$\frac{P_A}{\bar{R}a} = \frac{1}{a} \left[ \frac{1}{k_g} + \frac{He}{\sqrt{D_A K_2 C_{Bo}}} \right] \quad (3.43)$$

If  $K_2 C_{Bo}$  is varied, a plot of  $P/\bar{R}a$  against  $\frac{He}{\sqrt{D_A K_2 C_{Bo}}}$  will give

straight line of slope  $1/a$  and intercept  $1/k_g a$  so both  $a$  and  $k_g$  can be obtained.

### 3.3.6 Determination of Liquid Film Transfer Coefficient

Liquid film transfer coefficients can be found by absorption measurements, either allowing for the gas-side resistance or taking steps to eliminate it.

Volumetric liquid film transfer coefficient,  $k_L a$  can be estimated by physical absorption (absorption of  $CO_2$  in water) or by employing a relatively slow reaction (absorption of  $CO_2$  in a carbonate-bicarbonate solution under certain conditions).

By determining interfacial area ( $a$ ) independently,  $k_L$  can be calculated.

It is also possible to estimate the liquid film transfer coefficient by the chemical method where absorption is accompanied by a pseudo-first order reaction.

According to Danckwerts (41) the volumetric rate of absorption, for this case, is given by:

$$\overline{Ra} = a C_{Ai} \sqrt{D_A k_1 + k_L^2} \quad (3.44)$$

where  $k_1 = k_2 C_{Bo}$ , for a pseudo-first order reaction.

By changing the liquid concentration,  $C_{Bo}$ , volumetric rate of absorption can be measured experimentally. Then, provided the other parameters,  $C_{Ai}$  and  $D_A$  remain constant, the plot of  $(Ra)^2$  against  $k_1$  in equation (3.44) should give a straight line of slope  $(a C_{Ai})^2 D_A$  and intercept  $(k_L a C_{Ai})^2$ . This plot is known as the Danckwerts' plot, using values of the slope and the intercept  $k_L$  and  $(a)$  will be estimated.

## CHAPTER 4

### EQUIPMENT AND EXPERIMENTAL METHODS

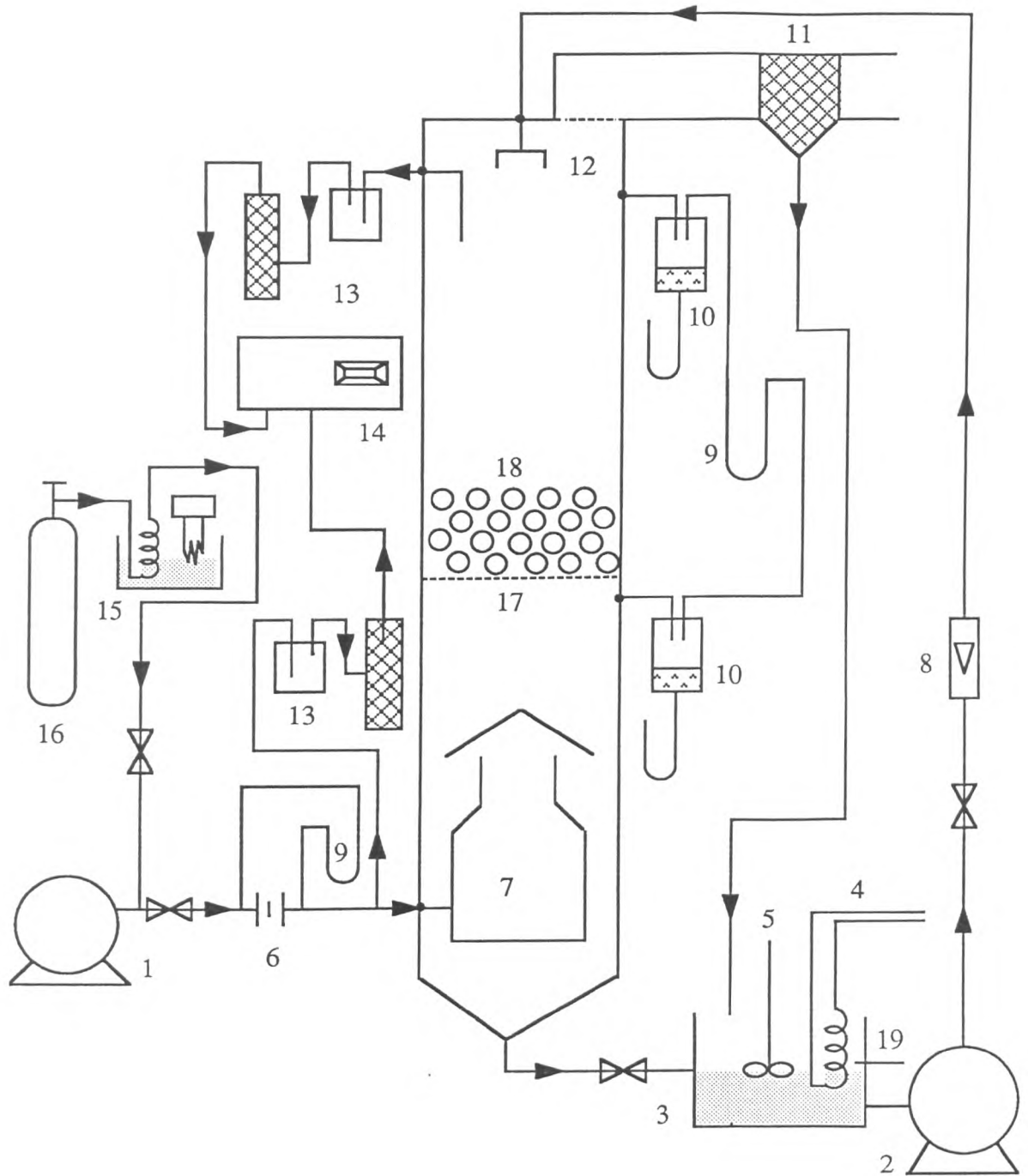
#### 4.1 Test Rig Design and Specifications

The rig, see figure (4.1), consisted of a perspex column of 22 cm internal diameter and 144 cm height with a stainless steel supporting grid of 72% open area. A gas-liquid separator is mounted on the top of the column which is made of PVC rectangular box (41 cm length, 20 cm width and 20 cm height) with a V shape attachment (9 cm height with sides of 12 cm) fitted to the bottom of the box. The knit mesh material was packed in the V section of the separator where the liquid is being separated from the leaving gas stream.

The air was supplied by a centrifugal fan and via a 10.5 cm diameter pipe containing a 57 mm diameter sharp edged orifice plate with D and D/2 tapings, was designed according to BS 1040, in order to measure air flow rate.

A special air flow distributor was constructed which consisted of a stainless steel vessel with a conical shape attachment connected to its top and with a plastic funnel fitted to the top of this attachment. The liquid was pumped from a storage tank through a rotameter and the packings were irrigated by a shower type distributor from the top of the column. A thermometer was fitted in the liquid tank in order to measure the liquid temperature together with a cooling water coil and a variable speed stirrer in order to maintain the liquid temperature and well mixed liquid.

Two pressure taps were fitted for pressure measurements 2 cm below the supporting grid and 20 cm below the top of the column to accommodate



1-Blower; 2-Pump; 3-Liquid Tank; 4-Cooling Coil; 5-Stirrer; 6-Orifice Plate; 7-Gas Distributor; 8-Rotameter; 9-Manometer; 10-Pressure Tap Separator; 11-Gas-Liquid Separator; 12-Liquid Distributor; 13-Gas Sampling Point and Dryer; 14-CO<sub>2</sub> Analyser; 15-Heating Water Tank; 16-CO<sub>2</sub> Cylinder; 17-Supporting Grid; 18-Packings; 19-Thermometer

Figure 4.1 Rig Arrangement

all the expanded bed heights. Any gas-liquid mixture entering the taps was separated in small containers from which the air line was connected to a U tube manometer.

A fan heater and a water immersed heating coil was placed in the CO<sub>2</sub> line in order to avoid carbon dioxide ice formation which occurs due to the evaporation cooling effect in CO<sub>2</sub> cylinder thereby securing a steady flow of carbon dioxide. The CO<sub>2</sub> flow rate was controlled by a valve and rotameter to maintain a chosen feed rate and concentration.

Two magnesium perchlorate driers were provided at the inlet and outlet gas sampling points. The dry sampled gas was introduced to the CO<sub>2</sub> analyser (Signal Analyser Series 2000) through a 3-way valve. The whole assembly was assembled inside a large PVC floor tray, so that in the case of a caustic solution leakage the liquid was safely retained.

## **4.2 Experimental Procedures**

### **4.2.1 Hydrodynamics Experimental Procedures**

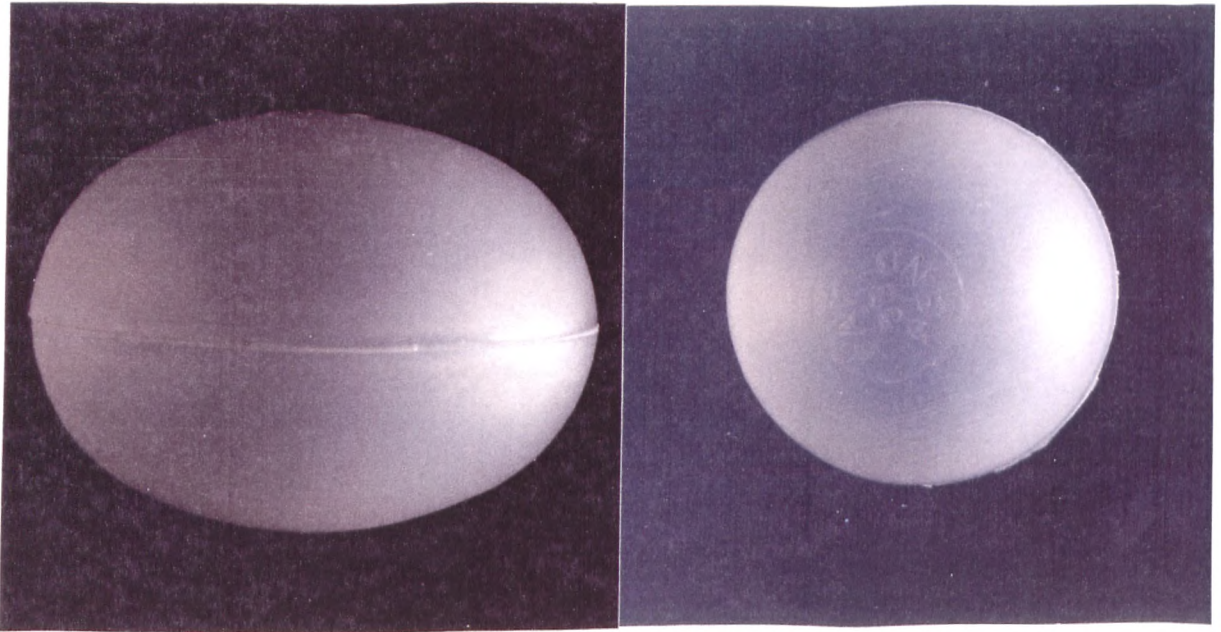
Four types of packing at two bed static heights of 10.5 and 16.5 cm were used throughout the experiments. The specifications of the packing are given in Table (4.1) and Fig. 4.2. Pressure drop, liquid hold up, expanded bed height and minimum fluidization velocity measurements were carried out in this study.

#### **4.2.1.1 Pressure Drop**

Bed pressure drop was measured by using a U tube manometer connected to two pressure tappings which are situated below and above the bed.

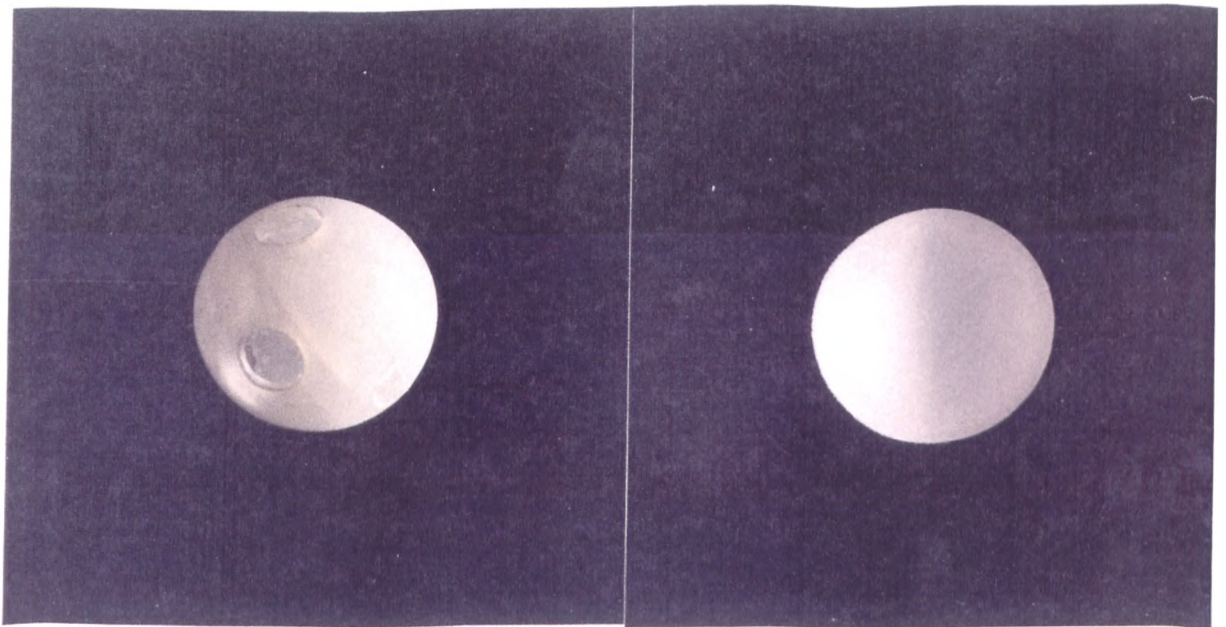
Table 4.1 Specifications of packing used in the present work.

Packing type	$d_p$ mm	Apparent packing density kg/m <sup>3</sup>	Solid surface area cm <sup>2</sup>	Packing weight gr	No. of Packings in bed		hole dia mm	hole No.
					$H_s=10.5$ cm	$H_s=16.5$ cm		
Oblate spheroid	50 x 38	162	69.0	8.08	50	75	-	-
Plain sphere	38	161	45.36	4.64	85	120	-	-
Plain sphere	25	327	19.63	2.68	275	360	-	-
Slotted sphere	25	293	30.89	2.4	275	360	7	6



Oblate Spheroid Packing  
Diameter = 50 x 38 mm

Plain Sphere Packing  
Diameter = 38 mm



Slotted Sphere Packing  
Diameter = 25 mm

Plain Sphere Packing  
Diameter = 25 mm

Figure 4.2 Type of Packings

#### 4.2.1.2 Expanded Bed Height

The expanded bed height was measured by reading a scale placed on the column. In the cases where fluctuation in the bed height is present, the minimum and maximum bed height was recorded and the average of these is reported as being the expanded bed height.

#### 4.2.1.3 Liquid Hold Up

The liquid hold up was measured by using the cut off method achieved by closing the valves on the liquid lines to the column and below the column simultaneously and then measuring the amount of liquid which was retained in the bed. This procedure was repeated five times in each run and the average of these readings was taken as the liquid hold up.

#### 4.2.1.4 Minimum Expanding Velocity

The minimum expanding velocity was determined as the velocity at which the bed starts to expand and the top layer of the bed is beginning to move very slowly.

### 4.2.2 Mass Transfer Experimental Procedures

Measurements of the interfacial area and liquid film transfer coefficient were conducted by the chemical absorption method at a bed static height of 10.5 cm for plain, slotted sphere and oblate spheroid packings. The specifications of the packing are shown in Table (4.1) and Fig. 4.2.

The air and liquid rates were varied between 1.82 to 2.79 m/s and  $2.32 \times 10^{-3}$  to  $10.9 \times 10^{-3}$  m/s respectively. Carbon dioxide was absorbed from air into aqueous solutions of sodium hydroxide. The carbon dioxide

concentration was 2% by volume and maintained constant during each run and for all of the experiments, by using an on-line CO<sub>2</sub> analyser.

For a given experimental condition four liquid recycle runs were carried out by using a bath of sodium hydroxide with four different initial concentrations of 2, 1.5, 1 and 0.3 g mol/lit. The liquid volume was 30 lit and its temperature was kept constant for each experimental condition. The degree of conversion of sodium hydroxide in all runs was not allowed to exceed 25 percent and was therefore considered to be characteristic of the rate of absorption into the fresh sodium hydroxide solution. The rate of absorption of CO<sub>2</sub> into NaOH was calculated on the basis of chemical analysis of the liquid samples. The liquid samples were analysed by titration method with hydrogen chloride. The end points were detected by Jenway 3020 pH meter whilst using a mixed indicator (cresol red and thymol blue) and screened methyl orange as indicators for hydroxyl and bicarbonate analysis. The correction for the concentration of sodium hydroxide due to evaporation from the liquid solution during absorption was made by multiplying the volume of acid used for titration of total sodium concentration for the final titration by the ratio of initial to the final volume.

## CHAPTER 5

### RESULTS AND DISCUSSION

#### 5.1 Hydrodynamic Results and Discussion

##### 5.1.1 Pressure Drop

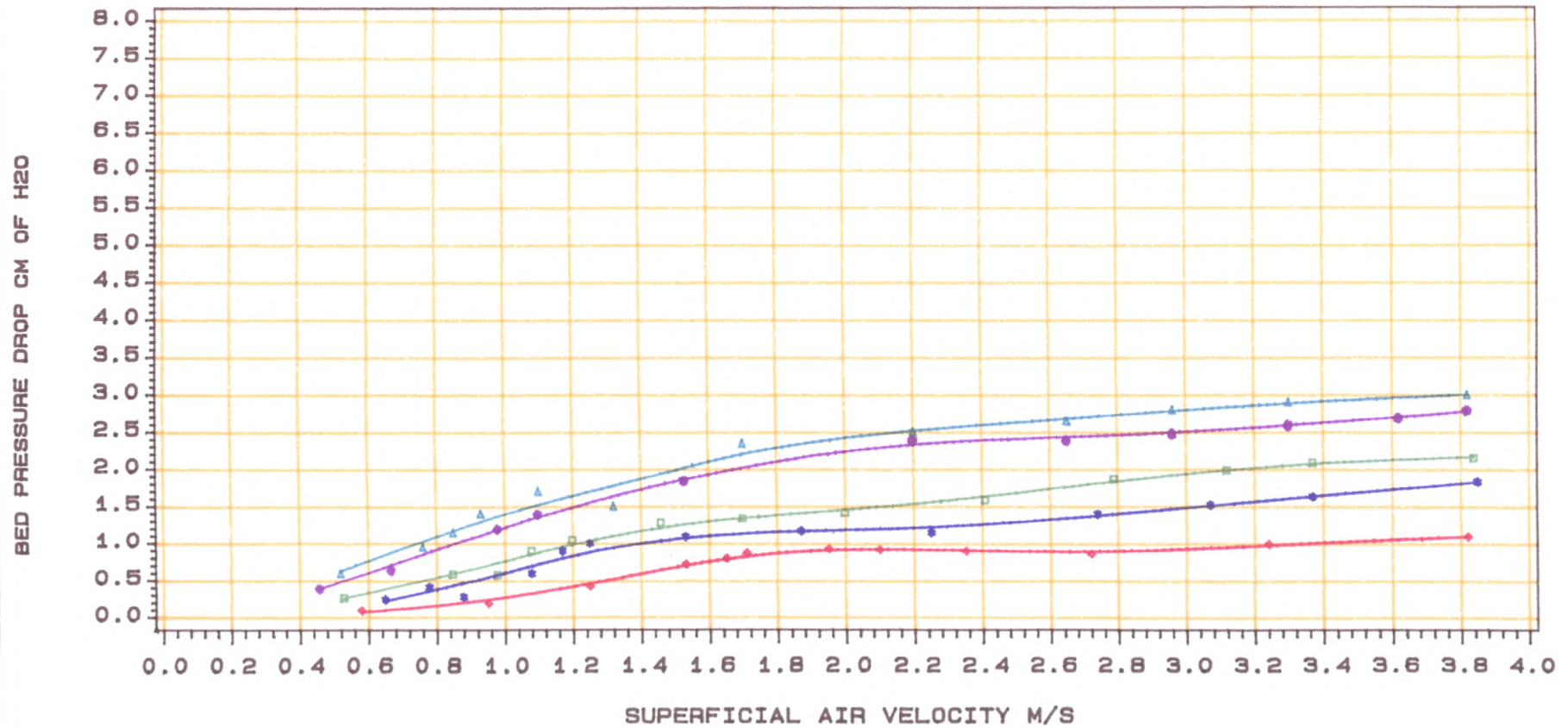
Variation of pressure drop with air velocity for 38 mm diameter plain sphere packing at bed static height of 10.5 cm and 16.5 cm are shown in figures 5.1.1 and 5.1.2. It can be seen that in the static bed region i.e. before fluidization, the pressure drop increases sharply with the air velocity as in the case of ordinary fixed bed, but, with further increase in the air velocity, the bed starts to expand slightly until the point of fluidization.

In this region the pressure drop decreases slowly until the whole bed is fluidized (complete fluidization) and with further increase in the air velocity, the pressure drop increases very slowly. This is because the bed expands and therefore gas voidage in bed increases in order to accommodate more air flow, however, the resistance to the air flow decreases.

From figures 5.1.1 and 5.1.2 it is also apparent that at a given air velocity, the pressure drop increases with liquid velocity. This is because the liquid hold up in the bed increases as the liquid velocity increases. These are the main features of Turbulent Contact Absorbers.

In all of the pressure drop experiments a similar behaviour was observed. Figures 5.1.3 and 5.1.4 show the effect of a change in bed static height ( $H_{st} = 10.5$  cm and  $H_{st} = 16.5$  cm) on the pressure drop for 38 mm diameter spherical packing whence it can be seen that at a given air and water velocity, the pressure drop for 16.5 cm static bed is

**Fig 5.1.1 Plot Of Pressure Drop Characteristics Of Plain Sphere Packing**  
**Packing Dia=38 mm Bed Static Height=10.5 Cm**  
**FOR VARIOUS SUPERFICIAL LIQUID VELOCITY**



DRY BED  
 $V_{min}=1.65$  M/S

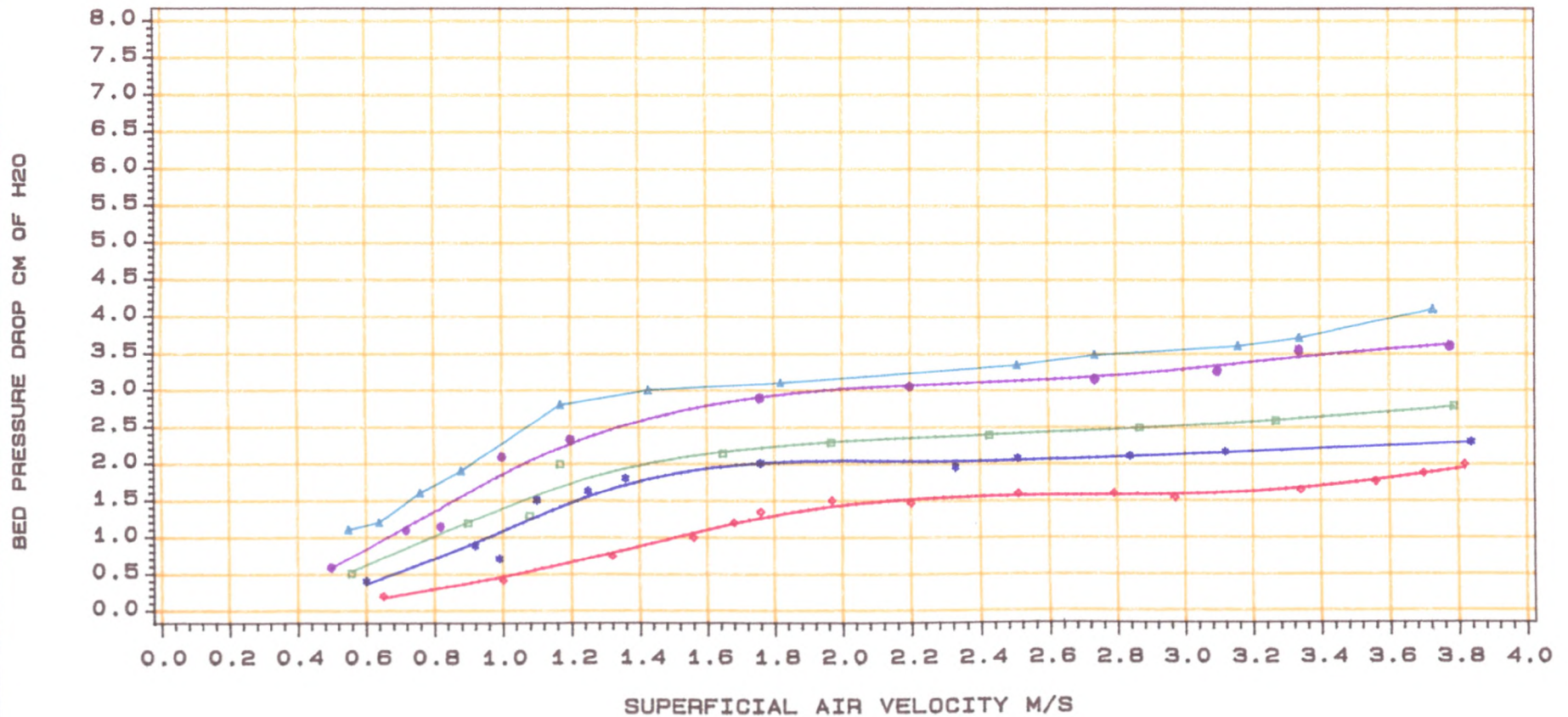
$VL=1E-3$  M/S  
 $V_{min}=1.17$  M/S

$VL=2.32E-3$  M/S  
 $V_{min}=1.08$  M/S

$VL=6.58E-3$  M/S  
 $V_{min}=0.98$  M/S

$VL=8.77E-3$  M/S  
 $V_{min}=0.85$  M/S

Fig 5.1.2 Plot Of Pressure Drop Characteristics Of Plain Sphere Packing  
 Packing Dia=38 mm, Bed Static Height=16.5 Cm  
 FOR VARIOUS SUPERFICIAL LIQUID VELOCITY



DRY BED  
 Vmin=1.68 M/S

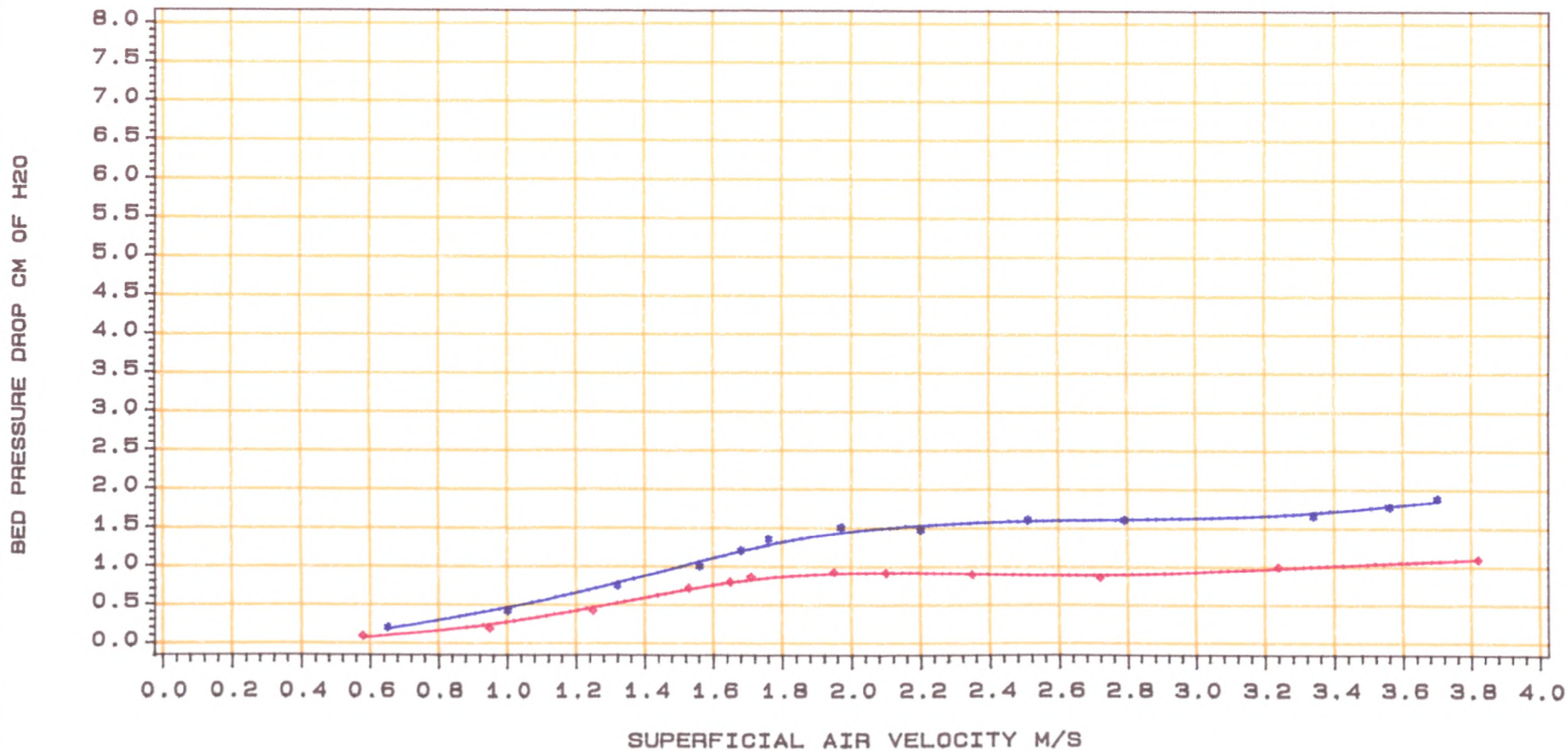
VL=1E-3 M/S  
 Vmin=1.25 M/S

VL=2.32E-3 M/S  
 Vmin=1.17 M/S

VL=6.58E-3 M/S  
 Vmin=1.00 M/S

VL=8.77E-3 M/S  
 Vmin=0.88 M/S

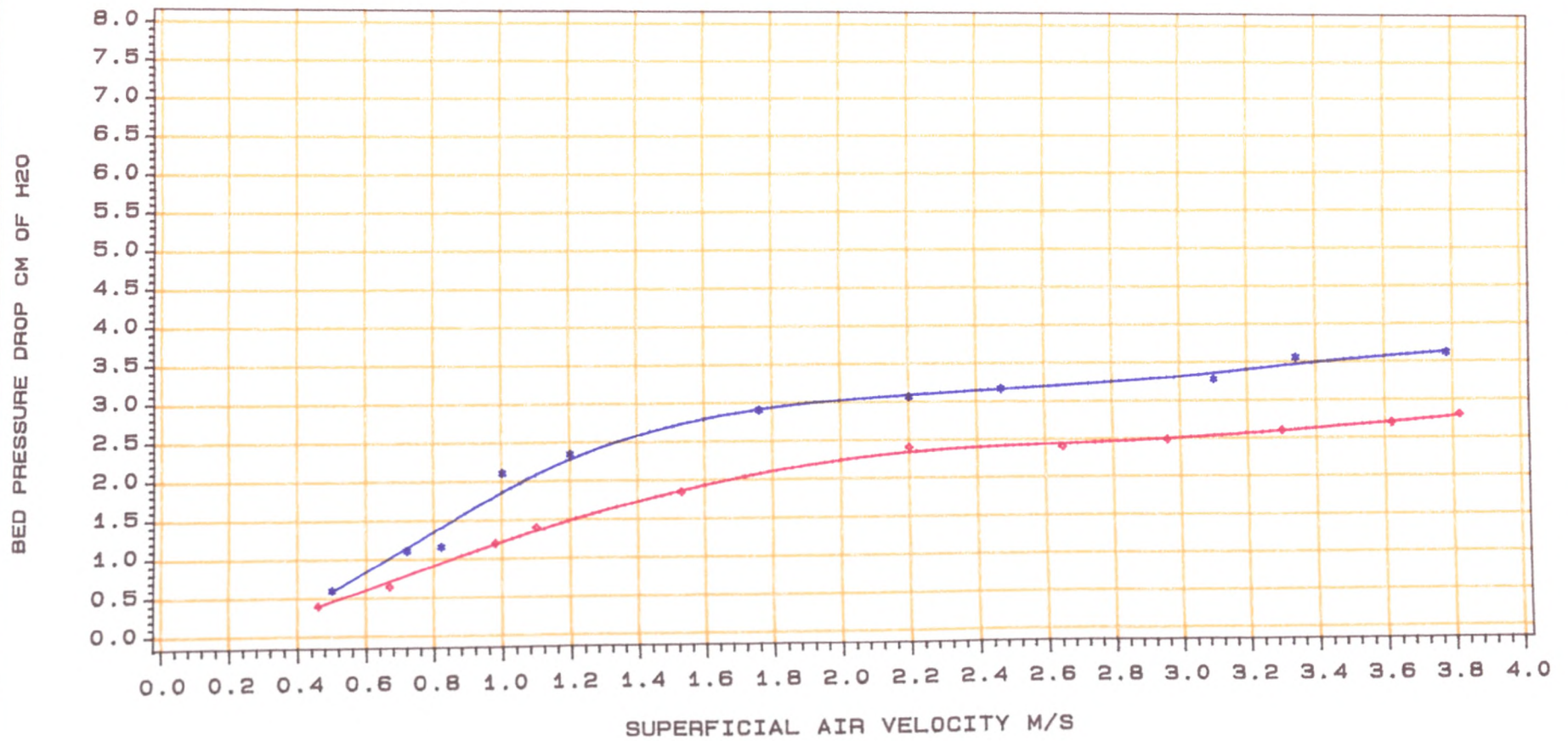
Fig 5.1.3 Plot Of Pressure Drop Characteristics Of Plain Sphere Packing  
Packing Dia=38 mm,H=10.5 CM AND H=16.5 CM  
FOR DRY BED



H=10.5 CM

H=16.5 CM

Fig 5.1.4 Plot Of Pressure Drop Characteristics Of Plain Sphere Packing  
 Packing Dia=38 mm,H=10.5 CM AND H=16.5 Cm  
 FOR SUPERFICIAL LIQUID VELOCITY=6.58E-3 M/S



H=10.5 CM

H=16.5 CM

higher than for 10.5 cm static bed. The higher pressure drop in the case of the deeper bed can be attributed mainly to the increase in the liquid hold up in the bed as the bed static height increases. In both cases for the dry bed, the pressure drop remains reasonably constant with an increase in the air velocity as in the case of two phase fluidization. This is because the effect of liquid hold up is not present and therefore the higher pressure drop for the dry bed in the case of a bed static height of 16.5 cm is only due to the larger number of packings in the bed.

These findings confirm the results of Balabekov et al (50), Strumillo et al (51) and Miconnet et al (52) who reported similar findings.

#### **5.1.2. Minimum Expanding Velocity.**

The effect of liquid velocity on the minimum expanding velocity for the 38 mm plain sphere is shown in figure 5.1.5. It can be seen that the minimum expanding velocity decreases with liquid velocity. This is because as the liquid velocity increases, the liquid hold up in the bed increases and this in turn will increase the interstitial air velocity in the bed and therefore the bed starts to expand at a lower superficial air velocity. It should also be mentioned that the reduction in the minimum expanding air velocity occurs at a higher pressure drop which is needed to support the bed.

This confirms the results of Tichy and Douglas (53), Kuroda and Tabei (10) and Kito et al (22).

Figures 5.1.6 to 5.1.8 show the variation of minimum expanding velocity with liquid rate for the oblate spheroid, 25 mm plain sphere

**Fig 5.1.5 Plot Of Variation Of Minimum Expanding Velocity With Liquid Rate For Plain Packing  
Packing Dia=38 mm Bed Static Height=10.5 Cm**

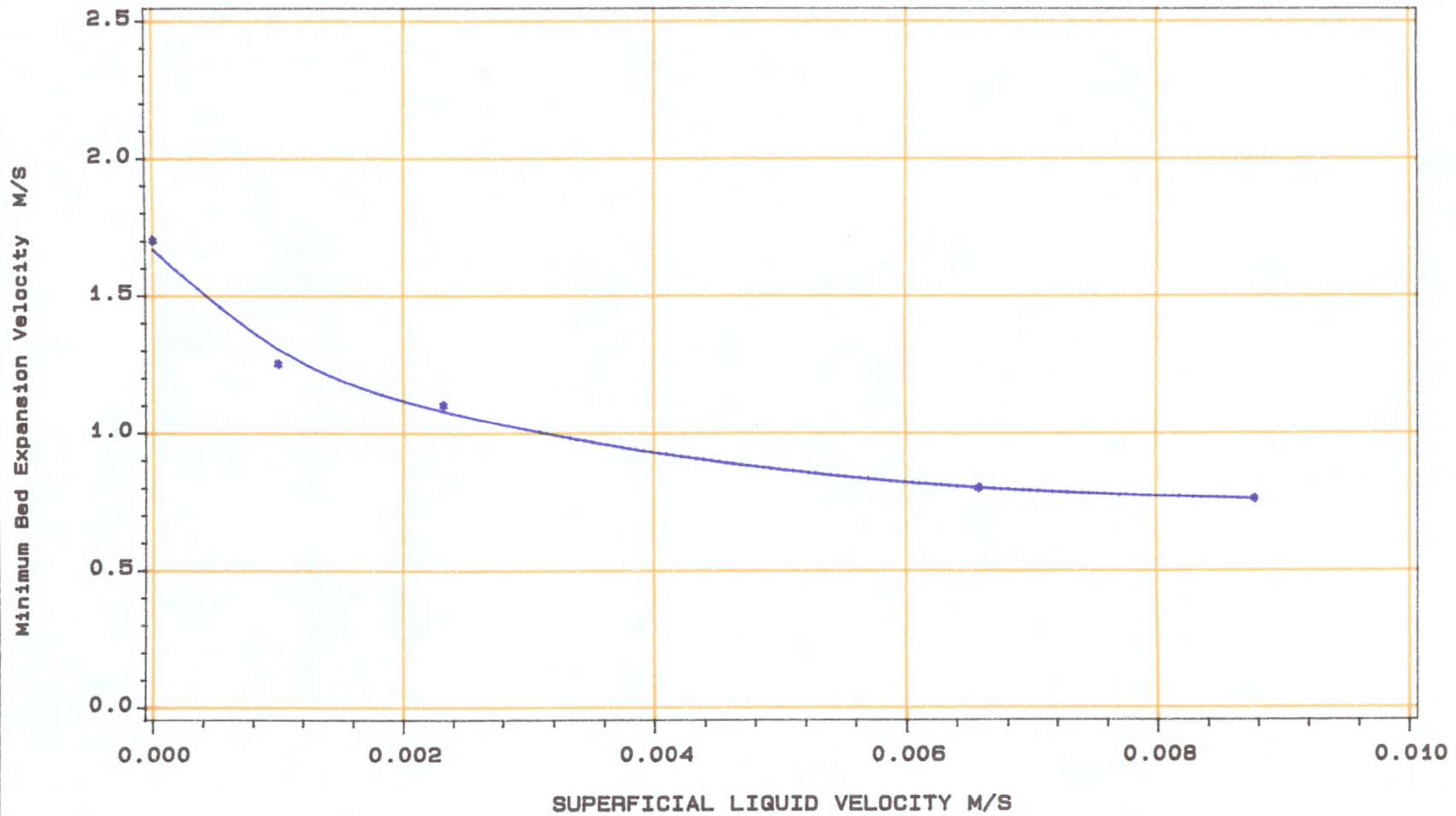


**Fig 5.1.6 Plot Of Variation Of Minimum Expanding Velocity With Liquid Rate For Oblate Spheroid Packing  
Packing Dia=50\*38 mm Bed Static Height=10.5 cm**

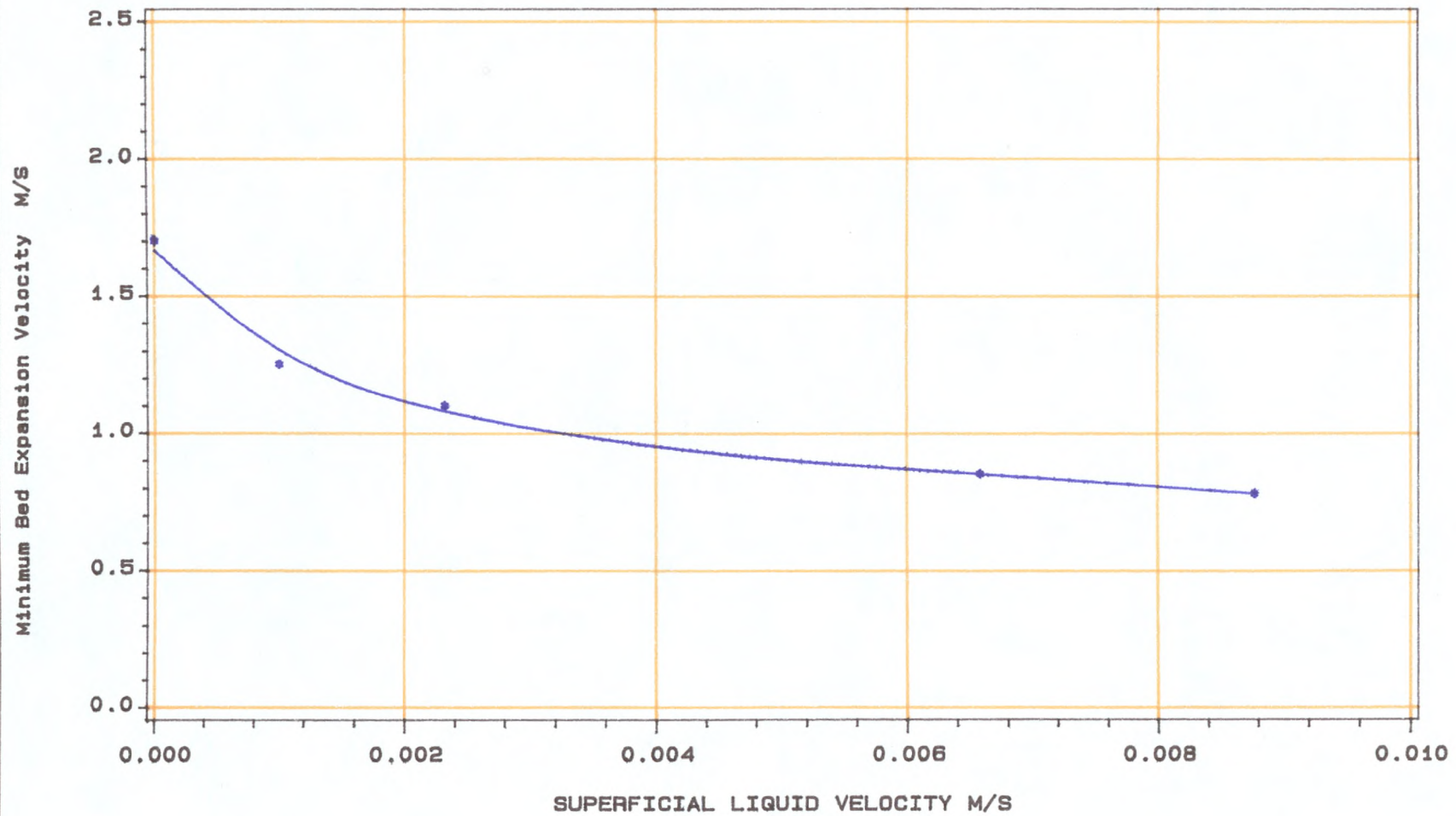


**Fig 5.1.7 Plot Of Variation Of Minimum Expanding Velocity With Liquid Rate For Plain Packing**  
**Packing Dia=25 mm Bed Static Height=10.5 Cm**

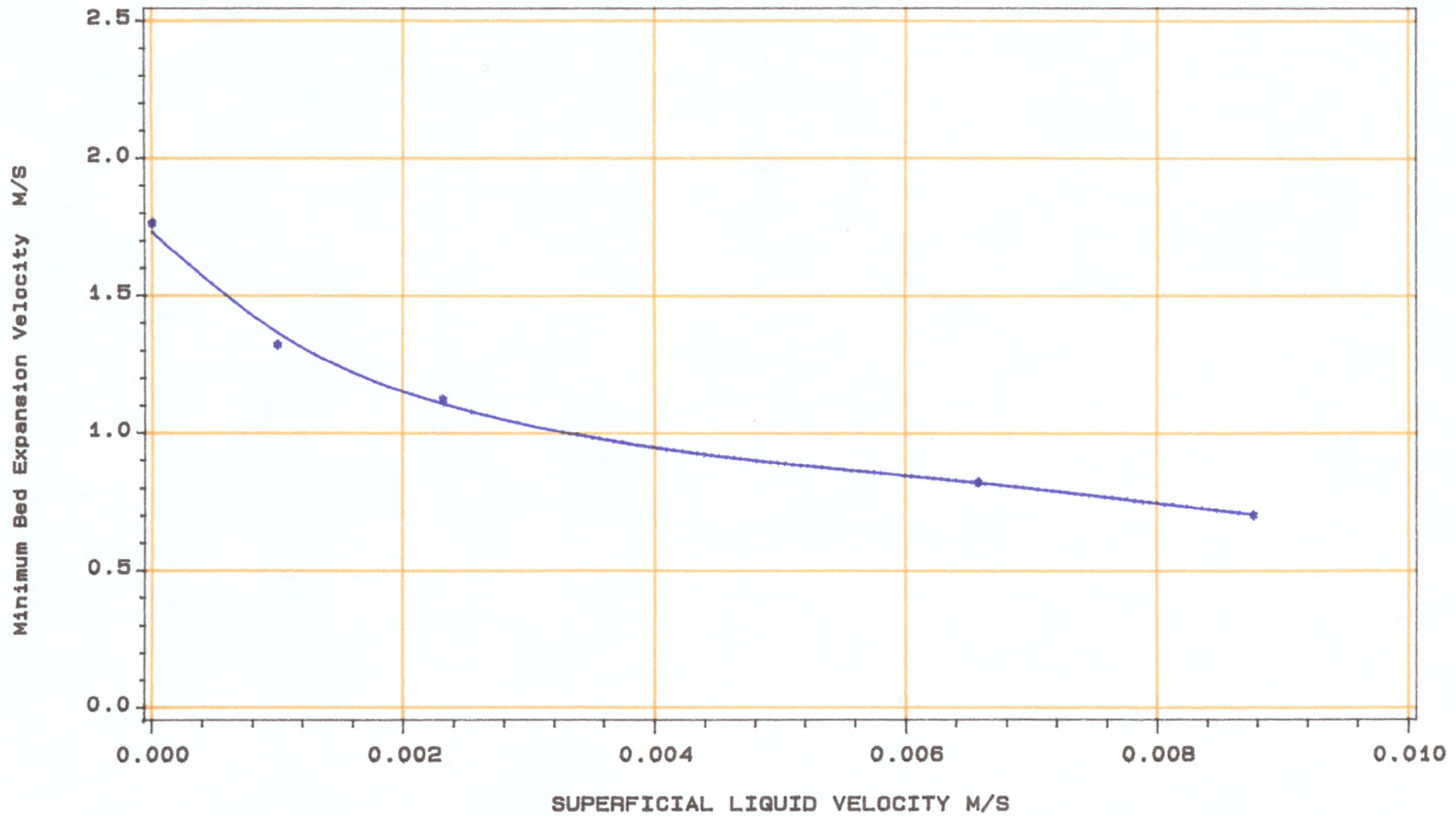
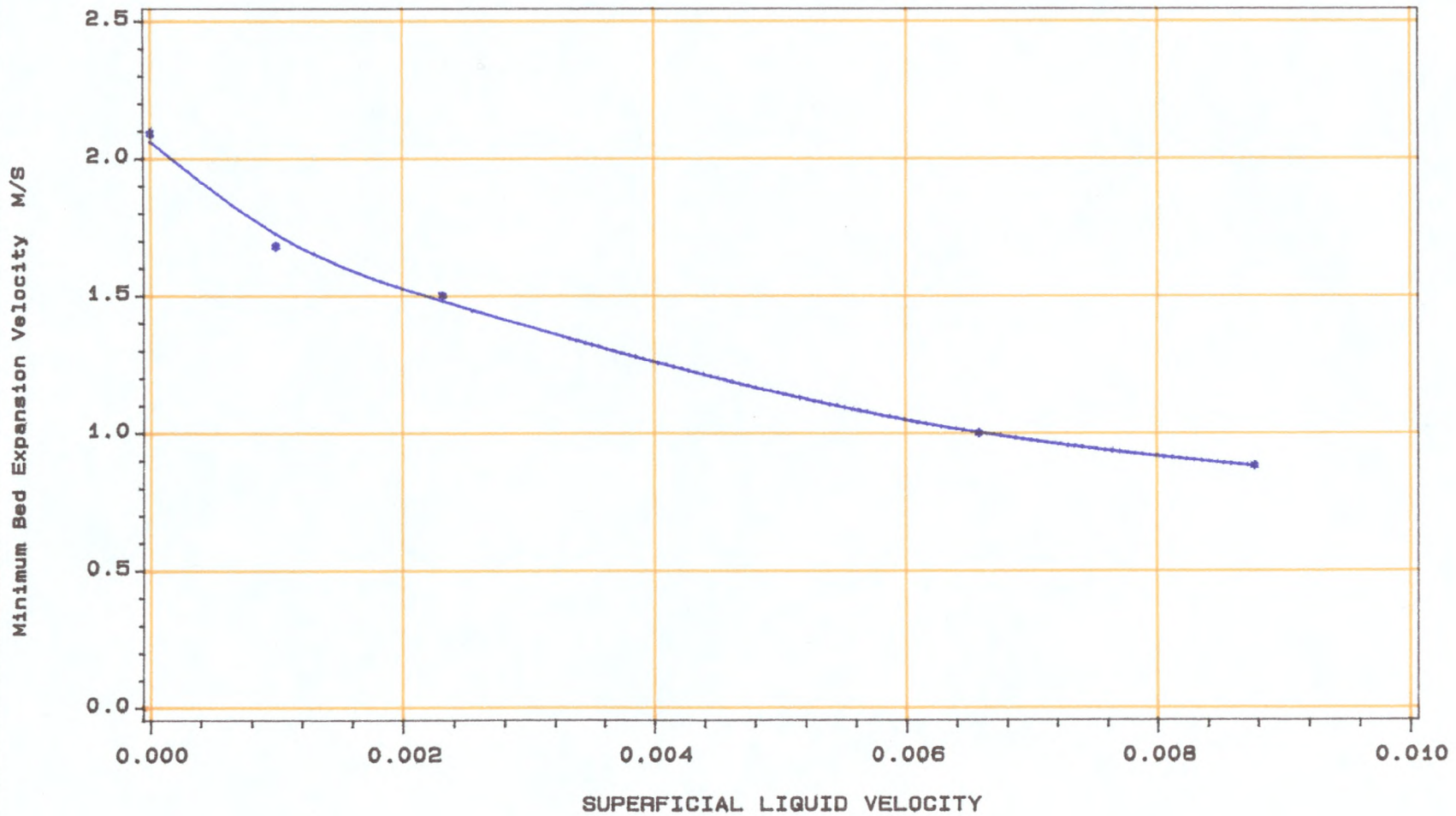


**Fig 5.1.8 Plot Of Variation Of Minimum Expanding Velocity With Liquid Rate For Slotted Packing**  
**Packing Dia=25 mm Bed Static Height=10.5 Cm**



and 25 mm slotted sphere packings, from which a similar behaviour is apparent as already observed in the case of 38 mm plain sphere packing.

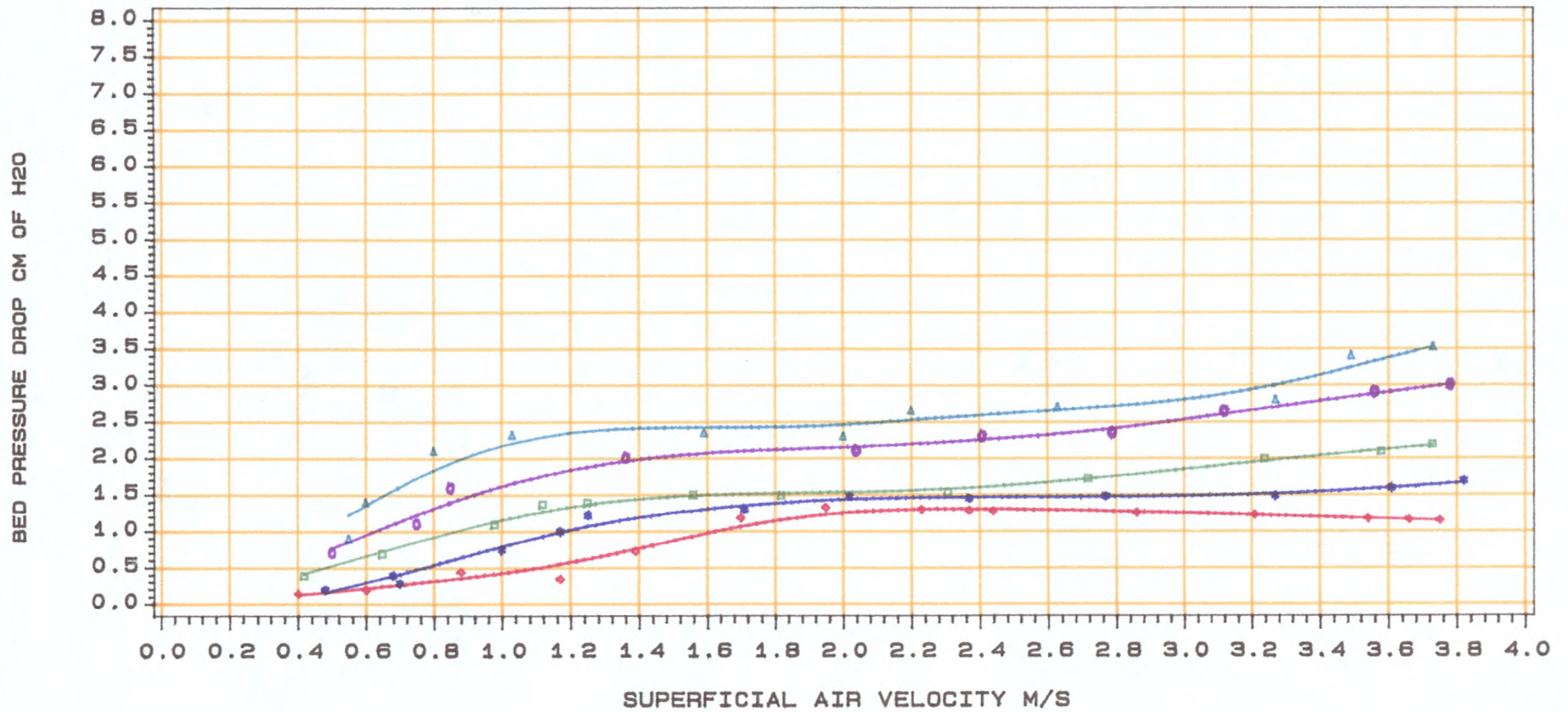
The variation of pressure drop with air and liquid velocities at bed static heights of 10.5 cm and 16.5 cm for oblate spheroids, 25 mm plain spheres and 25 mm slotted sphere packings are shown in figures 5.1.9 to 5.1.11 and 5.1.12 to 5.1.14. It can be seen that variation of pressure drop with air and liquid velocities for both bed static heights of 10.5 cm and 16.5 cm show a similar trend as in the case of the 38 mm diameter sphere packing.

Variation of pressure drop with bed static height for the oblate spheroid, 25 mm diameter plain sphere and slotted packing are shown in figures 5.1.15 to 5.1.17. It is apparent that the observed pressure drop variation with bed static height is greater for the bed static height of 16.5 cm since the weight of bed is increased due to the larger number of packings and higher liquid hold up.

### **5.1.3. Wall Effect.**

In the early stages of the pressure drop experiments, a star shaped liquid distributor with a 16 cm diameter length was used. In these experiments, an occasional wall effect manifested itself, especially at the higher liquid rates ( $6.58 \times 10^{-3}$  m/s and  $8.77 \times 10^{-3}$  m/s), due to only part of the liquid pouring on the central part of the bed, while the rest flowed off along the packings near the wall. Therefore, the motion of packings adjacent to the column wall due to the surface tension effect of water, was constrained and the packings at the wall did not fluidize effectively. The expanded bed height of the central part of bed was lower and consequently, as a result of this wall effect, the bed pressure drop was lowered.

Fig 5.1.9 Plot Of Pressure Drop Characteristics Of Oblate Spheroid Packing  
 Packing Dia=50\*38 mm Bed static Height=10.5 cm  
 FOR VARIOUS SUPERFICIAL LIQUID VELOCITY



DRY BED  
 $v_{min}=1.7$  M/S

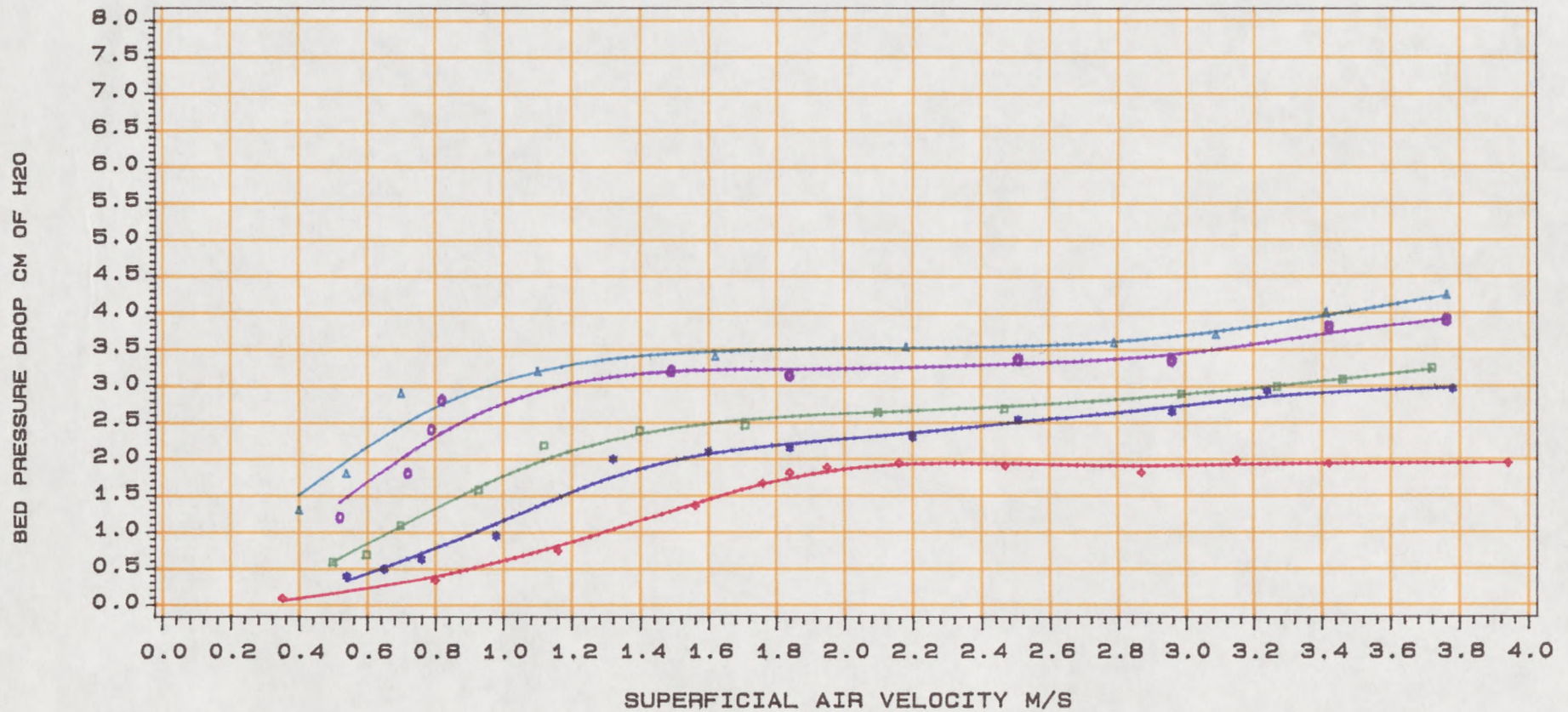
$VL=1E-3$  M/S  
 $v_{min}=1.25$  M/S

$VL=2.32E-3$  M/S  
 $v_{min}=1.10$  M/S

$VL=6.58E-3$  M/S  
 $v_{min}=0.85$  M/S

$VL=8.77E-3$  M/S  
 $v_{min}=0.80$  M/S

Fig 5.1.10 Plot Of Pressure Drop Characteristics Of Plain Sphere Packing  
 Packing Dia=25 mm, Bed Static Height=10.5 Cm  
 FOR VARIOUS SUPERFICIAL LIQUID VELOCITY



DRY BED  
 $V_{min}=1.76$  M/S

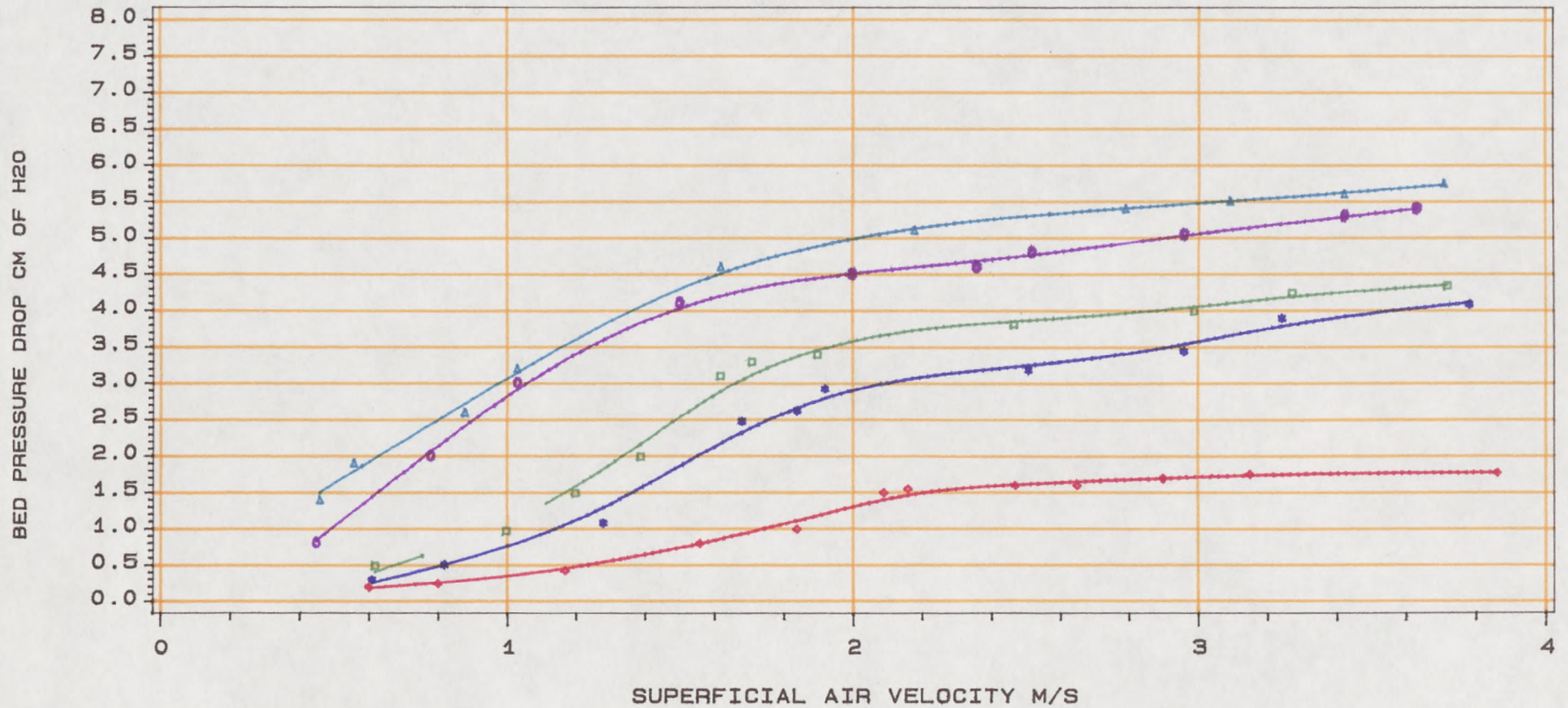
VL=1E-3 M/S  
 $V_{min}=1.32$  M/S

VL=2.32E-3 M/S  
 $V_{min}=1.12$  M/S

VL=6.58E-3 M/S  
 $V_{min}=0.82$  M/S

VL=8.77E-3 M/S  
 $V_{min}=0.70$  M/S

Fig 5.1.11 Plot Of Pressure Drop Characteristics Of Slotted Sphere Packing  
 Packing Dia=25 mm Open Area=0.11 Bed Static Height=10.5 Cm  
 FOR VARIOUS SUPERFICIAL LIQUID VELOCITY



DRY BED  
 V<sub>min</sub>=2.09 M/S

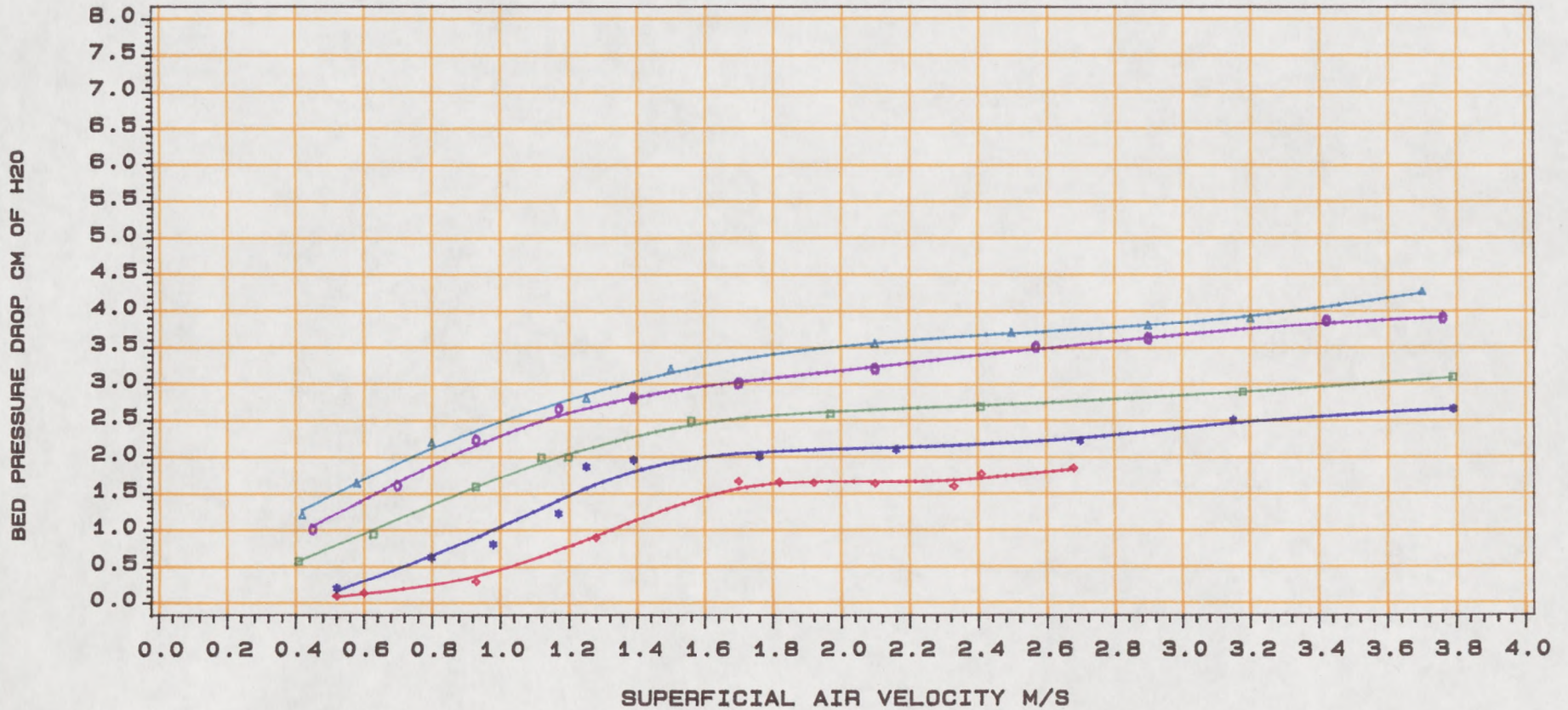
L=2.2 LIT/MIN  
 V<sub>min</sub>=1.68 M/S

L=5.3 LIT/MIN  
 V<sub>min</sub>=1.49 M/S

L=15 LIT/MIN  
 V<sub>min</sub>=1.03 M/S

L=20 LIT/MIN  
 V<sub>min</sub>=0.88 M/S

Fig 5.1.12 Plot Of Pressure Drop Characteristics Of Oblate Spheroid Packing  
 Packing Dia=5\*38 mm Bed Static Height=16.5 cm  
 FOR VARIOUS SUPERFICIAL LIQUID VELOCITY



DRY BED  
 V<sub>min</sub>=1.68 M/S

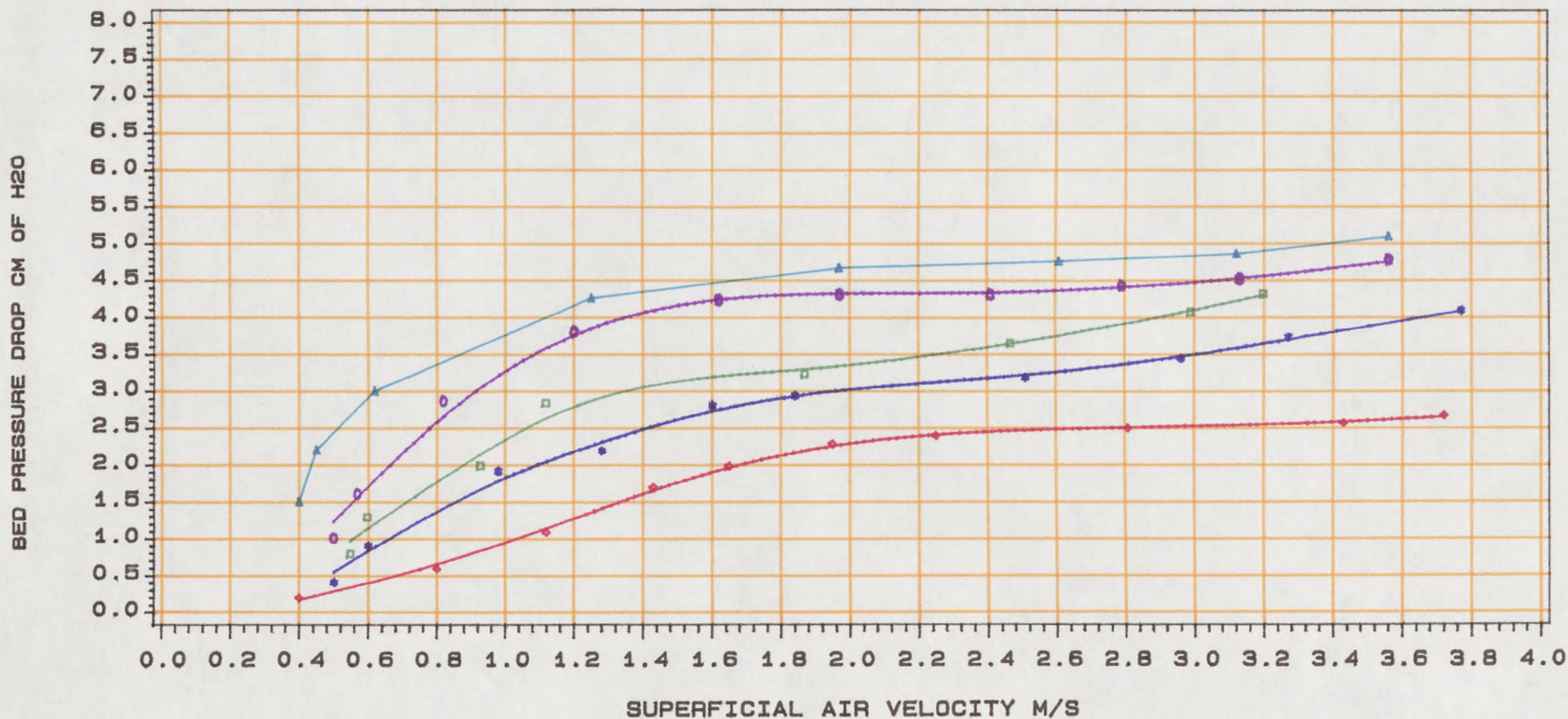
VL=1E-3 M/S  
 V<sub>min</sub>=1.25 M/S

VL=2.32E-3 M/S  
 V<sub>min</sub>=1.12 M/S

VL=6.58E-3 M/S  
 V<sub>min</sub>=0.93 M/S

VL=8.77E-3 M/S  
 V<sub>min</sub>=0.8 M/S

Fig 5.1.13 Plot Of Pressure Drop Characteristics Of Plain Sphere Packing  
 Packing Dia=25 mm Bed Static Height=16.5 Cm  
 FOR VARIOUS SUPERFICIAL LIQUID VELOCITY



DRY BED  
 $V_{min}=1.95$  M/S

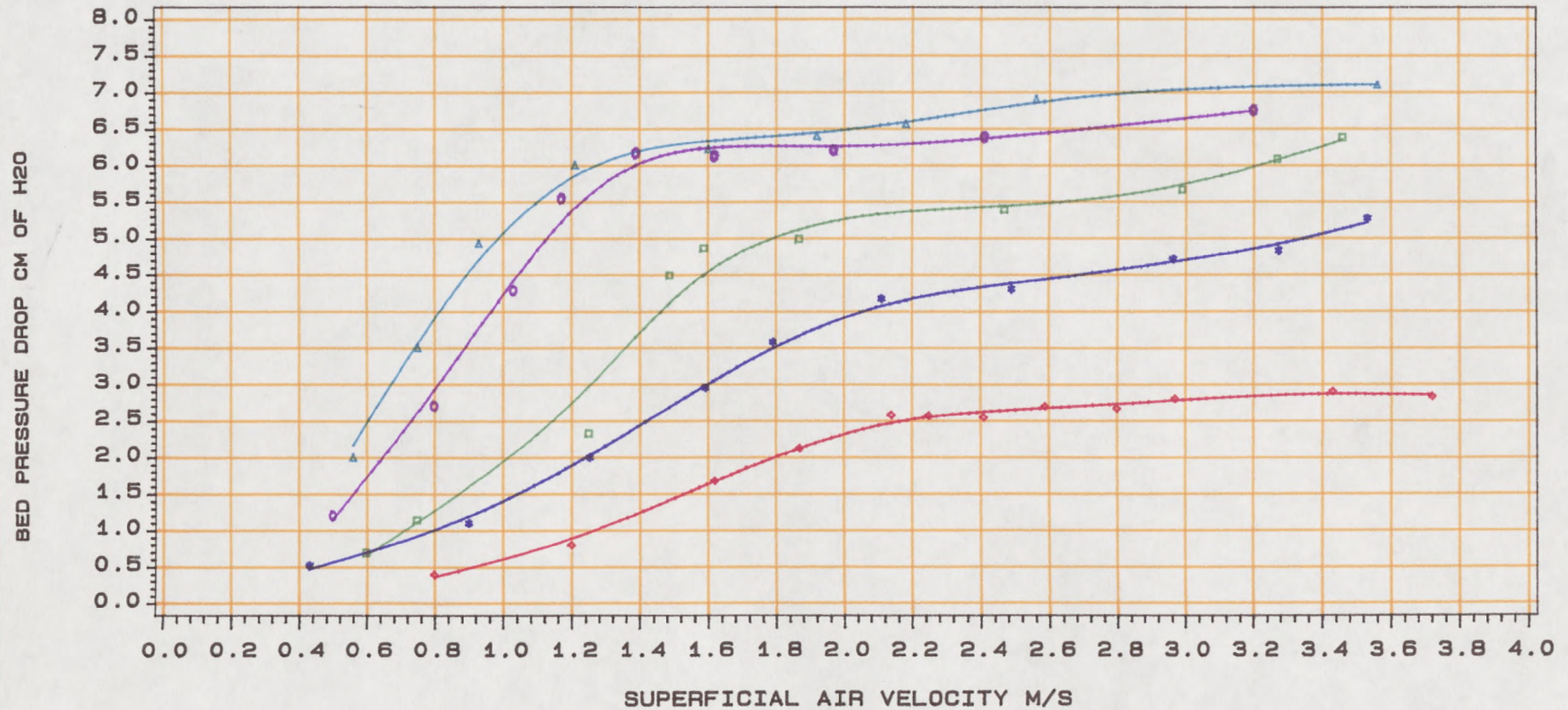
$V_L=1E-3$  M/S  
 $V_{min}=1.28$  M/S

$V_L=2.32E-3$  M/S  
 $V_{min}=1.12$  M/S

$V_L=6.58E-3$  M/S  
 $V_{min}=0.82$  M/S

$V_L=8.77E-3$  M/S  
 $V_{min}=0.62$  M/S

Fig 5.1.14 Plot Of Pressure Drop Characteristics Of Slotted Sphere Packing  
 Packing Dia=25 mm Open Area=0.11 Bed Static Height=16.5 Cm  
 FOR VARIOUS SUPERFICIAL LIQUID VELOCITY



DRY BED  
Vmin=2.14 M/S

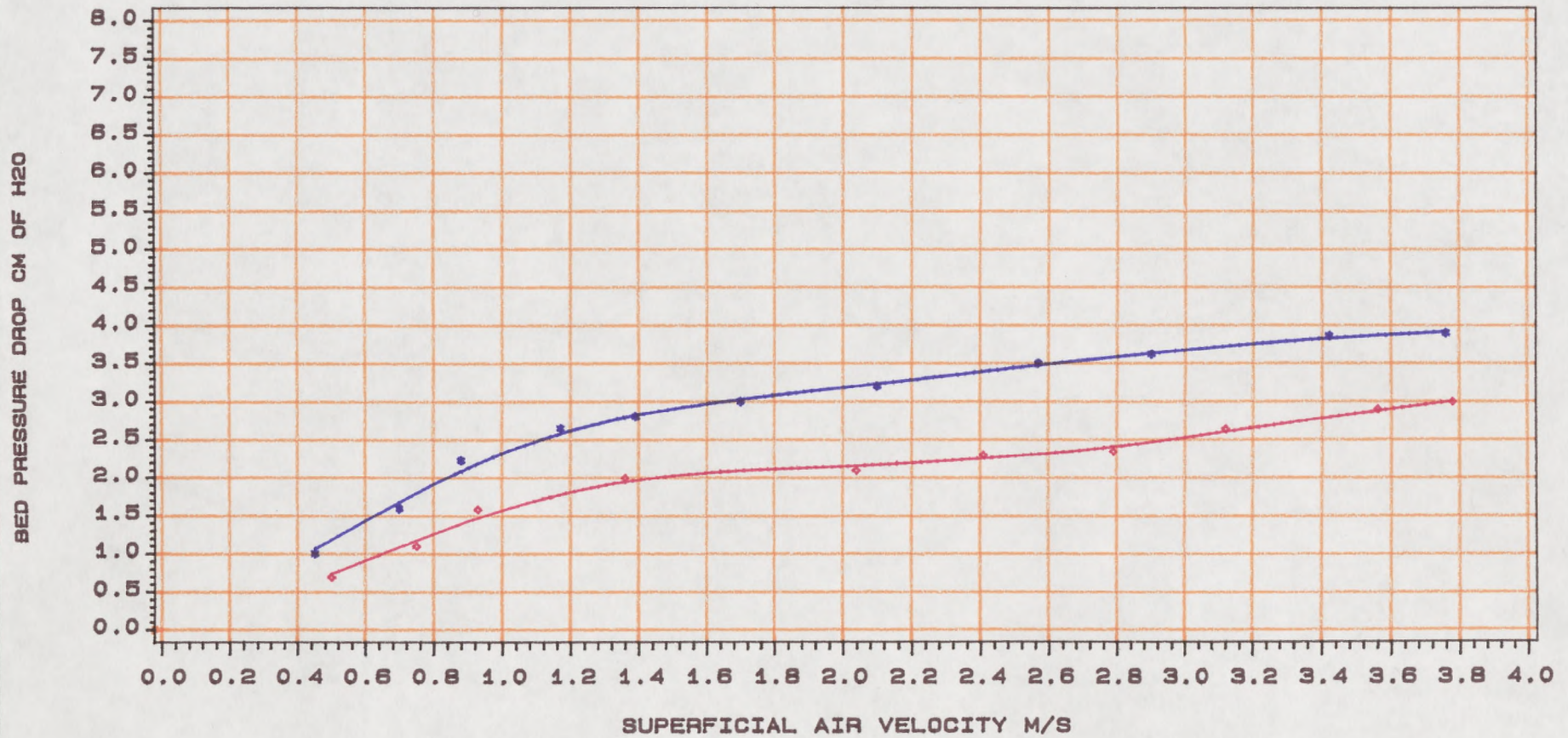
VL=1E-3 M/S  
Vmin=1.79 M/S

VL=2.32E-3 M/S  
Vmin=1.49 M/S

VL=6.58E-3 M/S  
Vmin=1.03 M/S

VL=8.77E-3 M/S  
Vmin=0.93 M/S

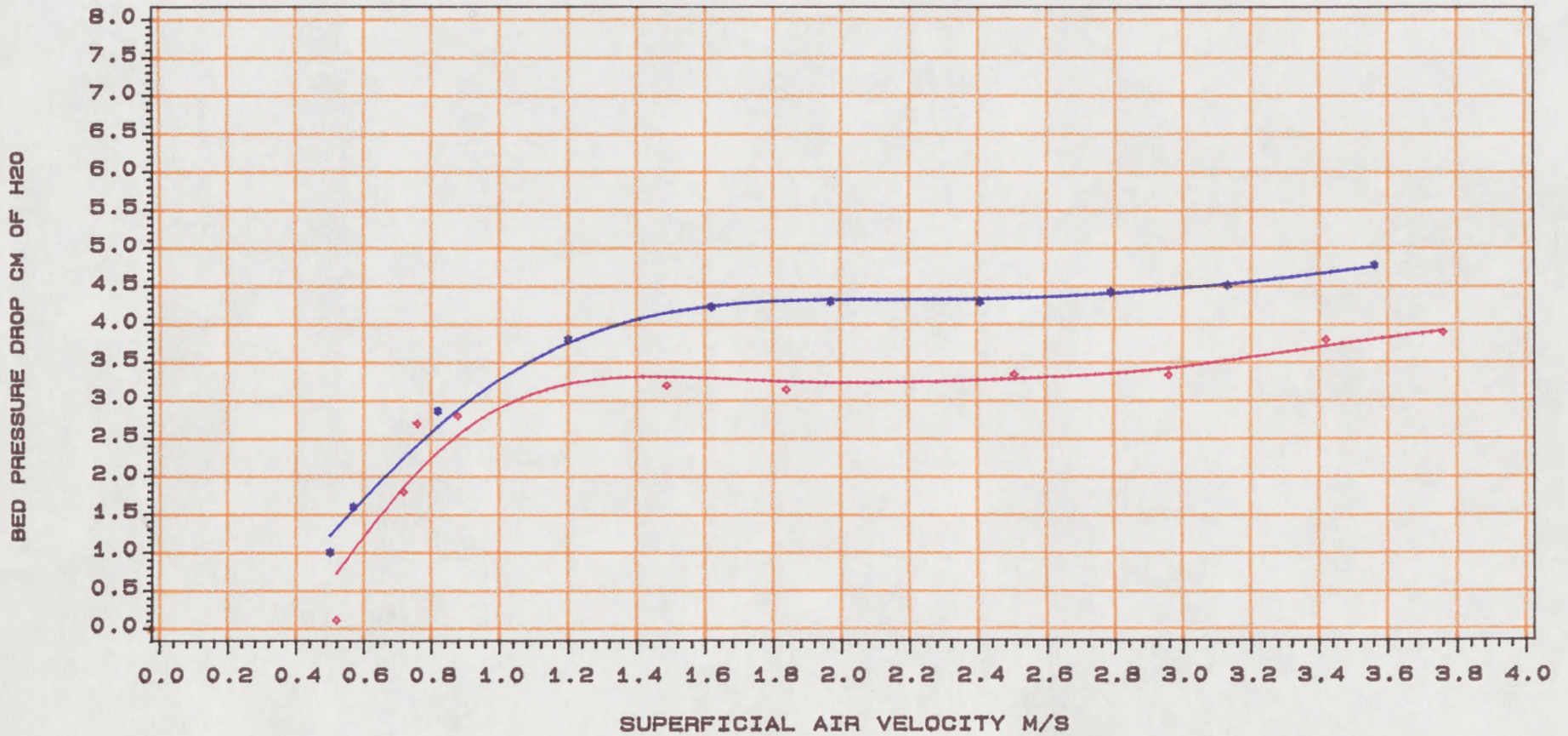
**Fig 5.1.15 Plot Of Pressure Drop Characteristics Of Oblate Spheroid Packing**  
**Packing Dia=25 mm,H=10.5 CM AND H=16.5 CM**  
**SUPERFICIAL LIQUID VELOCITY=8.77E-3 M/S**



H=10.5 CM

H=16.5 CM

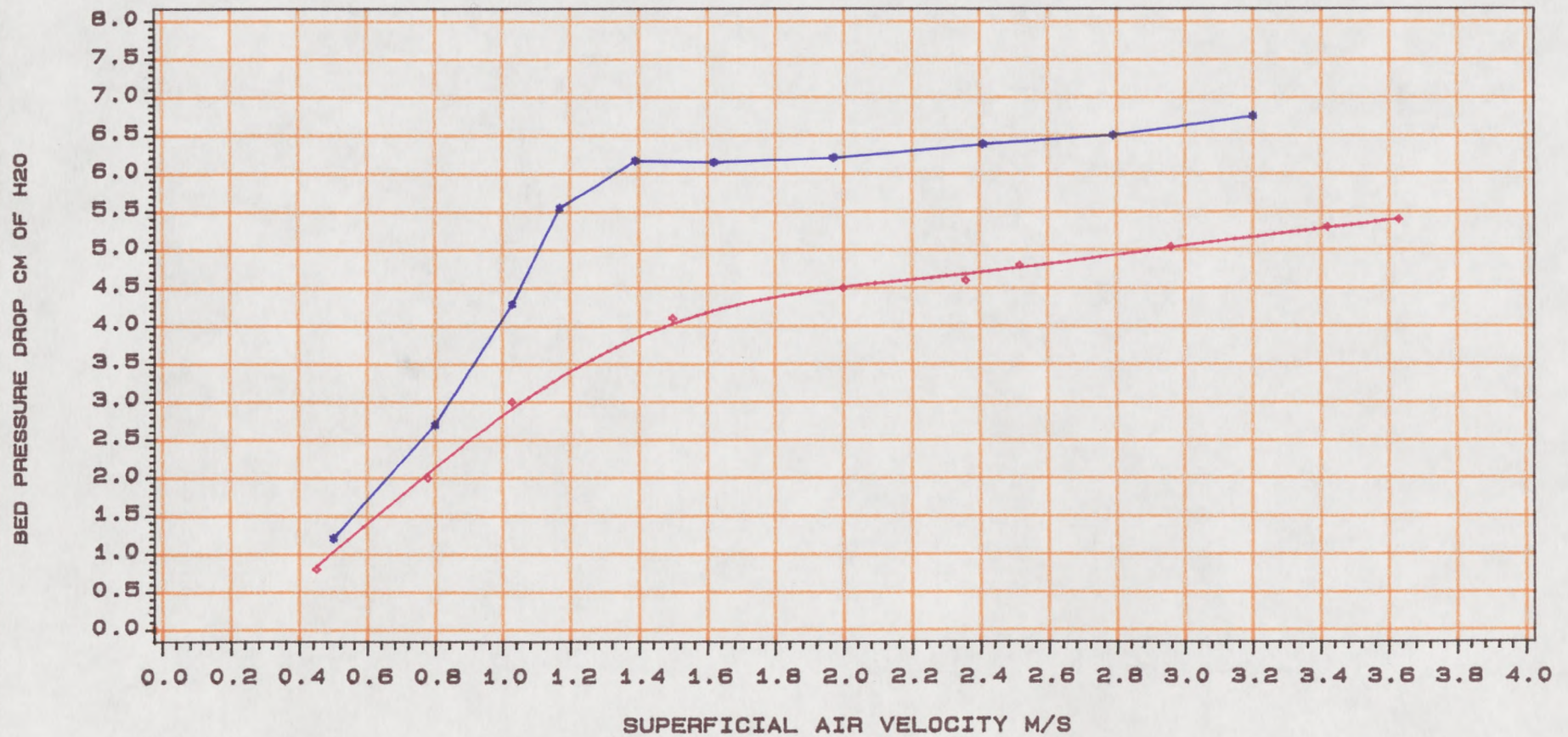
**Fig 5.1.16 Plot Of Pressure Drop Characteristics Of Plain Sphere Packing**  
**Packing Dia=25 mm,H=10.5 CM AND H=16.5 CM**  
**FOR SUPERFICIAL LIQUID VELOCITY=8.77E-3 M/S**



H=10.5 CM

H=16.5 CM

Fig 5.1.17 Plot Of Pressure Drop Characteristics Of Slotted Sphere Packing  
 Packing Dia=25 mm,H=10.5 CM AND H=16.5 CM  
 SUPERFICIAL LIQUID VELOCITY=8.77E-3 M/S



H=10.5 CM

H=16.5 CM

In order to avoid the wall effect, a shower type liquid distributor was then used which distributed water over the central part of the bed.

Figures 5.1.18 to 5.1.21 and 5.1.22 to 5.1.25 show wall effect on the pressure drop for the oblate spheroid, 38 mm plain sphere, 25 mm plain sphere and 25 mm slotted packing at two different liquid rates of  $2.32 \times 10^{-3}$  m/s and  $6.58 \times 10^{-3}$  m/s respectively.

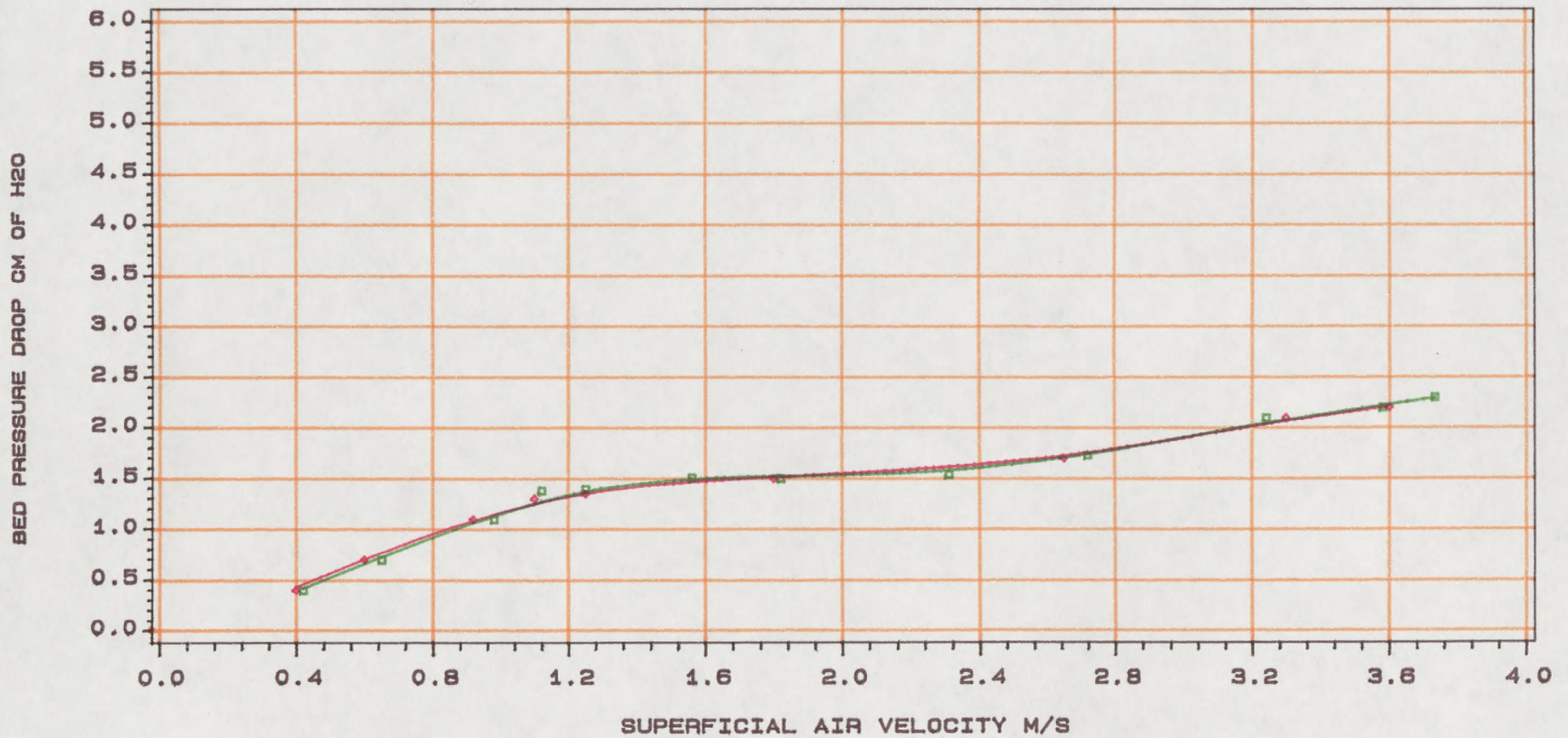
From figures 5.1.21 to 5.1.24 it can be seen that the wall effect is generally very small for the liquid rate of  $2.32 \times 10^{-3}$  m/s so that there is very little difference in the pressure drop between the cases where there is practically no wall effect.

Figures 5.1.22 to 5.1.25 show the wall effect on the pressure drop for a liquid rate of  $6.58 \times 10^5$  m/s. It can be seen that the effect of the wall is more pronounced at this liquid rate, especially for the slotted packing. This is because at the higher liquid rate, more liquid was residing between the packings and the wall, which is also the case for the slotted sphere packing.

Similar findings were observed by Rao et al. (24) and Tichy and Douglas (54). They reported that in some cases, a strong wall effect was present and a relatively immovable regularly stacked layer of packings built up at the wall. In dry fluidized beds, the wall effect is a function of the ratio of the column to the packing diameter as in the case of fixed beds.

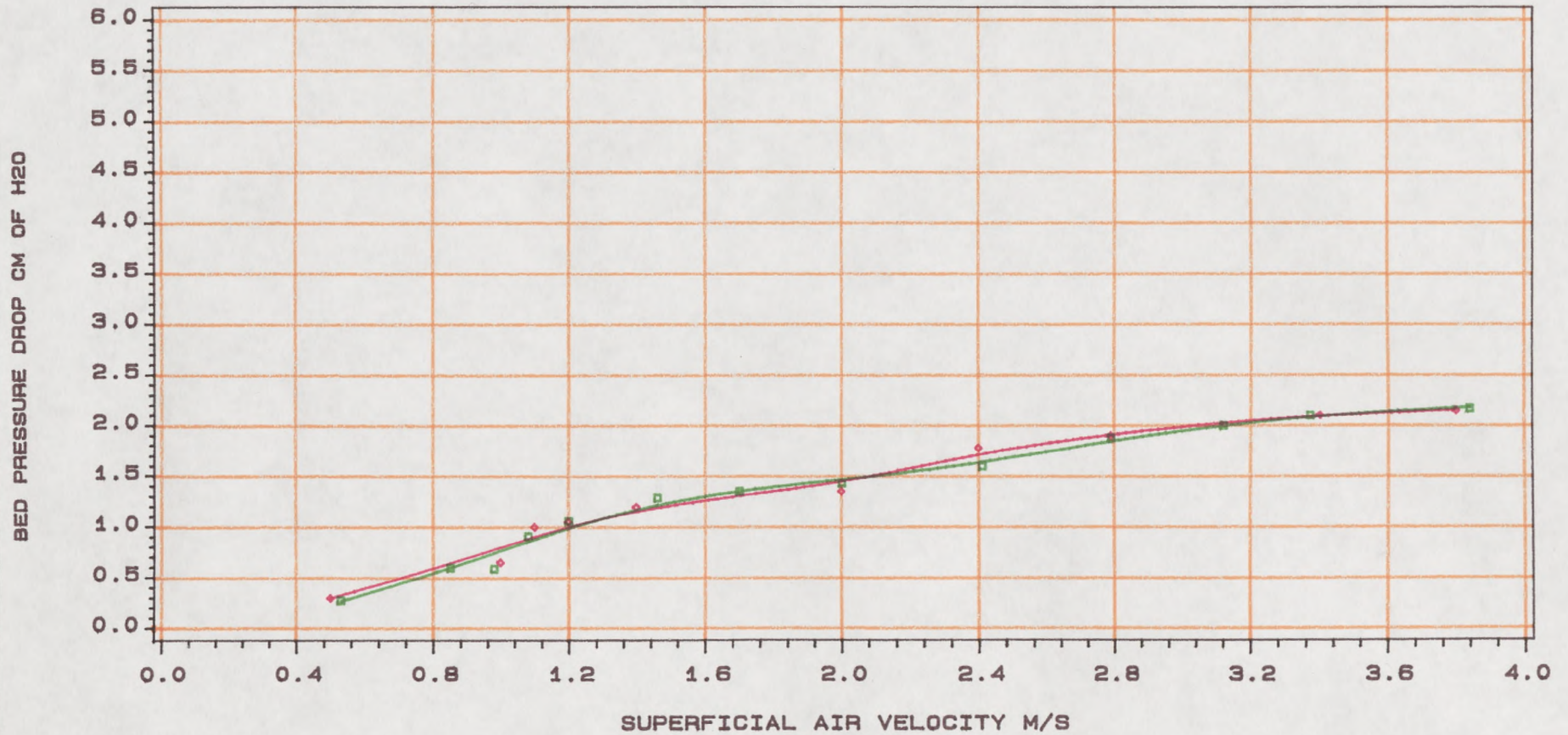
In order to reduce the wall effect, a fixed bed should have a ratio larger than about 10, Douglas et al (18) and Gelperin et al (8). In TCA, higher values of this ratio will improve the quality of

**Fig 5.1.18 Influence Of Wall Effect On Pressure Drop For Oblate Spheroid Packing**  
**Packing Dia=50\*38 mm Static Bed Height=10.5 cm**  
**SUPERFICIAL LIQUID VELOCITY=2.32E-3 M/S**



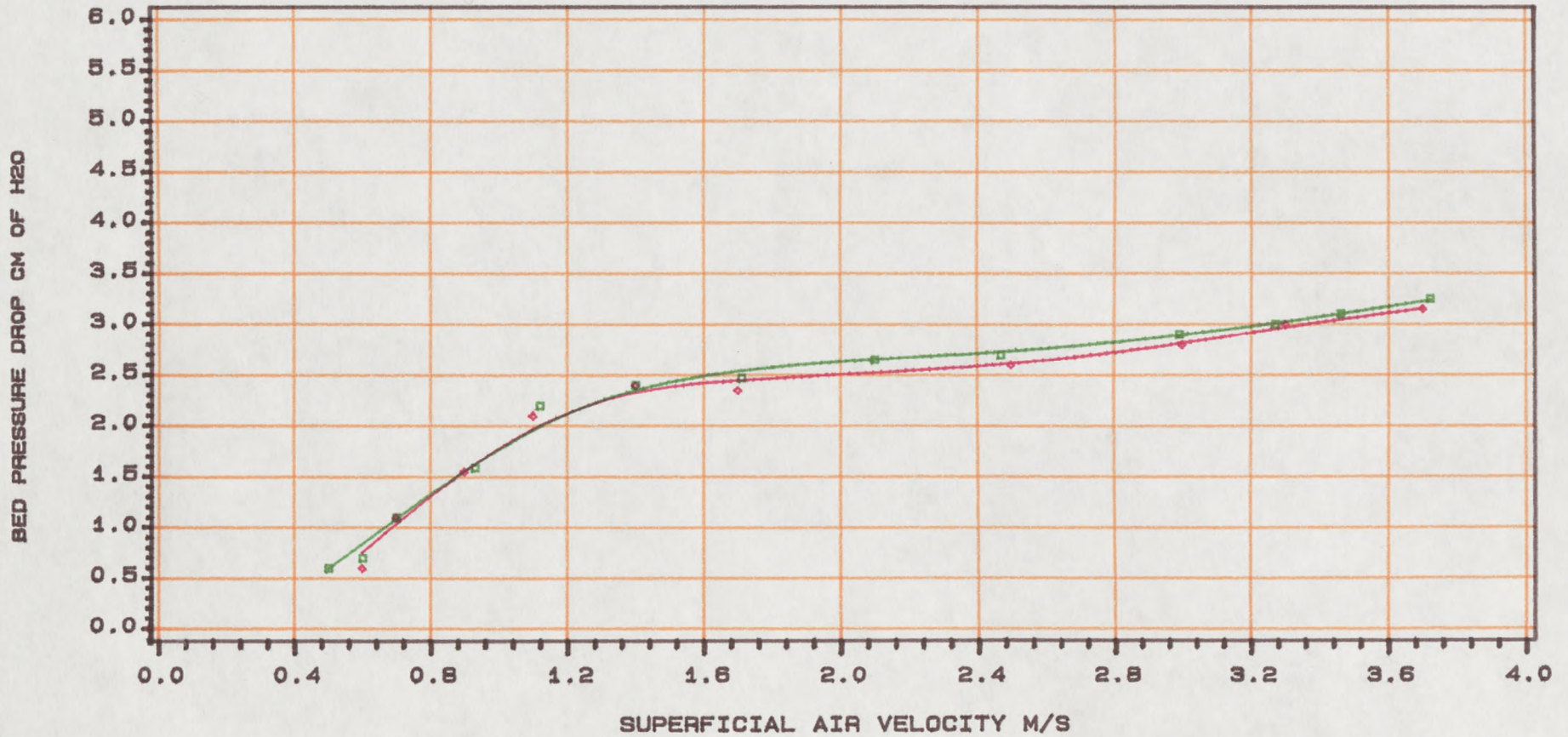
with wall effect      without wall effect

**Fig 5.1.19 Influence Of Wall Effect On Pressure Drop For Plain Sphere Packing**  
Packing Dia=38 mm Bed Static Height=10.5 CM  
SUPERFICIAL LIQUID VELOCITY=2.32E-3 M/S



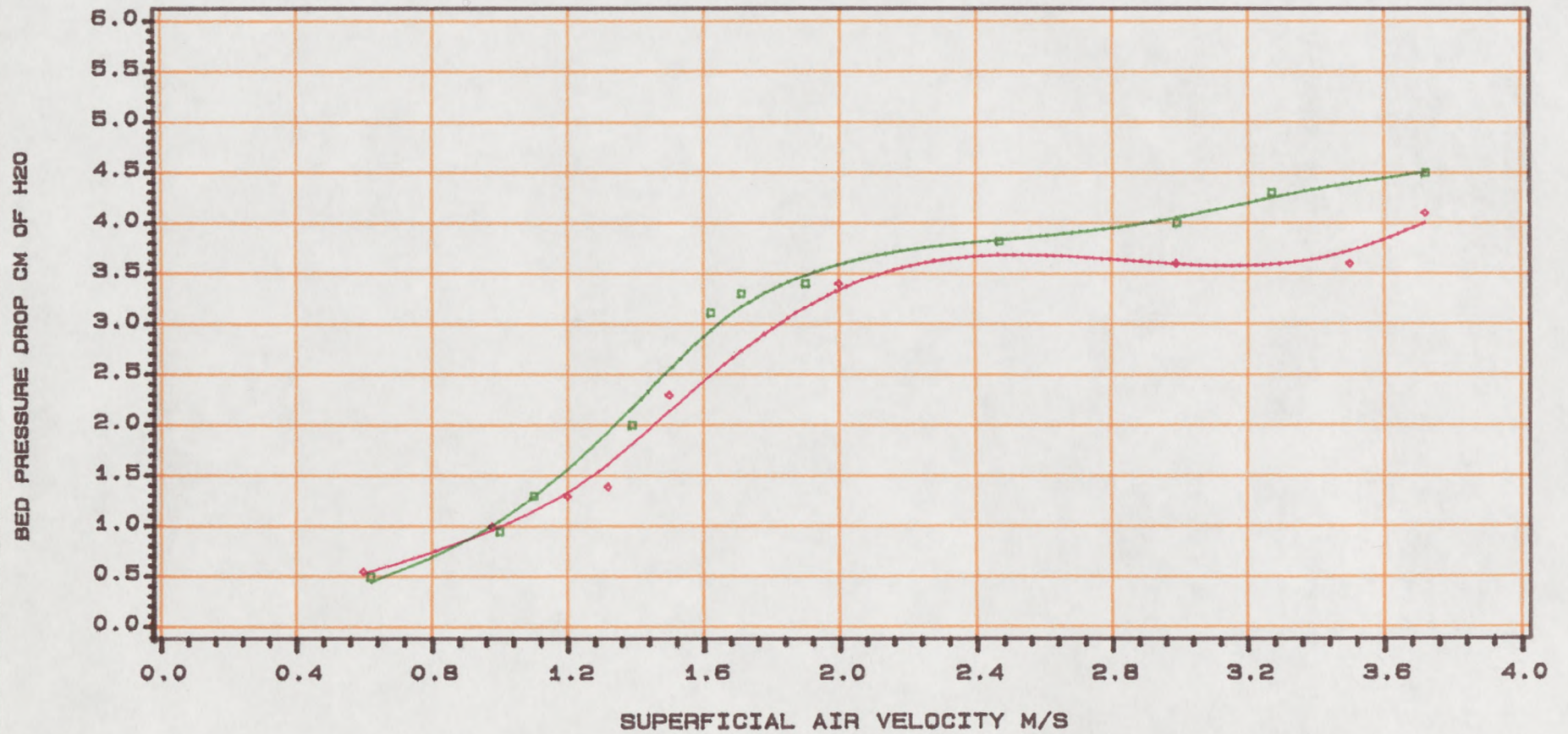
with wall effect      without wall effect

**Fig 5.1.20 Influence Of Wall Effect On Pressure Drop For Plain Sphere Packing**  
**Packing Dia=25 mm Bed Static Height= 10.5 CM**  
**SUPERFICIAL LIQUID VELOCITY=2.32E-3 M/S**



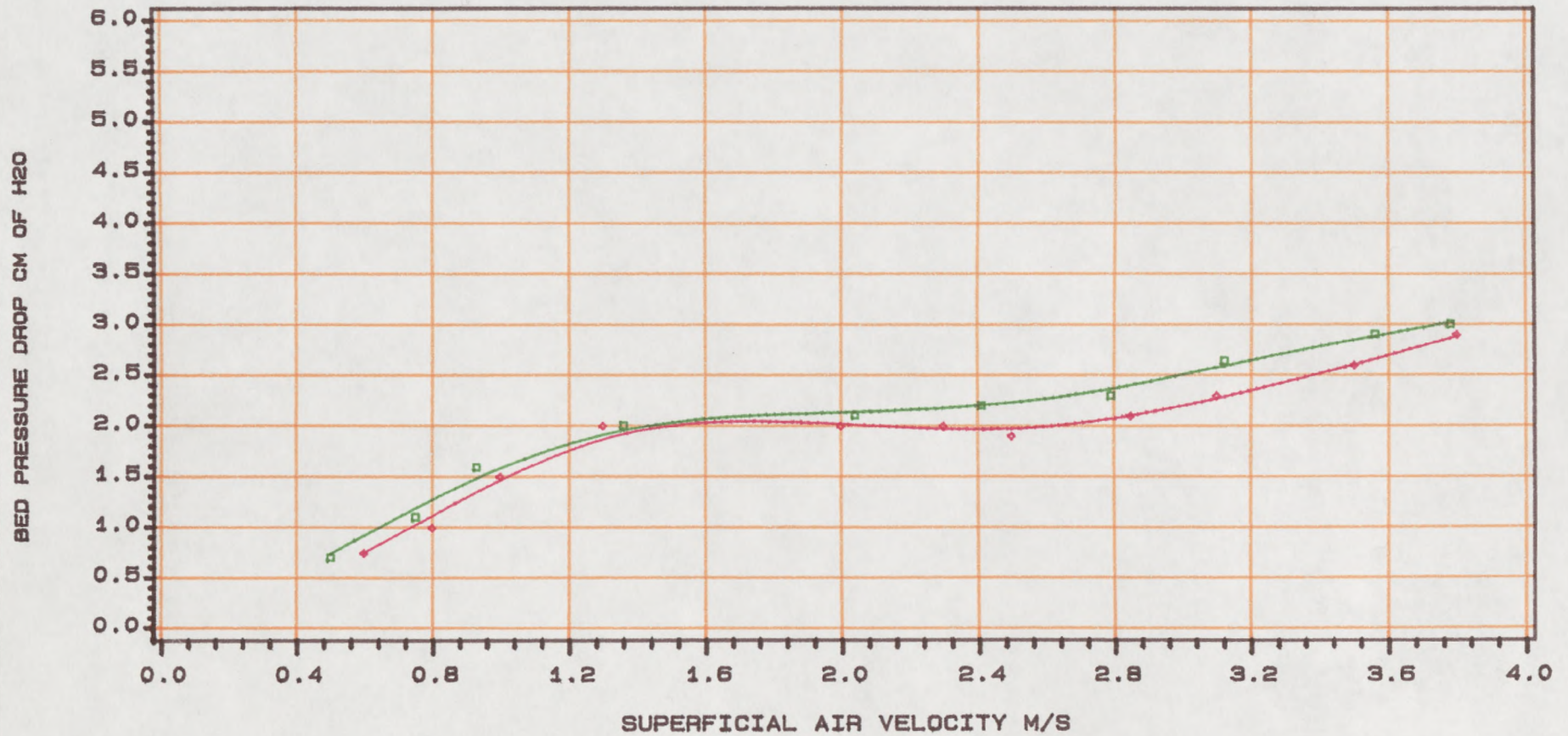
With wall effect      Without wall effect

Fig 5.1.21 Influence Of Wall Effect On Pressure Drop For Slotted Sphere Packing  
 Packing Dia=25 mm Open Area=0.11 Bed Static Height=10.5 Cm  
 SUPERFICIAL LIQUID VELOCITY=2.32E-3 M/S



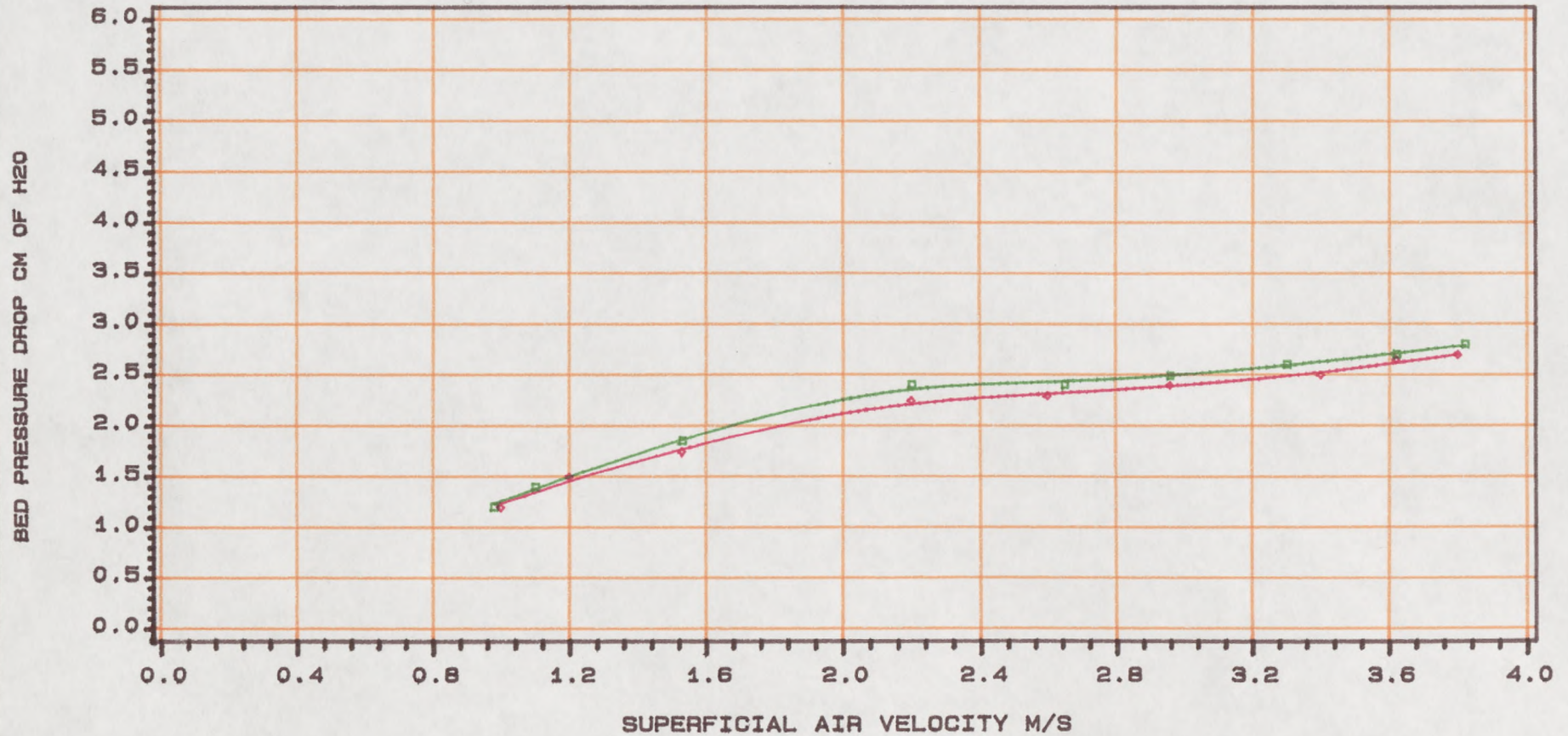
With wall effect      without wall effect

Fig 5.1.22 Influence Of Wall Effect On Pressure Drop For Oblate Spheroid Packing  
 Packing Dia=50\*38 mm Bed Static Height=10.5 cm  
 SUPERFICIAL LIQUID VELOCITY =6.58E-3 M/S



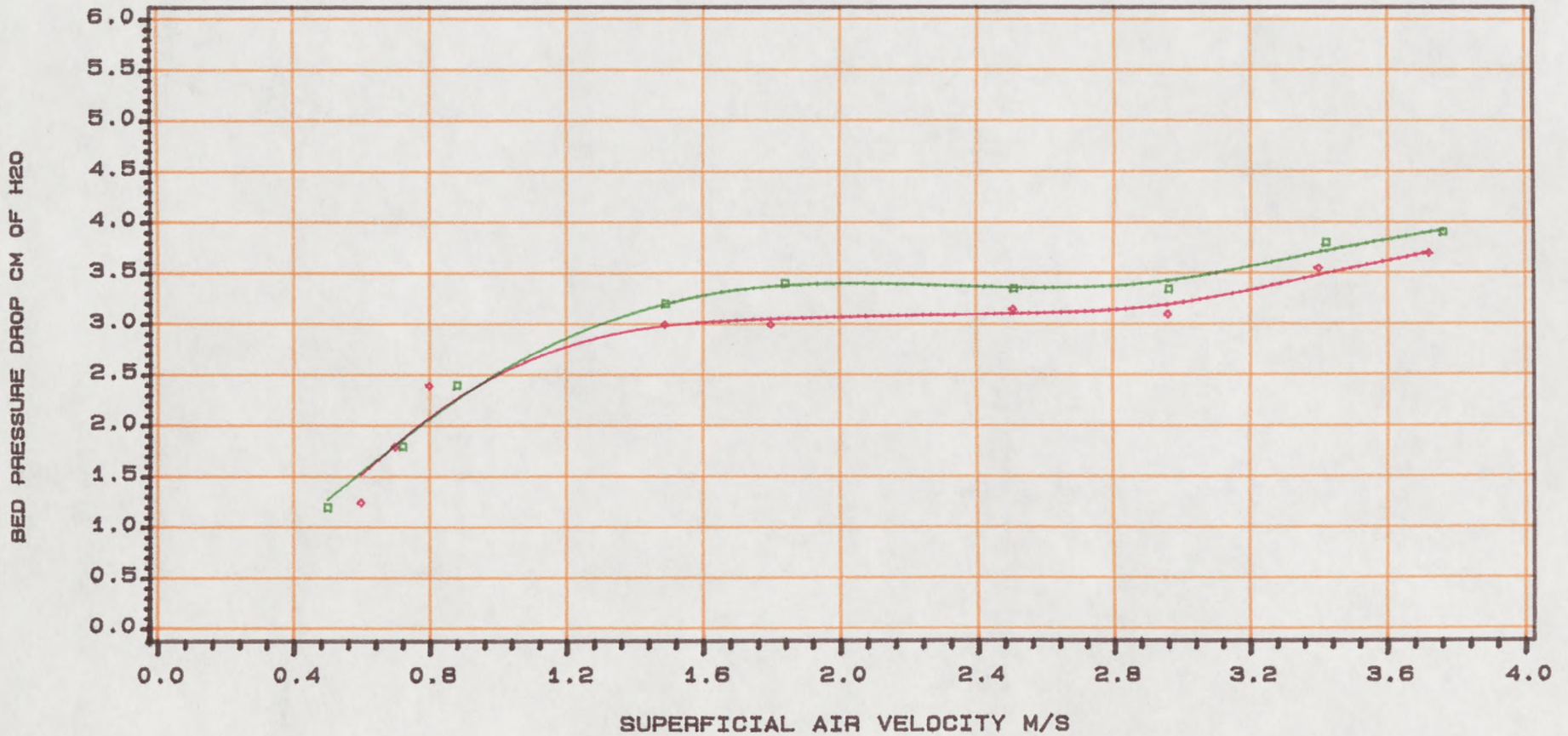
With wall effect      without wall effect

Fig 5.1.23 Influence Of Wall Effect On Pressure Drop For Plain Sphere Packing  
Packing Dia=38 mm Bed Static Height=10.5 CM  
Superficial Liquid Velocity=6.56E-3 M/S



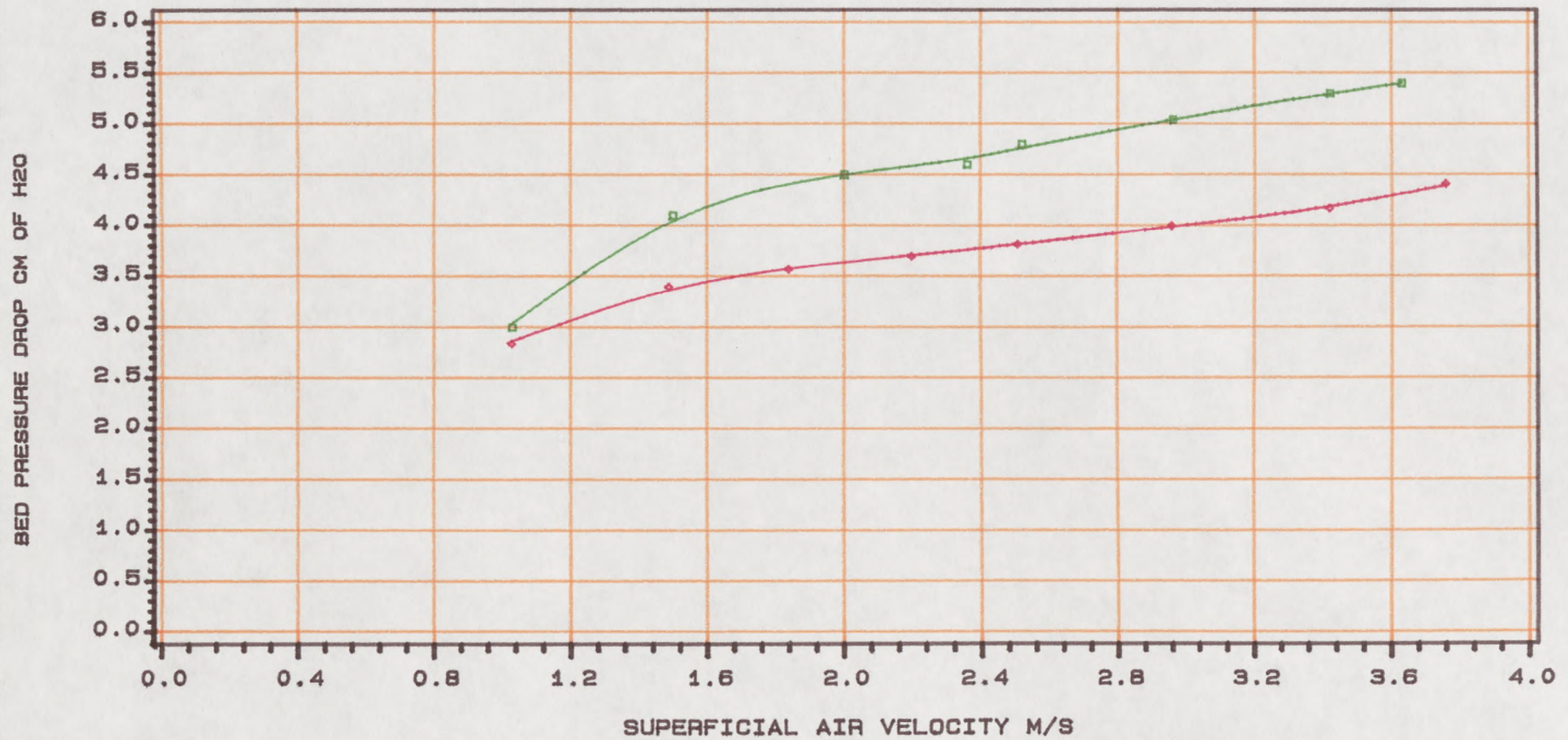
with wall effect      without wall effect

Fig 5.1.24 Influence Of Wall Effect On Pressure Drop For Plain Sphere Packing  
Packing Dia=25 mm Bed Static Height=10.5 CM  
SUPERFICIAL LIQUID VELOCITY=6.58E-3 M/S



With wall effect      without wall effect

Fig 5.1.25 Influence Of Wall Effect On Pressure Drop For Slotted Sphere Packing  
Packing Dia=25 mm Open Area=0.11 Bed Static Height=10.5 Cm  
SUPERFICIAL LIQUID VELOCITY=6.58E-3 M/S



with wall effect      without wall effect

fluidization. In dry fluidized beds, the wall effect is connected with the purely geometrical nature of the phenomenon, i.e, the ratio of column to packing diameter and the resulting voidage distribution, whereas in the irrigated bed, the action of the liquid surface (surface tension) encourages the flow of water to pass between the packings and the wall of the column, causing the packing to be held on to the wall. In this case the main feature displayed by the wall effect is produced by the action of the surface tension of the water being more important than the purely geometrical voidage distribution effect.

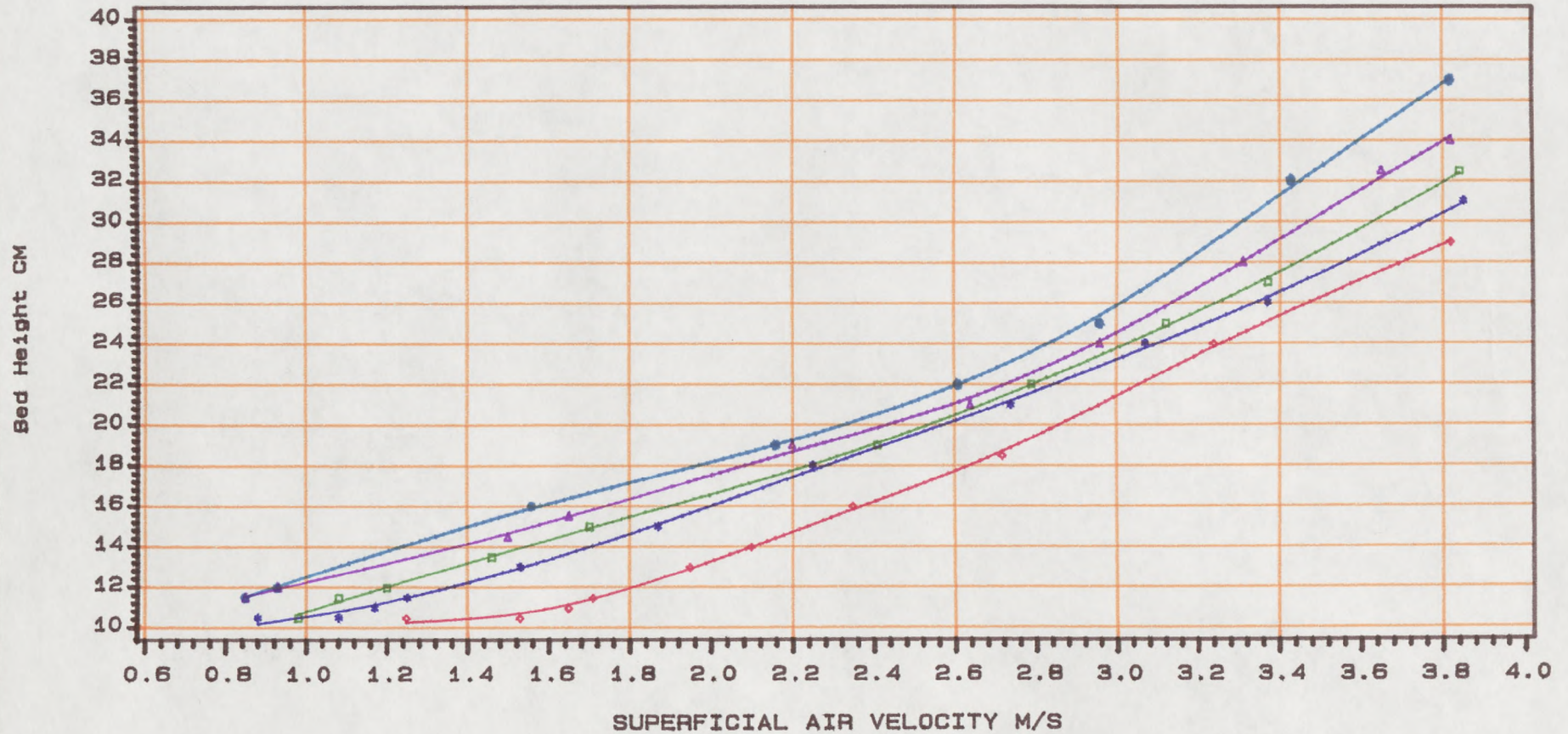
#### **5.1.4. Bed Expansion Characteristics.**

Figures 5.1.26 to 5.1.29 show the variation of expanded bed height with air and liquid velocity employing a bed static height of 10.5 cm for different packings. It can be seen that the bed height increases steadily with both air and liquid velocities.

The inspection of the bed expansion curves for the various packings and liquid rates suggests that the presence of gas channelling and by-passing is more noticeable at low fluidizing velocities and with the lowest liquid irrigation rates as indicated by the lower bed expansion rates. The higher rates of bed expansion observed at gas velocities above 2.5 m/s and with high liquid irrigation rates indicate the presence of more intimate uniform contacting between gas liquid and packings in these highly agitated beds.

Figures 5.1.30 to 5.1.33 show the effect of air and liquid velocities on the bed expansion for the oblate spheroids, 38 mm diameter plain spheres, 25 mm diameter slotted and plain spheres employing a bed static height of 16.5 cm. It can be seen that the variation of expanded bed height with air and liquid velocities, is similar to the case when

Fig 5.1.26 Plot Of Variation Of Bed Height With Superficial Air Velocity For Plain Sphere Packing  
 Packing Dia=38 mm Bed Static Height=10.5 Cm  
 For Various Superficial Liquid Velocity



Dry Bed

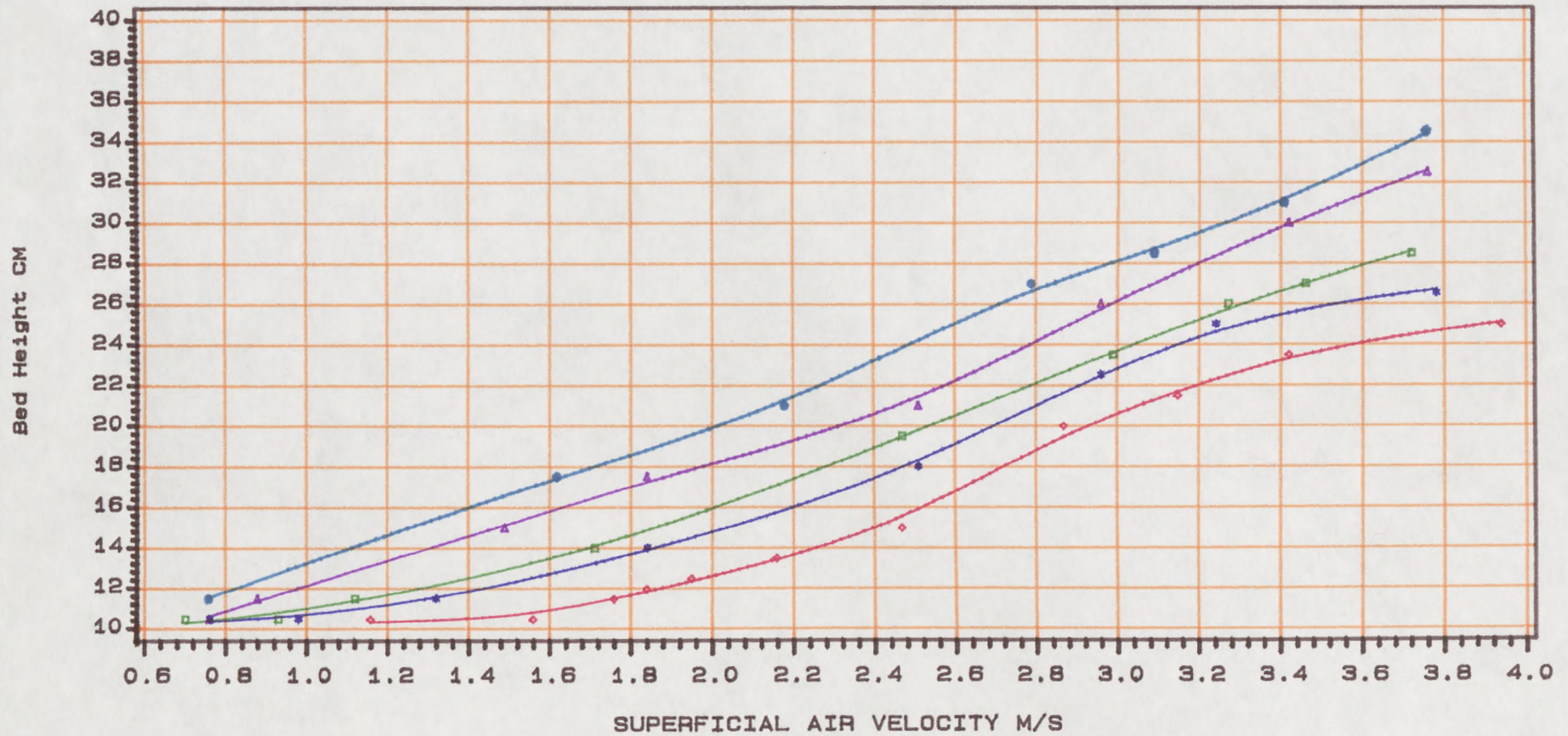
VL=1E-3 M/S

VL=2.32E-3 M/S

VL=6.58E-3 M/S

VL=8.77E-3 M/S

**Fig 5.1.27 Plot Of Variation Of Bed Height With Superficial Air Velocity For Plain Sphere Packing**  
**Packing Dia=25 mm Bed Static Height=10.5 Cm**  
**For Various Superficial Liquid Velocity**



Dry Bed

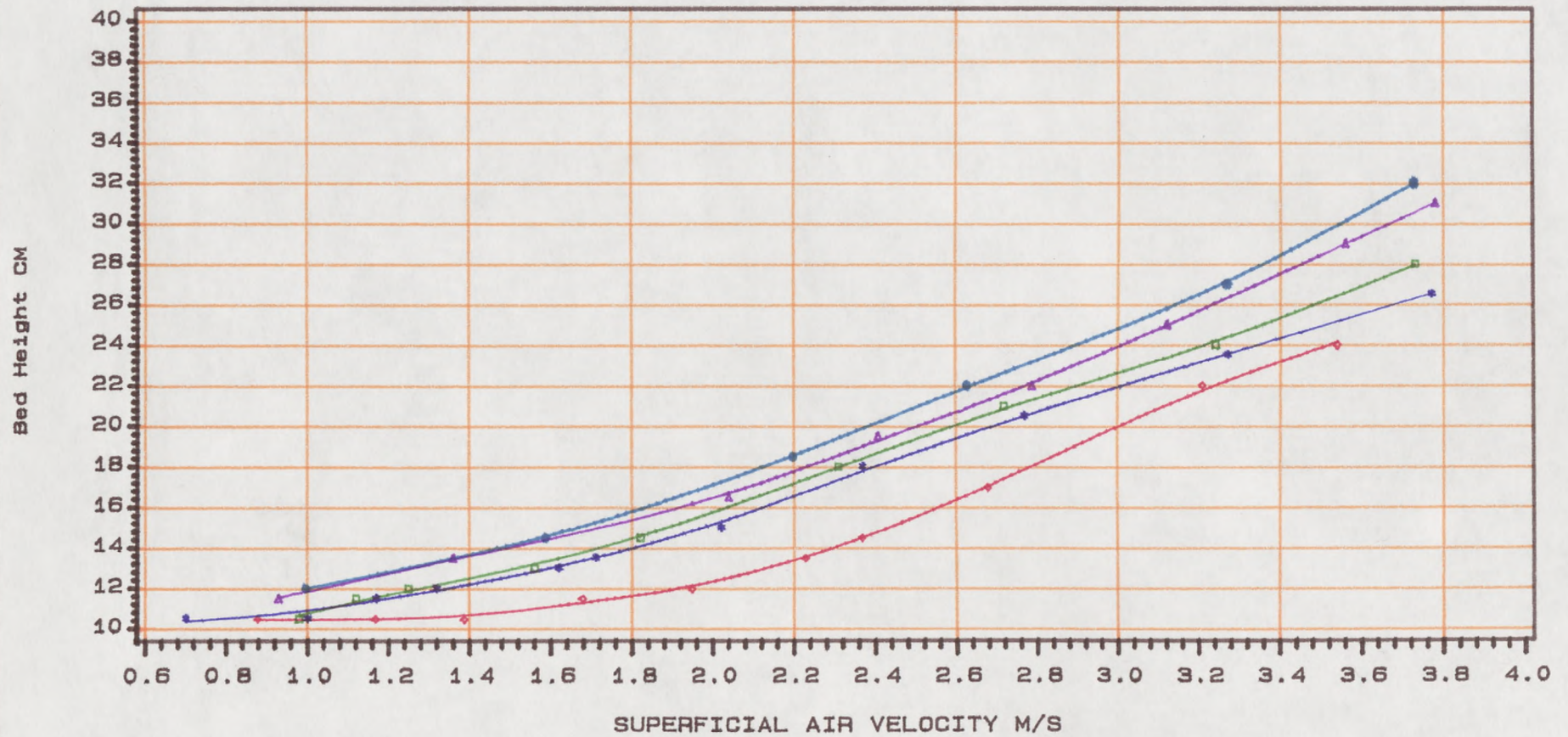
VL=1E-3 M/S

VL=2.32E-3 M/S

VL=6.58E-3 M/S

VL=8.77E-3 M/S

**Fig 5.1.28 Plot Of Variation Of Bed Height With Superficial Air Velocity For Oblate Spheroid Packing**  
**Packing Dia=50\*38 mm Bed Static Height=10.5 cm**  
**For Various Superficial Liquid Velocity**



Dry Bed

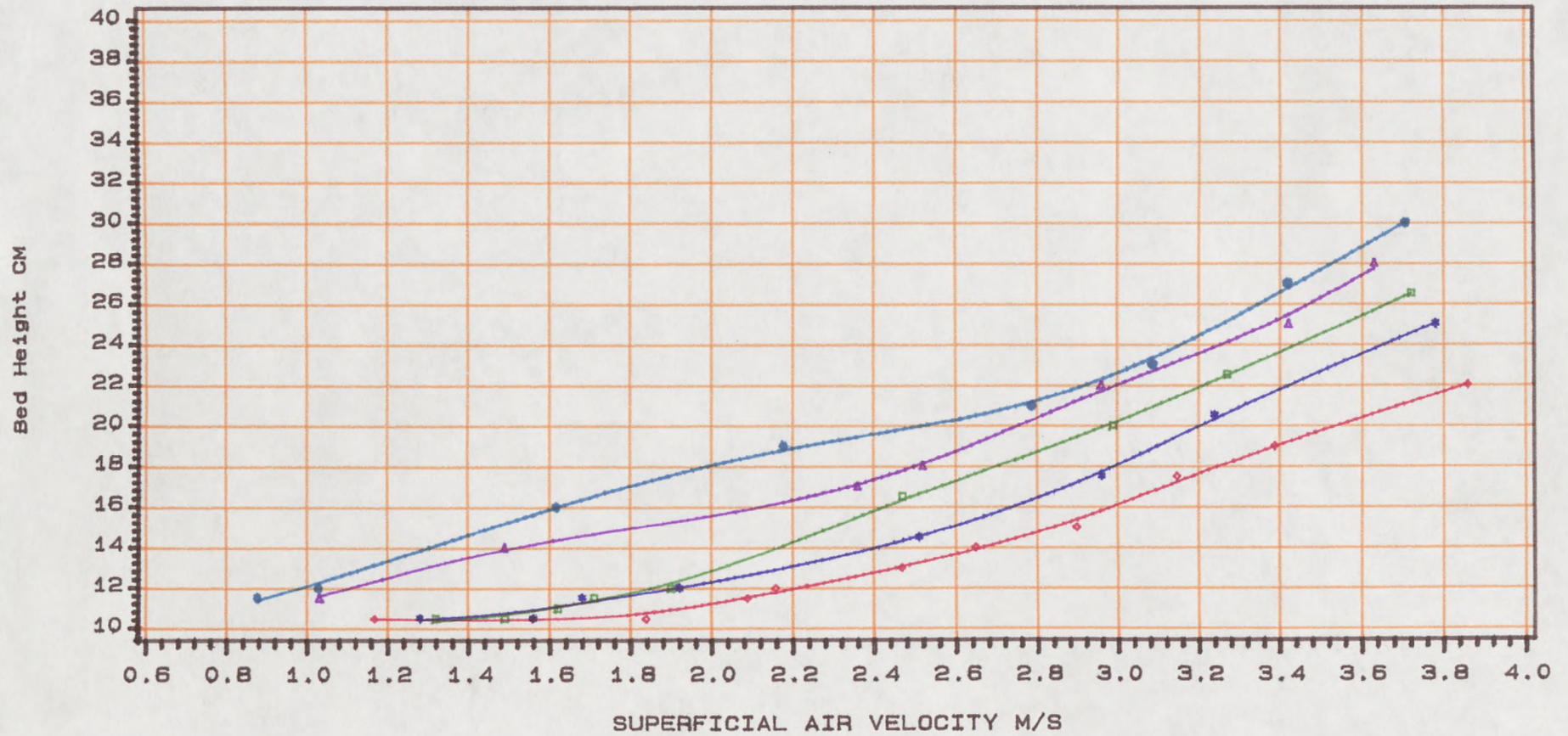
VL=1E-3 M/S

VL=2.32E-3 M/S

VL=6.58E-3 M/S

VL=8.77E-3 M/S

Fig 5.1.29 Plot Of Variation Of Bed Height With Superficial Air Velocity For Slotted Packing  
 Packing Dia=25 mm Bed Static height=10.5 Cm  
 For Various Superficial Liquid Velocity



Dry Bed

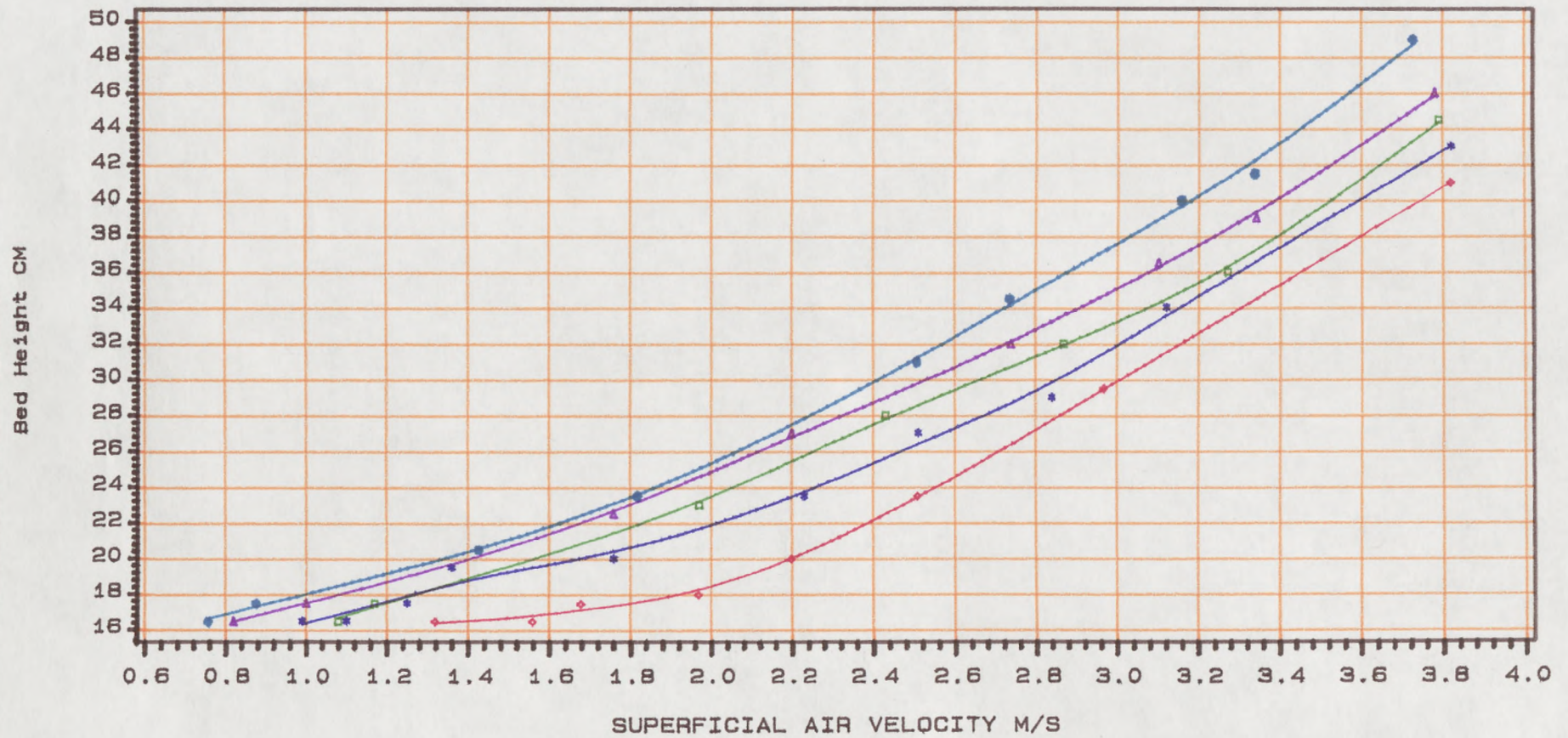
VL=1E-3 M/S

VL=2.32E-3 M/S

VL=6.58E-3 M/S

VL=8.77E-3 M/S

Fig 5.1.30 Plot Of Variation Of Bed Height With Superficial Air Velocity For Plain Sphere Packing  
 Packing Dia=38 mm Bed Static Height=16.5 Cm  
 For Various Superficial Liquid Velocity



Dry Bed

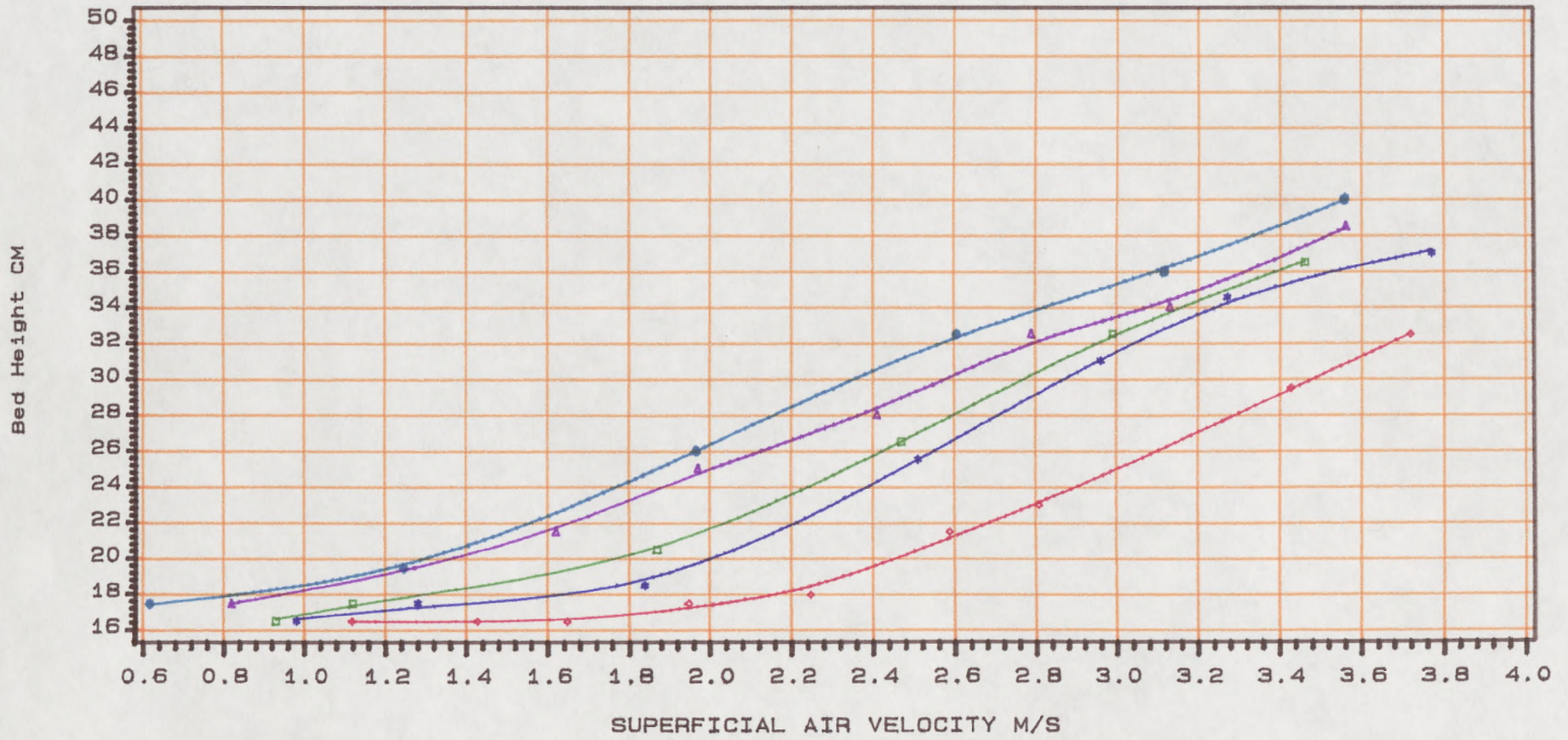
VL=1E-3 M/S

VL=2.32E-3 M/S

VL=6.58E-3 M/S

VL=8.77E-3 M/S

Fig 5.1.31 Plot Of Variation Of Bed Height With Superficial Air Velocity For Plain Sphere Packing  
 Packing Dia=25 mm Bed Static Height=16.5 Cm  
 For Various Superficial Liquid Velocity



Dry Bed

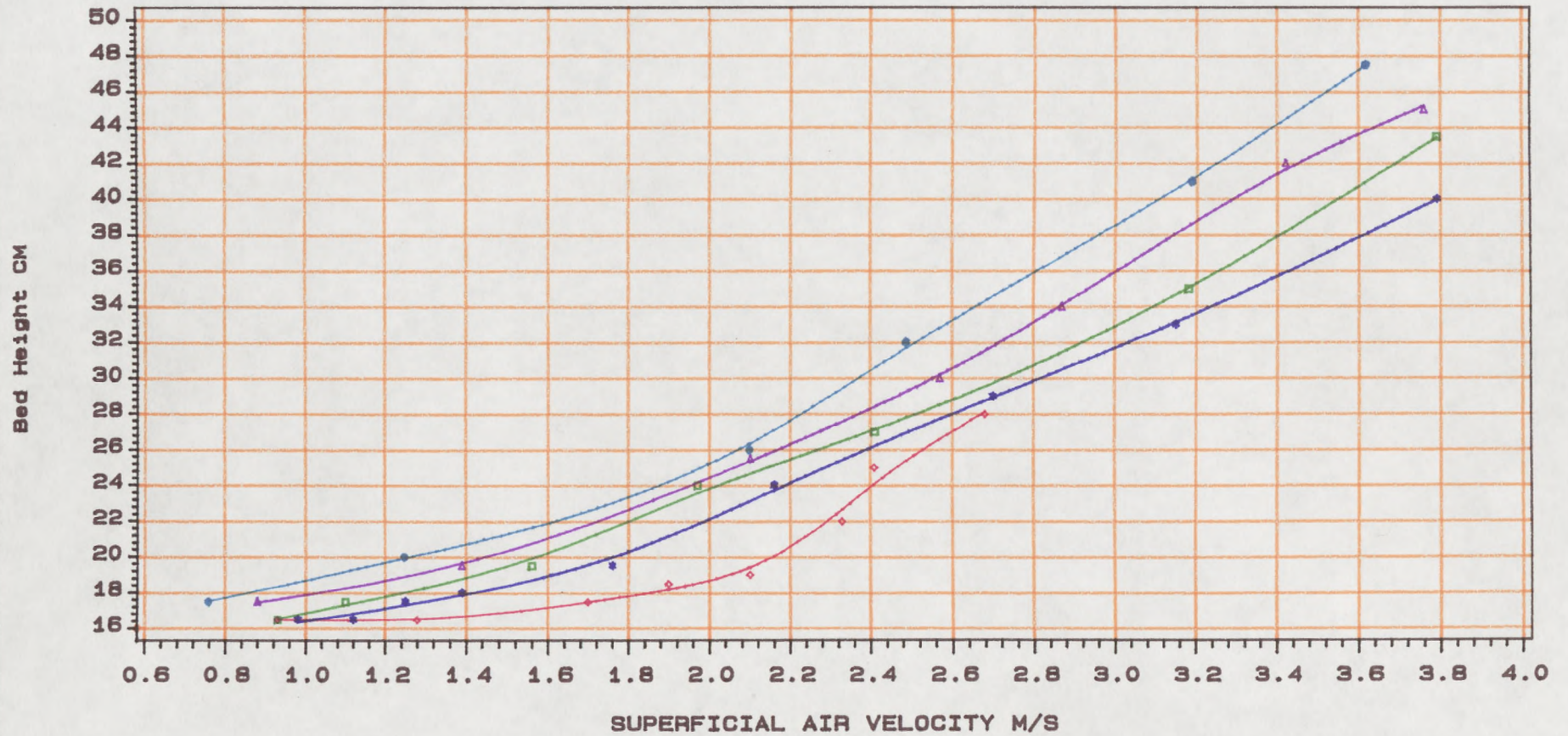
VL=1E-3 M/S

VL=2.32E-3 M/S

VL=6.58E-3 M/S

VL=8.77E-3 M/S

**Fig 5.1.32 Plot Of Variation Of Bed Height With Superficial Air Velocity For Oblate Spheroid Packing  
 Packing Dia=50\*38 mm Bed Static Height=16.5 cm  
 For Various Superficial Liquid Velocity**



Dry Bed

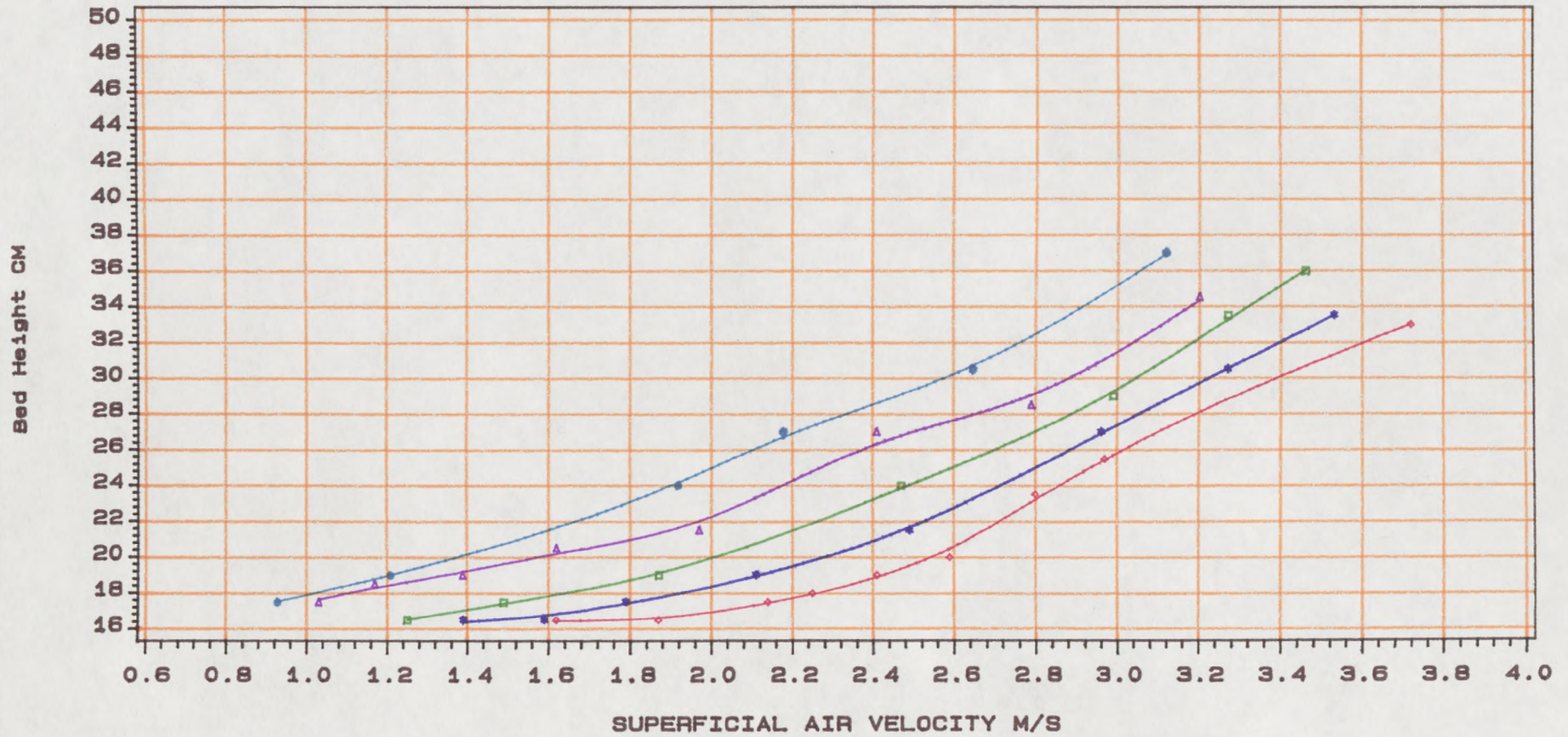
VL=1E-3 M/S

VL=2.32E-3 M/S

VL=6.58E-3 M/S

VL=8.77E-3 M/S

**Fig 5.1.33 Plot Of Variation Of Bed Height With Superficial Air Velocity For Slotted Packing**  
**Packing Dia=25 mm Bed Static Height=16.5 Cm**  
**For Various Superficial Liquid Velocity**



Dry Bed

VL=1E-3 M/S

VL=2.32E-3 M/S

VL=6.58E-3 M/S

VL=8.77E-3 M/S

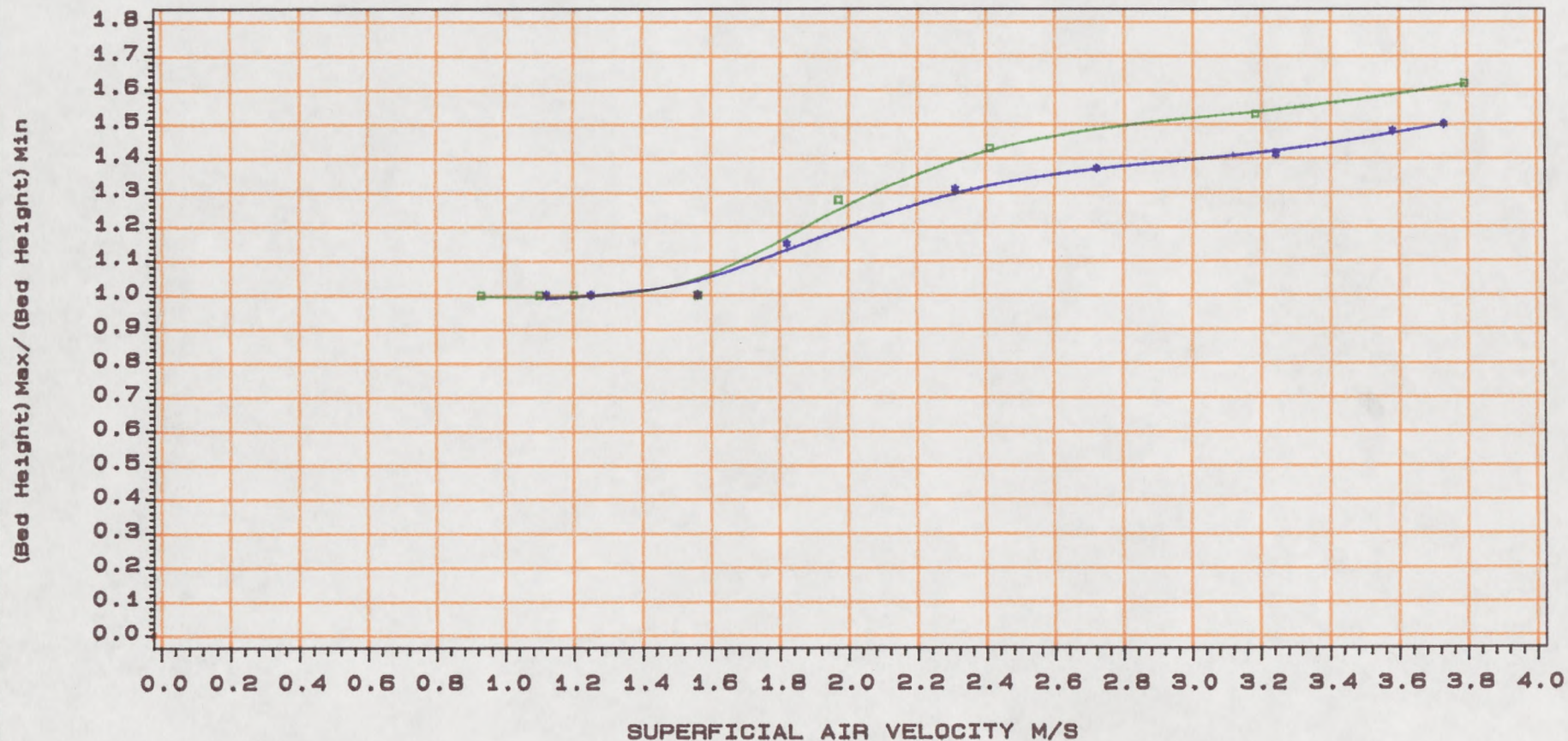
employing 10.5 cm bed static height, however, the fluctuation in expanded bed height was more pronounced with the 16.5 cm bed static height. The largest effect of increasing liquid rate on bed expansion and bed expansion rate is observed with the slotted packing having a bed static height of 16.5 cm.

The effects of bed static height on the fluctuation of fluidized bed height for all of the packings are shown in figures 5.1.34 to 5.1.37. It can be seen that the fluctuation between maximum and minimum bed height is larger for the case with a bed static height of 16.5 cm than with a 10.5 cm bed static height.

Similar results regarding the general effect of bed static height and air velocity on the bed expansion and fluctuation of the bed have been reported by Gelperin et al (8), Strumillo et al (51) and Tichy and Douglas (54). Thus, a substantial increase in the fluctuation of the bed height will result in a slugging bed. In this case, the whole bed or part of the bed moves upwards as a slug with the packing elements at the bottom end of the slug falling back individually to form another slug immediately above the support mesh. The top slug eventually decays back into the second slug which now becomes the top slug and itself decays back into the succeeding slug and this motion continues until so called flooding is reached.

Figure 5.1.38 shows the sequence of formation of slugs in a slugging bed. Visual observation of the turbulent agitation of the liquid and packings in the mobile bed suggests that the beds having lower fluctuations in expanded bed height are contacting the gas and liquid streams more homogeneously and more intimately, thus offering the possibility of more efficient interphase mass transfer.

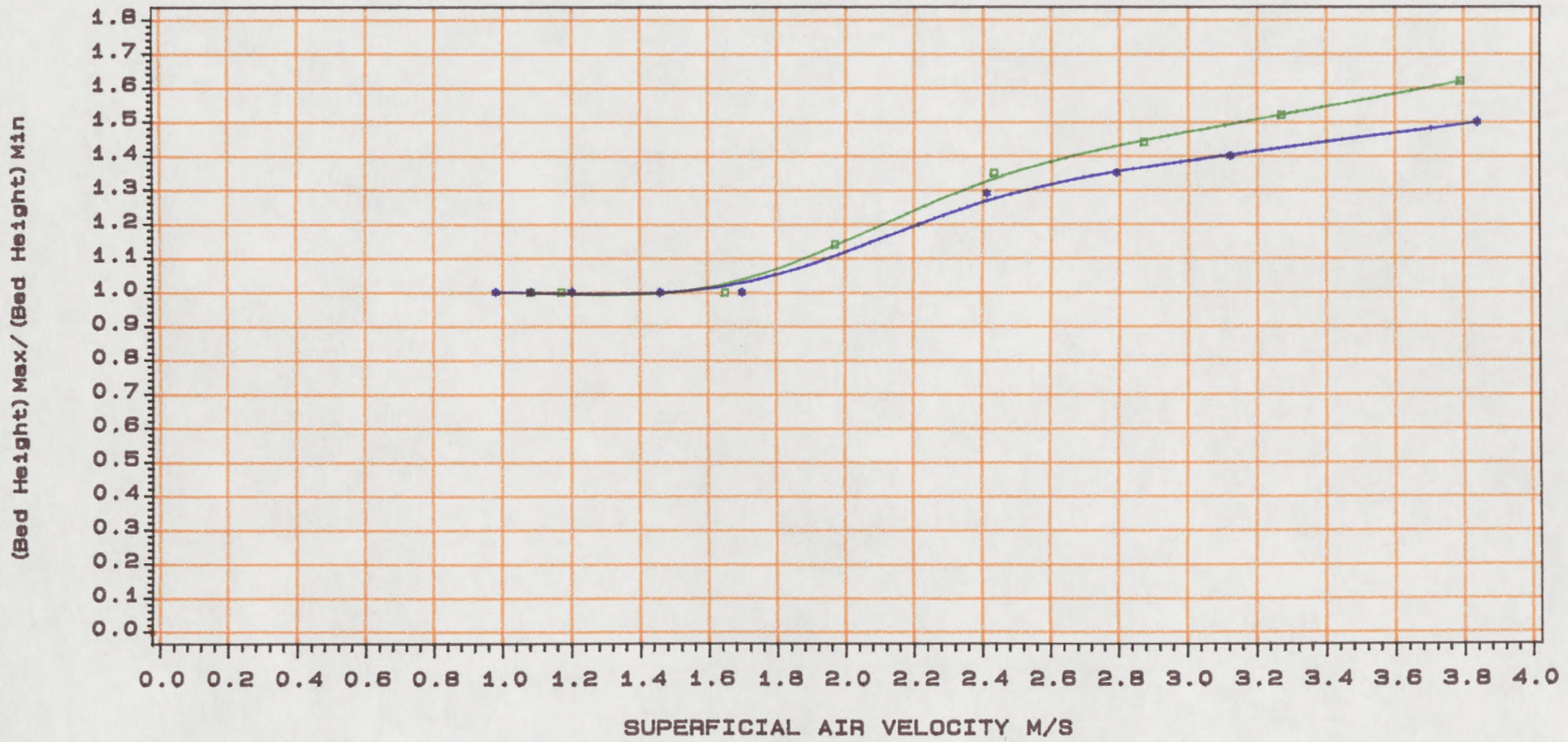
**Fig 5.1.34 Plot Of Variation Of Fluctuation Of Bed Height With Air Velocity For Oblate Spheroid Packing**  
 Packing Dia=50\*38 mm H=10.5 cm And H=16.5 cm  
 SUPERFICIAL LIQUID VELOCITY=2.32E-3 M/S



BED STATIC HEIGHT=10.5 CM

BED STATIC HEIGHT= 16.5 CM

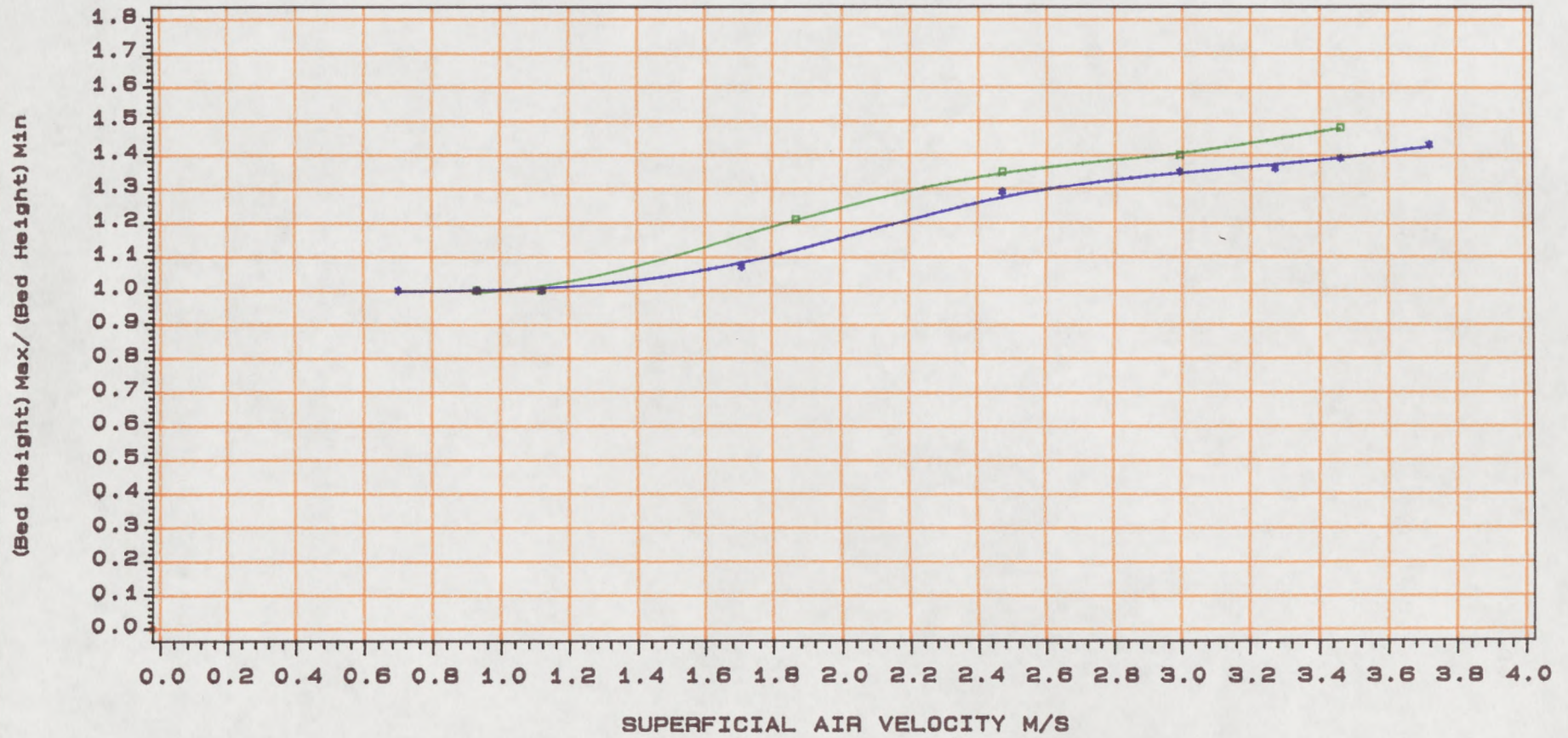
**Fig 5.1.35 Plot Of Variation Of Fluctuation Of Bed Height With Air Velocity For Plain Packing**  
**Packing Dia=38 mm H=10.5 cm And H=16.5 cm**  
**SUPERFICIAL LIQUID VELOCVITY=2.32E-3 M/S**



BED STATIC HEIGHT=10.5 CM

BED STATIC HEIGHT= 16.5 CM

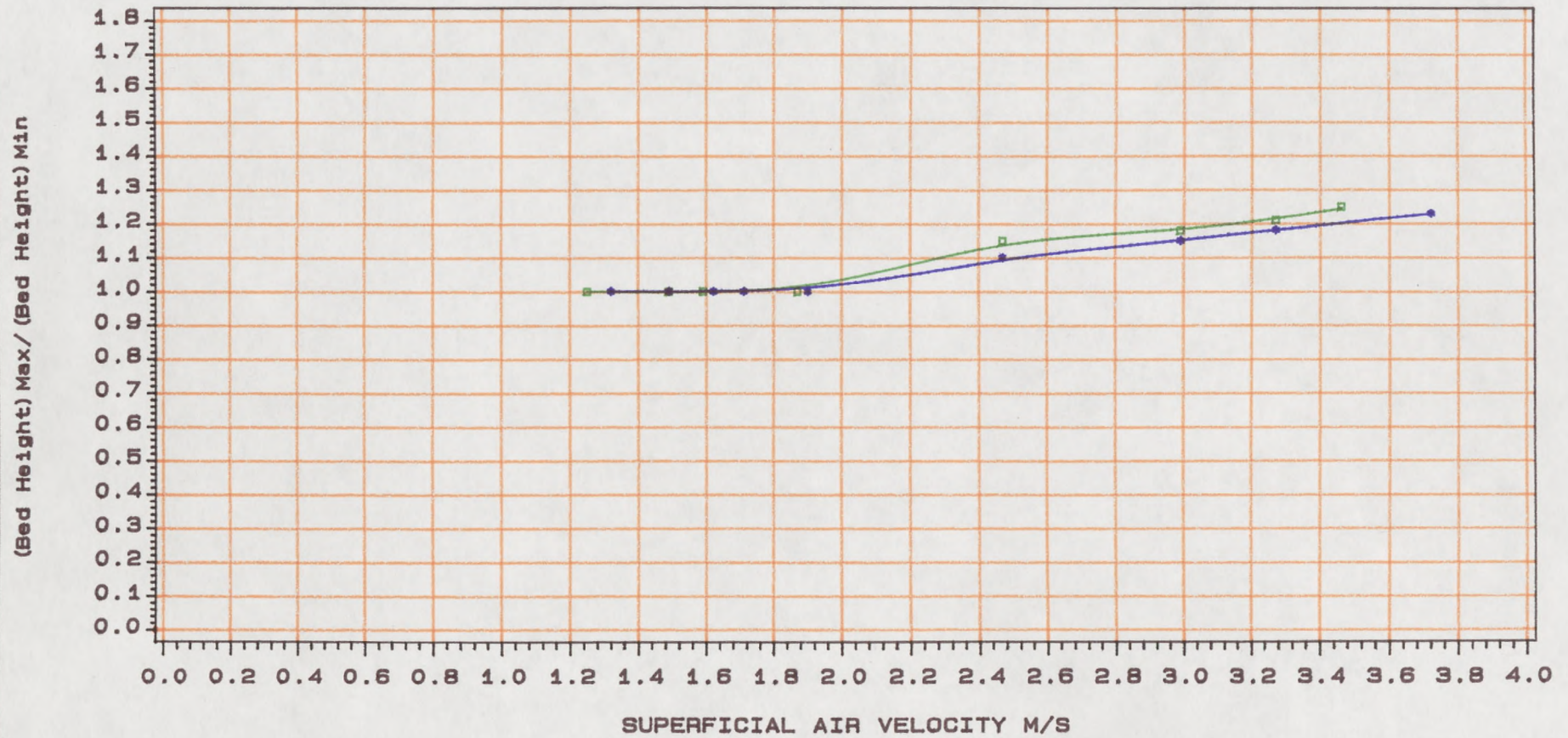
**Fig 5.1.36 Plot Of Variation Of Fluctuation Of Bed Height With Air Velocity For Plain Packing**  
 Packing Dia=25 mm H=10.5 cm And H=16.5 cm  
 SUPERFICIAL LIQUID VELOCITY=2.32E-3 M/S



BED STATIC HEIGHT=10.5 CM

BED STATIC HEIGHT= 16.5 CM

Fig 5.1.37 Plot Of Variation Of Fluctuation Of Bed Height With Air Velocity For Slotted Packing  
 Packing Dia=25 mm H=10.5 cm And H=16.5 cm  
 SUPERFICIAL LIQUID VELOCITY=2.32E-3 M/S



BED STATIC HEIGHT=10.5 CM

BED STATIC HEIGHT= 16.5 CM

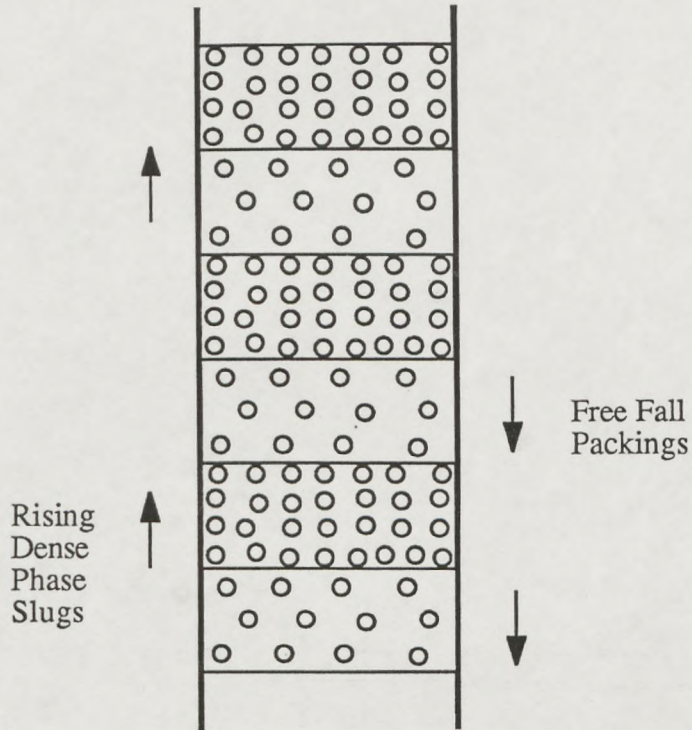


Figure 5.1.38 Sequence of formation of slugs in a slugging bed

Figure 5.1.37 confirms that fluidized beds of slotted packings fluidize more smoothly and homogeneously than plain packings which is also apparent from visual observation.

#### 5.1.5. Liquid Hold Up.

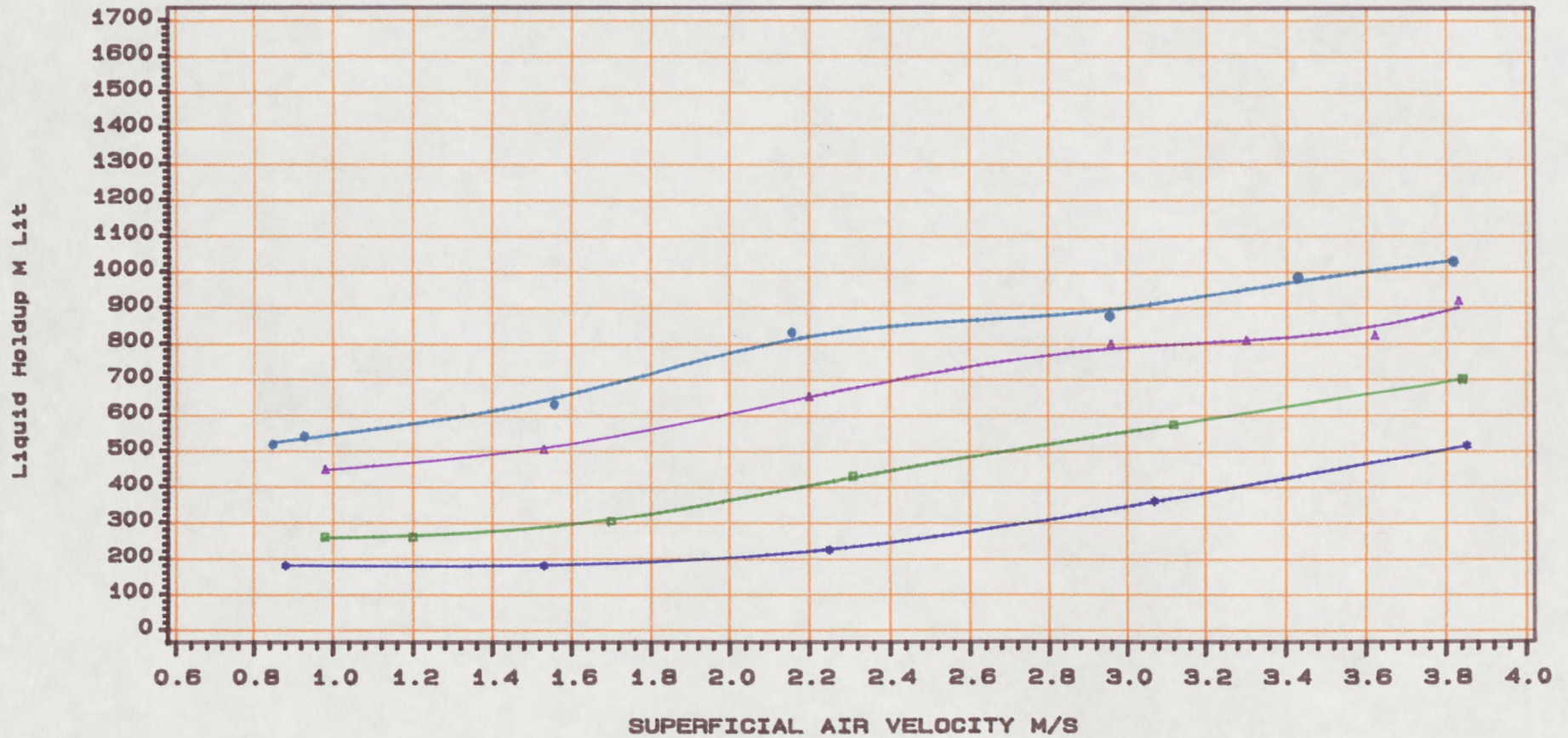
The effect of varying air and liquid velocity on the liquid hold up for all of the packings at a bed static height of 10.5 cm is shown in figures 5.1.39 to 5.1.42. It can be seen that the liquid hold up increases with both increasing air and liquid velocity. The increase in the liquid hold up with increasing liquid rate is to be expected as the amount of liquid retained in the bed also increases. This finding confirms the results of Gelperin et al (8), Chen and Douglas (21). Also, the increase in the air velocity will result in more support for liquid hold up by air velocity and therefore increase the liquid retained in the bed.

Chen and Douglas (21), Ushida et al (3) and Kito et al (2) reported that the liquid hold up was not affected significantly by the air velocity within the range of air and liquid velocities investigated in their experiments. Whereas Gelperin et al (8), Balabekov et al (50), Rao et al (24) and Groeneveld (55) found that the liquid hold up increases with both increasing air and liquid velocities.

#### 5.1.6. Summary of Comparative Hydrodynamic Studies.

Figure 5.1.43 compares the variation of minimum expanding gas velocity ( $V_{min}$ ) for the oblate spheroid, 38 mm diameter plain sphere, 25 mm plain sphere and 25 mm slotted sphere packings. It can be seen that the minimum expanding velocity is nearly the same for the oblate spheroid the 38 mm diameter plain sphere and 25 mm diameter plain sphere

**Fig 5.1.39 Plot Of Variation Of Liquid Hold Up With Air Velocity For Plain Sphere Packing**  
**Packing Dia=38 mm Bed Static Height=10.5 Cm**  
**For Various Superficial Liquid Velocity**



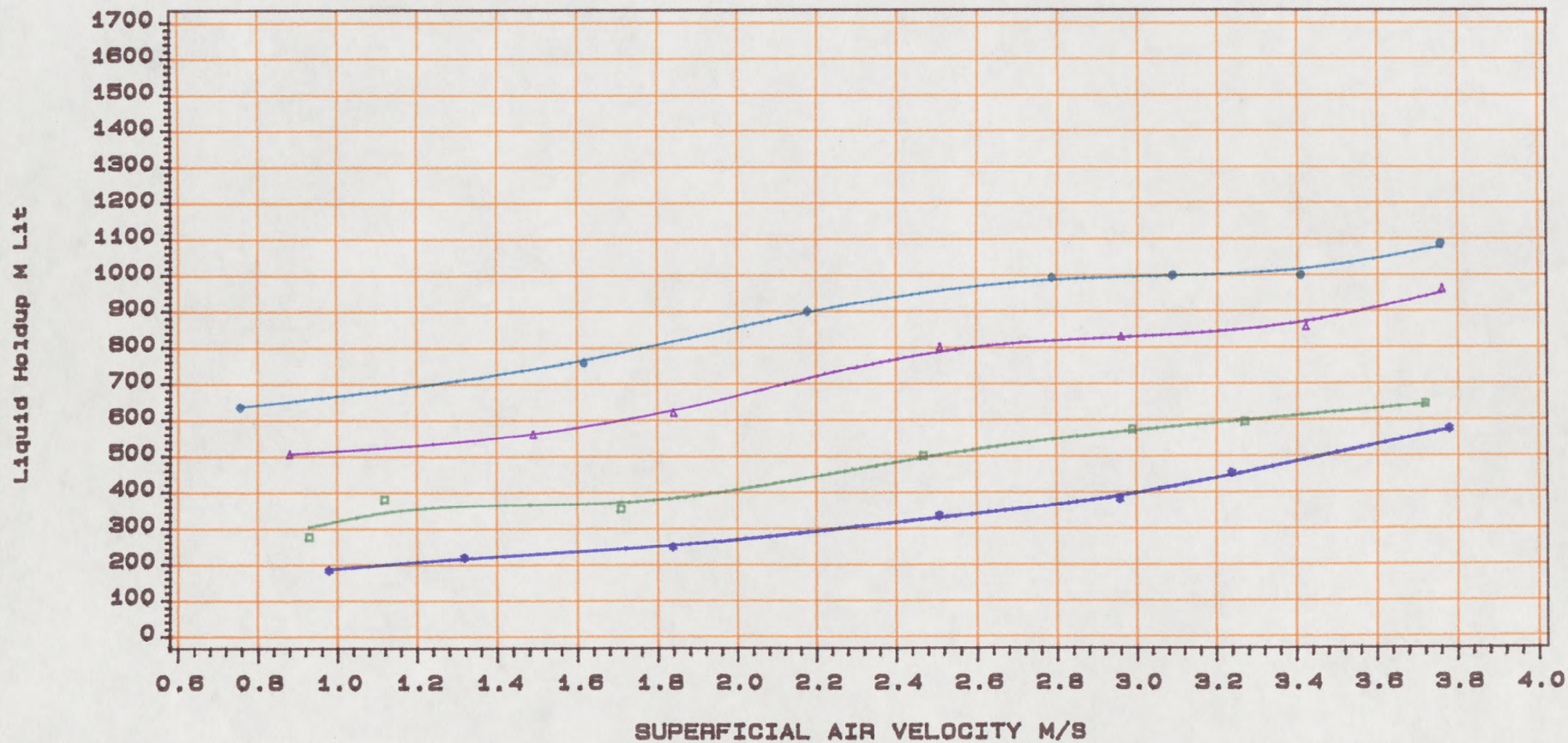
VL=1E-3 M/S

VL=2.32E-3 M/S

VL=6.58E-3 M/S

VL=8.77E-3 M/S

**Fig 5.1.40 Plot Of Variation Of Liquid Hold Up With Air Velocity For Plain Sphere Packing**  
**Packing Dia=25 mm Bed Static Height=10.5 Cm**  
**For Various Superficial Liquid Velocity**



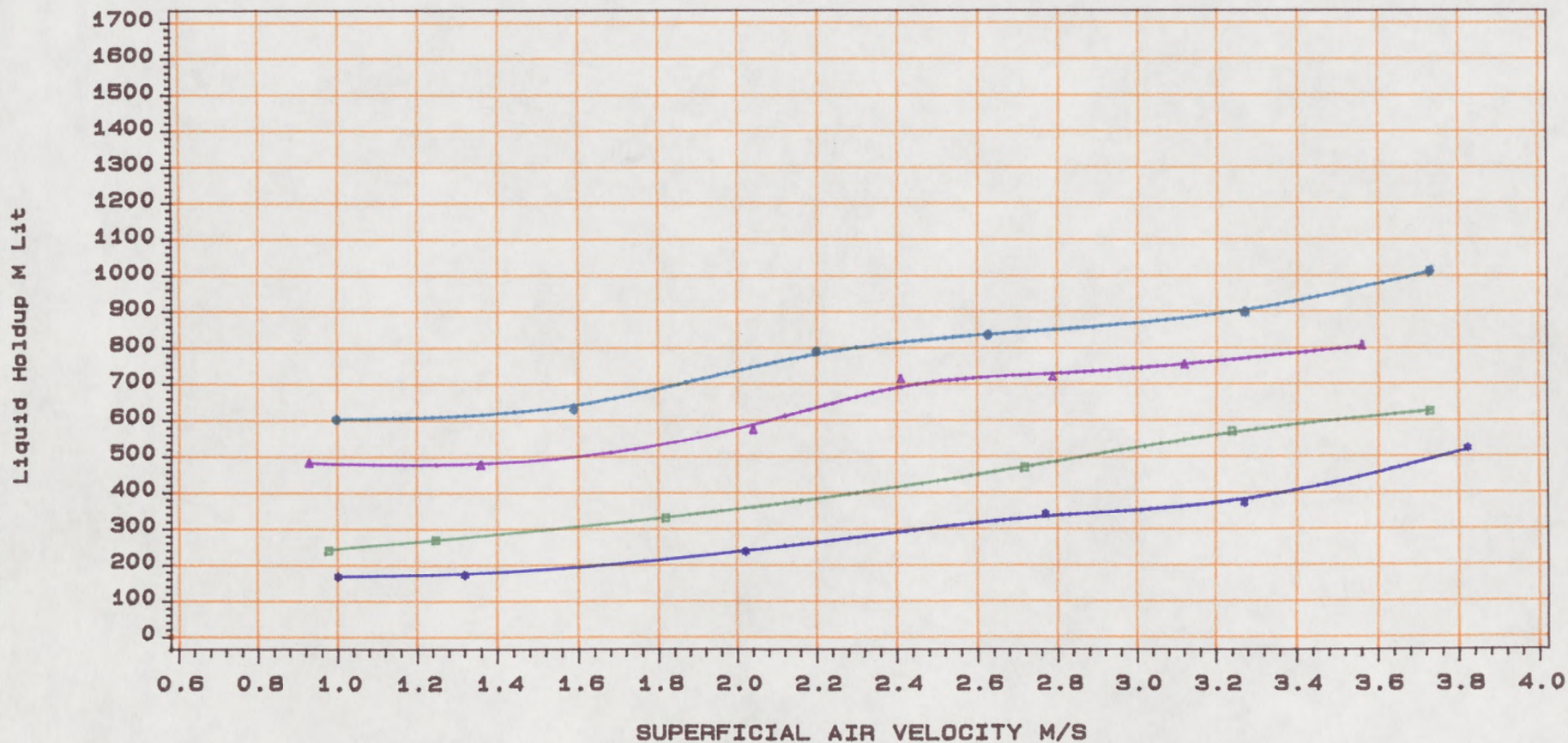
VL=1E-3 M/S

VL=2.32E-3 M/S

VL=6.58E-3 M/S

VL=8.77E-3 M/S

**Fig 5.1.41 Plot Of Variation Of Liquid Hold Up With Air Velocity For Oblate Spheroid Packing**  
**Packing Dia=50\*38 mm Bed Static Height=10.5 cm**  
**For Various Superficial Liquid Velocity**



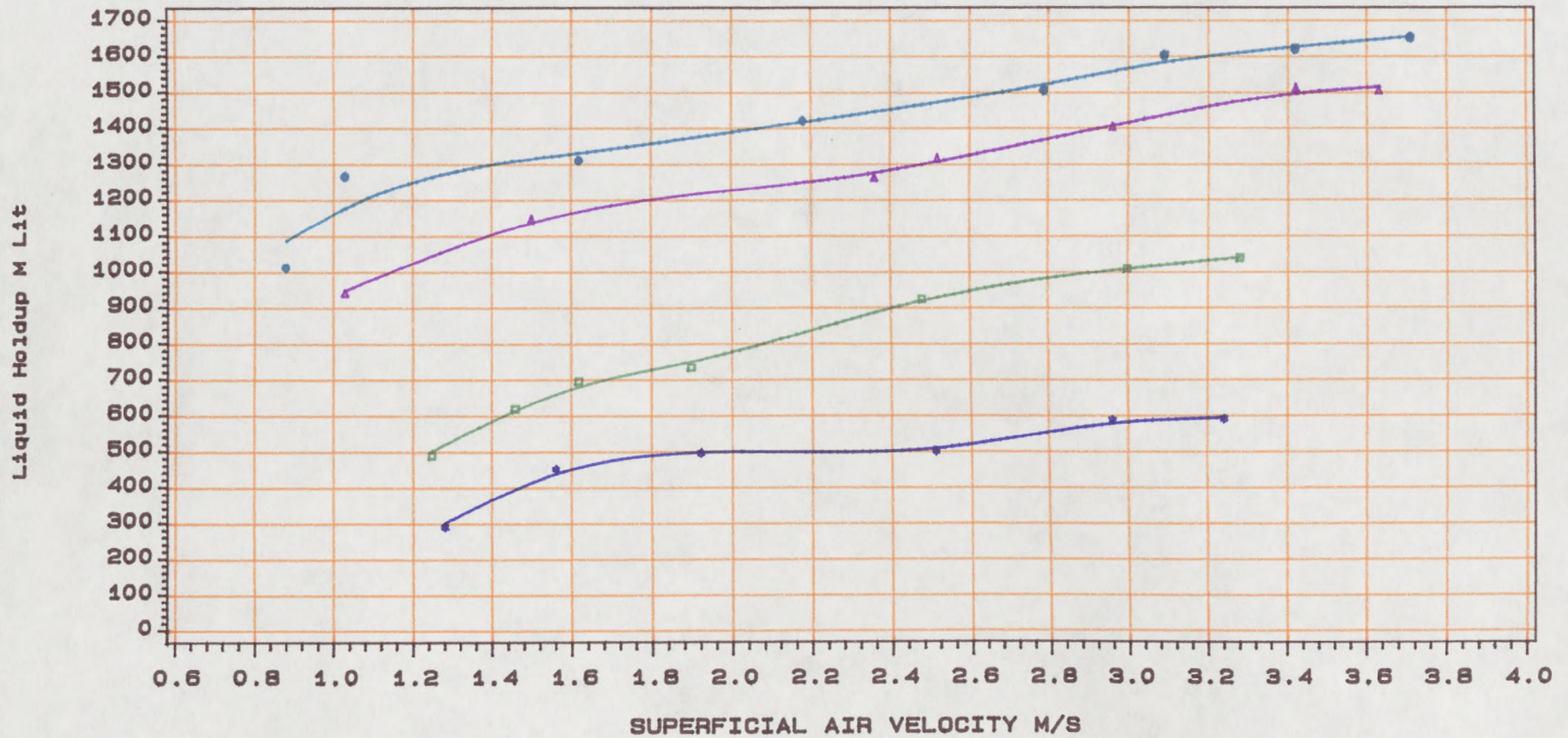
VL=1E-3 M/S

VL=2.33E-3 M/S

VL=6.58E-3 M/S

VL=8.77E-3 M/S

**Fig 5.1.42 Plot Of Variation Of Liquid Hold Up With Air Velocity For Slotted Sphere Packing  
 Packing Dia=25 mm Bed Static Height=10.5 Cm  
 For Various Superficial Liquid Velocity**



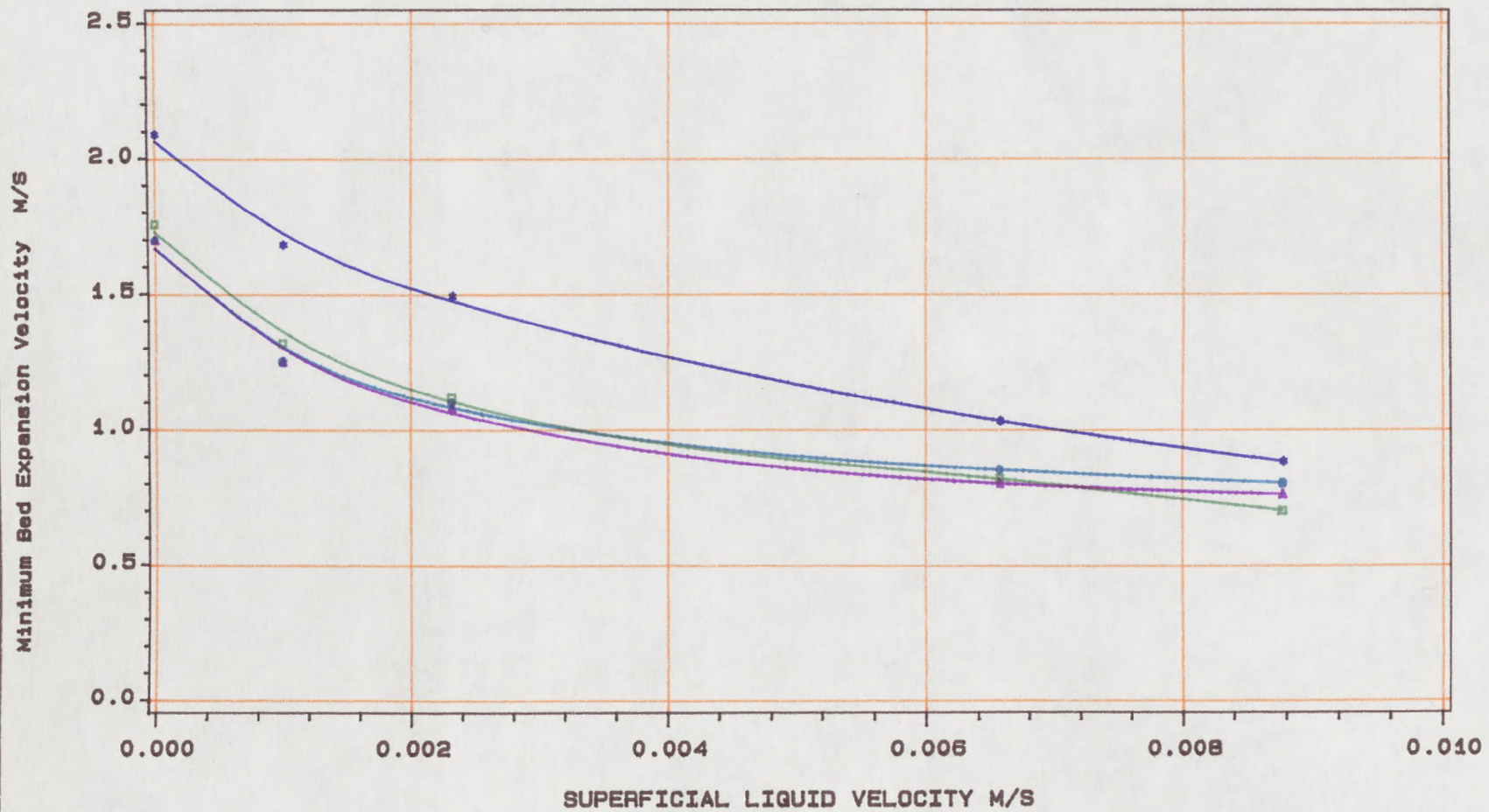
VL=1E-3 M/S

VL=2.32E-3 M/S

VL=6.58E-3 M/S

VL=8.77E-3 M/S

**Fig 5.1.43 Plot Of Variation Of Minimum Expanding Velocity With Liquid Rate For Mobile Bed Packings**  
**Bed static Height=10.5 Cm**



SLOTTED D=25 mm    PLAIN D=25 mm    PLAIN D=38 mm    Oblate D=50\*38 mm

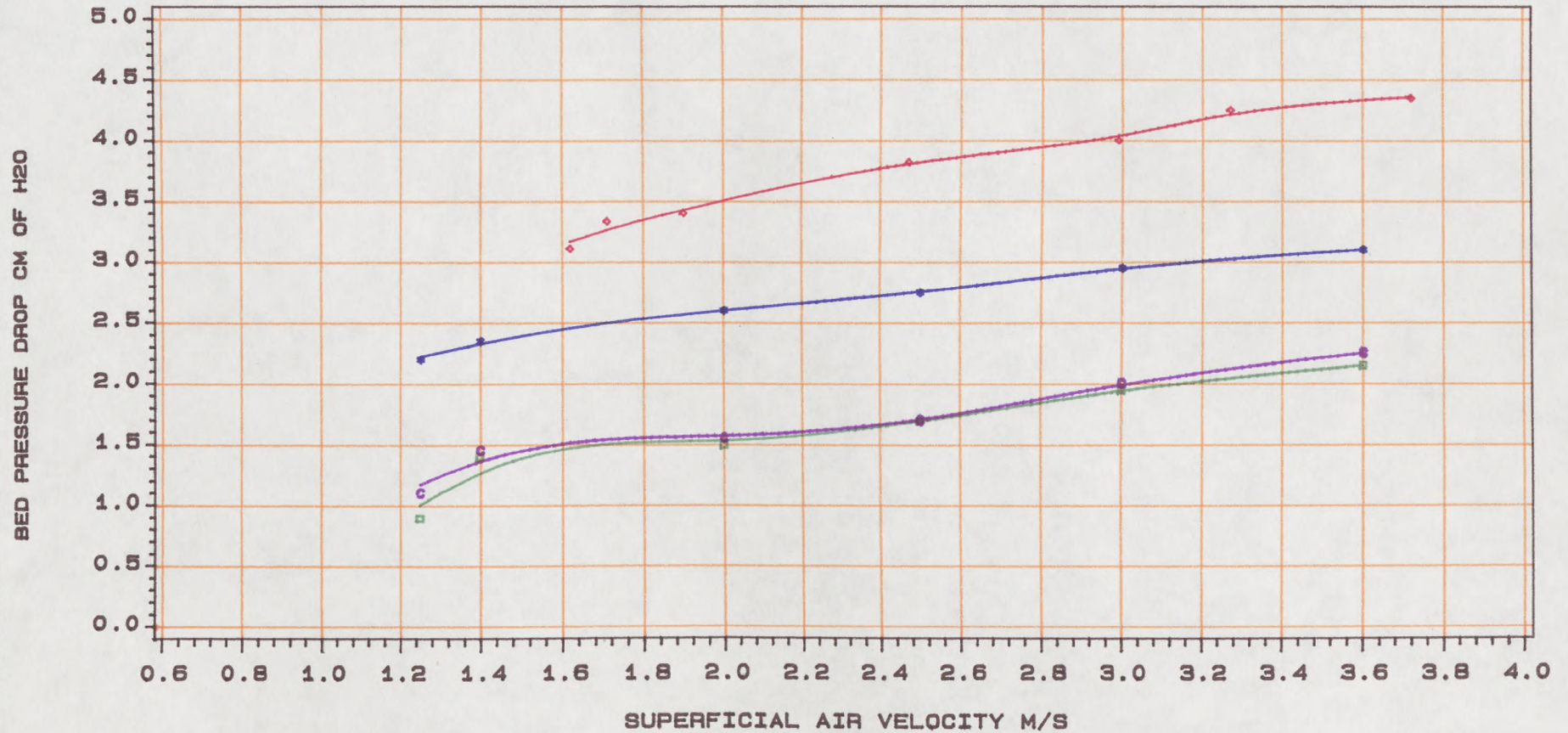
packings. On the other hand, ( $V_{min}$ ) for the slotted packing is considerably higher than for the other packings and as the liquid velocity increases, the ( $V_{min}$ ) for the slotted packing approaches the value of ( $V_{min}$ ) for the oblate spheroid, 38 mm diameter plain sphere and 25 mm diameter plain sphere packings. This is because in the case of dry beds and at low liquid velocities, the slotted packings offer lower resistance to the air flow and therefore higher air velocities are required in order to fluidize the packing, however, as the liquid velocity is increased, the corresponding increase in the liquid hold up for the slotted packing is greater than for the other packings which in turn causes a more rapid decrease in the minimum expanding velocity as compared with the other packings.

Figure 5.1.44 shows the effect of air velocity on the pressure drop for different packings. It is apparent that the pressure drop for the slotted packing is significantly higher than for the oblate spheroid and the plain packings. This is due to the presence of greater liquid hold up for the fluidized slotted packing as compared to the other plain packings.

It can also be seen that the pressure drop for the 25 mm diameter plain sphere packing is higher than for the 38 mm diameter plain sphere and oblate spheroid packings, again due to higher liquid hold up. Similar results were obtained as shown in figure 5.1.45 which compares the variation of pressure drop with liquid velocity for different packings.

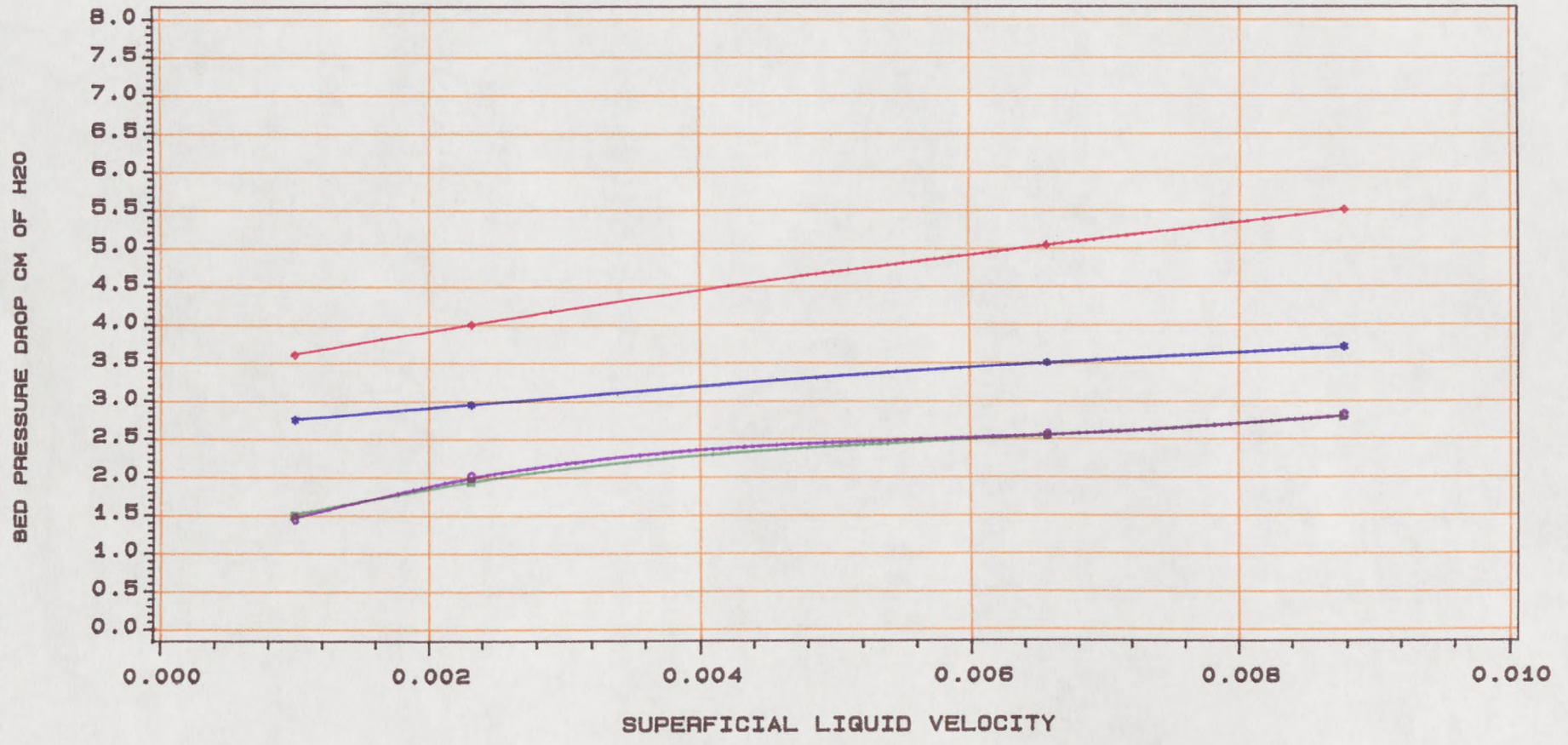
Figure 5.1.46 compares the effect of air velocity on the liquid hold up at a constant liquid rate for the different packings. It can be seen that the liquid hold up for the slotted packings is much higher

**Fig 5.1.44 Plot Of Pressure Drop Characteristics Of Mobile Packings**  
**Superficial Liquid Velocity=2.82E-3 M/S Bed Static Height=10.5 cm**  
**For Different Packings**



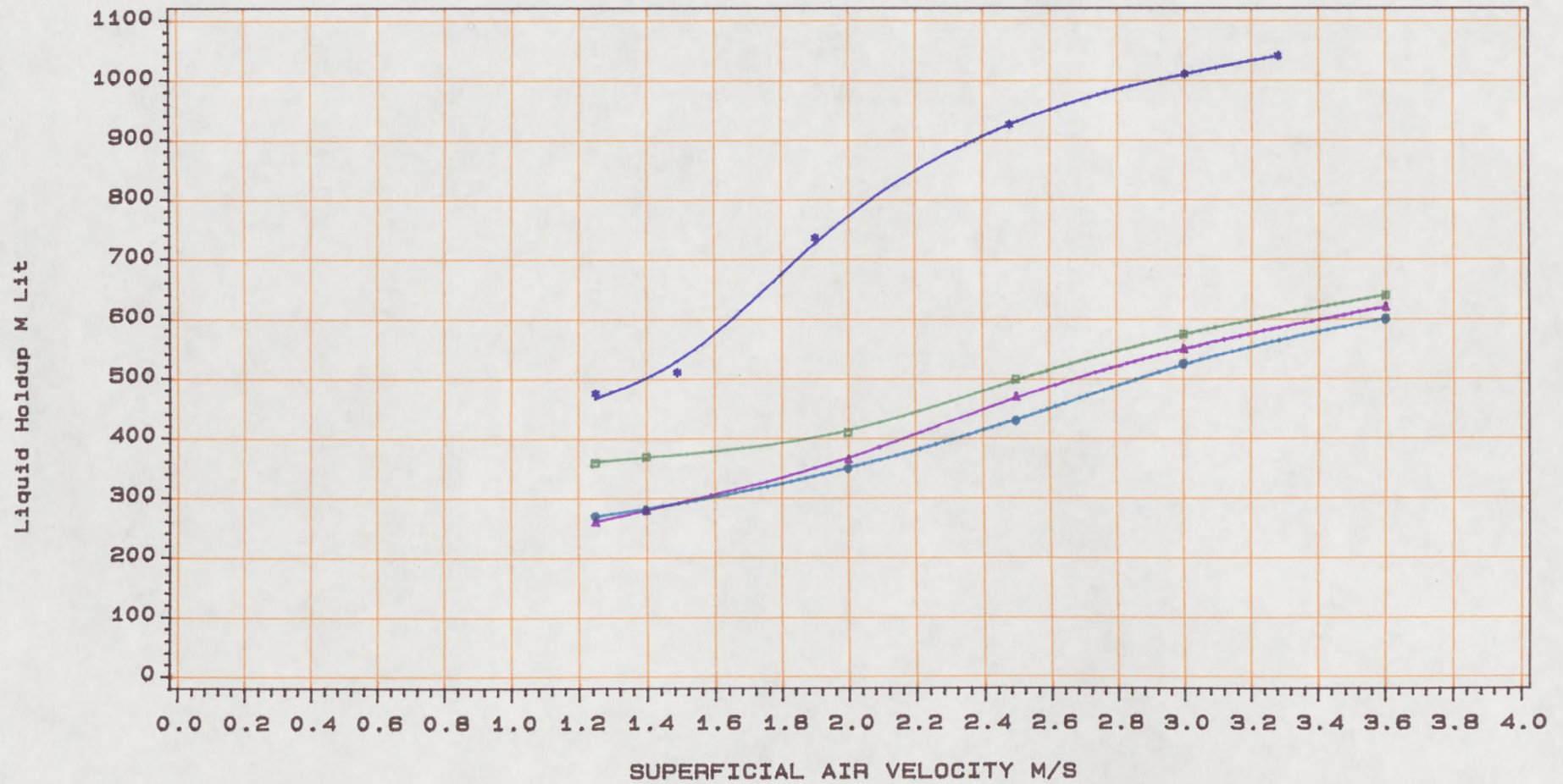
Slotted Dia=25 mm Plain Dia=25 mm Plain Dia=38 mm Oblate Dia=50x38 mm

**Fig 5.1.45 Plot Of Pressure Drop Characteristics Of Mobile Packings**  
**Superficial Air Velocity=3 M/S Bed Static Height=10.5 cm**  
**For Different Packings**



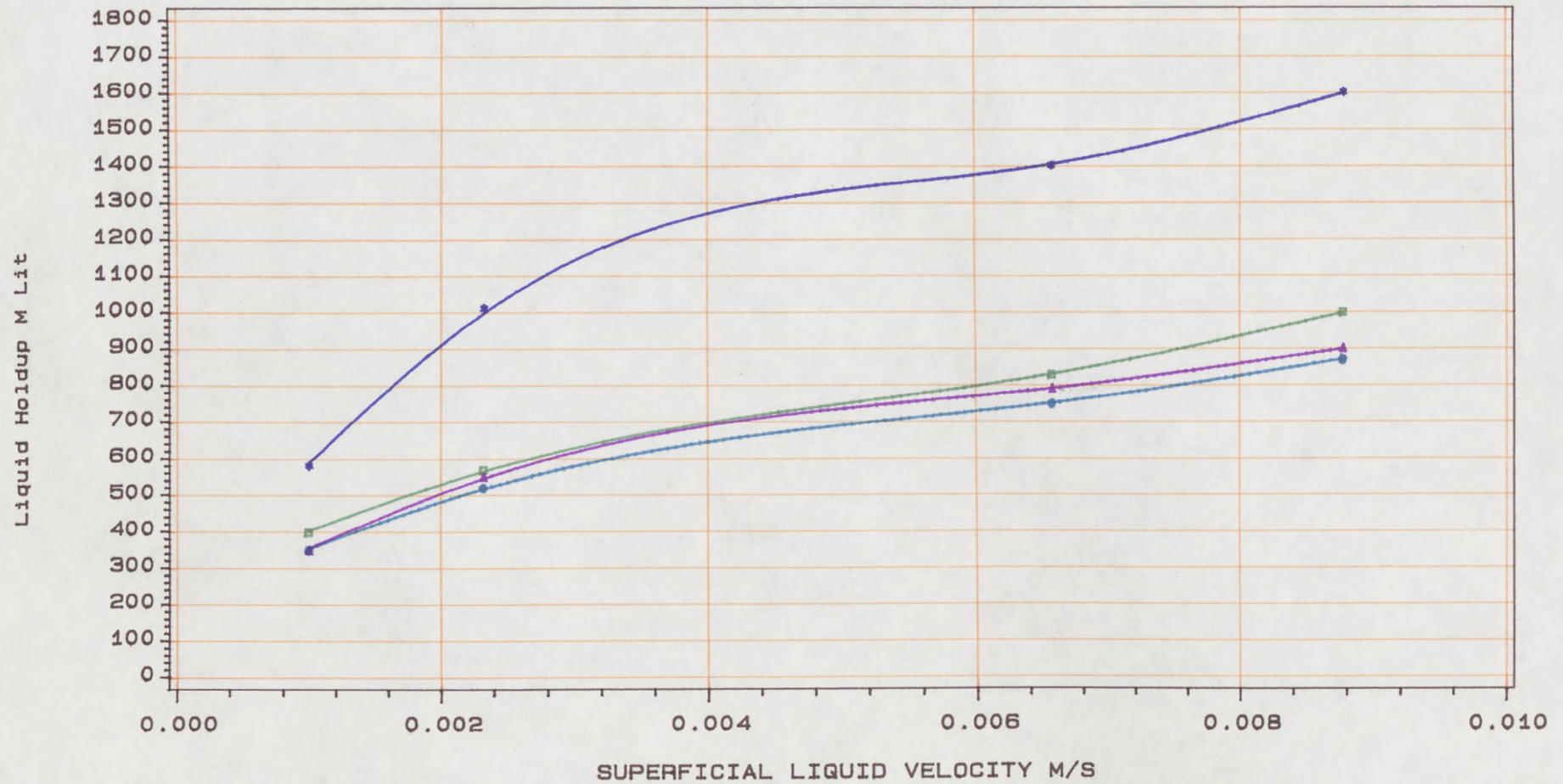
Slotted Dia=25 mm Plain Dia=25 mm Plain Dia=38 mm Oblate Dia=50\*38 mm

**Fig 5.1.46 Plot Of Variation Of Liquid Hold Up With Air Velocity For Mobile Bed Packings**  
**SUPERFICIAL LIQUID VELOCITY=2.32E-3 M/S BED STATIC HEIGHT=10.5 CM**



SLOTTED D=25 mm    PLAIN D=25 mm    PLAIN D=38 mm    QBLATE D=50\*38 mm

Fig 5.1.47 Plot Of Variation Of Liquid Hold Up With Liquid Rate For Mobile Bed Packings  
 Superficial Air Velocity=3 M/S Bed Static Height=10.5 cm



SLOTTED D=25 mm    PLAIN D=25 mm    PLAIN D=38 mm    OBLATE D=50x38 mm

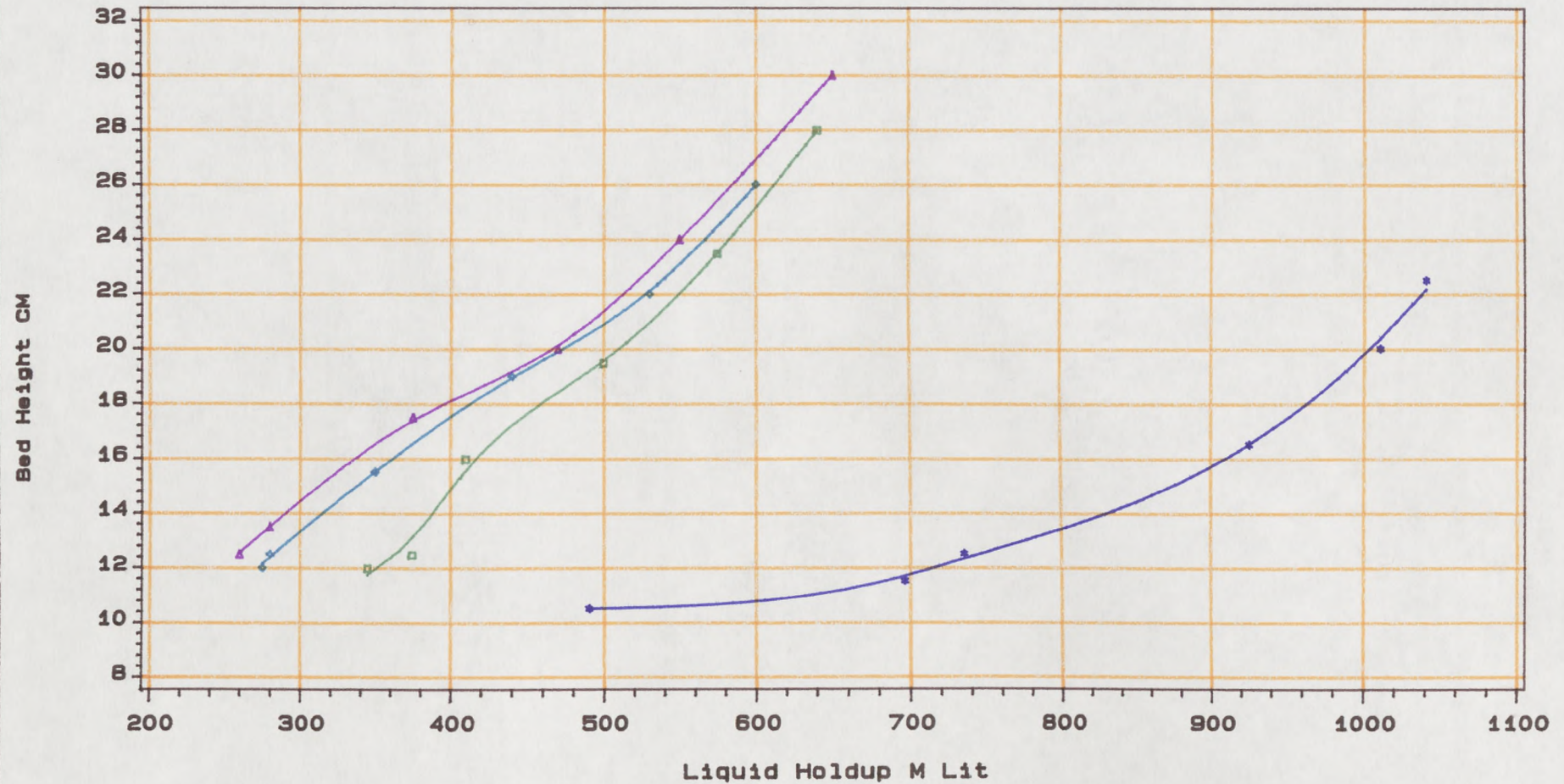
than for the other packings as the slotted packings are able to retain more liquid within the bed at the same air velocity as compared to the plain sphere and oblate spheroid packings. The liquid hold up is also slightly higher for the 25 mm diameter plain spheres. This is because the 25 mm plain sphere packing being smaller than the 38 mm diameter plain sphere and oblate spheroid packings, offers a larger surface area per unit volume of bed. Similar findings are to be found in figure 5.1.47 which compares the effect of liquid rate on the liquid hold up for various packings.

Figure 5.1.48 shows the variation of expansion in the bed height with liquid hold up for different packings. It can be seen that at a given expanded bed height, the liquid hold up for the slotted packings is much higher than for the other packings, which suggests that much of the liquid is being held up inside the slotted ball packing.

Figure 5.1.49 compares the variation of expanded bed height with air velocity for different packings. It is apparent that the expansion in the bed height for the slotted bed height is lower than for the other packings, as the slotted packings offer lower resistance to the air flow and requires higher air velocity for a given bed expansion.

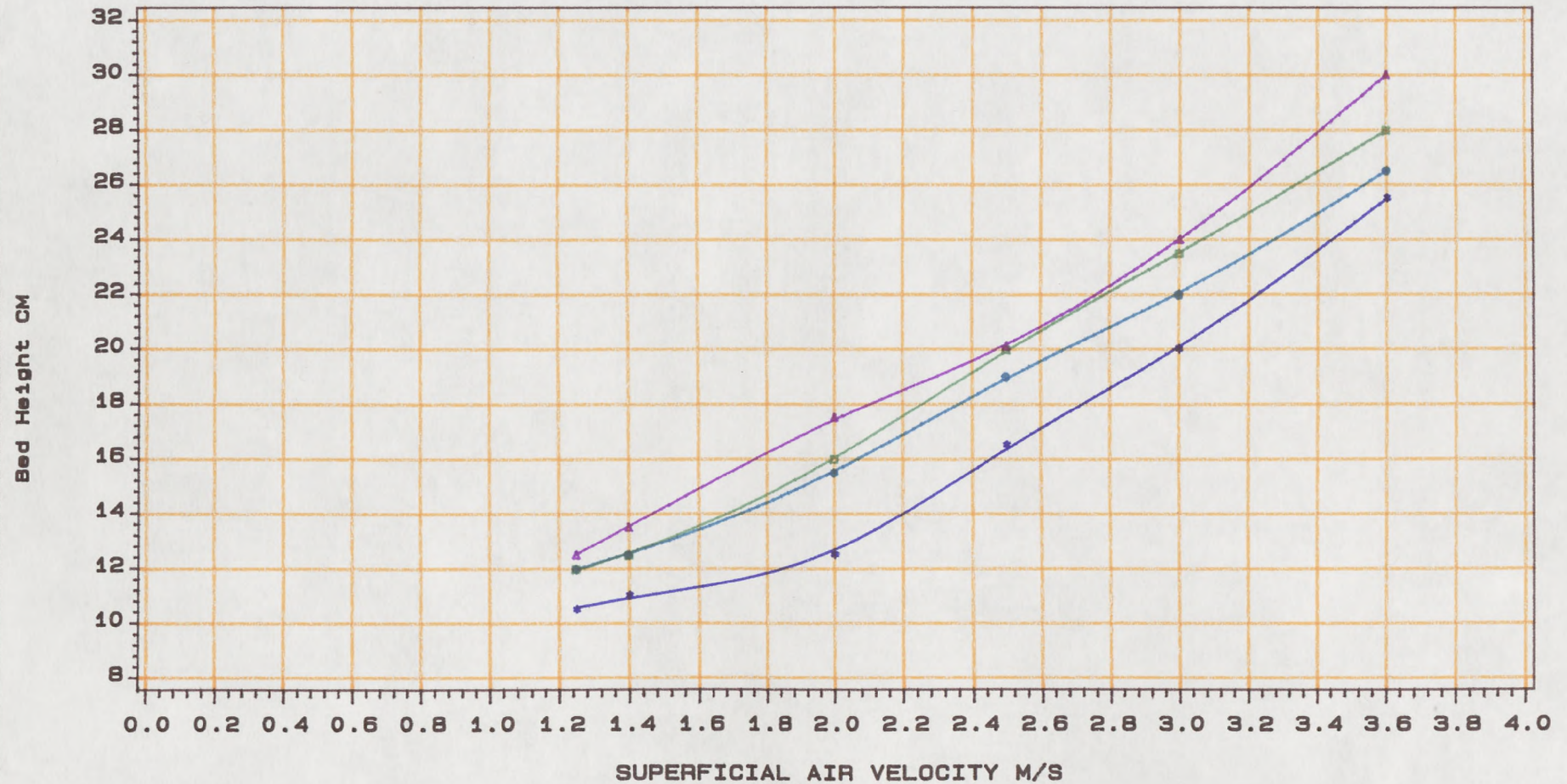
Figures 5.1.50 and 5.1.51 compare the effect of air velocity on the expanded bed height fluctuation for different packings at zero and  $8.77 \times 10^{-3}$  m/s liquid superficial velocities respectively. It can be seen that the fluctuation in the bed height is greater for the oblate spheroid and smaller for the slotted sphere packings as compared to the 38 mm and 25 mm plain sphere packings.

**Fig 5.1.48 Plot Of Variation Of Bed Height With Liquid Holdup For Mobile Bed Packings**  
**BED STATIC HEIGHT=10.5 CM SUPERFICIAL LIQUID VELOCITY =2.32E-3 M/S**



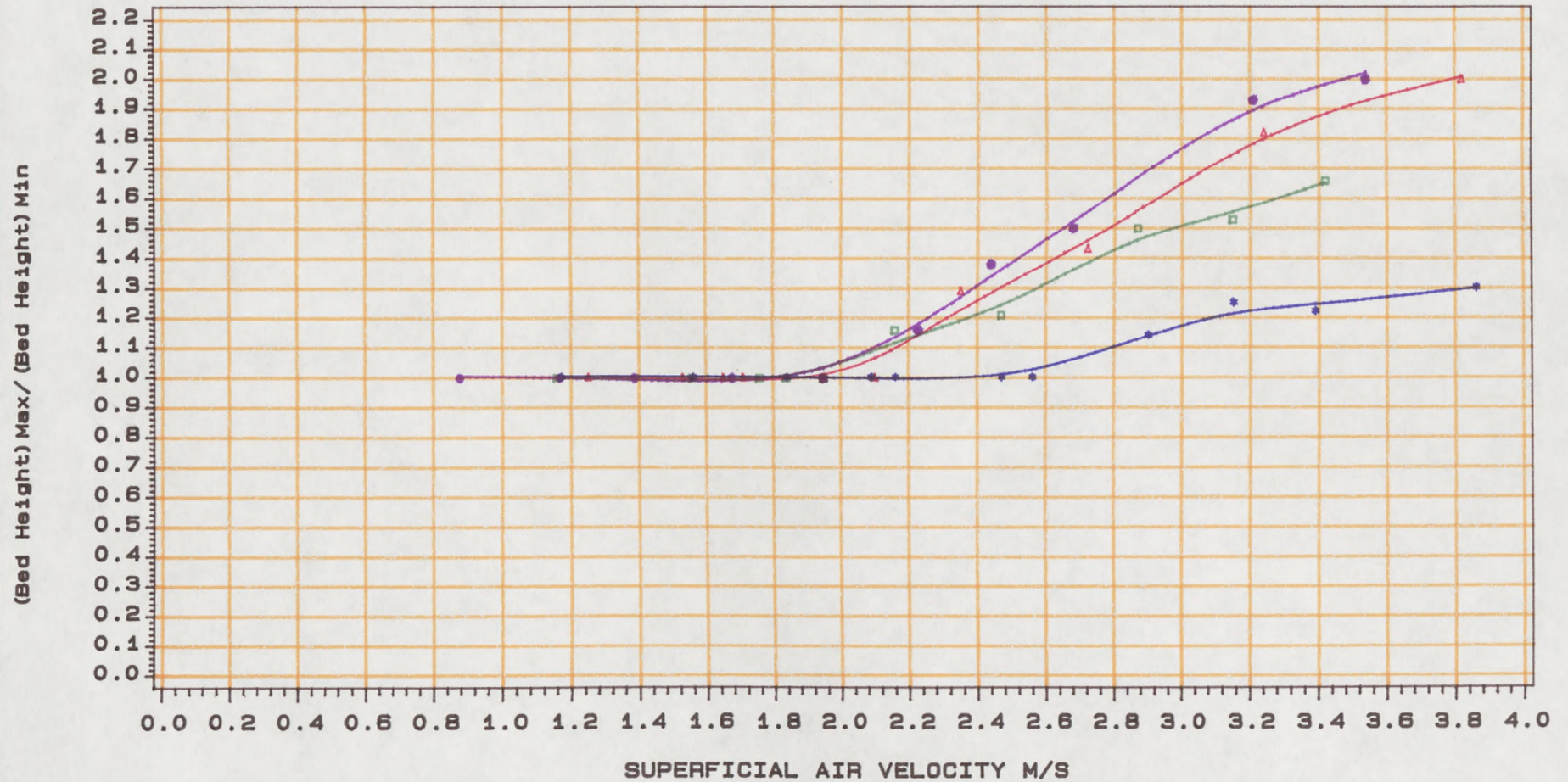
SLOTTED Dia=25 mm    PLAIN Dia=25 mm    PLAIN Dia=38 mm    OBLATE Dia=50\*38 mm

**Fig 5.1.49 Plot Of Variation Of Bed Height With Air Velocity For Mobile Bed Packings**  
**BED STATIC HEIGHT=10.5 CM SUPERFICIAL LIQUID VELOCITY=2.32E-3 M/S**



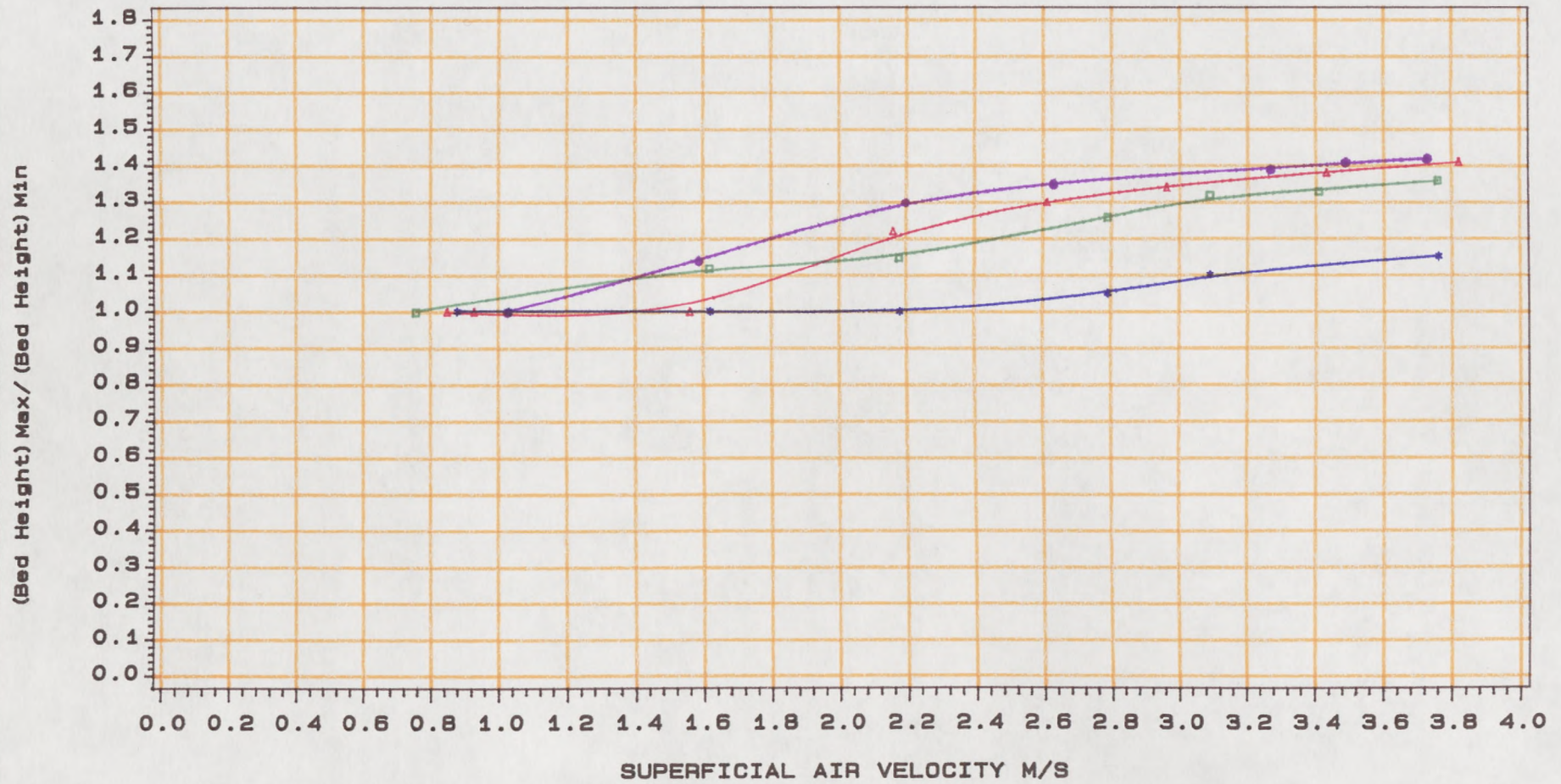
SLOTTED Dia=25 mm    PLAIN Dia=25 mm    PLAIN Dia=38 mm    OBLATE Dia=50\*38 mm

**Fig 5.1.50 Plot Of Variation Of Fluctuation Of Bed Height With Air Velocity For Mobile Bed Packings**  
**BED STATIC HEIGHT=10.5 CM DRY BED**



SLOTTED SPHERE DIA=25 mm
PLAIN SPHEREDIA=25 mm
PLAIN SPHERE DIA=38 mm
QBLATE DIA=50 mm

Fig 5.1.51 Plot Of Variation Of Fluctuation Of Bed Height With Air Velocity For Mobile Bed Packings  
 BED STATIC HEIGHT=10.5 CM LIQUID SUPERFICIAL VELOCITY=8.77E-3 M/S



SLOTTED SPHERE DIA=25 mm    PLAIN SPHERE DIA=25 mm    PLAIN SPHERE DIA=38 mm    OBLATE DIA=50\*38 mm

## 5.2 Mass Transfer Results and Discussion

### 5.2.1 Theoretical Model and Treatment of Data

The technique of gas absorption accompanied by an irreversible pseudo-first order reaction has been used to determine both the liquid film transfer coefficient and interfacial area. In this case the rate of absorption is given by Danckwerts' model for absorption accompanied by chemical reaction into an agitated liquid surface (41).

$$RA = AC_{Ai} \sqrt{DK_1 + k_L^2} \quad (5.2.1.1)$$

where  $C_{Ai} = PH_e$ , (RA) is the total rate of absorption and (A) is the total interfacial area between the gas and liquid and R is the rate of absorption per unit area after contact time (t),  $\text{gmol/cm}^2\text{s}$ .

Assuming the gas film resistance is negligible, squaring and rearranging equation (5.2.1.1) gives

$$\left[ \frac{RA}{C_{Ai}} \right]^2 = A^2 D K_1 + (k_L A)^2 \quad (5.2.1.2)$$

The rate of absorption was measured for four different sodium hydroxide concentrations and corresponding parameter values  $C_{Ai}$ ,  $D_A$  and  $K_2$  were calculated using equations given in Appendix (A) and writing a computer program, thus enabling  $(RA/C_{Ai})^2$  to be plotted against  $DK_1$  for each run, which is known as Danckwerts' plot. From the intercept and slope of the line of best fit of this plot the liquid film transfer coefficient ( $k_L$ ) and total interfacial area (A) for slotted, plain and oblate spheroid packing under the different experimental conditions were estimated.

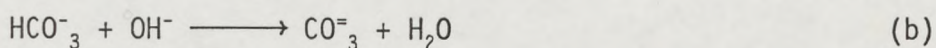
An alternative way of estimating the ( $k_L$ ) and (A) values is by using the Danckwerts' full model at low sodium hydroxide concentration and Danckwerts' short model at high sodium hydroxide concentration respectively. Comparisons of estimated values of (A) and ( $k_L$ ) for the two methods are given in Appendices (B and C).

It was also possible to calculate  $K_G a$  by measuring the rate of absorption and average  $\text{CO}_2$  concentration ( $\bar{P}_{\text{CO}_2}$ ) across the bed.

The overall volumetric mass transfer coefficient ( $K_G a$ ) should reflect chemical volumetric liquid film transfer coefficient, i.e.  $E k_L A$  values, where  $E$  is the enhancement factor due to chemical reaction.

### 5.2.2 Absorption of $\text{CO}_2$ in NaOH Solutions

The reaction systems of carbon dioxide and sodium hydroxide has been widely used by many workers in order to investigate mass transfer performance of different contactors (28, 31, 35, 37). The reaction is believed to take place in two steps,



Reaction (a) is second-order with respect to  $\text{CO}_2$  and hydroxyl ions, reaction (b) is an ionic reaction and is very much faster than reaction (a) (56). Thus the overall reaction is a second-order reaction between the dissolved carbon dioxide and hydroxyl ions, i.e.



For the special case where the concentration of sodium hydroxide is high enough and therefore does not drop appreciably near the surface

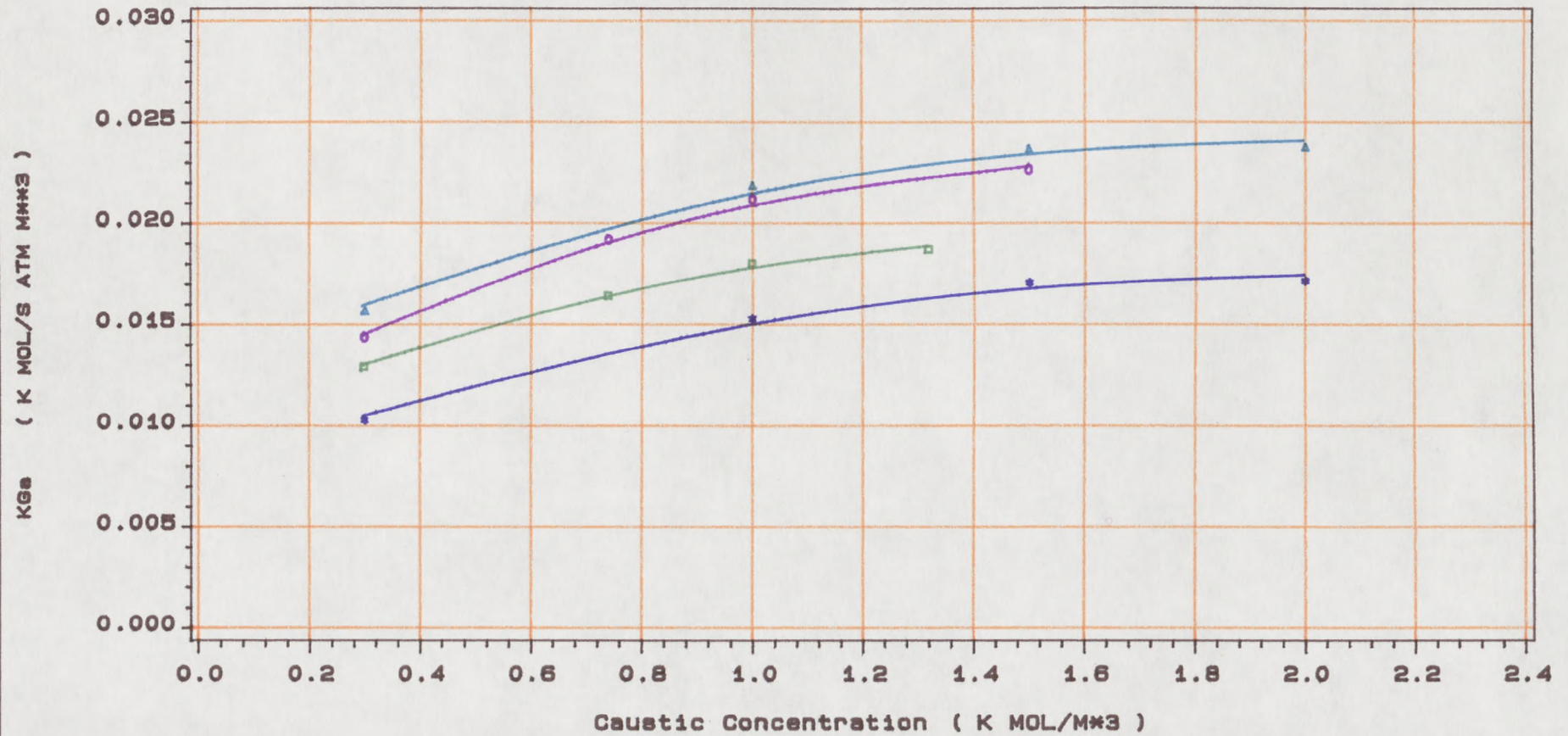
during the reaction, the reaction (c) can be considered to be a pseudo-first order reaction. Figures (5.2.1 to 5.2.4) show the effect of liquid rate and sodium hydroxide concentration on the overall volumetric mass transfer coefficient  $K_G a$  for oblate spheroid, slotted and plain packing. It can be seen that  $K_G a$  increases with both sodium hydroxide and liquid superficial velocity.

Similar behaviour has been reported by Wozniak and Ostergaard (30) and by Wales (31). The increase in the  $K_G a$  with reactant concentration (NaOH) is to be expected since the reaction is pseudo-first order reaction at high NaOH concentration. The increase in  $K_G a$  with liquid velocity can be attributed to the enhancement of mass transfer ( $k_L$ ) due to an increase in the turbulence and agitation of liquid and packing. Figure 5.2.4 compares the variation of  $K_G a$  with liquid velocity for slotted and oblate packing. It can be seen that the  $K_G a$  is substantially higher for the slotted packing than the oblate spheroid packing, indicating that the slotted packing offers more vigorous agitation of bed with a higher interfacial area and liquid film coefficient.

### 5.2.3. Estimation of Interfacial Area ( $a$ ) and Liquid Film Transfer Coefficient ( $k_L$ )

Typical Danckwerts' plots are presented in figures 5.2.5 to 5.2.8. In all cases the experimental points on Danckwerts' plot lay on a straight line which shows the applicability of Danckwerts' model in describing mass transfer in the beds of the mobile packing studied in this work. It is also evident from the plots that both the interfacial area and the liquid film transfer coefficient increase with both liquid and gas rates.

**Fig 5.2.1 Plot Of Overall Mass Transfer Coefficient VS Caustic Concentration For Oblate Air Velocity=2.1 M/S  
Packing Dia=50\*38 mm Bed Static Height=10.5 cm  
FOR VARIOUS SUPERFICIAL LIQUID VELOCITY**



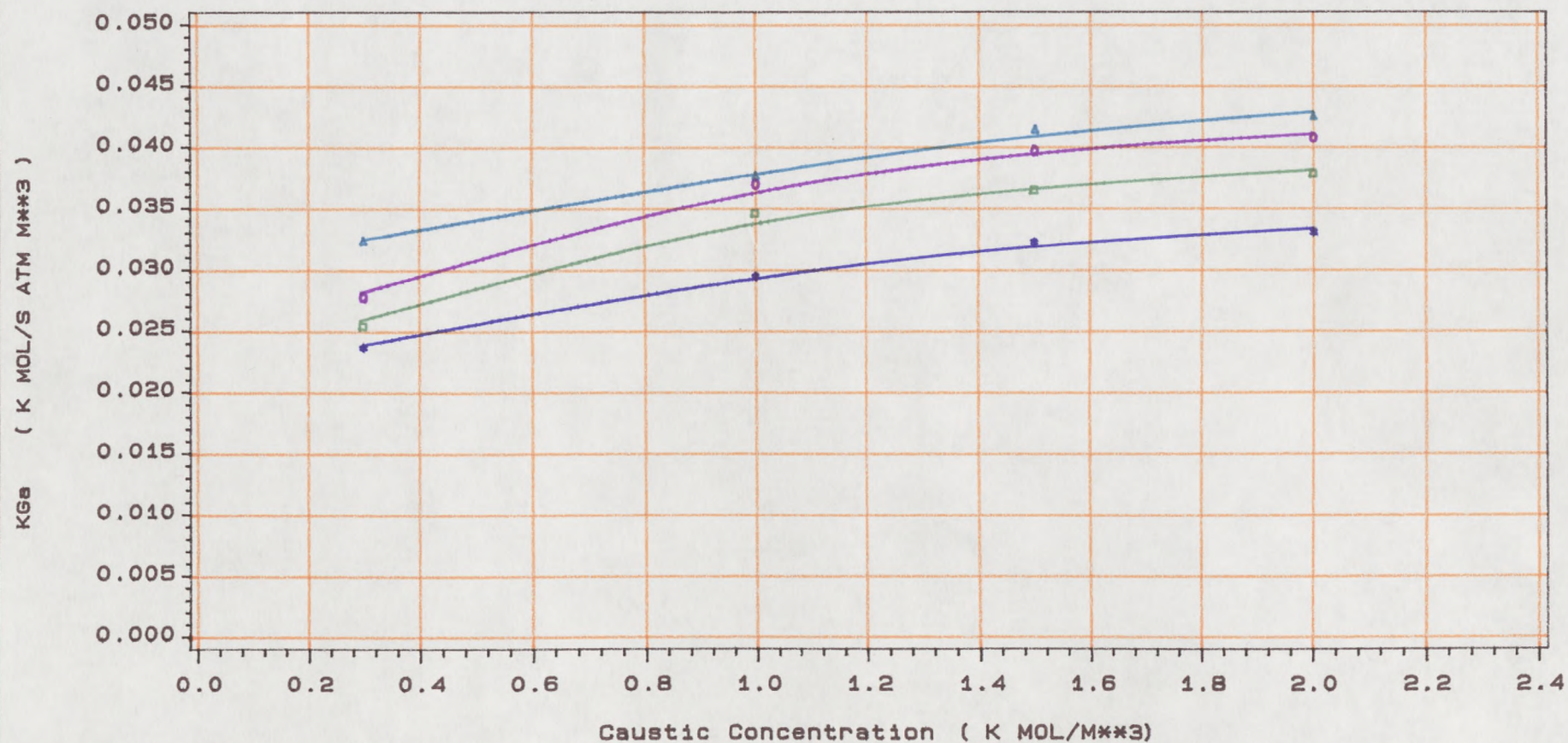
VL=2.32E-3 M/S

VL=4.38E-3 M/S

VL=6.58E-3 M/S

VL=10.96E-3 M/S

Fig 5.2.2 Plot Of Overall Mass Transfer Coefficient VS Caustic Concentration For Slotted Sphere Air Velocity=2.1 M/S  
 Packing Dia=25 mm Open Area=0.11 Bed Static Height=10.5 Cm  
 FOR VARIOUS SUPERFICIAL LIQUID VELOCITY



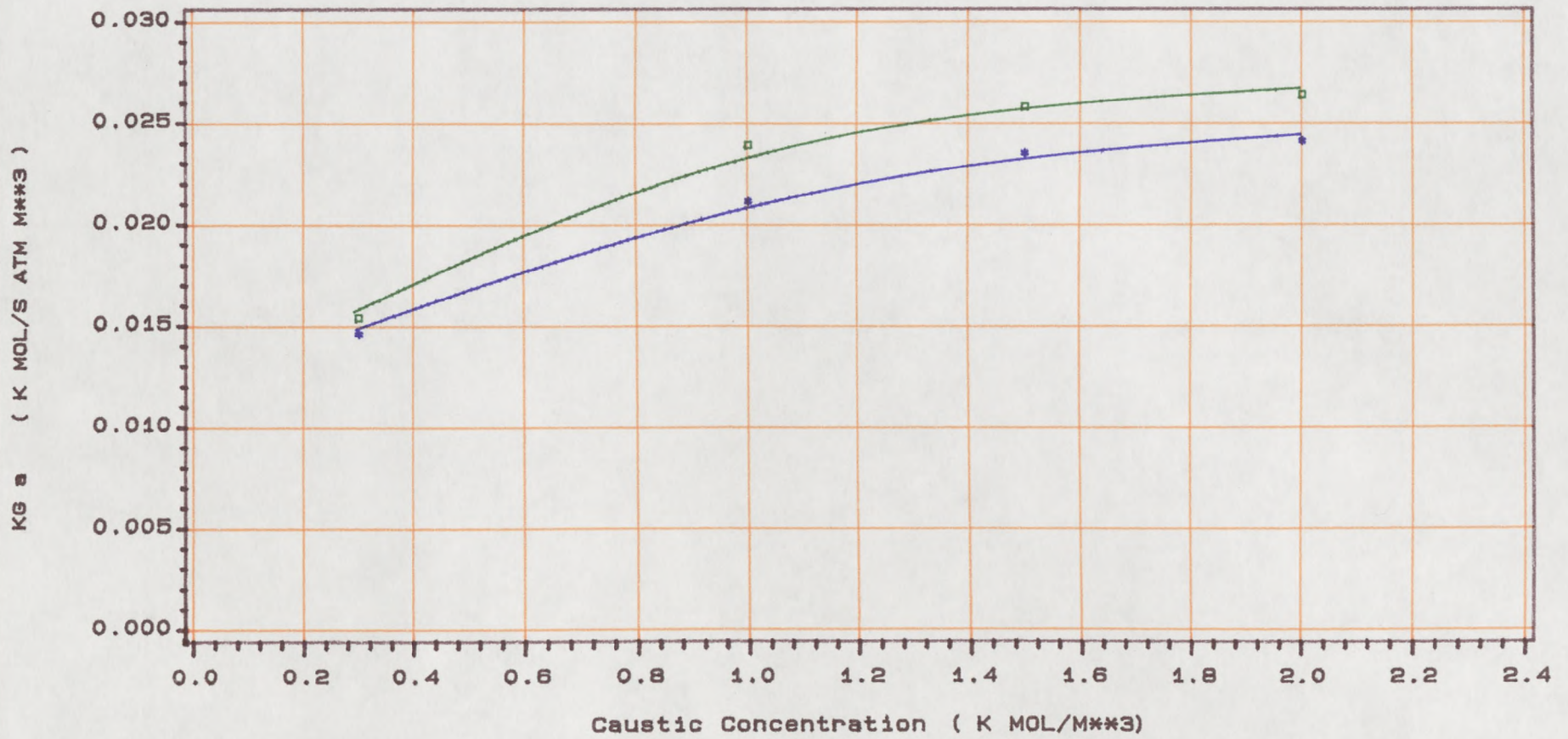
VL=2.32E-3 M/S

VL=4.38E-3 M/S

VL=6.58E-3 M/S

VL=10.9E-3 M/S

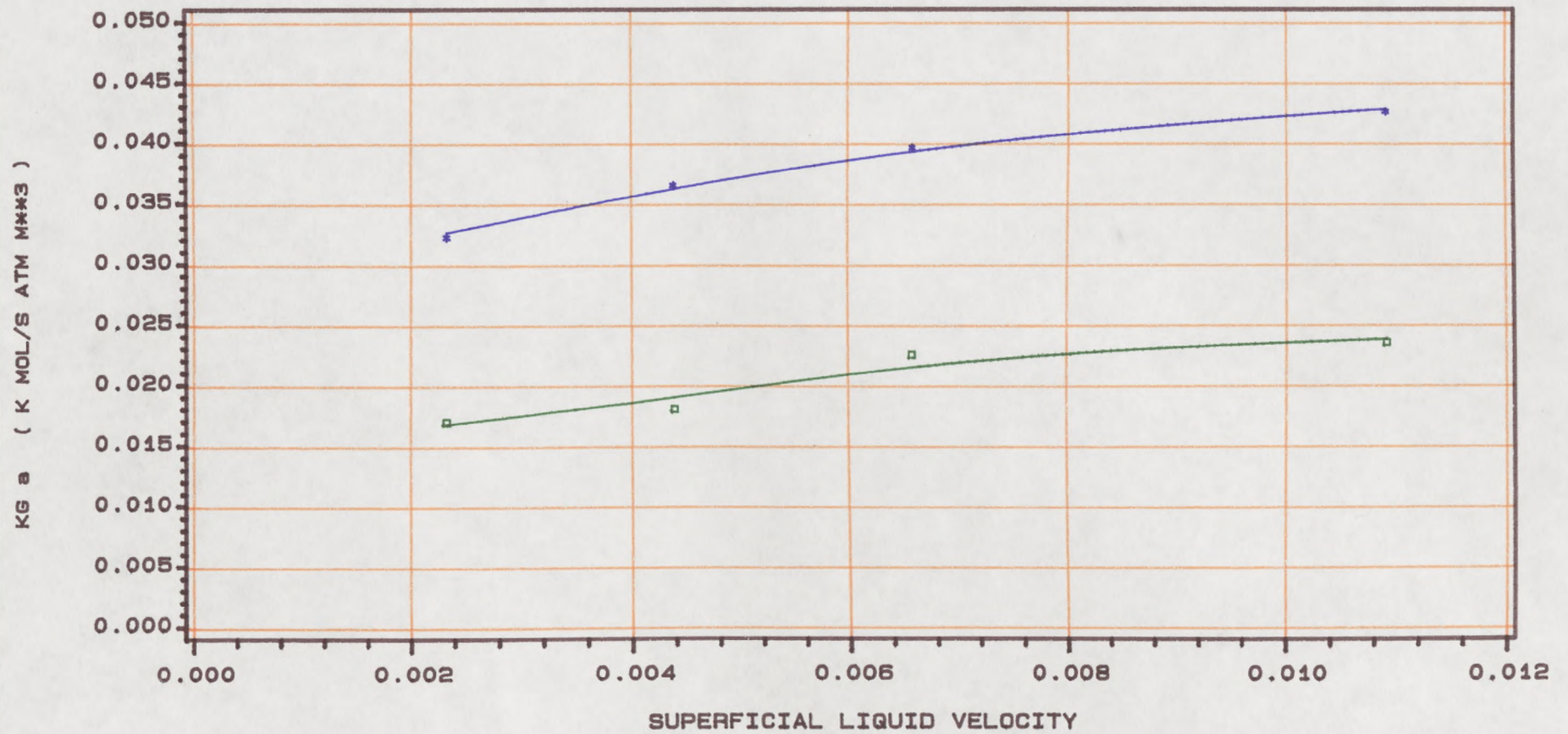
Fig 5.2.3 Plot Of Overall Mass Transfer Coefficient VS Caustic Concentration For Plain Sphere Air Velocity=2.1 M/S  
 Packing Dia=25 mm Bed Static Height=10.5 cm  
 FOR VARIOUS SUPERFICIAL LIQUID VELOCITY



VL=2.32E-3 M/S

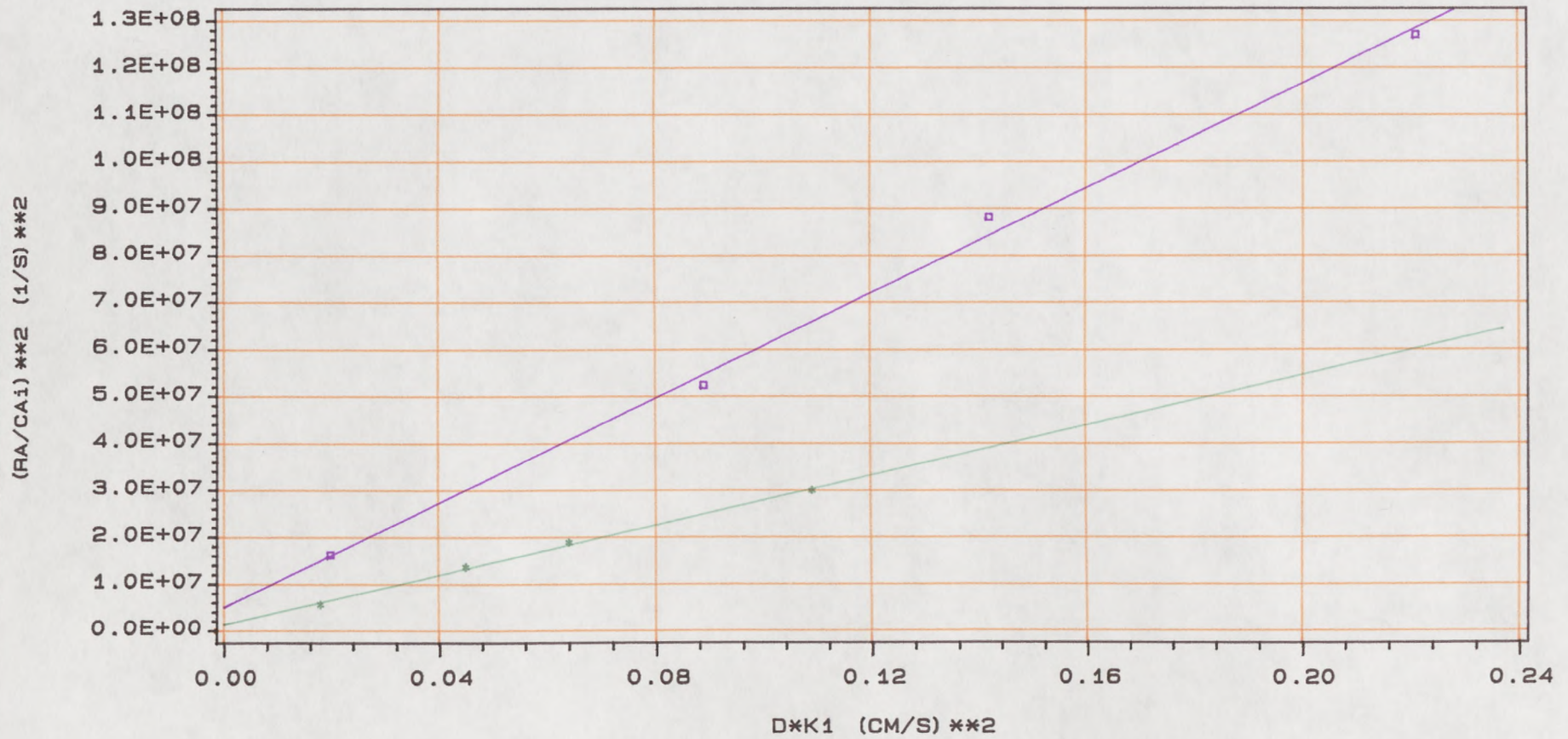
VL=6.58E-3 M/S

Fig 5.2.4 Plot Of OVERALL MASS TRANSFER Coefficient VS Liquid Rate At Superficial Air Velocity=2.1 M/S  
 Bed Static Height=10.5 cm  
 For Mobile Packings Caustic Concentration=1.5 K MOL/M\*\*3



Slotted Packing Dia=25 mm Open Area=0.11 Oblate Packing Dia=50\*38 mm

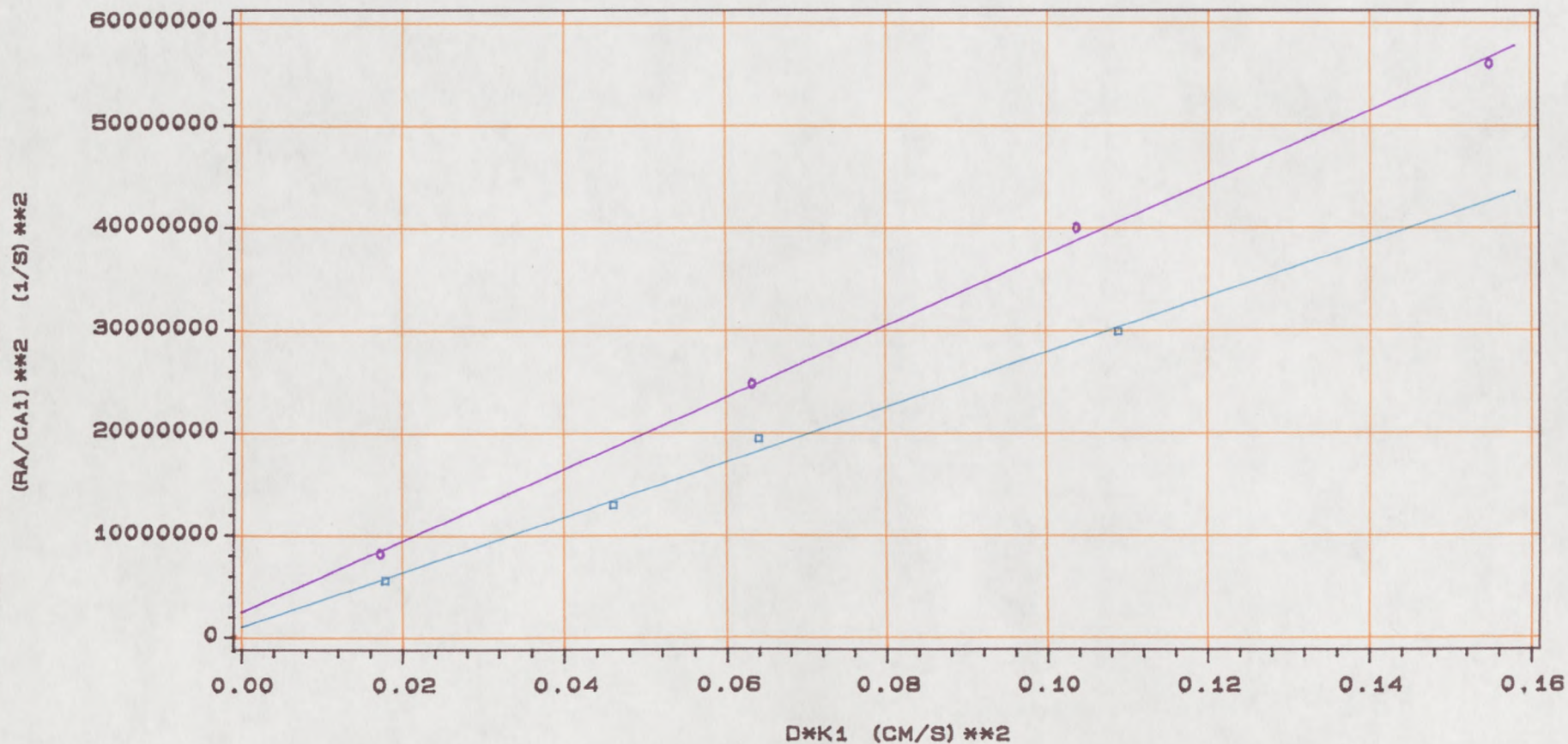
Fig 5.2.5 Plot Of Mass Transfer Characteristics Of Oblate Packing For Superficial Liquid Velocity= $6.58E-3$  M/S  
 Packing Dia=55 mm Bed Static Height=10.5 cm  
 FOR VARIOUS SUPERFICIAL AIR VELOCITY



$V_g = 2.1$  M/S

$V_g = 2.79$  M/S

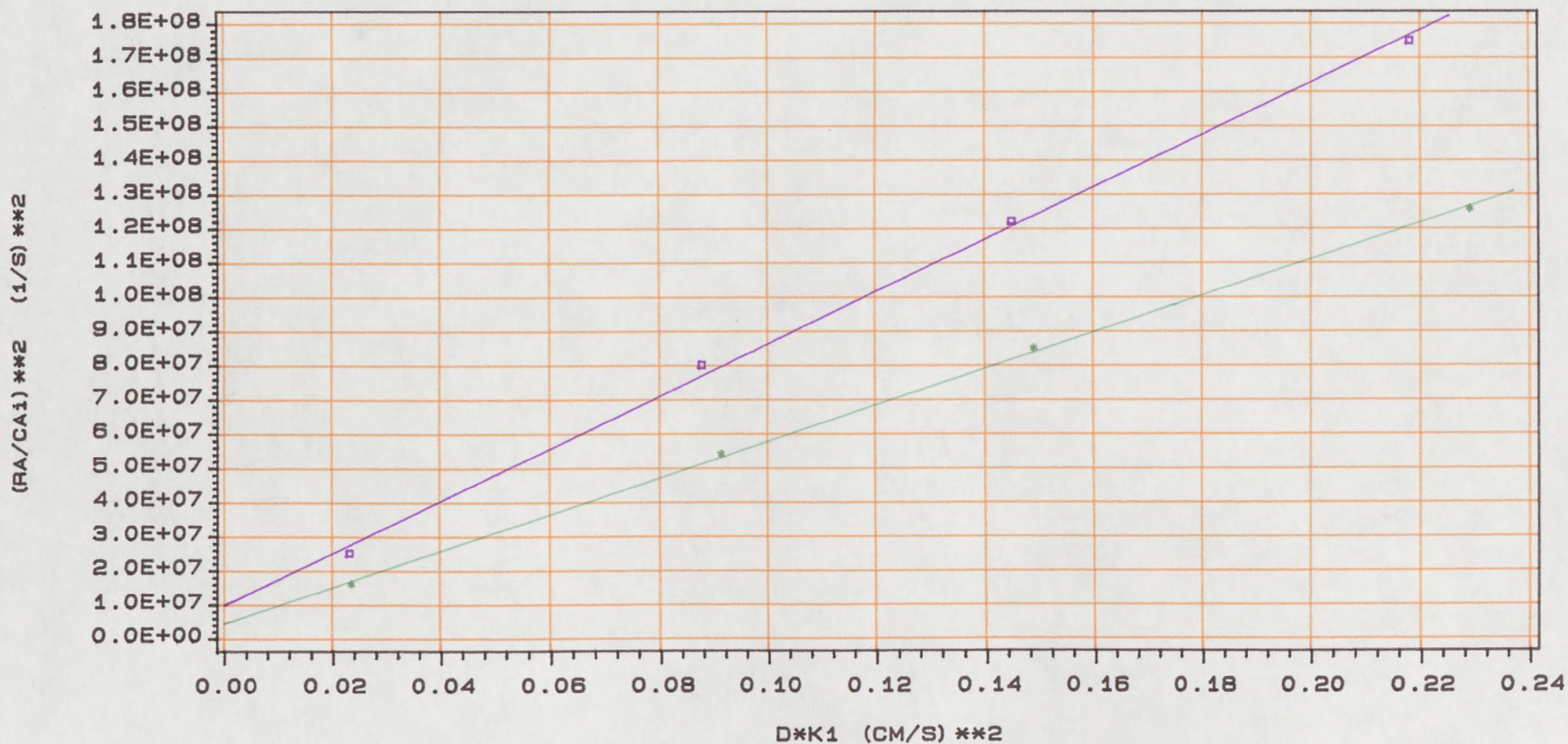
**Fig 5.2.6 Plot Of Mass Transfer Characteristics Of Oblate Packing For Superficial Air Velocity=2.1 M/S  
 Packing Dia=50\*38 mm Bed Static Height=10.5 cm  
 FOR VARIOUS SUPERFICIAL LIQUID VELOCITY**



$v_L = 6.58 \times 10^{-3}$  M/S

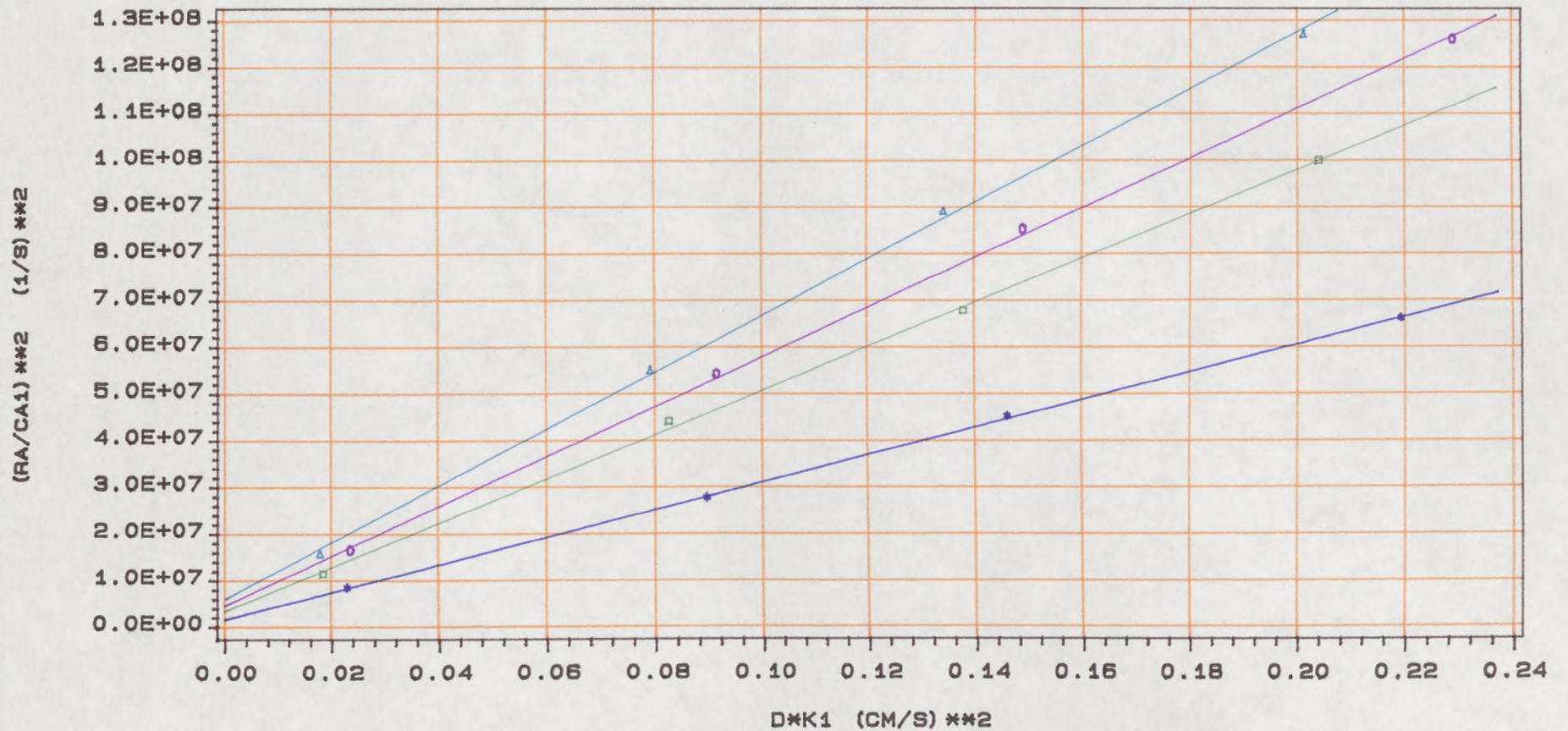
$v_L = 10.9 \times 10^{-3}$  M/S

Fig 5.2.7 Plot Of Mass Transfer Characteristics Of Slotted Sphere At Superficial Liquid Velocity= $6.58E-3$  M/S  
 Packing Dia=25 mm Open Area=0.11 Bed Static Height=10.5 Cm  
 FOR VARIOUS SUPERFICIAL AIR VELOCITY



$V_g = 2.1$  M/S       $V_g = 2.79$  M/S

**Fig 5.2.8 Plot Of Mass Transfer Characteristics Of Slotted Sphere At Superficial Air Velocity=2.1 (M/S)  
 Packing Dia=25 mm Open Area=0.11 Bed Static Height=10.5 Cm  
 FOR VARIOUS SUPERFICIAL LIQUID VELOCITY**



VL=2.32E-3 M/S

VL=4.38E-3 M/S

VL=6.58E-3 M/S

VL=10.9E-3 M/S

Figure 5.2.9 and 5.2.10 show the effect of air and liquid velocity on the interfacial area per unit of static bed ( $a_s$ ) i.e. the packing volume for the slotted and oblate packing.

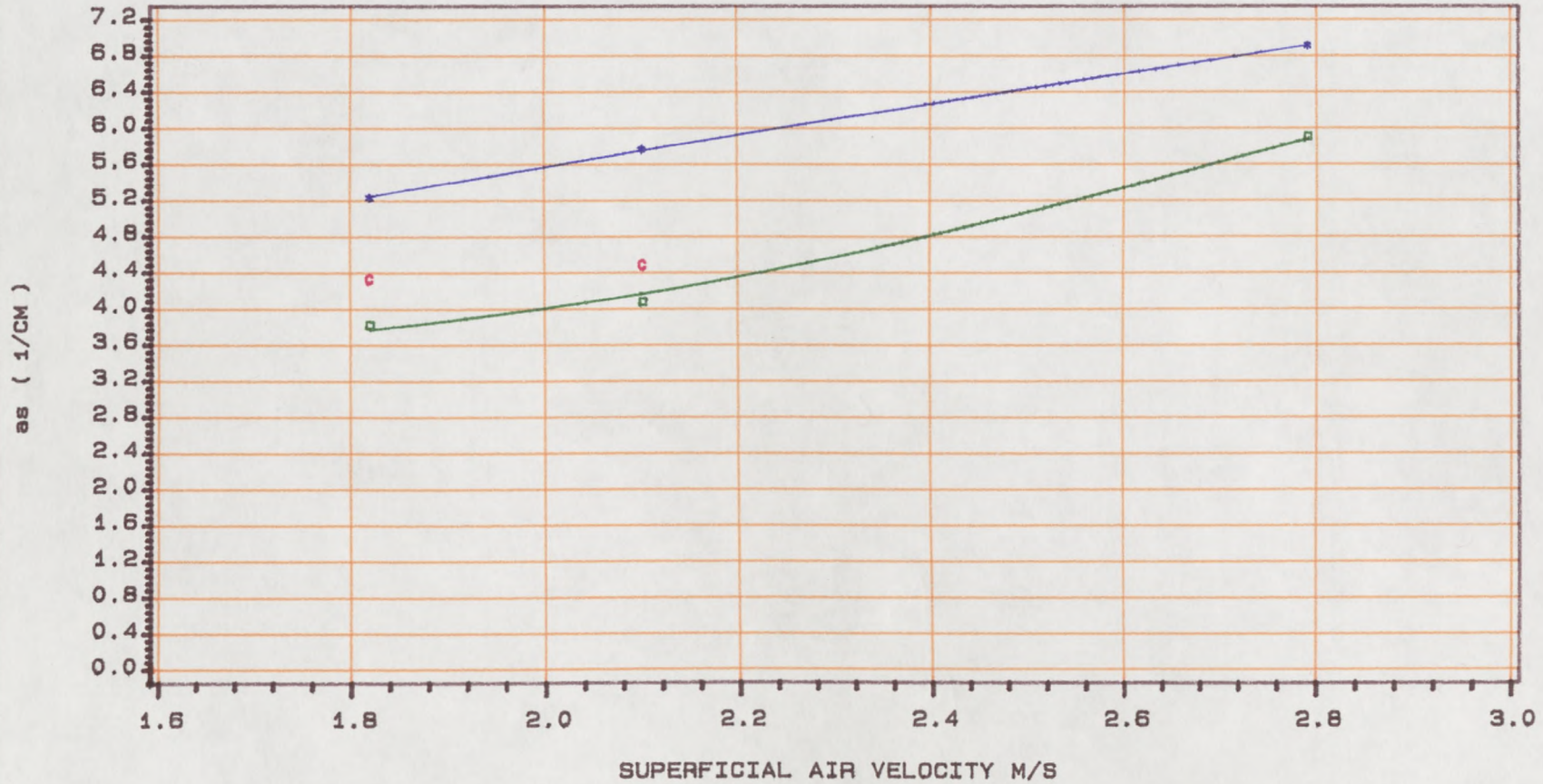
It can be seen that the interfacial area ( $a_s$ ) increases with both air and liquid velocity within the limited range of air and liquid velocity which was investigated. It can be seen that the increase in the interfacial area ( $a_s$ ) is greater for the slotted sphere packing than for the oblate spheroid packing. The higher interfacial area for slotted packing might be expected as the liquid hold up in the bed and the surface area of packing per unit volume of bed for the slotted packing is higher than for the oblate spheroid packing.

Tables 5.2.1 and 5.2.2 compare the interfacial area ( $a_s$ ), for plain and slotted packings at different air and liquid rates. It can be seen that at a given air and liquid rate the interfacial area ( $a_s$ ) for the slotted packing is higher than for the plain packing. When the air and liquid velocity (especially the air velocity) are increased to the stage that the bed height begins to fluctuate widely with the appearance of slugging in the bed. The presence of slugging in the bed disturbs the homogeneity of the bed.

Kossev et al (35), Strumillo and Kudra (37) and Kito et al (22) reported a decrease in the interfacial area at high gas velocities due to nonuniformity in the bed structure as a result of slugging phenomenon being present.

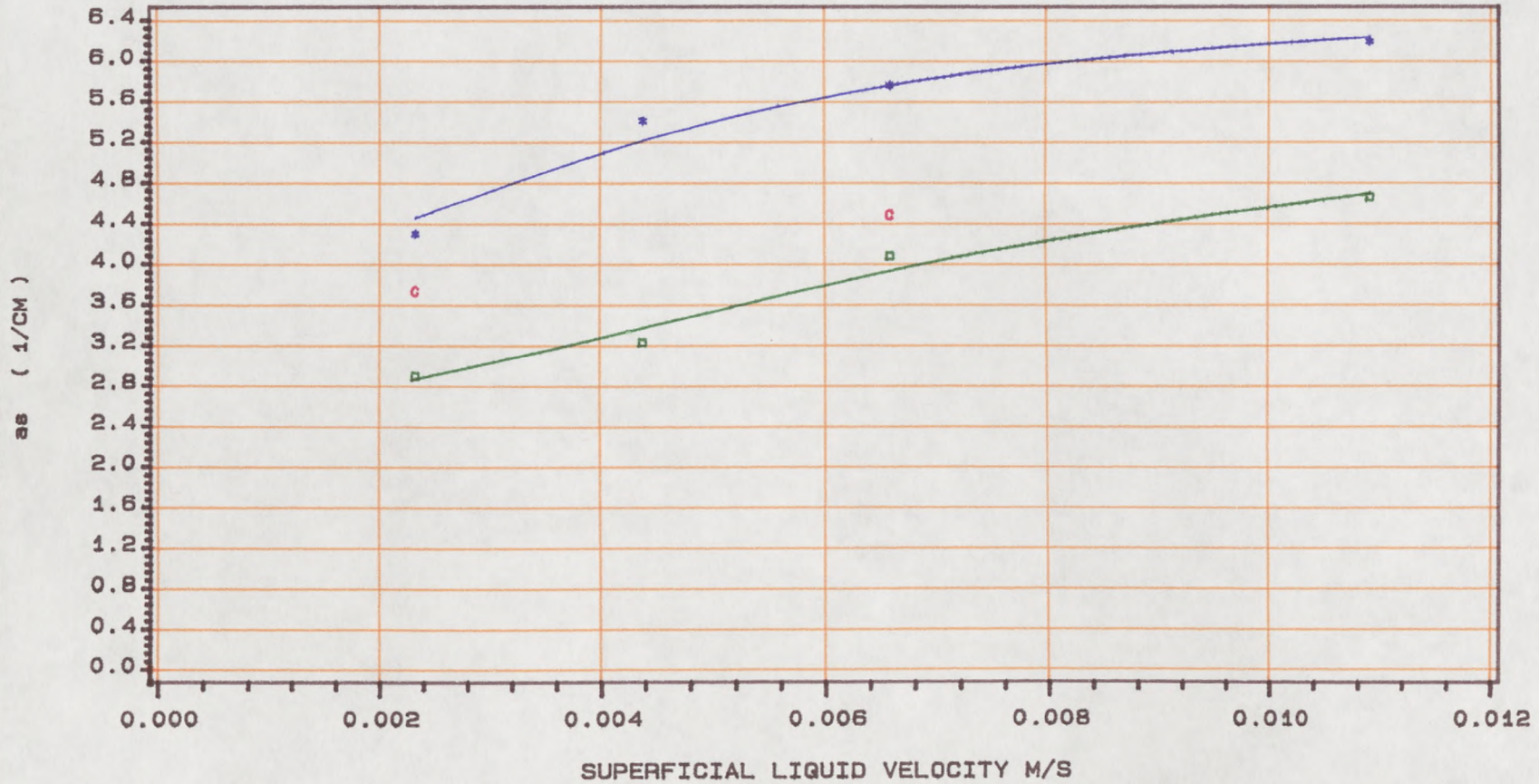
It is worth noting that an increase in the liquid rate from  $2.32 \times 10^{-3}$  m/s to  $1.09 \times 10^{-2}$  m/s, (nearly 4.7 times) the increase in liquid hold up is 85% for the slotted packing and 200% for the oblate spheroid packing which will increase the total interfacial area by 43% for the

Fig 5.2.9 Plot Of Interfacial Area Per Unit Volume Of Static Bed VS Superficial Air Velocity  
 Static Bed Height=10.5 cm Superficial Liquid Velocity=6.58E-3 M/S  
 For Mobile Packings



Slotted Packing Dia=25mm Open Area=0.11    Oblate Packing Dia=50\*38 mm    Plain Sphere Dia=25 mm

Fig 5.2.10 Plot Of Interfacial Area Per Unit Volume Of Static Bed VS Superficial Liquid Velocity  
 Static Bed Height=10.5 cm Superficial Air Velocity=2.1 M/S  
 For Mobile Packings



Slotted Packing Dia=25 mm Open Area=0,11 Oblate Packing Dia=50\*38 mm Plain Sphere Dia=25 mm

Table 5.2.1. Comparison of  $a_s$  and  $a_L$  at different gas velocity.

$V_g$ m/s	$a_s$ $\text{cm}^{-1}$		$a_L$ $\text{cm}^{-1}$	
	slotted	plain	slotted	plain
1.82	5.23	4.33	16.60	28.90
2.10	5.76	4.48	20.56	29.10

$$V_L = 6.58 \times 10^{-3} \text{ m/s}$$

Table 5.2.2. Comparison of  $a_s$  and  $a_L$  at different liquid velocity.

$V_L$ m/s	$a_s$ $\text{cm}^{-1}$		$a_L$ $\text{cm}^{-1}$	
	slotted	plain	slotted	plain
$2.32 \times 10^{-3}$	4.31	3.73	21.47	34.0
$6.58 \times 10^{-3}$	5.76	4.48	20.56	29.10

$$V_s = 2.1 \text{ m/s}$$

slotted packing and 60% for the oblate spheroid packing. Whereas an increase in air velocity from 1.82 m/s to 2.79 m/s (nearly 53%) increases liquid hold up by 6% for slotted packing and by 25% for oblate spheroid packing and will increase the total interfacial area by 32% for the slotted packing and 54% for the oblate spheroid packing. This is probably because the liquid hold up is being dispersed more efficiently with increasing air velocity than with increasing liquid velocity. In the case of the plain sphere packing an increase in the liquid velocity from  $2.32 \times 10^{-3}$  m/s to  $6.58 \times 10^{-3}$  m/s (produced an increase in the liquid hold up of 40%) with an increase in the total interfacial area of 20%. An increase in the air velocity however, from 1.82 m/s to 2.1 m/s, increases the total interfacial area by only 3%.

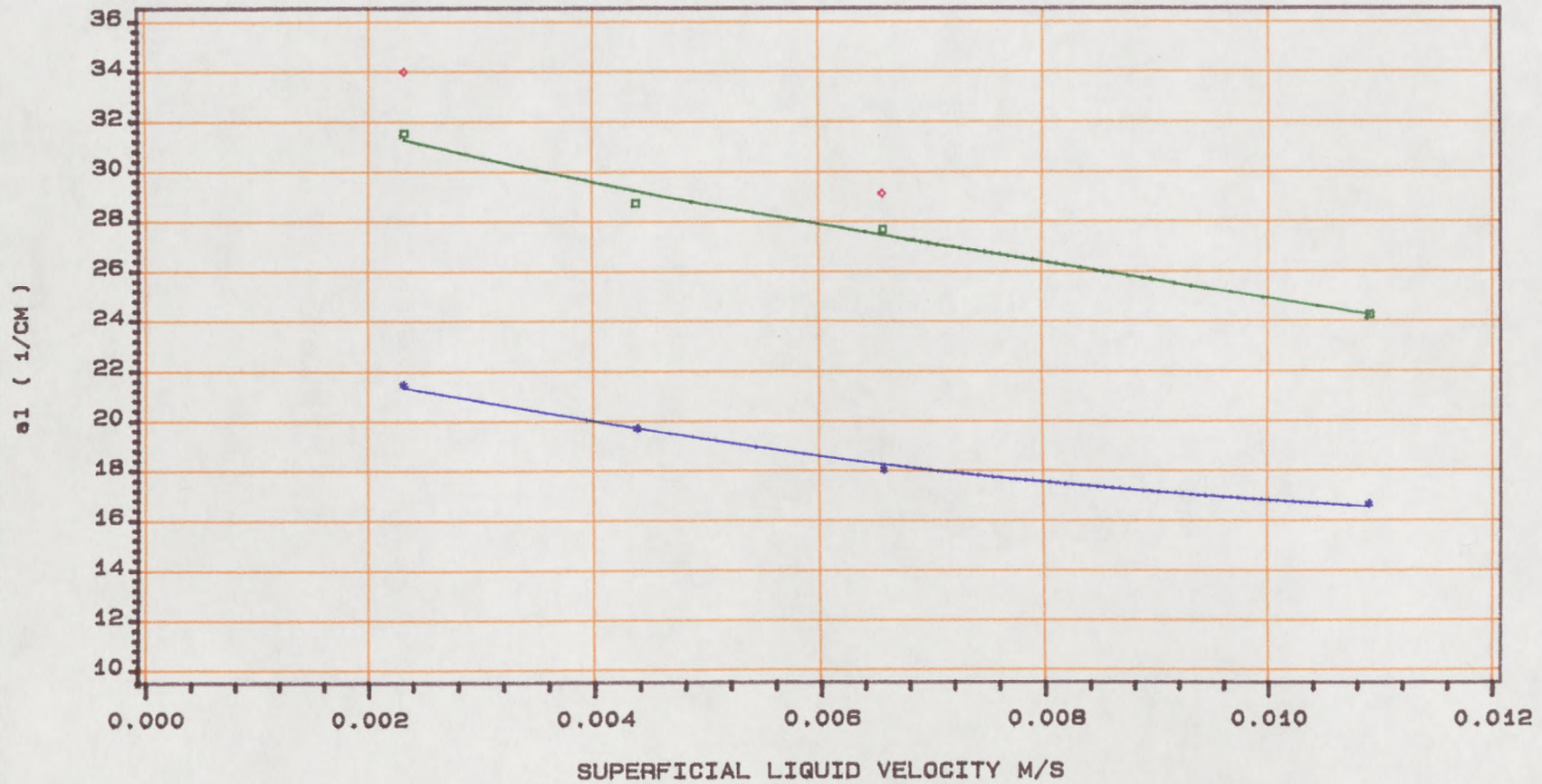
The effect of increasing liquid and air velocities on the interfacial area per unit volume of liquid hold up in the bed ( $a_L$ ) for the slotted and oblate packings is shown in figures 5.2.11 and 5.2.12. From figure 5.2.11 it can be seen that ( $a_L$ ) decreases with increasing liquid rate for both packings, but ( $a_L$ ) is higher for the oblate packing than for the slotted packing, probably indicating poor liquid dispersion inside the slotted packings.

The decrease in the ( $a_L$ ) with increasing liquid velocity is due to a relatively larger increase in liquid hold up as compared to the corresponding increase in interfacial area (see Table 5.2.3).

It is also shown that at a given liquid velocity the value of ( $a_L$ ) for the slotted packing is less than the corresponding value for the oblate spheroid and plain sphere packings. This is because the ratio of total interfacial area of the slotted packing to the oblate spheroid packing is smaller than the ratio of the liquid hold up of slotted ball to the oblate spheroid packing (see Table 5.2.3).

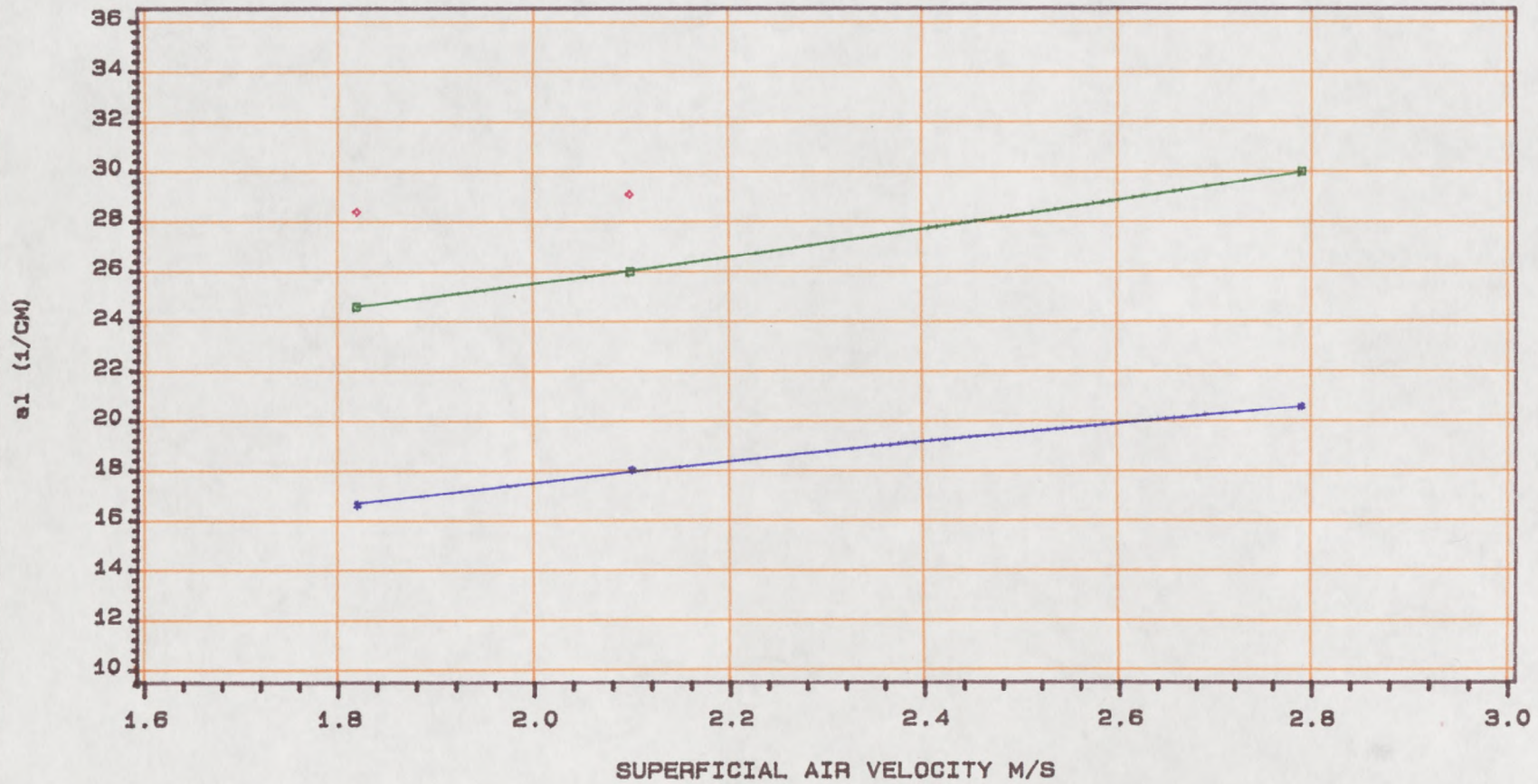
It may, however, be possible to increase and improve the contribution of the liquid hold up to the total interfacial area in the case of slotted packings by optimizing the hole size or numbers and thereby dispersing the present liquid within the bed more efficiently. Figure 5.2.12 shows the variation of ( $a_L$ ) with the air velocity for the slotted and oblate spheroid packings. It can be seen that ( $a_L$ ) increases with increasing air velocity for both the packings. This is because the factor by which the total interfacial area increases with air velocity is greater than the corresponding increase in the liquid hold up (see Table 5.2.4). It is also evident that ( $a_L$ ) for the slotted

**Fig 5.2.11 Plot Of Interfacial Area Per Unit Volume Of Liquid Hold Up VS Superficial Liquid Velocity**  
**Bed Static Height=10.5 cm Superficial Air Velocity=2.1 M/S**  
**For Mobile Packings**



Slotted Packing Dia=25mm Open Area=0.11    Oblate Packing Dia=50\*38 mm    Plain Packing Dia=25 mm

**Fig 5.2.12 Plot Of Interfacial Area Per Unit Volume Of Liquid Hold Up VS Superficial Air Velocity**  
 Bed Static Height=10.5 cm Superficial Liquid Velocity=6.58E-3 M/S  
 For Mobile Packings



Slotted Packing Dia=25mm Open Area=0.11    Oblate Packing Dia=50\*38 mm    Plain Packing Dia=25 mm

Table 5.2.3. Variation of  $\epsilon(h_L)$  and  $\epsilon(A)$  with liquid velocity for different packings.

Variation of liquid velocity $V_L$ m/s	Ratio of liquid hold up $\epsilon(h_L)$			Ratio of total interfacial area $\epsilon(A)$			Liquid velocity $V_L$ m/s	$\frac{A \text{ slotted}}{A \text{ oblate}}$	$\frac{h_L \text{ slotted}}{h_L \text{ oblate}}$
	slotted	oblate	plain	slotted	oblate	plain			
$2.32 \times 10^{-3}$ to $4.38 \times 10^{-3}$	1.37	1.21	-	1.26	1.11	-	$2.32 \times 10^{-3}$	1.48	2.16
$2.32 \times 10^{-3}$ to $6.58 \times 10^{-3}$	1.16	1.31	1.40	1.06	1.26	1.20	$4.38 \times 10^{-3}$	1.67	2.4
$6.58 \times 10^{-3}$ to $10.9 \times 10^{-3}$	1.15	1.30	-	1.07	1.14	-	$6.58 \times 10^{-3}$	1.41	2.17
							$10.9 \times 10^{-3}$	1.32	1.92

packings is smaller than the corresponding value for the oblate spheroid and plain sphere packings, again for the same reason explained above.

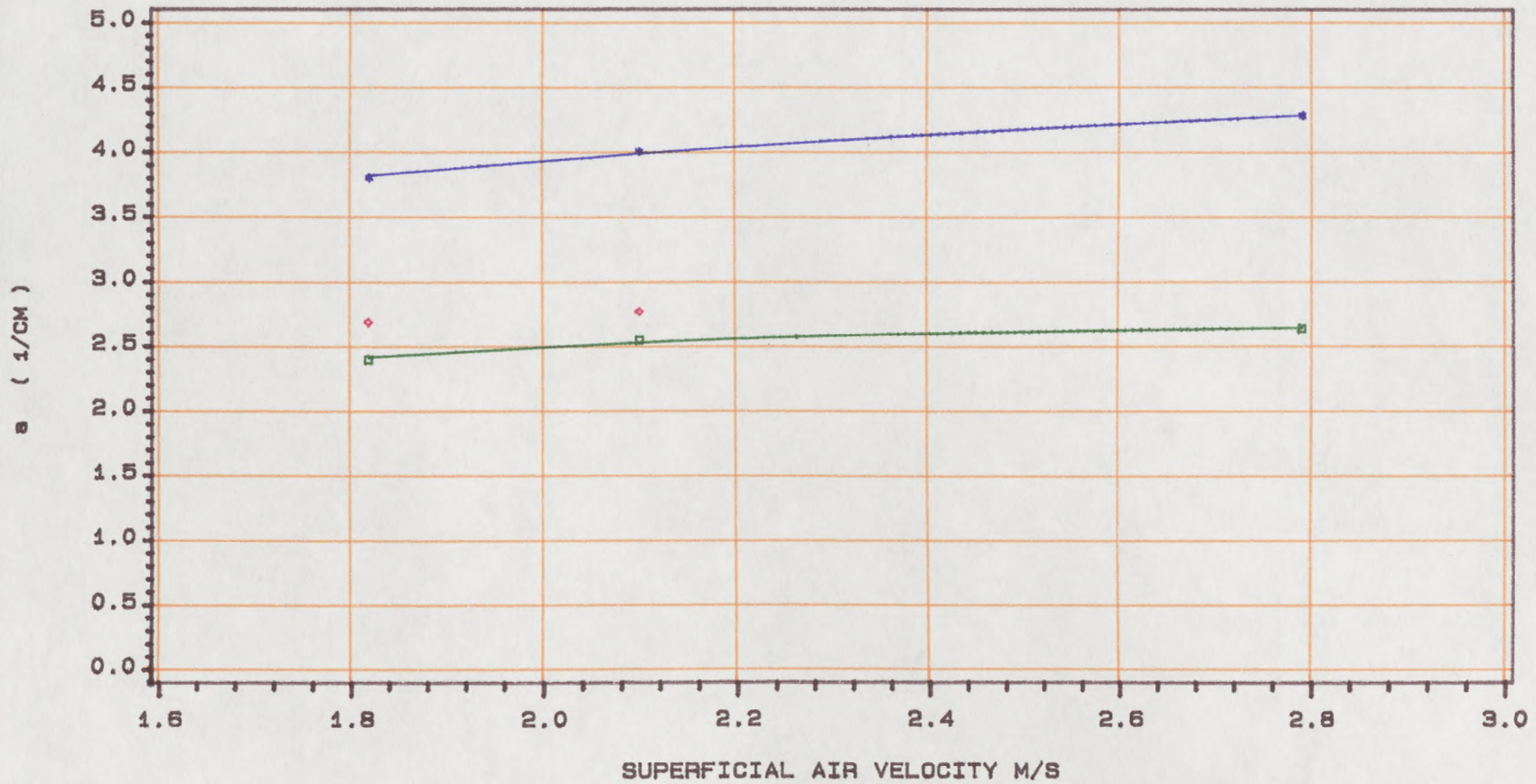
Table 5.2.4. Variation of  $\epsilon(h_L)$  and  $\epsilon(A)$  with gas velocity for different packings.

Variation of air velocity $V_g$ m/s	Ratio of liquid hold up $\epsilon(h_L)$			Ratio of total interfacial area $\epsilon(A)$		
	slotted	oblate	plain	slotted	oblate	plain
1.82-2.1	1.015	1.01	1.01	1.10	1.065	1.034
2.1 -2.79	1.05	1.24	-	1.20	1.45	-

$$V_L = 6.58 \times 10^{-3} \text{ m/s}$$

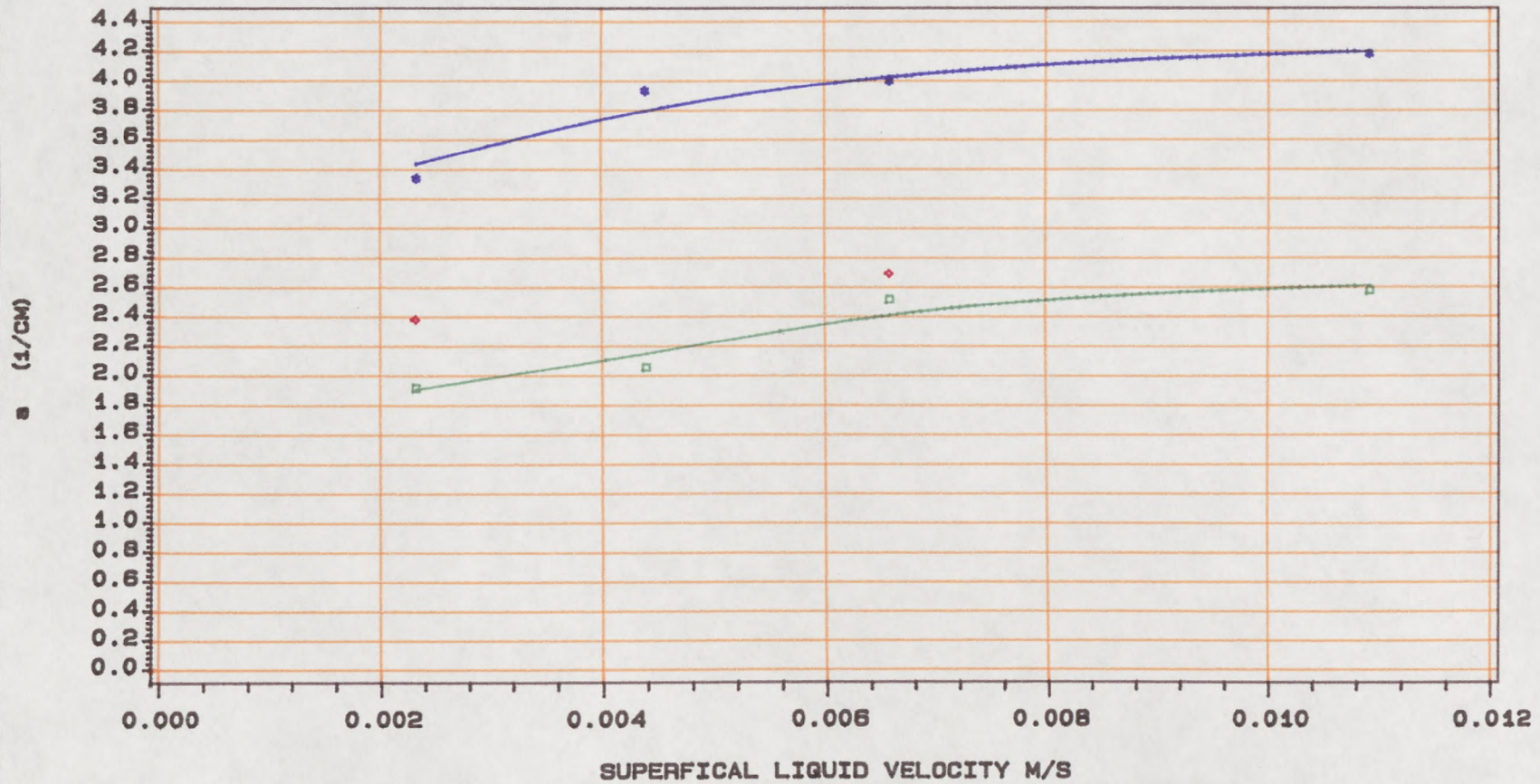
Tables 5.2.1 and 5.2.2 compare the  $(a_L)$  values for the slotted and plain packings. It can be seen that  $(a_L)$  decreases with increasing liquid rate and decreases with air velocity as for the case of slotted and oblate spheroid packings. Figures 5.2.13 and 5.2.14 show the effect of the air and liquid velocity on the interfacial area per unit volume of expanded bed height  $(a)$  for slotted, plain sphere and oblate spheroid packings. It is apparent that  $(a)$  increases consistently with an increase in both air and liquid velocity. This is because the relative increase in the total interfacial area of the bed due to higher air and liquid velocity, exceeds the relative increase in the height of the expanded bed. It can also be seen that  $(a)$  is higher for the slotted packing than for the oblate spheroid and plain sphere packings as on the one hand the total interfacial area of slotted packing is higher than the oblate and plain sphere packings, and, on the other hand the expansion of bed height is higher for the oblate spheroid and plain

**Fig 5.2.13 Plot Of Interfacial Area Per Unit Volume Of Expanded Bed VS Superficial Air Velocity**  
 Bed Static Height=10.5 cm Superficial Liquid Velocity=6.58E-3 M/S  
 For Mobile Packings



Slotted Packing Dia=25mm Open Area=0.11    Oblate Packing Dia=50\*38 mm    Plain Sphere Dia=25 mm

**Fig 5.2.14 Plot Of Interfacial Area Per Unit Volume Of Expanded Bed VS Superficial Liquid Velocity**  
**Bed Static Height=10.5 cm Superficial Air Velocity=2.1 M/S**  
**For Mobile Packings**



Slotted Packing Dia=25 mm Open Area=0.11 Oblate Packing Dia=50\*38 mm Plain Sphere Dia=25 mm

sphere packings than for the slotted packing (see Table 5.2.5). This means that for the same liquid and air throughput the slotted packing offers higher interfacial area and therefore a shorter column is needed as compared to that required for the oblate spheroid and plain packings.

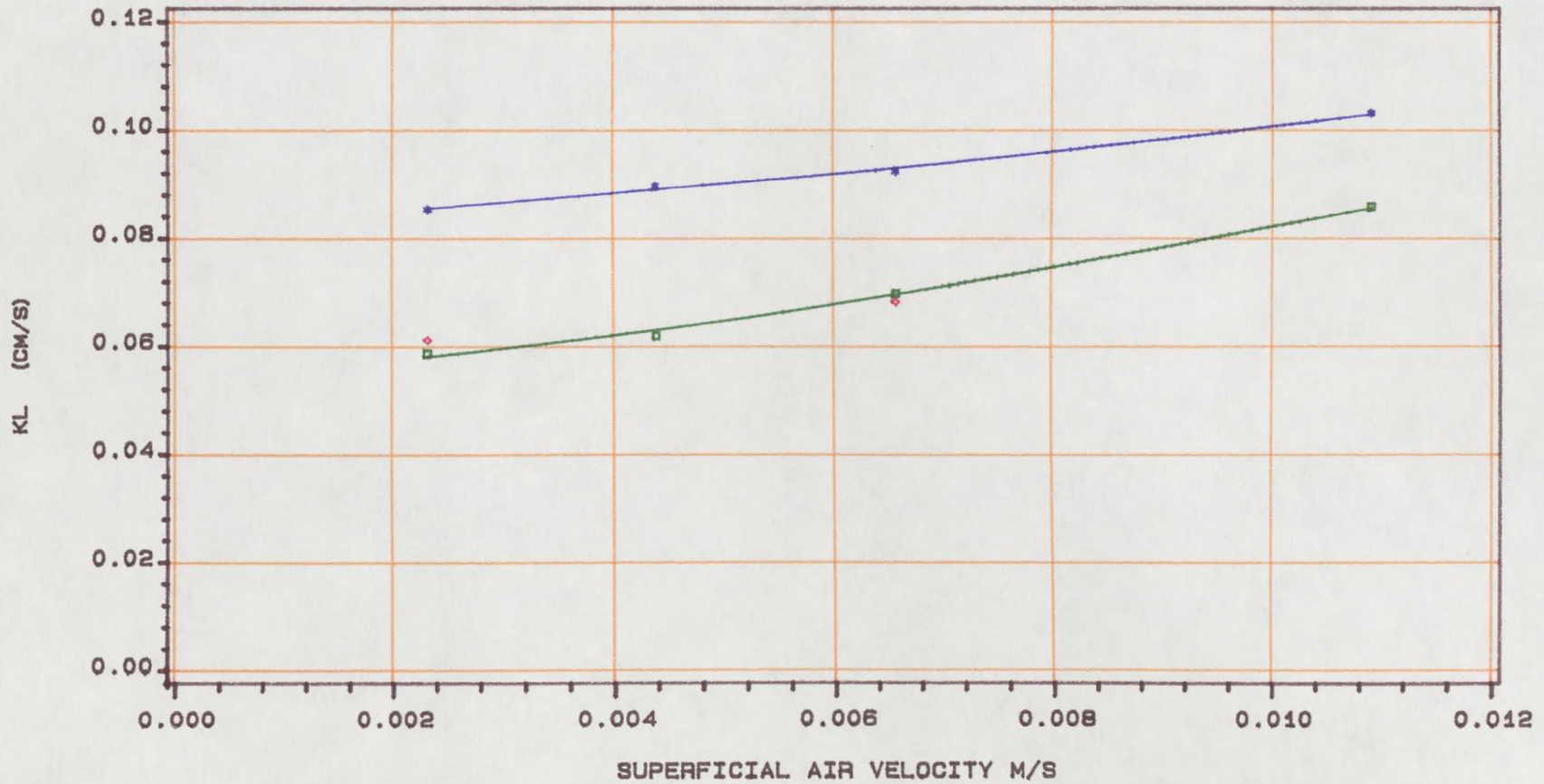
Tables 5.2.6 and 5.2.7 also show the (a) values for the slotted, plain and oblate spheroid packings at different air and liquid velocities.

Figures 5.2.15 and 5.2.16 show the effect of liquid and air velocity on the liquid film transfer coefficient ( $k_L$ ) for the slotted and oblate packings. It can be seen that ( $k_L$ ) increases consistently with both air and liquid velocity, because as the air and the liquid velocities increase, the agitation of packings in the bed appear to increase and therefore also the liquid film transfer coefficient ( $k_L$ ). This is in agreement with the findings of Kossev and Elenkov (36).

Figures 5.2.15 and 5.2.16 also show that ( $k_L$ ) for the slotted packing is higher than for the oblate packing. The higher ( $k_L$ ) for the slotted packing can be attributed on the one hand to the more vigorous agitation of slotted packing owing to the higher liquid hold up and, on the other, to the increasingly turbulent recirculation of liquid within the slotted packing.

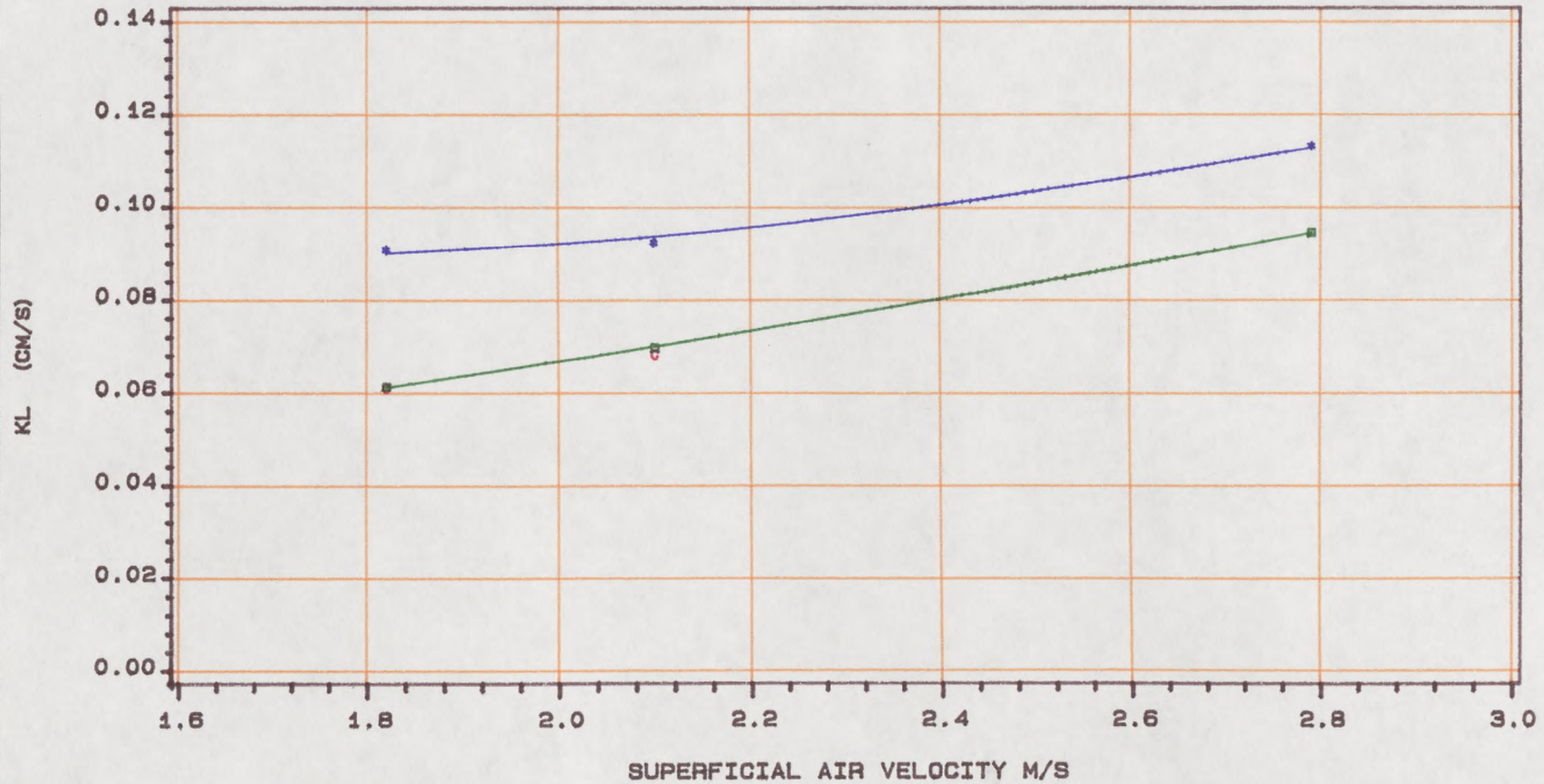
It is interesting to note that an increase in the liquid velocity from  $4.38 \times 10^{-3}$  to  $6.58 \times 10^{-3}$  m/s (nearly 50%, the corresponding increase in liquid hold up is 16% for slotted packing and 31% for oblate spheroid packing), increases the liquid film transfer coefficient by only 4% for the slotted packing and by 31% for the oblate spheroid packing.

**Fig 5.2.15 Plot Of Liquid Film Transfer Coefficient VS Superficial Liquid Velocity**  
**Bed Static Height=10.5 cm Superficial Air Velocity=2.1 M/S**  
**For Mobile Packings**



Slotted Packing Dia=25mm Open Area=0.11    Oblate Packing Dia=50\*38 mm    Plain Sphere Dia=25 mm

Fig 5.2.16 Plot Of Liquid Film Transfer Coefficient VS Superficial Air Velocity  
Bed Static Height=10.5 cm Superficial Liquid Velocity=6.58E-3 M/S  
For Mobile Packings



Slotted Packing Dia=25mm Open Area=0.11 Oblate Packing Dia=50\*38 mm Plain Sphere Dia=25 mm

Table 5.2.5. Comparison of  $\epsilon(A)$  and  $\epsilon(H_{dy})$  with liquid velocity for slotted packing with respect to oblate and plain packings.

Liquid velocity $V_L$ m/s	Ratio of total interfacial area $\epsilon(A)$		Ratio of expanded bed height $\epsilon(H_{dy})$	
	<u>slotted</u> oblate	<u>slotted</u> plain	<u>slotted</u> oblate	<u>slotted</u> plain
$2.32 \times 10^{-3}$	1.48	1.15	0.85	0.85
$4.38 \times 10^{-3}$	1.67	-	0.88	-
$6.58 \times 10^{-3}$	1.41	-	0.86	-
$10.9 \times 10^{-3}$	1.32	1.28	0.86	0.88

$$V_g = 2.1 \text{ m/s}$$

Table 5.2.6. Comparison of (a) for different packings at constant gas velocity of 2.1 m/s

$V_L$ m/s	a $\text{cm}^{-1}$		
	slotted	oblate	plain
$2.32 \times 10^{-3}$	3.34	1.92	2.46
$6.58 \times 10^{-3}$	4.00	2.45	2.77

$$V_g = 2.1 \text{ m/s}$$

Table 5.2.7. Comparison of (a) for different packings at constant liquid velocity of  $6.58 \times 10^{-3}$  m/s.

$V_g$ m/s	a $\text{cm}^{-1}$		
	slotted	oblate	plain
1.82	3.80	2.44	2.69
2.1	4.00	2.45	2.77

$$V_L = 6.58 \times 10^{-3} \text{ m/s}$$

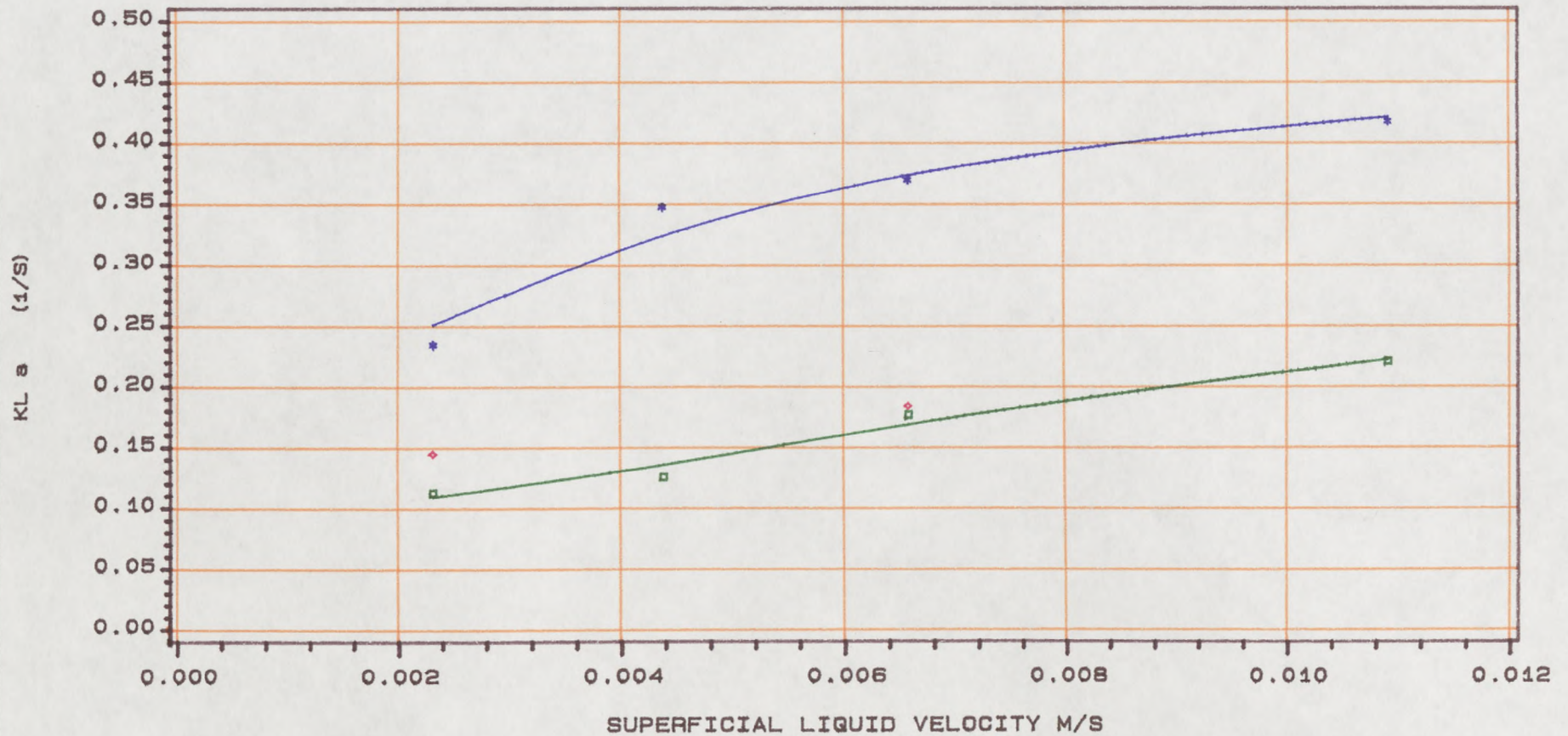
An increase in the air velocity of 53% (the corresponding increase in terms of liquid hold up being 6% for the slotted packing and 25% for oblate spheroid packing) increases the liquid film transfer coefficient by 24% and 54% for the slotted and oblate spheroid packings respectively.

In the case of the plain sphere packing increasing the liquid velocity by 238% (the corresponding increase in terms of liquid hold up being 40%) increases the  $(k_L)$  by 11% whereas a 15% increase in the air velocity increases the  $(k_L)$  by 11%, this means the increase in the air velocity for all of the packings causes more vigorous motion of packing than in a corresponding increase in liquid velocity. This finding was also confirmed by visual observations.

Kossev and Elenkov (36) reported similar results. Tables B1 and B2 in Appendix (B) compare the liquid film transfer coefficient for slotted and plain packings. It can be seen that  $(k_L)$  for the slotted packing is higher than  $(k_L)$  for the plain packing, presumably because the liquid hold up and turbulence in the motion of slotted packing is more vigorous than in the plain packing.

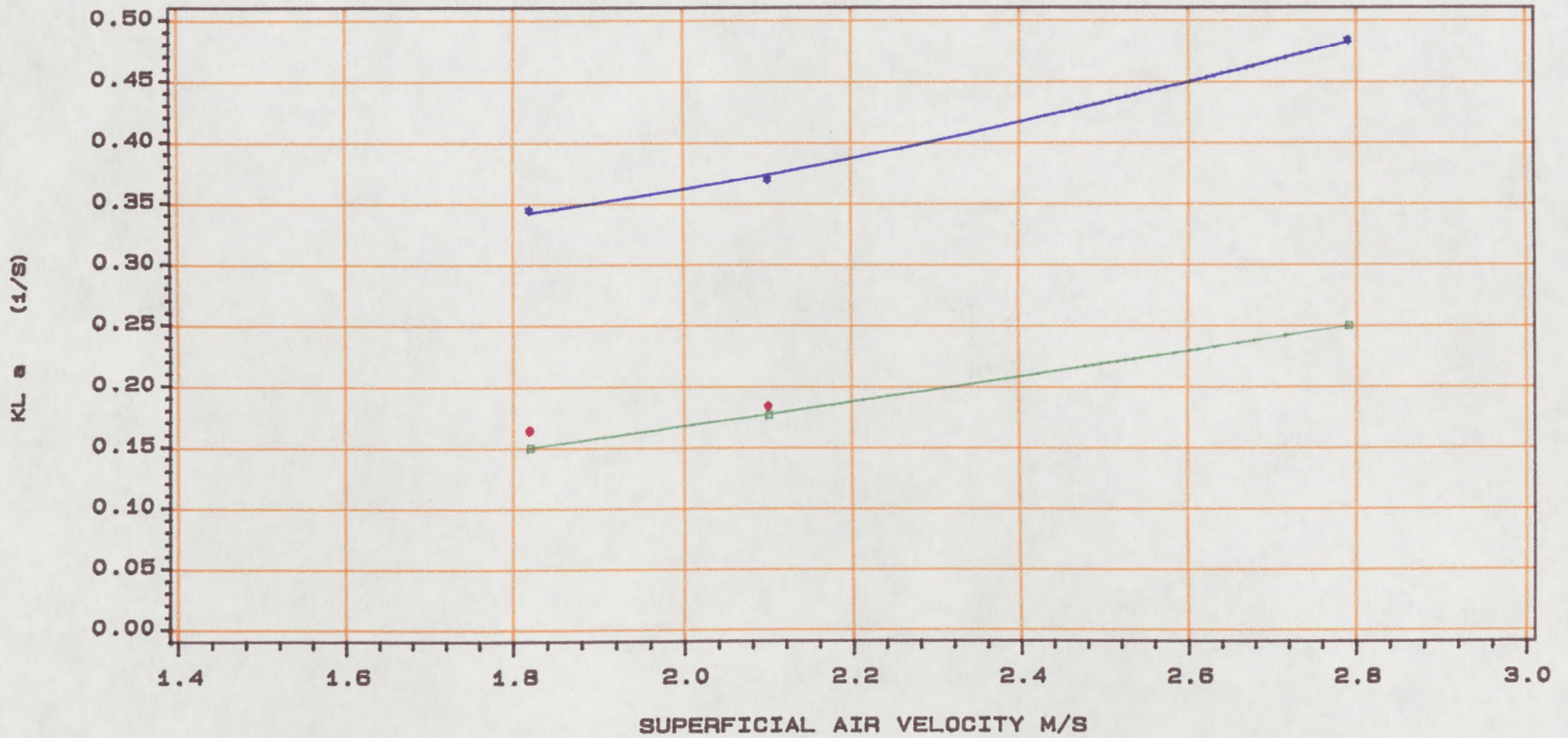
Figures 5.2.17 and 5.2.18 show the effect of liquid and air flow rates on the volumetric liquid film transfer coefficient  $(k_L a)$  for different packings. From figure 5.2.18 it is apparent that  $(k_L a)$  for slotted packing is higher than the oblate spheroid and 25 mm plain packings, this is to say mass transfer performance of slotted packing is higher than those of oblate spheroid and 25 mm plain packings. It can also be seen that  $(k_L a)$  for 25 mm plain packings is slightly higher than the oblate spheroid packing. The similar results are observed from

**Fig 5.2.17 Plot Of Volumetric Liquid Mass Transfer Coefficient VS Superficial Liquid Velocity**  
 Bed Static Height=10.5 cm Superficial Air Velocity=2.1 M/S  
 For Mobile Packings



Slotted Packings Dia=25 mm Open Area=0.11 Oblate packing Dia=50\*38 mm Plain Sphere Dia=25 mm

**Fig 5.2.18 Plot Of Volumetric Liquid Mass Transfer Coefficient VS Superficial Air Velocity**  
**Bed Static Height=10.5 CM Superficial Liquid Velocity=6.58E-3 M/S**  
**For Mobile Packings**



Slotted Packing Dia=25 mm Open Are a=0.11 Oblate Packing Dia=50\*38 mm Plain Sphere Dia=25 mm

Figure 5.2.19 which shows the variation ( $k_L a$ ) with air flow rate for all of the packings.

A parameter has been defined as the operational mass transfer efficiency,

$$\eta_{op} = \frac{k_L a H}{\Delta P V_g}$$

which relates the volumetric liquid film transfer coefficient to the power consumed to achieve such a performance. The plots of this efficiency against the liquid and gas flow rates for different packings are shown in figures 5.2.19 and 5.2.20.

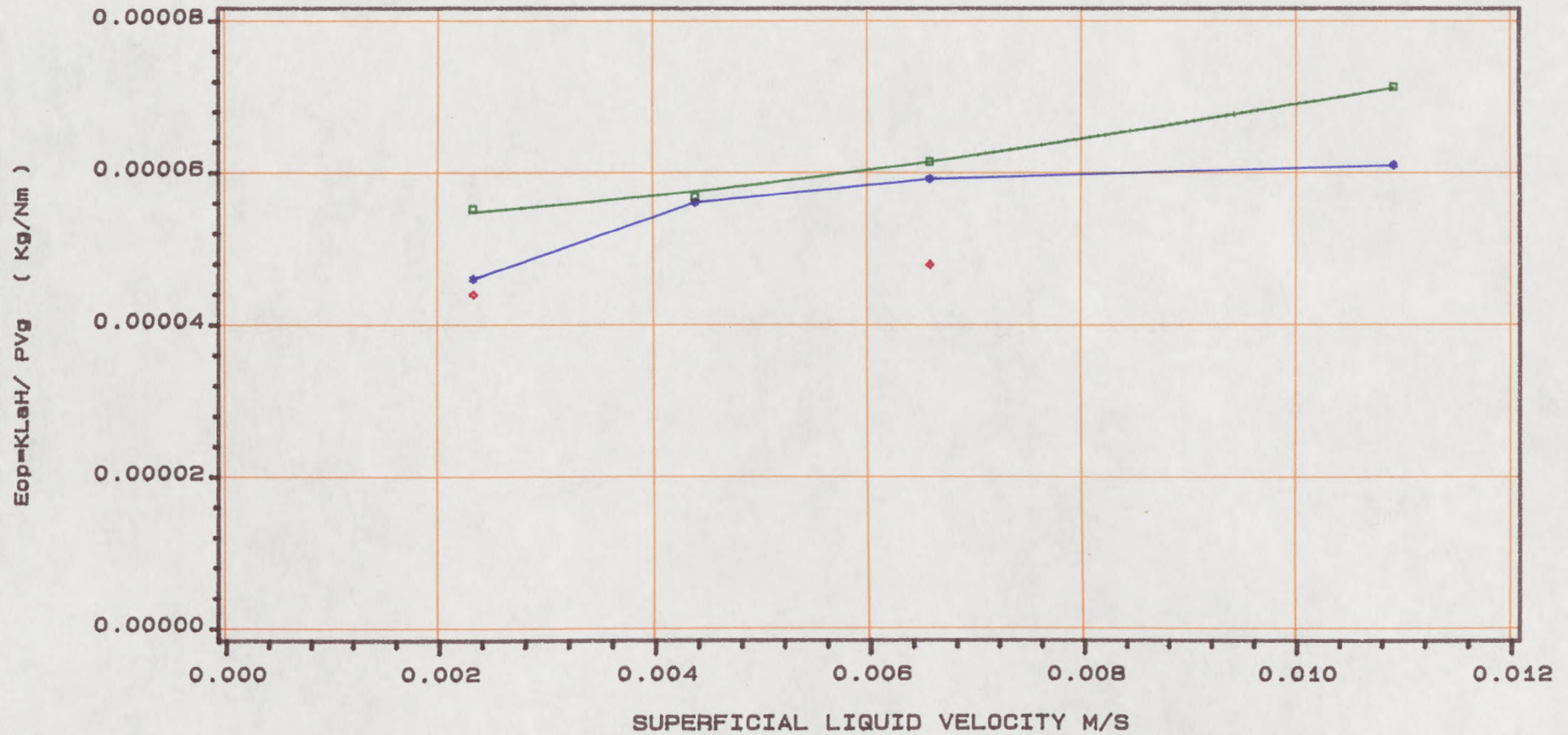
From figure 5.2.19, it can be seen that ( $\eta_{op}$ ) for oblate spheroid packing is higher than for slotted and 25 mm plain packings and ( $\eta_{op}$ ) for 25 mm plain packing is lower than slotted and oblate spheroid packings. This is also the case when ( $\eta_{op}$ ) is plotted against gas velocity for all of the packings (see Figure 5.2.20). This is because at a given gas and liquid rates, the ratio of ( $k_L a$ ) to the power consumption is higher for the oblate spheroid packing than for the other packings.

#### 5.2.4 Comparative Mass Transfer Performance for Different Systems

Comparison of values of interfacial area and liquid film mass transfer coefficient for different contacting systems as well as for the present work are given in Appendix (B).

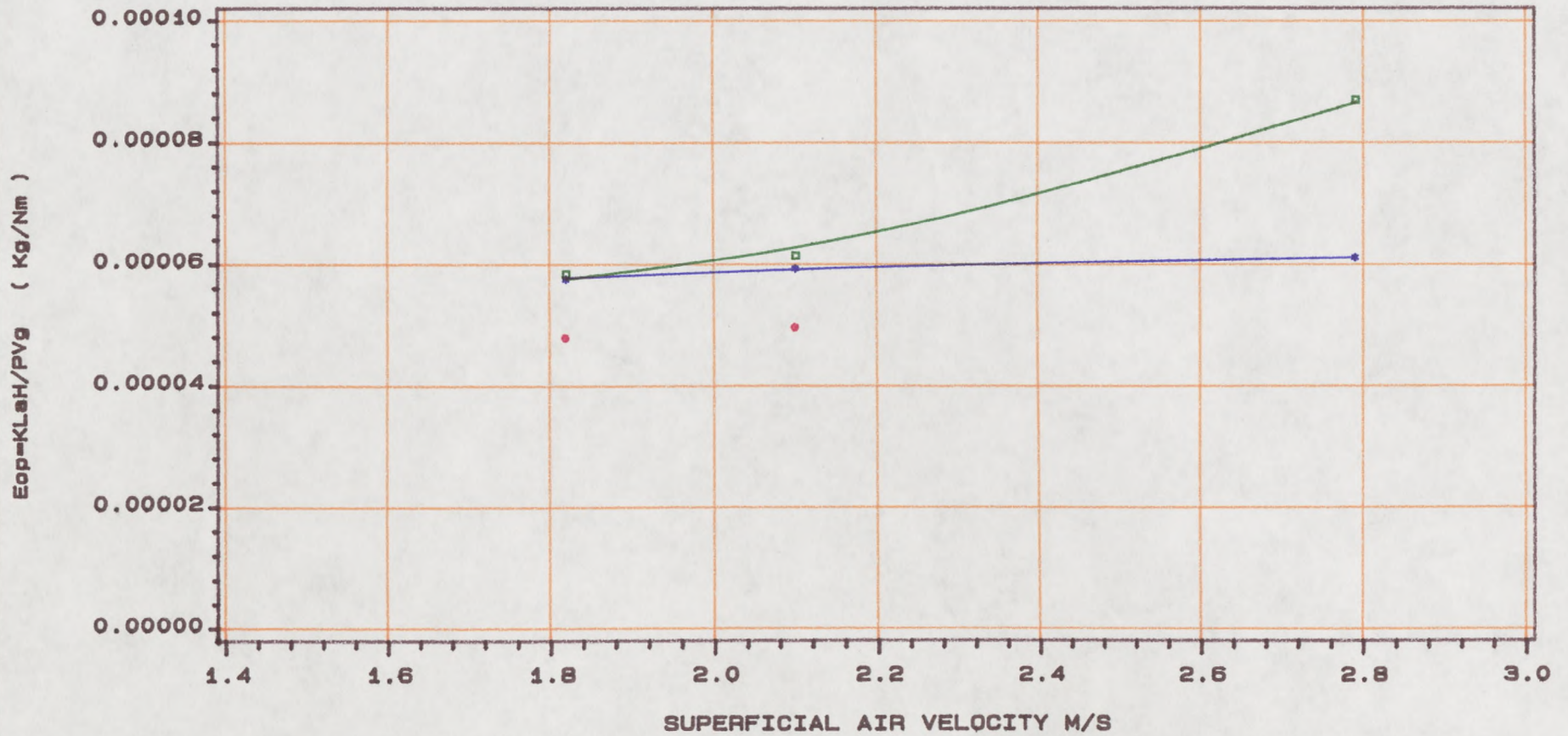
Because of the wide variation in experimental conditions, a direct comparison between the values of interfacial area and liquid film mass transfer coefficients as obtained in turbulent contact absorbers

Fig 5.2.19 Plot Of Operational Mass Transfer Efficiency VS Superficial Liquid Velocity  
 Bed Static Height=10.5 cm Superficial Air Velocity=2.1 M/S  
 For Mobile Packings



Slotted Packings Dia=25 mm Open Area=0.11 Oblate packing Dia=50\*38 mm Plain Sphere Dia=25 mm

**Fig 5.2.20 Plot Of Operational Mass Transfer Efficiency VS Superficial Air Velocity**  
 Bed Static Height=10.5 CM Superficial Liquid Velocity=6.58E-3 M/S  
 For Mobile Packings



Slotted Packing Dia=25 mm Open Area=0.11 Oblate Packing Dia=50x38 mm Plain Sphere Dia=25 mm

including the present work and those obtained on sieve plates is difficult to make.

In general, however, it appears that the values observed for TCAs are higher than those for sieve plates having a percentage open area greater than about 20%.

It is also difficult to compare the values of interfacial area and liquid film transfer coefficient obtained in the present work with those obtained in turbulent contact absorbers having plain spherical packings, since in most cases small diameter packings, higher liquid velocities and a wider range of supporting grid open areas have been used.

Fractional hole area in the supporting grid may have a considerable affect on the mass transfer performance of both TCA columns and sieve plate dispersions. If the fractional hole area is small then it is likely that high velocity gas jets will be present immediately above the packing supporting grid thus generating increased liquid mixing and packing agitation. The mass transfer performance of the mobile bed will therefore be enhanced by the presence of the supporting grid acting as a sieve plate. On the other hand a TCA having a supporting grid with relatively high free area (more than about 70%) will have mass transfer characteristics which are more typical of the inherent performance of the mobile bed alone.

Comparison of the values of  $(a)$  and  $(a_s)$  obtained by Wozniak (28) at a superficial liquid velocity of 0.0106 m/s which is closer to the experimental conditions of the present work shows that  $(a)$  and  $(a_s)$  for both the slotted sphere and oblate spheroid packings are higher than the ones obtained by Wozniak (28) (table B5).

Comparison of values of  $k_L$  obtained by Elenkov and Kossev (36) (table B6), with those of the present work (tables B1 and B2), shows that the liquid film transfer coefficients for the oblate spheroid and slotted sphere packings are higher than corresponding values reported by Elenkov and Kossev (36).

In spite of the difficulties encountered in making objective comparisons with other gas liquid contacting systems, it would appear that the volumetric mass transfer coefficients present in mobile beds of oblate spheroid and slotted sphere packings are amongst the highest values reported in the literature.

## CHAPTER 6

### GRAPHICAL PRESENTATION OF INTERPHASE MASS TRANSFER

Interphase mass transfer rate calculations must inevitably incorporate the possible effects of gas and liquid film resistances together with the interfacial solubility equilibrium requirement. The equations for calculating interphase mass transfer rates are well established, however the procedure and results of these calculations are not generally considered or presented in the absorption literature.

A graphical procedure and presentation of interphase mass transfer rates has therefore been devised as an aid to understanding the factors influencing actual absorption rates under given mass transfer and solubility coefficients and for rapid calculation of the interphase transfer rates.

The absorption flux of an absorbing gas across the gas film is given by

$$F = k_g (P_A - P_{Ai}) \quad \text{mol/cm}^2 \text{ s} \quad (6.1)$$

where  $P_A$  = partial pressure of gas in gas bulk

$P_{Ai}$  = partial pressure of gas at the interface.

The absorption flux into the liquid film is given by

$$F = E k_L C_{Ai} \quad \text{mol/cm}^2 \text{ s} \quad (6.2)$$

where  $C_{Ai}$  = concentration of gas at liquid interface

$E$  = enhancement factor for absorption into a liquid film having an effective physical mass transfer coefficient  $k_L$ .

At the liquid surface equilibrium is assumed to exist according to Henry's law.

$$\text{i.e. } P_{Ai} = H_A C_{Ai} \quad (6.3)$$

where  $H_A$  is the Henry's law solubility coefficient (at  $\text{cm}^3/\text{g mol}$ ).

Equations (6.1), (6.2) and (6.3) may be combined as follows,

$$F = k_g (P_A - H_A C_{Ai})$$

$$F = k_g \left[ P_A - \frac{H_A F_A}{E k_L} \right]$$

$$F = \frac{k_g P_A}{\left[ 1 + \frac{H_A k_g}{E k_L} \right]}$$

The maximum absorption flux will occur when there is no liquid film resistance, i.e.  $E k_L \rightarrow \infty$ .

$$\text{Hence } F_{\max} = k_g P_A.$$

The relative absorption efficiency is defined as

$$\frac{F}{F_{\max}} \text{ and}$$

$$\eta_{\text{rel}} = \frac{F}{F_{\max}} = \left[ \frac{1}{1 + \frac{H_A k_g}{E k_L}} \right]$$

$$\eta_{\text{rel}} = \frac{E k_L}{E k_L + H_A k_g} \quad (6.4)$$

The equation (4) clearly expresses the dependence of absorption flux ( $F$ ) and relative absorption efficiency ( $\eta_{rel}$ ) on the gas and liquid film mass transfer coefficients ( $k_g$  and  $k_L$ ), the liquid film enhancement factor ( $E$ ) and the gas solubility coefficient ( $H_A$ ).

The following features should be emphasised:

1. As  $E k_L$  increases then  $\eta_{rel}$  increases continuously to approach a maximum value of 1.0.
2. As  $E k_L$  decreases to zero, then  $\eta$  also decreases to zero.
3. As  $E k_L$  becomes very small, then  $\eta_{rel}$  becomes proportional to  $E k_L$ , i.e.  $\eta_{rel}$  approaches  $\gamma$ .

$$\gamma = \frac{E k_L}{H_A k_g} \quad (6.5)$$

This confirms that the graphical plot of  $\eta_{rel}$  against  $E k_L$  is a hyperbola with two asymptotes (see Fig. 6.1).

At high  $E k_L$ ,  $\eta_{rel} = 1.0$ .

$$\text{At low } E k_L, \eta_{rel} \rightarrow \frac{E k_L}{H_A k_g} \text{ and } \gamma = \frac{E k_L}{H_A k_g}$$

this is the equation of straight line passing through the origin with a slope of  $1/H_A k_g$ . The point of intersection of the two asymptotes has the coordinates  $\eta_{rel} = 1.0$  at  $E k_L = H_A k_g$ . The relative absorption efficiency ( $\eta_{rel}$ ) corresponding to this point of intersection is 0.50, i.e.  $\eta_{rel} = 0.5$  at  $E k_L = H_A k_g$ . Therefore, the 50% relative efficiency point is a point at which the gas and liquid film resistances may be regarded as equal.

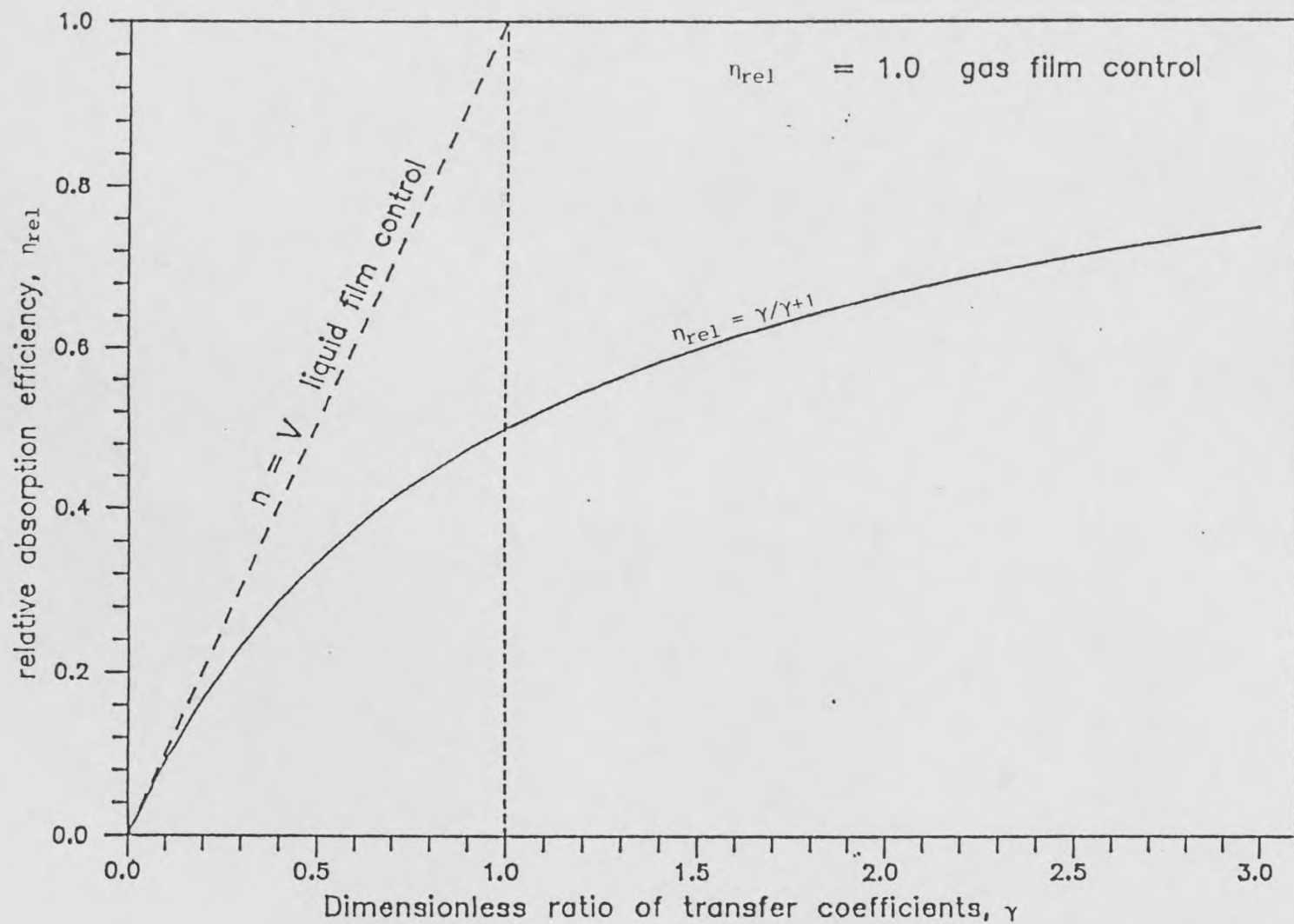


Figure 6.1

Dimensionless plot of relative absorption efficiency,  $\eta_{rel}$ , versus the transfer coefficient ratio,  $\gamma$ .

For  $E k_L < H_A k_g$  the liquid film resistance is larger than the gas film resistance.

For  $E k_L > H_A k_g$  the gas film resistance is larger than the liquid film resistance.

The shape of the curve for  $\eta_{rel}$  against  $E k_L$  is clearly dependent on the value of  $H_A k_g$  present, so that liquid film control is observed over a smaller range of  $E k_L$  values as the value of  $H_A k_g$  is reduced. Correspondingly gas film control extends to lower values of  $E k_L$  as  $H_A k_g$  is reduced. The family of curves obtained by plotting  $\eta_{rel}$  against  $E k_L$  for various values of  $H_A k_g$  may be combined into a single master curve by plotting  $\eta_{rel}$  against the dimensionless group

$$\gamma = \frac{E k_L}{H_A k_g}$$

as shown in Fig. 6.1 and

$$\eta_{rel} = \frac{\gamma}{\gamma + 1}$$

It is clear from this graph that values of  $\gamma$  between zero and one lead to relatively low absorption rates which are predominantly liquid film controlled. On the other hand, values of  $\gamma > 1$  lead to relatively high mass transfer rates which are predominantly gas film controlled.

An example is given below using experimental results of Vidwans and Sharma (65), who absorbed dilute  $CO_2$  in sodium hydroxide under the following conditions:

$$P_{CO_2} = 0.0695 \text{ atm}$$

$$\begin{aligned}C_{O\bar{H}} &= 1.765 \text{ N} \\H_{CO_2} &= 1.49 \times 10^{-5} \text{ g mol/cm}^3 \text{ at} \\k_L &= 4.53 \times 10^{-3} \text{ cm/s} \\k_g &= 5.64 \times 10^{-5} \text{ g mol/cm}^2 \text{ s at} \\E &= 162\end{aligned}$$

For this data

$$\begin{aligned}E k_L &= 0.734 \text{ cm/s.} \\H k_g &= 3.78 \text{ cm/s} \\\gamma &= 0.194 \\\eta_{rel} &= 0.163\end{aligned}$$

Note that  $E k_L$  is much less than  $H k_g$  and the absorption process is mainly liquid film controlled (83.9% of total resistance).

## CHAPTER 7

### CONCLUSIONS

#### 7.1. Hydrodynamics

For all of the packings, the pressure drop at a constant liquid flow rate was found to increase sharply with increasing air velocity in the static bed state, but to increase only slowly above the minimum fluidization velocity (i.e. in the fluidization state). This is because the pressure drop increases as in the fixed bed whereas in the fluidized state, the bed expands and packings are set in motion, therefore, the voidage in the bed increases, this in turn provides a freer passage for the air flow and pressure drop increases slowly due to an increase in the liquid hold up.

In the case of a dry bed, the pressure drop above the point of fluidization (in the fluidization state) remains reasonably constant because the effect of liquid hold up is not present. The pressure drop also increases with an increase in the liquid flow rate. An increase in the static bed height also increases the bed pressure drop for the same reasons as explained above. It was found that the minimum expanding gas velocity decreases with increasing liquid flow rate, this is because the increase in the liquid flow rate increases the liquid hold up and this in turn tends to increase the interstitial gas velocity and the bed pressure drop sufficient to achieve fluidization.

The increase in both liquid and air flow rates will increase the liquid hold up, since the volume of liquid which is retained in the bed increases as the liquid rate increases and an increase in the air flow rate will provide more support for the liquid flowing down the column and thus increase the liquid hold up.

Increases in air and liquid flow rates also increase the expanded bed height (especially increases in the air flow rate), however, substantial increases in the air velocity also increases the fluctuation of the expanded bed height reflecting the presence of slugging in the bed.

The pressure drop for the 25 mm slotted sphere packing at a given air and liquid velocity is higher than for the oblate spheroid, 38 mm plain sphere and 25 mm plain sphere packings, as the liquid hold up for the slotted packing is higher than for the other packings. It was also found that the pressure drop for the 25 mm plain sphere packing is higher than for the 38 mm plain sphere and oblate spheroid packings.

The liquid hold up for the slotted packing is much greater compared to the rest of the packings because the slotted packing can retain more liquid within the bed, presumably within the packing itself. The liquid hold up for the 25 mm plain sphere packing is also higher than for the oblate spheroid and the 38 mm plain sphere packings reflecting liquid hold up on the increased surface area associated with the smaller size packings.

The minimum expanding velocity was higher for the slotted packing especially in the case of a dry bed, or at low liquid rates. This is because the slotted packing offers an intrinsically lower resistance to the air flow rate and therefore a higher air flow rate is needed to generate the pressure drop required to lift the packings. At the higher liquid rates however, the liquid hold up in the bed increases and if present inside the packings will significantly increase the resistance to air flow, thereby reducing the minimum expanding gas velocity.

The expanded bed height and fluctuation in the bed height was higher for the oblate spheroid and lower for the slotted packing.

There was some occasional wall effect present in the bed fitted with the star shaped liquid distributor due to part distribution of liquid over the central part of the bed while the rest flowed off the packings on to the wall of the column. This problem was overcome by using a uniform shower type liquid distributor which kept the liquid feed away from the wall.

The conclusions from the comparative hydrodynamic studies may be summarized as follows:

1. All packings exhibit a similar general behaviour, suggesting that beds expand in order to minimise pressure drop at a particular gas velocity whilst allowing the liquid stream to pass in the form of streamlined or turbulent flowing films on the packing surfaces. At increasing gas and liquid velocities the liquid begins to froth and spray into the available space between and inside the packings. This must increase the intensity of mixing and turbulence present in both the gas and liquid phases passing through the bed.
2. Spherical and oblate spheroid packings appear to have almost identical hydrodynamic behaviour although the oblate spheroid packing shows more fluctuation in expanded bed height at high gas velocities.
3. Slotted sphere packings although showing the same general hydrodynamic behaviour, requires much higher gas velocities to achieve the same degree of bed expansion and also shows a greater liquid hold up at the same degree of bed expansion thus indicating that the gas is

passing through as well as around the slotted packings and that the increased liquid hold up is present within the packings.

The fluidization of the slotted packings appears to be more homogeneous and to offer more intensive liquid turbulence, with reduced slugging of the bed. Comparison of the bed expansion curves for the various packings and liquid rates suggests that the presence of gas channelling and by-passing is more noticeable at low fluidizing gas velocities and with the lowest liquid irrigation rates. The high rates of bed expansion observed at gas velocities above 2.5 m/s and with high liquid irrigation rates indicate the presence of more intimate uniform contacting between gas and liquid and packings in these strongly agitated and highly expanded beds.

## 7.2. Mass Transfer.

It was found that the interfacial area per unit volume of static bed height ( $a_s$ ) and per expanded bed height ( $a$ ) is higher for the slotted packing than for the 25 mm diameter plain and oblate spheroid packings. This is due to the higher packing surface area per unit volume of bed and also the increased liquid hold up for the slotted packing. The ( $a_s$ ) and the ( $a$ ) for the 25 mm diameter plain packing was also higher than for the oblate spheroid packing for the same reasons as explained above. The interfacial area per unit volume of static bed height ( $a_s$ ) and per unit volume of expanded bed height ( $a$ ) for all of the packings increases with both liquid and gas velocities.

The interfacial area per unit volume of liquid hold up ( $a_l$ ) at a given air and liquid velocity, was found to be lower for the slotted packing than for the 25 mm plain sphere and oblate spheroid packings. This is probably because the additional liquid hold up in a bed of

slotted packings is present inside the packings and is itself not as well dispersed as the liquid hold up on the outside of the packings.

It was also found that  $a_L$  decreases with increasing liquid rate for all of the packings, this is due to a relatively larger increase in liquid hold up as compared to the corresponding increase in the total interfacial area. Interfacial area per unit volume of liquid hold up ( $a_L$ ) also increased as the air velocity was increased, this being due to the factor by which the total interfacial area increases with air velocity being higher than the corresponding increase in the liquid hold up.

The liquid film transfer coefficient ( $k_L$ ) for the slotted packing is higher than for the other packings. This is attributed to the more vigorous motion of slotted packing and the recirculation of liquid within the slotted packing. The liquid film transfer coefficients for the oblate spheroid and 25 mm diameter packings were almost the same. The liquid film transfer coefficient was found to increase with both liquid and gas velocities due to increasing agitation of liquid in the bed.

The operational mass transfer efficiency for the oblate spheroid packing was found to be higher than for both 25 mm slotted and 25 mm plain sphere packings, particularly at the highest gas velocities. This efficiency ratio was also higher for the slotted packing than for the plain packing. The operational mass transfer efficiency for all of the packings was found to increase, with increases in both gas and liquid velocities.

Conclusions arising from the comparative mass transfer studies may be summarized as follows:

1. As the gas and liquid flow rates are increased, there is a corresponding increase in liquid being held up in the form of froth and spray thus leading to a general increase in the liquid film transfer coefficient and the interfacial area over the range of experimental conditions investigated.
2. Slotted packings offer the greatest liquid film transfer coefficients and interfacial areas but with a significant increase in pressure drop. The bed however appears to fluidize more intimately and turbulently with less fluctuation in bed height.
3. The oblate spheroid packing has a similar mass transfer performance to that of the 25 mm plain sphere packing. However, its operational mass transfer efficiency is higher than for both the slotted and plain sphere packings of 25 mm diameter.
4. Mobile packings generally offer high through put, with exceptionally high volumetric mass transfer rates. A high gas distributor pressure drop is not required and the liquid flow is self-distributing. Liquid backing mixing in turbulent contact beds is very substantial so that countercurrent processing would require multi-staged operation as in a tray tower.

## CHAPTER 8

### RECOMMENDATIONS FOR FURTHER WORK

The results and conclusions from this investigation have been generally encouraging, demonstrating that both oblate spheroid and slotted sphere packings can significantly increase the interfacial area and the liquid film transfer coefficient in fluidized bed dispersions.

The fluidized beds appear to offer an improving mass transfer performance at increasing gas and liquid rates, leading to significant intensification of the contacting process.

Further research is therefore recommended in order to achieve a better understanding of the hydrodynamic and mass transfer performance of oblate spheroid and slotted sphere packings.

The following recommendations are of particular importance:

1. Investigation of the effects of packing slot diameter shape and numbers.
2. Investigation of gas film mass transfer coefficients.
3. Investigation of a wider range of liquid and gas velocities.
4. Confirmation of the volumetric liquid film transfer coefficients by alternative established method such as the desorption of oxygen from water.
5. Slotted packings may also offer good performance characteristics in the fixed bed condition and similar investigations of hydrodynamics and mass transfer should be undertaken with a view to comparison and assessment of their full potential.

## APPENDIX A

## DETERMINATION OF THE PHYSICO-CHEMICAL PARAMETERS

A1 - Concentration Of CO<sub>2</sub> At The Interface

The concentration of dissolved gas  $C_{Ai}$  in equilibrium with partial pressure of gas  $P_{Ai}$  is determined from Henry's Law Relation

$$C_{Ai} = P_{Ai} H_e.$$

The solubility of a gas in electrolyte solutions ( $H_e$ ) can be obtained by the equation given by Van Krevelen and Hoftyzer (49).

$$\log \left[ \frac{H_e}{H_w} \right] = - \sum hI.$$

The solubility of CO<sub>2</sub> in partly-carbonated caustic solution is calculated from

$$\log \left[ \frac{H_e}{H_w} \right] = - [h_1 I(\text{NaOH}) + h_2 I(\text{Na}_2\text{CO}_3)]$$

where  $H_w$  is the solubility of dissolved CO<sub>2</sub> in water,  $I(\text{NaOH})$  and  $I(\text{Na}_2\text{CO}_3)$  are the contributions to the ionic strength of the solution from sodium hydroxide and sodium carbonate respectively;  $h_1$  and  $h_2$  are salting coefficients.

The solubility coefficient of CO<sub>2</sub> in water ( $H_w$ ), is given by (49).

$$\log (H_w) = \frac{1140}{(273+t')} - 5.30$$

$t'$  = temperature of solution in degrees centigrade. The ionic strength ( $I$ ) is calculated from the equation below.

$$I = 0.5 \sum_{i=1}^n C_i Z_i^2$$

where  $C_i$  is the concentration of ions in the solution and  $Z_i$  is the valency of ions. The salting coefficient is the sum of the contributions due to the species of gas  $h_g$  and to the species of positive  $h^+$  and negative  $h^-$  ions present in the solution, therefore

$$h = h^+ + h^- + h_g.$$

The contributions to ionic strength from sodium hydroxide and sodium carbonate are,

$$I(\text{NaOH}) = [\text{NaOH}] \text{ and } I(\text{Na}_2\text{CO}_3) = 3 [\text{Na}_2\text{CO}_3].$$

Therefore the ionic strength of the solution is

$$I = [\text{NaOH}] + 3 [\text{Na}_2\text{CO}_3]$$

where  $[\text{NaOH}]$  and  $[\text{Na}_2\text{CO}_3]$  are concentrations in gr mole/litre.

Values of  $h^+$  and  $h^-$  (l/g ion) for  $\text{Na}^+$ ,  $\text{OH}^-$  and  $\text{CO}_3^{=}$  are (49, 57)

$$h(\text{Na}^+) = 0.094, \quad h(\text{OH}^-) = 0.061, \quad h(\text{CO}_3^{=}) = 0.021$$

Therefore:

$$h(\text{NaOH}) = 0.094 + 0.061 + h_g = 0.155 h_g$$

$$h(\text{Na}_2\text{CO}_3) = 0.094 + 0.021 + h_g = 0.115 h_g$$

values of  $h_g$  can be obtained from (58)

$$h_g = - 0.005 - 0.00053 t' \text{ lit/g ion.}$$

## A2 - Rate Constant For The Reaction Of CO<sub>2</sub> With Hydroxyl Ions, K<sub>2</sub>.

Reaction rate constant for the reaction of CO<sub>2</sub> with NaOH solutions is calculated from the equation given by Nijssing, Hendriksz and Kramer (59),

$$\log \frac{k_2}{k_{2,\infty}} = 0.133 I$$

where  $k_{2,\infty}$  is the reaction rate constant at infinite dilution and is given by (41),

$$\log k_{2,\infty} = 13.635 - \frac{2895}{273+t'}$$

Hence the reaction rate constant,  $k_2$ , for CO<sub>2</sub> - NaOH reaction is given by,

$$\log k_2 = 13.635 - \frac{2895}{273+t'} + 0.133 I$$

### A3 - The Diffusivity Of Dissolved CO<sub>2</sub> In Hydroxide Solutions.

The diffusivity of dissolved CO<sub>2</sub> in hydroxide solutions was calculated from the equation proposed by barrett (58).

$$D_A = D_w (a + b) C$$

where  $D_w$  is the diffusivity of CO<sub>2</sub> in water (cm<sup>2</sup>/s) given by the equation,

$$\log D_w = - 4.1764 + \frac{712.52}{(273+t')} - \frac{2.5907}{(273+t')^2} \times 10^5$$

Expressions for a, b and c as functions of sodium, hydroxyl and carbonate ions concentrations are as follows,

$$a = 1.0 - 0.145 [\text{Na}^+] + 0.0112 [\text{Na}^+]^2$$

$$b = 3.7 \times 10^{-4} (t' - 20) ([\text{OH}^-] + 0.75 [\text{CO}_3^{=}] )$$

$$c = 1.0 - 0.5 \frac{[\text{CO}_3^{=}]}{[\text{Na}^+]} (1 - \exp(- 0.0516 [\text{Na}^+]))$$

## APPENDIX B

Table B1 Variation of  $k_L$  with liquid velocity at  $V_g = 2.1$  m/s in present work estimated from Danckwerts' plot.

$V_L$ m/s	$k_L$ m/s		
	oblate spheroid	slotted sphere	plain sphere
$2.32 \times 10^{-3}$	$0.0588 \times 10^{-2}$	$0.0702 \times 10^{-2}$	$0.0612 \times 10^{-2}$
$4.38 \times 10^{-3}$	$0.0612 \times 10^{-2}$	$0.0884 \times 10^{-2}$	-
$6.58 \times 10^{-3}$	$0.0699 \times 10^{-2}$	$0.0923 \times 10^{-2}$	$0.0683 \times 10^{-2}$
$10.9 \times 10^{-3}$	$0.0859 \times 10^{-2}$	$0.103 \times 10^{-2}$	-

$$V_g = 2.1 \text{ m/s}$$

Table B2 Variation of  $k_L$  with gas velocity  $V_L = 6.58 \times 10^{-3}$  m/s in present work estimated from Danckwerts' plot.

$V_g$ m/s	$k_L$ m/s		
	oblate spheroid	slotted sphere	plain sphere
1.82	$0.0614 \times 10^{-2}$	$0.0907 \times 10^{-2}$	$0.061 \times 10^{-2}$
2.10	$0.0699 \times 10^{-2}$	$0.0923 \times 10^{-2}$	$0.0683 \times 10^{-2}$
2.79	$0.0946 \times 10^{-2}$	$0.11 \times 10^{-2}$	-

$$V_L = 6.58 \times 10^{-3} \text{ m/s}$$

Table B3 Variation of  $\eta_{op}$  with liquid velocity at  $v_g = 2.1$  m/s in present work.

$V_L$ m/s	$\eta_{op}$ kg/Nm		
	oblate spheroid	slotted sphere	plain sphere
$2.32 \times 10^{-3}$	$5.52 \times 10^{-5}$	$4.60 \times 10^{-5}$	$4.39 \times 10^{-5}$
$4.38 \times 10^{-3}$	$5.68 \times 10^{-5}$	$5.88 \times 10^{-5}$	-
$6.58 \times 10^{-3}$	$6.15 \times 10^{-5}$	$5.92 \times 10^{-5}$	$4.79 \times 10^{-5}$
$10.9 \times 10^{-3}$	$7.13 \times 10^{-5}$	$6.10 \times 10^{-5}$	-

$$v_g = 2.1 \text{ m/s}$$

Table B4 Variation of  $\eta_{op}$  with air velocity at  $V_L = 6.58 \times 10^{-3}$  m/s in present work.

$V_g$ m/s	$\eta_{op}$ kg/Nm		
	oblate spheroid	slotted sphere	plain sphere
1.82	$5.85 \times 10^{-5}$	$5.89 \times 10^{-5}$	$4.79 \times 10^{-5}$
2.10	$6.15 \times 10^{-5}$	$5.92 \times 10^{-5}$	$4.96 \times 10^{-5}$
2.79	$8.70 \times 10^{-5}$	$6.10 \times 10^{-5}$	-

$$v_L = 6.58 \times 10^{-3} \text{ m/s}$$

Table (B5) Typical values of interfacial area in TCA.

References	$D_c$ cm	f %	$d_p$ cm	$\rho_p$ kg/m <sup>3</sup>	$H_s$ cm	$v_L$ m/s	$v_g$ m/s	a cm <sup>-1</sup>	$a_s$ cm <sup>-1</sup>	$a_L$ cm <sup>-1</sup>	Type of packing
Kosseve et al. (35)	19	60	1.8	167	14	0.0167 0.0119	2.85 2.85	242 218	685 657	2142 1744	Plain sphere
Gelperin et al. (26)	14.5	30	1.55	470	45 9 13.5	0.0111	2.0 3.0 2.0 3.0 2.0 2.5	506 508 342 327 293 285	1444 1956 856 1111 689 904	2387 3234 1867 2423 1768 2319	
Wozniak and Ostergaard (30)	10.0		0.97	3.88	22	0.02	0.7	520	656	4936	
Wozniak (28)	20	60	1.96	260	29	0.0106 0.02	1.7 3.0 1.7 3.8	206 207 280 254	363 541 555 741	1793 2657 1820 2440	
Tabei et al. (34)	10.2	82	1.95	170	10	0.01 0.02 0.02	2.0 2.0 1.8	220 392 304	396 890 587	2075 2284 1985	

Table B5 continued.

References	$D_c$ cm	$f$ %	$d_p$ cm	$\rho_p$ kg/m <sup>3</sup>	$H_s$ cm	$v_L$ m/s	$v_g$ m/s	$a$ cm <sup>-1</sup>	$a_s$ cm <sup>-1</sup>	$a_L$ cm <sup>-1</sup>	Type of packing
Strumillo and Kudra (37)	8.5	65	1.0	1050	8	0.0139	1.0	234	469	862	Plain sphere
						0.0222	1.5	300	813	1106	
							2.0	310	975	1328	
							3.0	279	1188	1611	
				10	0.0222	2.0	309	800	1609		
Present work	22	72	2.5	293	10.5	0.00658	1.82	380	523	1660	Slotted sphere (open area 11%)
						0.00658	2.1	400	576	1800	
						0.00658	2.79	428	699	2056	
						0.0109	2.1	410	619	1663	
	22	72	5x3.8	162	10.5	0.00658	1.82	244	383	2620	Oblate spheroid
						0.00658	2.79	264	591	3240	
						0.0109	2.1	258	466	2422	
	22	72	2.5	327	10.5	0.00658	1.82	269	433	2840	Plain sphere
						0.00658	2.1	277	448	2910	

Table B6 Typical Values of  $k_L$  in TCA.

References	$D_c$ cm	$f$ %	$d_p$ cm	$\rho_p$ kg/m <sup>3</sup>	$H_s$ cm	$v_L$ m/s	$v_g$ m/s	$k_L$ m/s
Z. Palaty (33)	5.8	65.5	0.6	1000	-	-	-	$0.044 \times 10^{-2}$
Elenkov and Kosev (36)	19	79.0	1.7	930	20	0.0143	3.5	$0.062 \times 10^{-2}$
Strumillo and Kudra (37)	8.5	65.0	0.5-1.0	1050	2-16	0.0091-0.03	0.5-3.5	$0.12 \times 10^{-2}$

Table B7 Typical liquid film mass transfer coefficient and interfacial area for sieve plates.

References	Tray Characteristics	$v_g$ m/s	$v_L$ m/s	$a$ $m^{-1}$	$k_L$ m/s	$k_L a$ $s^{-1}$
Sharma and Gupta (62)	hole dia = 6.35 mm free area = 29.6%	2.0	0.0144	400	$0.033 \times 10^{-2}$	0.132
	hole dia = 6.35 mm free area = 14.5%	1.2	0.00289	500	$0.044 \times 10^{-2}$	0.22
Nagy et al. (63)	hole dia = 1 mm free area = 16%	0.4	-	630	$0.08 \times 10^{-2}$	0.5
		1.4	-	810	$0.1 \times 10^{-2}$	0.81
Pohorecki (64)	hole dia = 5.56 mm free area = 5.5%	0.86	-	820	$0.069 \times 10^{-2}$	0.573
		1.44	-	863	$0.074 \times 10^{-2}$	0.638

### APPENDIX C

The value of the total interfacial area in the bed can be calculated at a relatively high concentration of sodium hydroxide concentration (2N) by assuming  $D_A K_1 \gg k_L^2$  and using the short version of Danckwerts' model (41) for the rate of absorption of a pseudo-first order reaction, i.e.

$$RA = C_{Ai} A \sqrt{D_A k_1}$$

using this value of (A) and Danckwerts' full model at low concentration (0.3N) i.e.

$$RA = C_{Ai} A \sqrt{D_A K_1 + k_L^2}$$

the liquid film mass transfer coefficient may be obtained by employing appropriate values of  $D_A K_1$  and  $C_{Ai}$ .

The values of ( $a_s$ ) and  $k_L$  so obtained are given in tables C1 and C2

A sample calculation of ( $k_L$ ) and ( $a_s$ ) for the slotted sphere packing at gas velocity of 2.1 m/s and liquid velocity of  $6.58 \times 10^{-3}$  m/s is given below:

The required estimated parameters are tabulated in the table below:

RA	$C_{Ai}$	$\left(\frac{RA}{C_{Ai}}\right)^2$	$D_A$	$K_1$	[NaOH]
$\frac{\text{g mol}}{\text{s}}$	$\frac{\text{g mol}}{\text{cm}^3}$	$\frac{\text{cm}^6}{\text{s}}$	$\frac{\text{cm}^2}{\text{s}}$	$\frac{1}{\text{s}}$	$\frac{\text{g mol}}{\text{lit}}$
$4.62 \times 10^{-3}$	$4.119 \times 10^{-7}$	$1.258 \times 10^8$	$0.130 \times 10^{-4}$	$1.76 \times 10^4$	2.00
$2.90 \times 10^{-3}$	$7.205 \times 10^{-7}$	$0.162 \times 10^8$	$0.164 \times 10^{-4}$	$0.139 \times 10^4$	0.30

At concentrations of 2.0N

$$RA = C_{Ai} A \sqrt{D_A K_1}$$

$$4.62 \times 10^{-3} = 4.119 \times 10^{-7} \times A \sqrt{0.130 \times 10^{-4} \times 1.76 \times 10^4}$$

$$A = 2.34 \times 10^4 \text{ cm}^2$$

$$a_s = \frac{A}{(V_{\text{bed}})_s}$$

where  $A$  = total interfacial area in the bed

$(V_{\text{bed}})_s$  = volume of the bed based on the bed static height.

$$a_s = \frac{2.34 \times 10^4}{3990} \quad a_s = 586 \text{ m}^{-1}$$

At concentration of 0.3N

$$\left(\frac{RA}{C_{Ai}}\right)^2 = A^2(DK_1 + k_L^2)$$

$$0.162 \times 10^8 = 5.475 \times 10^8 (0.164 \times 10^{-4} \times 0.139 \times 10^4 + k_L^2)$$

$$k_L = 0.082 \text{ cm/s.}$$

Table C1 Variation of ( $a_s$ ) and ( $k_L$ ) with liquid velocity at  $v_g = 2.1$  m/s using short and full Danckwerts' model.

$V_L$ m/s	$a_s$ m <sup>-1</sup>			$k_L$ m/s		
	oblate spheroid	slotted sphere	plain sphere	oblate spheroid	slotted sphere	plain sphere
$2.32 \times 10^{-3}$	288	433	383	$0.053 \times 10^{-2}$	$0.068 \times 10^{-2}$	$0.058 \times 10^{-2}$
$4.38 \times 10^{-3}$	326	549	-	$0.056 \times 10^{-2}$	$0.078 \times 10^{-2}$	-
$6.58 \times 10^{-3}$	416	586	451	$0.0668 \times 10^{-2}$	$0.082 \times 10^{-2}$	$0.059 \times 10^{-2}$
$10.9 \times 10^{-3}$	476	629	-	$0.077 \times 10^{-2}$	$0.084 \times 10^{-2}$	-

$$v_g = 2.1 \text{ m/s}$$

Table C2 Variation of ( $a_s$ ) and ( $k_L$ ) with liquid velocity at  $v_L = 6.58 \times 10^{-3}$  m/s using short and full Danckwerts' model.

$V_g$ m/s	$a_s$ m <sup>-1</sup>			$k_L$ m/s		
	oblate spheroid	slotted sphere	plain sphere	oblate spheroid	slotted sphere	plain sphere
1.82	386	531	438	$0.052 \times 10^{-2}$	$0.081 \times 10^{-2}$	$0.053 \times 10^{-2}$
2.10	416	586	451	$0.0668 \times 10^{-2}$	$0.082 \times 10^{-2}$	$0.059 \times 10$
2.79	599	709	-	$0.091 \times 10^{-2}$	$0.0966 \times 10^{-2}$	-

$$v_L = 6.58 \times 10^{-3} \text{ m/s}$$

Table C2 Variation of ( $a_s$ ) and ( $k_L$ ) with liquid velocity at  $v_L = 6.58 \times 10^{-3}$  m/s using short and full Danckwerts' model.

$V_g$ m/s	$a_s$ m <sup>-1</sup>			$k_L$ m/s		
	oblate spheroid	slotted sphere	plain sphere	oblate spheroid	slotted sphere	plain sphere
1.82	386	531	438	$0.052 \times 10^{-2}$	$0.081 \times 10^{-2}$	$0.053 \times 10^{-2}$
2.10	416	586	451	$0.0668 \times 10^{-2}$	$0.082 \times 10^{-2}$	$0.059 \times 10$
2.79	599	709	-	$0.091 \times 10^{-2}$	$0.0966 \times 10^{-2}$	-

$$v_L = 6.58 \times 10^{-3} \text{ m/s}$$

## NOMENCLATURE

$a$	Interfacial area per unit volume of expanded bed.
$a_b$	Contact area in the bubbling bed in the absence of packing.
$a_L$	Interfacial area per unit volume of liquid hold up.
$a_s, a_{st}$	Interfacial area per unit volume of static bed.
$A, A_f$	Total interfacial area in the column.
$A_{bed}$	Total interfacial area of bed.
$A_s$	Total interfacial area in the separation area.
$C_A$	Concentration of gas.
$C_{Ai}$	Concentration of gas at the interface.
$C_{Ao}$	Concentration of gas in the bulk of liquid.
$d$	Equivalent diameter of slot or orifice.
$d_p, d_{sph}, d_w, d_p$	Packing diameter.
$D$	Equivalent diameter for the free area.
$D_A$	Diffusivity of gas.
$D_c$	Column diameter.
$D_L$	Diffusivity of liquid.
$E$	Enhancement factor.
$E_i$	Enhancement factor for a instantaneous reaction.
$F, F_{op}, F_o, F_g$	Fractional open area of grid.
$Fr_L$	Froude number.
$F_A$	Absorption flux.

$F$	Column cross sectional area.
$g$	Acceleration due to gravity.
$G$	Gas velocity.
$G_{mf}$	Minimum fluidization velocity.
$G_p$	Packing weight.
$h$	Expanded bed height.
$h_L, H_L$	Volume of liquid in the bed.
$h_o$	Operational liquid hold up.
$h_t$	Total liquid hold up.
$h_{to}$	Liquid hold up at minimum fluidization velocity.
$H, H_{dy}, H_{dyn}$	Expanded bed height.
$H_e$	Henry low constant.
$H_o, H_p, H_s, H_{st}$	Bed static height.
$H_w$	Solubility of gas in water.
$I$	Ionic strength of solution.
$K$	Reaction rate constant.
$k_g$	Gas film transfer coefficient.
$K_G$	Overall mass transfer coefficient based on gas side.
$k_L$	Liquid film transfer coefficient.
$k_L a$	Volumetric liquid film transfer coefficient.
$M$	Defined by eqn. 3.21.
$P_A$	Bulk pressure of gas.
$P_{Ai}$	Partial pressure of gas at the interface.

$Q$	Amount of gas absorbed by unit area during contact time.
$Q_L$	Liquid rate.
$r$	Rate of reaction per unit volume.
$R$	Rate of absorption in time $t$ .
$\bar{R}$	Average rate of absorption.
$Re_g$	Reynolds number for the gas phase.
$Re_L$	Reynolds number for the liquid phase.
$S$	Rate of surface renewal.
$Sc_L$	Schimidt number.
$t$	Time.
$t'$	Temperature.
$U_g, V_g, W$	Superficial gas velocity.
$U_L, V_L$	Superficial liquid velocity.
$U_{mf}, V_{min}$	Minimum fluidization velocity.
$W_{cr}$	Defined by eqn. 2.9.
$W_{cr}^o$	Minimum fluidization velocity of dry bed.
$W_{go}$	Gas velocity referred to the open area of dry grid.

### GREEK LETTERS

$\epsilon, \epsilon_{sp}$	Void fraction of dry bed.
$\epsilon_g$	Fractional gas hold up.
$\epsilon_l, \epsilon_L$	Fractional liquid hold up.
$\epsilon_{l,op}, \epsilon_{l,st}$	Operating fractional liquid hold up.
$\epsilon_o$	Void fraction of static dry bed.

$\epsilon_{sL}$	Fractional liquid hold up defined by eqn. 2.26a.
$\mu_g$	Gas viscosity.
$\mu_L$	Liquid viscosity.
$\xi_f$	Geometrical hydraulic resistance coefficient.
$\xi_g, \xi_{gr}$	Hydraulic resistance coefficient of grid.
$\sigma$	Surface tension.
$\tau$	Proportion of open area of grid.
$\gamma_g, \rho_g$	Gas density.
$\gamma_l, \rho_L$	Liquid density.
$\rho_p, \rho_s, \gamma_p, \gamma_{sph}$	Packing density.
$\theta$	Time
$\eta$	Defined by eqn. 3.22.
$\eta_{op}$	Operational absorption efficiency.
$\eta_{rel}$	Relative absorption efficiency.

### SUBSCRIPTS

A	Component A.
B	Component B.
C	Column.
dy, dyn	Expanded or dynamic.
fd	Flooding.
g, G	Gas.
l, L	Liquid.
i	Interface.
O	Bulk.
o, S, St	Static.

## REFERENCES

1. Douglas, W.J., et al., Chem. Eng. Progr, Vol. 59, No. 12 (1963).
2. Kito, M., et al., Ind. Eng. Chem. Process Des. Dev., Vol. 17, No. 4 (1978).
3. Uchida, et al., Canad, J. Chem. Eng., Vol. 55 (1977).
4. Levsh, J.P., et al., Inter. Chem. Eng., Vol. 8, No. 2 (1968).
5. Blyakhor, I.G., et al., Inter. Chem. Eng., Vol. 7, No. 3 (1967).
6. Kasatkim, A.G., Khim, Prom, No. 3 (1958).
7. Elgin, J.C., Weiss, F.B., Ind. Eng. Chem. 31, 435 (1939).
8. Gelperin, N.I., et al., Theo. Found. Chem. Eng., Vol. 2 (1968).
9. Bain, W.A., Hougen, O.A., Trans. Amer. Inst. Chem. Engrs. 40. No. 1, 29 (1944).
10. Kuroda, M., Tabei, K., Int. Chem. Eng., Vol. 21, No. 2 (1981).
11. O'Neill, B.K., et al., Canad, J., Chem. Eng, 50, 595 (1972).
12. Uchida, S.T., et al., Canad, J., Chem. Eng, 58, 406 (1980).
13. Sherwood, T.K., et al., Ind. Chem. Eng., 80, 768 (1938).
14. Barile, R.G., Meyer, D.W., Chem. Eng. progr. Symp. Series, No. 119, Vol. 67, 134 (1971)
15. Barile, R.G., et al., A.I. Chem. Eng. Symp. Series, 701, 154 (1975).
16. Wozniak, M., Int. Chem. Eng., 17, 553 (1977).
17. Mayak, V.I., Matrozov, V.I., Theor. Found. Chem. Eng., 3, 64 (1969).
18. Tichy, J., et al., Canad, J., Chem. Eng., Vol. 50 (1972).

19. Vunjak-Novakovic, G.V. and Vukovic, D.V., Ind. Eng. Chem. Res., Vol. 26, No. 5, p.967 (1987).
20. Vunjak - Novakovic, G.V. and Vukovic, D.V., Ind. Eng. Chem. Res., 26, No. 5, p.958 (1987).
21. Chen, B.H., and Douglas, W.J.M., Canad, J., Chem. Eng. Vol. 46 (1968)
22. Kito, M., et al., Int. Chem. Eng., Vol. 16, No. 4 (1976).
23. Gelperin, N.I., et al., Khimicheskoe. Heftyanoe. Mashinostroenie, No. 1, p.36 (1968).
24. Rao, D.P., et al., Canad, J., Chem. Eng., Vol. 61 (1983).
25. Leva, M., p.52, U.S. Stoneware Co, Akron, Ohio, U.S.A.
26. Gelperin, N.I., et al., Theo. Found. Chem. Eng., Vol. 6 (1972).
27. Kito, M., et al., Int. Chem. Eng., Vol. 16, No. 4 (1976).
28. Wozniak, M., Int. Chem. Eng., Vol. 17, No. 3 (1977).
29. Kolar, V., Col. Checosl. Chem. Com. 35, p.3678 (1970).
30. Wozniak, M., and Ostergaard, K.A., Chem. Eng. Science, Vol. 28 (1973).
31. Wales, C.E., A.I.Ch.E.J., Vol. 12, No. 6 (1966).
32. Dodge, B.F., and Tepe, J.B., Trans. Am. Inst. Chem. Engrs., 39, 255 (1943).
33. Palaty, Z., Chem. Biochem. Eng. Q, 3 (1989).
34. Tabei, K., et al., Int. Chem. Eng., Vol. 29, No. 4 (1989).
35. Kossev, A., et al., Verfahrens. Technik, Vol. 5, p.230 (1971).

36. Kossev, A., and Elenkov, D., Theo. Found. Chem. Eng., Vol. 4, p.100 (1970).
37. Strumillo, C., and Kudra, T., Chem. Eng. Sci., Vol. 32 (1977).
38. Pasiuk, Branikowska, W., Chem. Eng. Sci., Vol. 24 (1969).
39. Fick, A., Ann. Phys. Lpz. 170 (1855), 59.
40. Fourier, J.B., Theorie. analytique de la chaleur. Euvres de Fourier (1822).
41. Danckwerts, P.V., Gas-Liquid Reactions, McGraw - Hill Book Company, New York (1970)
42. Astarita, G., Mass Transfer with Chemical Reactions, Elsevier, Amsterdam (1967).
43. Whitman, W.G., Chem. and Met. Eng., 29 (1023) 147.
44. Nernst, W.Z., Phys. Chemie, 47 (1904) 52.
45. Higbie, R., Trans. Am. Inst. Chem. Engrs. 35 (1935) 365.
46. Danckwerts, P.V., Ind. Eng. Chem., 43 (1951).
47. Hikita, H., and Asai, S., Int. Chem. Eng., Vol. 4, No. 2 (1964).
48. Danckwerts, P.V., and Sharma, M.M., The. Chem. Engrs. (1966).
49. Sharma, M.M., and Danckwerts, P.V., British Chem. Engng., Vol. 15, No. 4 (1970).
50. Balabekov, O.S., et al., J. App. Chem. USSR, Vol. 42, pp.1454-1458 (1969).
51. Strumillo, C., et al., Int. Chem. Eng., Vol. 14, No. 4 (1974).
52. Miconnet, M., et al., Int. Chem. Eng., Vol. 22, No. 1 (1982).

53. Tichy, J., and Douglas, W.J.M., *Canad. J. Chem. Eng.*, Vol. 50 (1972).
54. Tichy, J., and Douglas, W.J.M., *Canad. J. Chem. Eng.*, Vol. 51 (1973).
55. Groeneveld, K.J., Dissertation, Technische Hogeschool, Delft (1967).
56. Rehm, T.R., et al., *A.I.Ch.E.J.*, 9 (1963).
57. Brirley, R.J.P., et al., *I. Chem. Eng. Symp.*, No. 56 (1979).
58. McLachlan, C.N.S., and Danckwerts, P.V., *Trans. Inst. Chem. Engrs.*, Vol. 50 (1972).
59. Nijssing, R.A.T.O., et al., *Chem. Eng. Sci.*, Vol. 10 (1959).
60. Douglas, H.R., et al., *Chem. Eng. Progr.*, Vol. 59, No. 12 (1963).
61. Vukovic, D.V., et al., *Canad. J. Chem. Eng.*, Vol. 52 (1974).
62. Sharma, M.M., and Gupta, R.K., *Trans. Inst. Chem. Engrs.*, Vol. 45 (1967).
63. Nagy, E., et al., *Int. Chem. Eng.*, Vol. 26, No. 4 (1986).
64. Pohorecki, R., *Chem. Eng. Sci.*, Vol. 31 (1976).
65. Sharma, M.M., and Vidwans, *Chem. Eng. Sci.*, Vol. 22 (1967).